INFORMATION TO USERS

This manuscript has been reproduced from the microfilm master. UMI films the text directly from the original or copy submitted. Thus, some thesis and dissertation copies are in typewriter face, while others may be from any type of computer printer.

The quality of this reproduction is dependent upon the quality of the copy submitted. Broken or indistinct print, colored or poor quality illustrations and photographs, print bleedthrough, substandard margins, and improper alignment can adversely affect reproduction.

In the unlikely event that the author did not send UMI a complete manuscript and there are missing pages, these will be noted. Also, if unauthorized copyright material had to be removed, a note will indicate the deletion.

Oversize materials (e.g., maps, drawings, charts) are reproduced by sectioning the original, beginning at the upper left-hand corner and continuing from left to right in equal sections with small overlaps.

Photographs included in the original manuscript have been reproduced xerographically in this copy. Higher quality 6" x 9" black and white photographic prints are available for any photographs or illustrations appearing in this copy for an additional charge. Contact UMI directly to order.

ProQuest Information and Learning
300 North Zeeb Road, Ann Arbor, MI 48106-1346 USA
800-521-0600

Ion Transport and Electron Transfer at Self-Assembled Alkylthiol/Gold Monolayers

Emmanuelle Boubour

Department of Chemistry
McGill University, Montréal
(Québec) Canada

March 2000

A thesis submitted to the Faculty of Graduate Studies and Research in partial fulfilment of the requirements of the degree of

Doctor of Philosophy

A mes parents Eliane et Jean,
et à mes sœurs et frère.

A José, eau, soleil, sève de mon inspiration.

Abstract

The electrical and electrochemical properties of self-assembled *n*-alkylthiol monolayers (SAMs) on gold are important if SAMs are to be used as molecular building blocks in biomimetic membranes and in micro- or nano-electronics. Ion transport and electron transfer at SAM/electrolyte interfaces are two important processes which have been characterized by cyclic voltammetry and a.c. impedance spectroscopy. Ion transport from an aqueous phase to the hydrophobic SAM region has been addressed by investigating the insulating properties of a wide variety of $X(CH_2)_nS$/Au SAMs (X = CH_3, OH, CO_2H and CF_3, and n = 7, 9, 11, 15). It was established that when the phase angle at a frequency characteristic of ion diffusion processes (*i.e.* 1 Hz) is ≥ 88°, the SAM is defect-free and obeys the Helmholtz ideal capacitor model. However, when $\varphi_{1Hz} < 88°$, the SAM is no longer an ionic insulator and ion/water penetration from the electrolyte into the SAM hydrophobic region is observed. The behavior of the phase angle with frequency was used to characterize the permeability of SAMs to electrolyte ions (K^+, $H_2PO_4^-$, and HPO_4^{2-}) as a function of the applied d.c. potential. A critical potential, V_c, was identified for each type of SAM corresponding to a transition from an insulating state to a more permeable state. When X = CH_3, V_c becomes more cathodic with increasing chainlength, *i.e.* V_c = –0.15 V (*vs.* Ag/AgCl) for n = 7, – 0.25 V for n = 9, 11, and – 0.35 V for n = 15. The SAM ionic permeability can also be modulated by maintaining n constant (15) and by varying the terminal group X. V_c is considerably more anodic for hydrophilic SAM/electrolyte interfaces (+ 0.25 V *vs.* Ag/ AgCl for X = OH and + 0.15 V for X = CO_2H) than for hydrophobic interfaces (– 0.35 V for X = CH_3). The kinetics of electron transfer at $CH_3(CH_2)_{15}CH_3$ SAMs have been investigated by a.c. impedance

spectroscopy at various d.c. overpotentials with three redox couples, $Ru(NH_3)_6^{3+/2+}$, $Fe(CN)_6^{3-/4-}$, and $Co(bpy)_3^{3+/2+}$. Fits of σ - E (Warburg coefficient as a function of applied d.c. potential) curves to theoretical models reveal that electron transfer at SAM-coated electrodes is irreversible with $Co(bpy)_3^{3+/2+}$, and operates *via* a CE (chemical reaction followed by electron transfer) mechanism with $Ru(NH_3)_6^{3+/2+}$. The kinetics of $Fe(CN)_6^{3-}$ reduction at SAM-coated electrodes is complex and cannot be resolved in terms of σ - E plots. Finally, measurements of the surface potential $\Delta\phi$ of C_nS/Au ($n = CH_3(CH_2)_{n-1}$, $4 \leq n \leq 20$) SAMs show that $\Delta\phi$ increases linearly with n for $n > 6$. Moreover, the $\Delta\phi$ value is systematically greater by 122 mV for odd-numbered SAMs than for the corresponding even-numbered SAMs. The net dipole orientation of the methyl terminal group is suggested to be at the origin of this odd/even effect.

Résumé

L'utilisation de monocouches organiques auto-assembées ("Self-Assembled Monolayers", SAMs) comme constituants élémentaires de membranes biologiques biomimétiques ou de dispositifs micro/nano-électroniques requiert une bonne compréhension de leurs propriétés électriques et électrochimiques. Le transport ionique ainsi que le transfert électronique aux interfaces SAM/électrolyte sont par conséquent des processus importants et ont été étudiés par voltammétrie cyclique et par spectroscopie d'impédance. Le transfert d'ions de la phase aqueuse à la région hydrophobe de la monocouche organique a été caractérisé en étudiant les propriétés isolantes d'une grande variété de monocouches d'alkylthiols adsorbées sur des surfaces métalliques d'or: $X(CH_2)_nS$/Au SAMs avec $X = CH_3$, OH, CO_2H et CF_3, et n = 7, 9, 11 et 15. Il a été démontré que la valeur de l'angle de déphasage φ à des fréquences auxquelles se déroulent généralement les processus de diffusion ionique (c'est-à-dire 1 Hz) permet d'évaluer efficacement les propriétes isolantes des SAMs face aux ions électrolytiques. Ainsi, lorsque $\varphi_{1Hz} \geq 88°$, la monocouche est dénuée de défauts structuraux et elle peut être modélisée par une capacité. Par contre, si $\varphi_{1Hz} < 88°$, la monocouche ne se comporte plus comme un isolant et la diffusion d'ions à l'intérieur de la monocouche est mesurable. L'étude des variations de l'angle de déphasage en fonction de la fréquence permet de caractériser la perméabilité des SAMs aux ions électrolytiques (K^+, $H_2PO_4^-$ et HPO_4^{2-}) en fonction du potentiel d.c. appliqué. Un potentiel critique V_c a été identifié pour chaque type de SAM et correspond à une transition entre un état isolant et un état perméable. Pour $X = CH_3$, V_c est d'autant plus cathodique que la chaîne alkylée est longue: $V_c = -0.15$ V (*vs.* Ag/AgCl) quand $n = 7$, -0.25 V quand $n = 9$ ou 11, et -0.35 V quand $n = 15$.

La perméabilité ionique des SAMs peut aussi être modulée en maintenant n constant (à 15 par exemple) et en faisant varier la fonction terminale X. V_c est nettement plus anodique lorsque l'interface SAM/électrolyte est hydrophile (+ 0.25 V vs. Ag/AgCl quand $X = OH$ et + 0.15 V quand $X = CO_2H$) que lorsqu'elle est hydrophobe (– 0.35 V quand $X = CH_3$). Par ailleurs, la cinétique de transfert électronique à travers une monocouche $CH_3(CH_2)_{15}S/Au$ a été étudiée par spectroscopie d'impédance à plusieurs valeurs de surtensions d.c. avec trois couples rédox: $Ru(NH_3)_6^{3+/2+}$, $Fe(CN)_6^{3-/4-}$ et $Co(bpy)_3^{3+/2+}$. Les résultats sont interprétés à l'aide de modèles théoriques développés par Sluyters et Sluyters-Rehbach. A partir des courbes $\sigma(E)$ (coefficient de Warburg en fonction du potentiel d.c. appliqué), il est montré que le transfert électronique à travers des SAMs $CH_3(CH_2)_{15}S/Au$ est irréversible avec $Co(bpy)_3^{3+}$ et répond à un mécanisme CE (réaction chimique suivie du transfert électronique) avec $Ru(NH_3)_6^{3+/2+}$. La cinétique de réduction du $Fe(CN)_6^{3-}$ à travers une SAM $CH_3(CH_2)_{15}S/Au$ est complexe et ne peut être clarifiée par des courbes $\sigma(E)$. Finalement, des mesures de potentiel de surface $\Delta\phi$ de SAMs C_nS/Au (n = $CH_3(CH_2)_{n-1}$, $4 \leq n \leq 20$) montrent que $\Delta\phi$ augmente linéairement avec n quand $n > 6$. De plus, les valeurs de potentiel de surface sont systématiquement supérieures de 122 mV pour les chaînes ayant un nombre impair d'atomes de carbone par rapport à celles où n est pair. Il est suggéré que l'orientation dipolaire de la fonction terminale méthyle soit à l'origine de cet effet pair-impair.

Foreword

In accordance with guideline C of the "Guidelines for Thesis Preparation" (Faculty of Graduate Studies and Research), the following text is cited:

> "As an alternative to the traditional thesis format, the dissertation can consist of a collection of papers that have a cohesive, unitary character making them a report of a single program of research. The structure for the manuscript-based thesis must conform to the following:
>
> Candidates have the option of including, as part of the thesis, the text of one or more papers submitted, or to be submitted for publication, or the clearly-duplicated text (not the reprints) of one or more published papers. These texts must conform to the "Guidelines for Thesis Preparation" with respect to font size, line spacing and margin sizes and must be bound together as an integral part of the thesis. (Reprints of published papers can be included in the appendices at the end of the thesis).
>
> The thesis must be more than a collection of manuscripts. All components must be integrated into a cohesive unit with a logical progression from one chapter to the next. In order to ensure that the thesis has continuity, connecting texts that provide logical bridges between the different papers are mandatory.
>
> As manuscripts for publication are frequently very concise documents, where appropriate, additional material must be provided (*e.g.* in appendices) in

sufficient detail to allow a clear and precise judgement to be made of the importance and originality of the research reported in the thesis.

In general, when co-authored papers are included in a thesis the candidate must have made substantial contribution to all papers included in the thesis. In addition, the candidate is required to make an explicit statement in the thesis as to who contributed to such work and to what extent. This statement should appear in a single section entitled "Contributions of Authors" as a preface to the thesis. The supervisor must attest to the accuracy of this statement at the doctoral oral defense. Since the task of the examiners is made more difficult in these cases, it is in the candidate's interest to clearly specify the responsibilities of all the authors of the co-authored papers.

When previously published copyright material is presented in a thesis, the candidates must obtain, if necessary, signed waivers from the co-authors and publishers and submit these to the thesis Office with the final deposition."

This dissertation is written in a form of five papers. The papers each comprise one chapter in the main body of the thesis (Chapters 2 to 6), with a general introduction to this work in the first chapter and conclusions in the seventh chapter. Following normal procedures, the papers have either been published, submitted, or to be submitted in scientific journals. A list of the papers is given below:

Chapter 2: *Langmuir* **2000**, *16*, 4222-4228.
Chapter 3: *J. Phys. Chem. B.* (submitted)
Chapter 4: *Langmuir* (submitted)
Chapter 5: *J. Phys. Chem. B.* (to be submitted)
Chapter 6: *Langmuir* (to be submitted)

Acknowledgments

I wish to first thank all those who triggered the realization of my graduate studies by having me enjoy the very first steps in research, that is Professors Benoît Marsan and Daniel Bélanger (Université du Québec à Montréal), and Dr. Jean-Yves Huot (Centre de Technologie Noranda).

I wish to express my sincerest gratitude to my research director, Professor R. Bruce Lennox for his endless encouragement and devotion to this work. His continuous support and precious advice have made these years an extremely rich and fantastic experience. In addition to having created a stimulating learning environment, his human qualities have driven my enthusiasm and curiosity and inspired my creativity.

I would like to extend my gratitude to Professor Antonella Badia who has been a great source of inspiration and comfort. Her friendship and continuous encouragement have made this experience a unique one. I will always remember the trials made on the side "just-for-fun". Without the synthesis of alkylthiols and the preparation of some gold evaporated substrates, parts of this study could not have been achieved. Moreover, her judicious advice during the writing of the general introduction and the surface potential study is greatly appreciated.

I am grateful to Dr. Louis Cuccia for his encouragement, inspiration and for having taught me many aspects of phospholipid research. His support has given me confidence in pursuing my studies: "Don't worry, everything will go fine!".

Past and present members of this research group deserve a very special thanks for their discussions and friendship. These include Joy Klass, Pollyanna Peters, Isabelle Lawrence, Aziz Houmam, Daniela Loock, Valérie Gandubert, Michal Goren, Vicki Meli, Muriel Corbière, Brian Seivewright, Caroline Bourg, Janine Mauzeroll, Michelle Nahas, Franklin Wu, Linette Demers, Bruce Constantine, Hélène Schmidt,

Gabrielle Farkas, Tara Heitner, Juliet Cox, Fuyan Ma and Zhigang Qi. I am grateful to Valérie Gandubert and Isabelle Lawrence for the drawings and help in formatting this thesis. The typing of this thesis would not have been free from computer hazards without the help from Lawrence Lee. A special thanks to Dr. Francis Chubb for the genuine enthusiasm and wisdom he has propagated throughout the lab.

I would like to extent my thanks to Prof. Daniel Bélanger, Drs. Florence Fusalba, and Isabelle Lawrence for their helpful discussions on a.c. impedance spectroscopy. I am grateful to Professors David Ronis and Martin Zuckermann (Department of Physics) for their discussions on surface potential. I was fortunate to have worked with fantastic undergraduate students: Janine Mauzeroll, Michelle Nahas and Franklin Wu. Their inputs through their work on impedance spectroscopy and surface potential have been fruitful.

I sincerely acknowledge Mr. Fred Kluck (machine shop), Mr. Georges Kopp (glass blower), and Mr. Rick Rossi (electrician) for their help in designing and fabricating pieces of equipment that have been very useful in performing these experiments.

I would also like to thank my colleagues whose cooperation have led to the realization of certain science-related projects very dear to my heart. It includes Caroline Bourg and Luc Desbaumes for the radio broadcasting of *Digital Delirium*, Sandra Carriero, Erwin Schultz, Catherine Edgar, Alessandra Mezzetti, and François Ravenelle for the organization of the *Seventh and Eighth Visiting Speaker Ventures*.

I am grateful to the Natural Sciences and Engineering Research Council of Canada and to the Fonds pour la Formation de Chercheurs et l'Aide à la Recherche du Québec, Sigma Xi-The Scientific Research Society, and the Faculty of Graduate Studies and Research (McGill University) for financial support.

Finally, I wish to thank my family for their encouragement and support, as well as Nicole, Thierry, Rachèle, and Jean-Philippe. I sincerely wish to express my gratitude to José for his endless encouragement, support, and love.

Table of Contents

Chapter Two

INSULATING PROPERTIES OF SAMs MONITORED BY IMPEDANCE SPECTROSCOPY

Chapter Three

ION PENETRATION INTO *n*-ALKYLTHIOL SAMs MONITORED BY A.C. IMPEDANCE SPECTROSCOPY

Chapter Four

THE DEPENDENCE OF ω-FUNCTIONALIZED SAM STABILITY ON APPLIED POTENTIAL MONITORED BY A.C. IMPEDANCE SPECTROSCOPY

Chapter Five

KINETICS OF ELECTRON TRANSFER AT SELF-ASSEMBLED MONOLAYERS PROBED BY A.C. IMPEDANCE SPECTROSCOPY

List of Frequently Used Symbols

a_o, a_r $= D_i / \delta_i k_{sh}^a$, $i = O$ or R

C^* $= C_o^* + C_r^*$, concentration of electroactive species in the bulk of the solution or the electrode material, in mol cm^{-3}

C_p^* $= C_o^*(K+1)/K$

CE Chemical-Electrochemical mechanism

CEC Chemical-Electrochemical-Chemical mechanism

C_d capacitance of defects in defect-laden SAMs

C_{dl} double-layer capacitance

C_m monolayer capacitance

D_o, D_r diffusion coefficients in cm^2 s^{-1}

E applied d.c. potential

$E_{1/2}^r$ reversible half-wave potential

E_o standard potential

E_m minimum potential for σ in σ - E curves

f frequency in hertz

F Faraday constant = 96,480 C mol^{-1}

j $\sqrt{-1}$

K $= k_1 / k_2$, equilibrium constant of the chemical reaction

k $k_1 + k_2$

k_f forward rate constant of the charge transfer reaction

k_{sh} standard heterogeneous rate constant of charge transfer reaction in cm s^{-1}

k_{sh}^{a} "apparent" k_{sh} in cm s^{-1}

L represents the influence of the chemical reaction in a CE mechanism, as defined by Jacq's reaction layer treatment

n number of exchanged electrons involved in charge transfer

n in $X(CH_2)_nS/Au$ SAMs, represents the number of methylene units

R gas constant = 8.314 J K^{-1} mol^{-1}

R_{ct} charge transfer resistance

$(R_{ct})_m$ minimum value of R_{ct}

R_d resistance of defects in defect-laden SAMs

R_m SAM resistance

R_s solution resistance

V_{app} applied d.c. potential

V_c critical potential

RS/Au *n*-alkylthiol chemisorbed on gold

RSH *n*-alkylthiol

T temperature, 298 °K

$|Z|$ modulus of the impedance

Z_f' real component of the faradaic impedance

Z_f'' imaginary component of the faradaic impedance

Z_w Warburg impedance

α anodic transfer coefficient in Chapter 5

exponent of a Constant Phase Element in $Z_{CPE} = A(j\omega)^{-\alpha}$ (Chapters 2-4)

β cathodic transfer coefficient

$\Delta\phi$ surface potential (or contact potential difference)

φ phase angle of the impedance; φ_{1Hz} is the phase angle at one hertz

δ_o, δ_r thickness of the Nernst diffusion layer

ε dielectric constant of a material

ε_o permittivity of free space, 8.85×10^{-14} F cm^{-1}

η overpotential with respect to the reversible half-wave potential, $E_{1/2}^{r}$

List of Tables

List of Figures

List of Tables

Chapter 1

General Introduction

1.1 Self-Assembled Monolayers (SAMs) as Model Organic Surfaces

Organic monolayers can be formed by deposition on solid surfaces using the Langmuir-Blodgett[1,2] technique (transfer from air-water interface to the surface) or by chemisorption from dilute solution.[3-11] Structurally well-defined organic monolayers often derive from the spontaneous organization of individual molecules on the substrate where the driving force is dominated by molecule-substrate interactions and intermolecular forces. This spontaneous organization is often referred to as ***molecular self-assembly*** and the resulting film as a self-assembled monolayer (SAM). Different types of SAMs have been reported in the literature, including organosilanes on hydroxylated surfaces such as silicon oxide and glass [12-17], fatty acids on aluminum oxide[9,10] and silver,[18] and alkylthiols (RSH) or dialkyldisulfides (RSSR) on gold, silver, and copper.[4]

The first work describing the formation of self-assembled monolayers by the adsorption of surfactant molecules on a clean metal surface was reported by Zisman as early as 1946.[19] However, it is only four decades later that the full impact of SAMs was revealed for the engineering of model organic surfaces by the groups of Nuzzo and Allara (AT&T Bell Laboratories) and Whitesides (Harvard U.). These first reports involved the use of alkylthiols and *n*-dialkyl disulfides for the formation of SAMs on metal surfaces.[20-22] Since then, SAMs have become a versatile tool in the design of organic interfaces with well-defined thickness, composition, and structure.

This often makes them excellent candidates for the investigation of surface chemistry phenomena such as wetting, adhesion, lubrication, corrosion, protein adsorption, and cell attachment since SAMs with desired physical properties can be prepared rather easily from a number of functionalized organosulfur molecules.[3-6,23]

1.2 RS/Au SAM Preparation on Gold Surfaces

Thiols and disulfides on metal surfaces are the most widely used systems to date, since the resulting SAMs can withstand strong acid or base conditions,[24-26] and in some cases, physiological environments.[27-29] These SAMs are usually prepared by immersing a clean metal substrate into a solution (typically 10^{-3} M) of an alkylthiol or alkyldisulfide solubilized in an appropriate organic solvent (ethanol, THF, toluene, acetonitrile). The monolayer is spontaneously and irreversibly adsorbed onto a planar metal substrate by a self-assembly process (Figure 1.1). The metal surface reacts preferentially with the sulfur groups, exposing the chain end group at the SAM/air or SAM/solvent interface.[6,30,31] In addition to the more commonly used ω-functionalized alkylthiols (*i.e.* $X(CH_2)_nSH$ where X = CH_3, OH, CO_2H, NH_2), more complex molecules such as thiolipids[32-38] and thiocrown ethers[39,40] have been employed to build model lipid membranes or as chelating agents where the thiol group anchors the chelator to the metal surface.

Although SAMs can be prepared on a variety of metal substrates (Au, Ag, Pt, Cu. Hg), gold remains the most widely used metal due to the fact that under ambient conditions, its surface is not readily contaminated by the spontaneous formation of an oxide layer. Gold substrates include single crystals, polycrystalline bulk electrodes, and thin film gold formed by the evaporation or sputtering of gold onto mica, glass, or silicon substrates.[41]

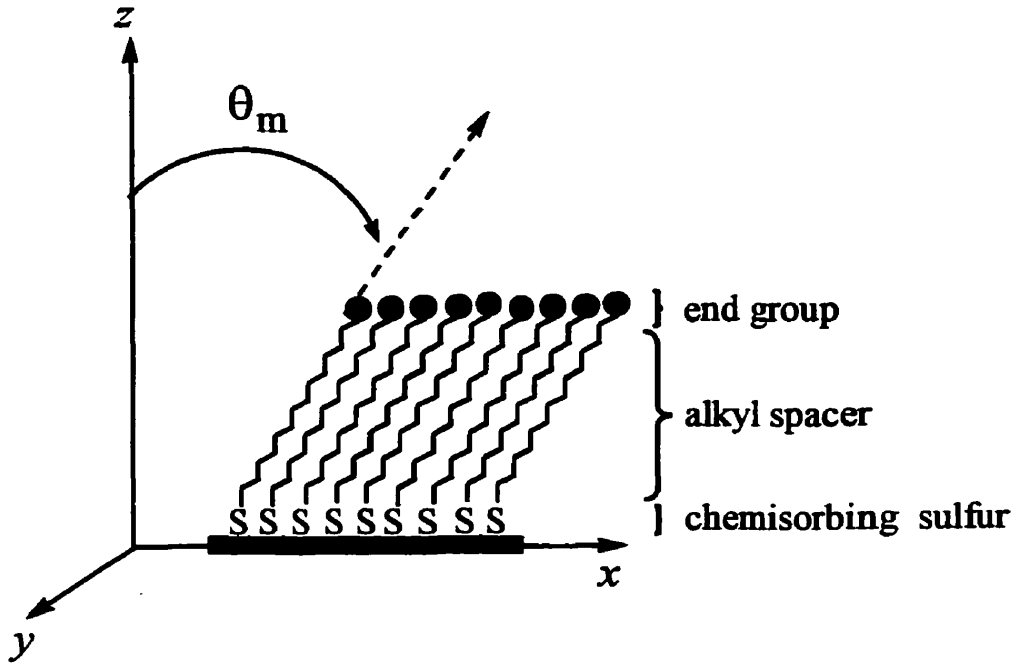

Figure 1.1. Schematic illustration of a $X(CH_2)_nS/Au$ self-assembled monolayer (SAM). The SAM surface properties can be modulated by choosing an appropriate end group *X*, rendering the surface hydrophobic (*e.g.* $X = CH_3$, CN, CF_3, OCH_3, RCO_2CH_3) or hydrophilic (*e.g.* $X = OH$, CO_2H, NH_2, $CONH_2$, Br, Cl). The degree of chain order increases with *n* and small size end groups. Three main types of interactions determine the SAM structure: $Au^{\delta+}$-$S^{\delta-}$ bond, interchain van der Waals interactions, and end group/air or electrolyte interactions. The molecular tilt θ_m takes on values depending on the nature of the gold substrate (polycrystalline *vs.* single crystal) and the chemical structure of the thiol. Adapted from Delamarche *et al. Adv. Mater.* **1996**, *8*, 719-729 and Xu *et al. J. Colloid Interface Sci.* **1995**, *176*, 138-149.

Single crystals (Au(111), Au(100) or Au(110)) must be used when SAMs are analyzed by surface analytical techniques requiring highly ordered or atomically flat surfaces, such as electron diffraction, He atom scattering, scanning tunneling microscopy, and atomic force microscopy. However, the construction of defect-free SAMs does not seem to require a single crystal surface.[42] Rigorous cleaning of the gold surface prior to thiol adsorption is the critical step for obtaining a defect-free, ionically-insulating SAM. Several procedures have been used to generate clean gold surfaces, including flame annealing,[43] electrochemistry,[44] or chemical etching with Piranha solution (3:1 H_2SO_4:H_2O_2).[45]

In addition to passive chemisorption from solution,[30,46,47] thiol molecules can be deposited using vapor deposition for short chain volatile thiols[48] and by electrochemical deposition at oxidative potentials.[49,50] Many factors can influence the order of a SAM, including the thiol concentration in the deposition solution, the incubation time, and the temperature. The most common deposition conditions are room temperature and a millimolar concentration of the alkylthiol in anhydrous ethanol. The incubation time can vary from minutes to days. It appears that a "recipe" has to be worked out for each type of thiol and gold substrate. This non-standardized preparation process often prevents a meaningful comparison of data from laboratory to laboratory in terms of the chemical, structural and physical properties of these SAMs.[51]

1.3 Structure of SAMs Made of *n*-Alkylthiols: $X(CH_2)_nS/Au$ SAMs

The affinity between the gold surface and the sulfur atoms is the driving force for the formation of RS/Au SAMs. The exact mechanism for Au-S bond formation is not known, but may be described formally as an oxidative addition of the S-H bond to the gold surface, followed by a reductive elimination of the hydrogen as H_2:[52]

$$XRSH + Au(0)_n \rightarrow XRS^{-}Au(I) \bullet Au(0)_{n-1} + \frac{1}{2}H_2 \qquad (1)$$

The reaction is exothermic ($\Delta H \sim -21$ kJ mol^{-1}).[53] The strength of the Au-S bond is 170-210 kJ mol^{-1}.[54] Evidence for the loss of the thiol proton is given by spectroscopy (surface IR and Raman) where the S-H stretching band for a SAM-coated metal (Au, Ag or Pt) is absent.[7,8,55-58] Moreover, XPS measurements suggest that the surface adsorbed species is a thiolate.[8,54,59,60] However, there is as yet no direct experimental evidence for the evolution of hydrogen gas.

In a general sense, the ordering and orientation of the tethered alkyl chains is driven by the interchain or lateral van der Waals interactions (~ 6 to 8 kJ mol^{-1} per CH_2)[4] and the electrostatic or hydrogen bonding interactions between polar end groups (Figure 1.1).[4,5,55] The S-S spacing and the alkyl chain packing density is largely dictated by the underlying metal lattice. Under well-defined experimental conditions, a densely packed monolayer (100 % surface coverage) is obtained with a chain density of $\sim 5 \times 10^{14}$ molecules per cm^2.[53,61] On Au(111), the chains are parallel to one another with a tilt angle of typically ~ 30° from the surface normal since the spacing between adjacent sulfur overlayers (4.99 Å) is greater than the distance of closest approach of the alkyl chains (4.24 Å).[3,4,61] The effective SAM thickness varies from ~ 1 to 3 nm, depending on the alkyl chainlength and the tilt angle θ_m. For alkyl chains $\geq$ 12 carbons, a well-organized two-dimensional phase is obtained with the chains extending perpendicularly from the plane of the surface in a predominantly all-*trans* configuration.

The most important issues for the characterization of RS/Au SAMs addressed so far are:

i) SAM structure (molecular conformation and orientation of the chains) and packing density

ii) Nature of the gold-sulfur interaction and the identity of adsorbed species

iii) Surface coverage of the thiol (defect density)

iv) SAM electrochemical/electrical properties.

The structural properties of self-assembled monolayers of thiols on gold have been widely studied by grazing incidence infrared spectroscopy,[8,55,59,62,63] low energy helium diffraction,[61,64-66] grazing incidence X-ray diffraction[64,67,68], electron diffraction[69] and scanning tunneling microscopy.[67,70-81] Macroscopic SAM properties such as the surface wettability and film thickness have also been determined by contact angle measurements[5,22,60,82,83] and ellipsometry,[8,30] respectively. Most reports on the SAM structure converge to the description shown in Figure 1.1.

However, it is important to mention that these SAMs should not be viewed as static systems. Their description as "hydrocarbon slabs" may be useful at some level of discussion, but is a rather naïve representation because of chain dynamics, reorganization of polar end groups, surface migration of thiolate gold species and the presence of film defect sites. Molecular dynamic simulations have been particularly useful at providing a picture of the chain dynamics in RS/Au SAMs. These predict the existence of *trans-gauche* bond isomerization, chain rotation and reorientational motions.[84-86] He diffraction intensities show that at room temperature, the chain ends of long chain thiols are highly mobile and disordered.[3] Surface IR spectroscopy and surface enhanced Raman spectroscopy studies have also revealed the presence of both chain end and internal *gauche* defects.[8,57,87-89] The energy associated with each *trans-gauche* isomerization is approximately 2.9 kJ mol^{-1}.[4] Thus, the number of *gauche* conformational chain defects has been found to increase with temperature and with shorter alkyl chains.[87,90] The relative humidity and the possible adsorption of contaminants from air or from the electrolyte at the SAM interface can also influence the orientation (disorder) of the chain ends.[91-95]

At the atomic scale, SAMs are far from being perfect structures. High gap impedance UHV-STM has enabled the imaging of the two-dimensional structure of RS/Au(111) monolayers with unprecedented molecular resolution (Figure 1.2).

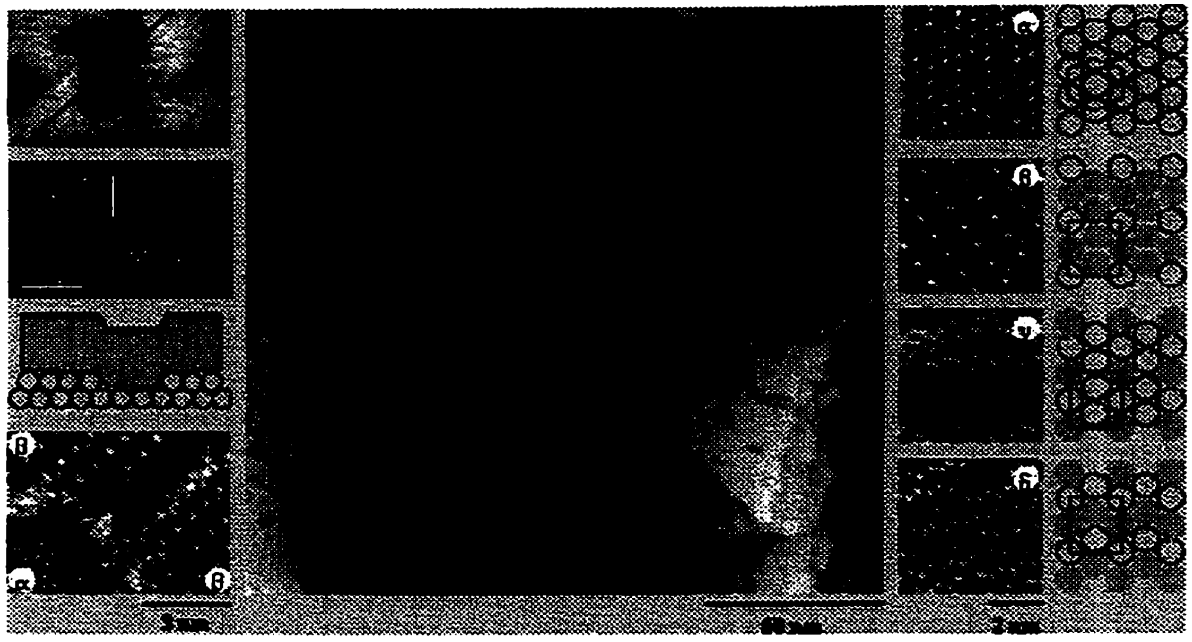

Figure 1.2. STM image of a $CH_3(CH_2)_{11}S$/Au(111) SAM. Monoatomic gold terraces are observed as darker lines delineating Au(111) terraces (from ref [73]). The presence of black holes is not due to defects in the SAM, but to etch pits (0.24 nm high) originating from a reconstruction of the gold surface by the thiols. The domain boundaries in the SAM correspond to zones of disorder and lower packing and are observed as a series of narrow (1 nm) lines. Reprinted with permission from *Langmuir* **1994**, *10(9)*, 2869-2871, copyright 1994 American Chemical Society; and from *Adv. Mater.* **1996**, *8(9)*, 719-729, copyright 1996 Wiley-VCH.

The STM images reveal that the alkylthiolates form positionally ordered domains of various molecular arrangements which are separated by domain boundaries (regions of disorder and defects) and etch pits, and are prone to structural defects associated with the underlying gold substrate.[96] The characteristic ordered domain size is only ~ 5 - 15 nm (*i.e.* 90 - 800 molecules per domain), even though the Au substrate domain size is > 100 nm. The overall effect can be likened to a mosaic of densely-packed, chain domains superimposed on a larger array of single-crystal Au domains. The imaging of RS/Au SAM requires state-of-the-art STM and AFM instrumentation and is challenging given that SAMs are extremely good insulators and are softer than the metal or inorganic substrates.

1.4 The Electrochemical Properties of SAMs

A major contributor to the SAM literature, H. O. Finklea (U. of West Virginia) has remarked that the "formation of a well-organized monolayer for the electrochemical experiment is at best an art".[42]

A wide variety of SAMs have been extensively studied by a number of electrochemical chemical methods, including cyclic voltammetry, differential capacitance measurements, and a.c. impedance spectroscopy. The fundamental questions arising from electrochemical studies of SAMs are:

i) What constitutes a defect-free SAM from an electrochemical viewpoint?

ii) Are SAMs impermeable to electrolyte ions?

iii) What is the mechanism of electron transfer across SAMs?

The presence of a nanometer-thick SAM on gold surface considerably reduces the interfacial capacitance, compared to that of a bare gold electrode. The blocking capacity of SAMs to ion transport and to heterogeneous electron transfer from redox probes are difficult to assess since the nature of the electrolyte, the type of redox couple used, and the magnitude of the applied potential all contribute to the level of blocking observed. By far, the most widely used parameter for the characterization of SAM electrochemical properties is the capacitance. The capacitance of a defect-free

SAM is 20 to 100 times lower than that of bare gold, owing to the very low dielectric constant of the alkyl monolayer. The Helmoltz model (parallel plate capacitor with a dielectric material as the spacer) is often used to describe SAM-coated electrodes,[8,97]

$$C_{SAM} = \frac{\varepsilon_{SAM}\varepsilon_o A}{d} \qquad (2)$$

where d is the thickness of the dielectric layer, A is the electrode area (in cm^2), ε_{SAM} is the SAM dielectric constant, and ε_o is the permittivity of free space (8.85×10^{-14} F cm^{-1}). The capacitance data obtained for $CH_3(CH_2)_nS$/Au SAMs was fitted to the Helmholtz model for alklythiol/Au SAMs for $n > 9$.[8,98,99] However, the Helmholtz model only applies when the SAM is defect-free. There is experimental evidence that eq 2 does not systematically hold since *i*) a linear relationship between the measured capacitance and the ellipsometric film thickness is not always observed[100] and *ii*) the SAM dielectric "constant" (ε_{SAM}) may not, in fact, be constant, but instead decreases as n increases, as indicated by surface potential measurements.[101]

For a given alkyl chainlength, the chemical speciation of the terminal group X affects the capacitance of SAM-coated electrodes,[83,102] in the sequence (increasing capacitance) for $n = 9$, CH_3 (~ 1.6 μF cm^{-2}) < OH < CN < CO_2H (~ 2.5 μF cm^{-2}). This trend leads to the conclusion that even though the hydrophilic character of the SAM/electrolyte interface affects its ionic permeability, it is probably not the only factor. The size of X also affects the packing density of the SAM. For instance, CO_2H-terminated SAMs have a greater population of *gauche* bonds compared to OH-, CH_3-, and CN-terminated SAMs, as shown by FT-IR spectroscopy for a chainlength of 10 carbons.[83]

One of the greatest challenges in the characterization of SAMs by electrochemical means is the non-intrusive determination of the surface coverage and the characterization of *pinholes* and *defect sites* (size and distribution). There is difficulty in the SAM literature in precisely defining what pinholes and defects actually are, since their meaning may vary from laboratory to laboratory. For the purpose of this discussion, a *pinhole* is described as a small-sized gold site that is

directly exposed to the electrolyte solution. This is the case when at least one chain is missing. On the other hand, *defects* arise from a structural disordering of the chains. This is more likely to happen near the chain terminus where *gauche* conformations are present. These defects may have a sufficient lifetime and size to allow ions, water or redox molecules to approach the gold substrate. In other words, defects may lead to the penetration of foreign species to a distance from the substrate which is shorter than the full width of the SAM. The (indirect) characterization of pinholes using a redox couple in solution has been the focus of most of the reported electrochemical studies, leaving the question of ion penetration (through defects) largely unanswered.

Evidence for a *pinhole*-free SAM is difficult to obtain since *i*) most of the techniques used actually generate/induce pinholes, and *ii*) the sensitivity for the detection of pinholes depends on the technique used. The general approach used assumes that a pinhole-mediated electrochemical response differs significantly from that of a defect-free SAM. Five approaches have been commonly employed to estimate the quantity of pinholes (or the surface coverage) of a given SAM:

i) Determination of the gold oxide stripping current (at + 0.9 V *vs.* SCE) by cyclic voltammetry in 0.1 M H_2SO_4. This procedure assumes that the areas covered with the densely-packed monolayer are electrochemically inert.[83,100,103-107] The alkylthiolate surface coverage ($1 - \theta$) is obtained from the ratio of the charge under the gold oxide stripping peak of the SAM-coated electrode to that of a bare gold of the same surface area. However, this technique damages the SAM.

ii) Measurement of the oxidation peak of an adsorbed layer of iodine. Iodine spontaneously forms a monolayer at the bare gold spots (pinholes) after a few minutes of immersion in a dilute solution (of iodine).[108-110] The ratio of the anodic current for iodine oxidation at a SAM-coated electrode over that of the bare gold yields ($1 - \theta$). Methods *i*) and *ii*) should give the same values of ($1 - \theta$). The I_2 technique also damages the SAM.

iii) Inhibition of metal deposition on the gold electrode, *i.e.* under potential deposition (UDP) of Cu^{2+} in H_2SO_4.[111] The current suppression obtained from cyclic voltammetry is due to the restricted access of the copper ions to the electrode surface and/or inhibited nucleation.

iv) Suppression of simple faradaic processes measured by cyclic voltammetry using redox couples in solution *(i.e.* $Fe(CN)_6^{3-/4-}$, $Ru(NH_3)_6^{2+/3+}$, $Mo(CN)_8^{3-/4-}$, $Fe^{2+/3+}$ and $Fe(bpy)(CN)_4^{1-/2-}$)[8,11,71,99,100,103-106,112-119] or a redox couple tethered to the alkyl chain end (viologens, $pyRu(NH_3)_5^{2+/3+}$, ferrocene).[11,71,120-128] One must keep in mind that the measured blocking properties depend on the physical and chemical characteristics of the SAM, the SAM/electrolyte interface, and on the nature of the redox couple. The unfavorable energetics of forcing a charged (hydrophilic or hydrophobic) redox molecule into and across a close-packed, non-polar hydrocarbon layer play a role in the observed signal.

v) The attenuation of the rate of heterogeneous electron transfer of the redox probe is characteristic of a blocking organic layer. This approach is used in the case where the SAM-coated electrode presents deliberately pre-formed pinholes. The system can then be treated as an array of microelectrodes. Assuming that the pinholes are conducting sites of well-defined dimensions and spacings on an insulating plane, the pinhole parameters (density, size and distribution) can be calculated from a.c. impedance data, using the methodology developed by Rubinstein and co-workers, [103,104,106] based on the work of Matsuda[129] and on the Amatore-Savéant-Tessier theory.[130] The microelectrode array model assumes that non-linear diffusion at pinhole sites is mathematically equivalent to a CEC (chemical-electrochemical-chemical) mechanism. The electrochemical response can thus be modeled using CEC formalisms.

In conclusion, the relationship between the SAM structure and its blocking properties at room temperature to ion transport and electron transfer is not straightforward. As mentioned above, factors such as the type of substrate used and the deposition method (thiol concentration, incubation time, and temperature) can affect the blocking properties of a SAM. Other factors such as the thiol chain composition and the presence of phase transitions (such as the melting transition between crystalline and liquid-like phases)[131] can greatly influence the electrochemical response. There has been great interest in the development of methods for the reproducible preparation of defect-free SAMs and increasingly sensitive SAM characterization techniques. Defect/pinhole-free SAMs seem to be ideal candidates for investigating long-range electron transfer processes. The exponential relationship between the measured faradaic current and the SAM thickness, and the (curved) Tafel (ln i - E) behavior are usually invoked as evidence for an electron tunneling mechanism[99,116-118,121,132] This however is somewhat controversial as it also seems to support a defect-dominated electron transfer model.[100,103-106] While these descriptions are internally consistent, it is unlikely that both are operative for what is ostensibly the same system. The interpretation of the electron transfer barrier properties of RS/Au SAMs obviously awaits development of another mechanistic model.

1.5 The Electrical Properties of SAMs

Materials are usually classified as being either conductors or insulators. In conductors, the current is carried out by electrons and/or ions. *Electronic* conductors include metals, inorganic oxides and sulfides (*i.e.* PbO_2, Ag_2S), semiconductors (*n*-type, *p*-type, intrinsic), conducting polymers, and organic metals (*i.e.* tetrathiafulvalene tetracyanoquinodimethane, TTF-TCNQ). *Ionic* conductors owe their conductivity to the motion of anions and/or cations. Examples are solutions of electrolytes, molten salts, solid ionic conductors (or solid electrolytes, such as zirconia) and doped crystals such as $LaBF_3$ doped by EuF_2. The most important

technique used to measure both the ionic and electronic conductivity of materials and the mechanism of conduction is a.c. impedance spectroscopy.

Curiously, the electrical (rather than electrochemical) properties of SAMs have not been the subject of many studies. This probably stems from the fact that in spite of their size (10 - 40 Å thick), they are extremely good insulators. Current across a well-formed SAM is typically in the range of 10 nA cm^{-2} and therefore requires very sensitive measuring equipment. The electrical properties of ultrathin organic films were originally investigated in the early 1970s using fatty acids deposited on Hg, Al, Pb, and Au by Mann and Kuhn.[133] Their methodology was then applied to alkyltrichlorosilanes ($CH_3(CH_2)_nSiCl_3$)[134-139] and Langmuir-Blodgett monolayers of hexadecylquinolinium tricyanoquinodimethanide sandwiched between two metal electrodes.[140] In this all-solid configuration (metal/SAM/metal or semiconductor), the electrical properties of alkylsiloxane SAMs are probed by measuring the conductivity *via* current-voltage measurements. The measured conductivity of such systems, typically 3×10^{-15} Ω^{-1} cm^{-1}, stems from the intrinsic properties of the materials as the contribution from electron tunneling is negligible.[137,138] The conductivity in Hg-$S(CH_2)_nCH_3$/$CH_3(CH_2)_nS$-Hg ($15 < n < 33$) systems is ~ 6×10^{-15} Ω^{-1} cm^{-1}, and is chainlength independent, confirming that electron tunneling is negligible.[141] When electron tunneling is the conduction mechanism, the tunneling conductivity σ decreases exponentially with SAM chainlength d (in Å) following the relation:

$$\sigma = \sigma_o e^{-\beta d} \qquad (3)$$

where σ_o is the conductivity measured on the bare substrate and β is the electron tunneling constant (in $Å^{-1}$). The major difficulty in the characterization of metal/SAM/metal systems is avoiding alternative conductive pathways through the SAM. Short-circuits and electron tunneling arising from metal indentations at each of the sandwiched surfaces can both contribute to the measured current.

Under well-controlled preparation procedures, alkylthiol SAMs can sustain electric fields as high as 6×10^6 V cm^{-1} (when $n > 14$) before monolayer breakdown occurs, a value similar to that of bilayer lipid membranes.[142] The measured electrical

breakdown voltage (BDV) of a Hg-$S(CH_2)_nCH_3/CH_3(CH_2)_nCH_3$-M' system was found to depend on the nature of M', the alkyl chainlength and whether the measurements are made in solution or in gas phase. The difference in the SAM packing density and tilt angle obtained for M' = Ag, Hg, Cu and Au can account for the difference in the measured BDV.[143] The BVD values are considerably lower when a dilute electrolyte is present between the two monolayers, owing to ion penetration within the SAMs.[143]

Metal-SAM-metal junctions have also been built using a STM tip as the second metal surface. This set-up has allowed the measurement of the electrical properties of single RSH molecules.[144-147] This research is motivated by the development of organic molecular wires (conjugated molecules) which requires one to understand carrier motion in both single molecules and in assemblies of molecules.

1.6 SAMs as Building Blocks of Molecular Architectures for Model Membranes

Nanomolecular thiol-based systems are used as the building blocks of molecular architectures on a scale of 1 to 100 nanometers.[148] The emergence of nanostructures as a topic of study has created considerable interest in the scientific community, given that matter at the nanoscale can exhibit physical and chemical properties that are quite different from that of the bulk. The alignment of nanostructures is a major challenge and chemical strategies based on self-assembly have been attempted.[149] Self-assembly and self-ordering are of course very important processes in biological systems and play an important role in DNA hybridization, the assembly of cell membranes, and protein folding. Chemists are now exploiting covalent modifications and non-covalent interactions (hydrogen bonds, ionic bonds, and van der Waals forces) to develop new supramolecular architectures.

The biomimetic capacity and the biocompatibility of SAMs are important considerations for their applications in chemical and biochemical sensors. SAMs have the advantage of being easier to handle and considerably more stable than the well-

known Black Lipid Membranes (BLMs)[142] which are formed by painting a dilute lipid solution across a micrometer size hole. A stable BLM is a very efficient insulator whose capacitance is low (typically 0.5 – 1 $\mu F\ cm^{-2}$) and can resist high electric fields (~ $10^6\ V\ cm^{-1}$). Upon the insertion of a protein within a BLM, it has been possible to elucidate some of the molecular mechanisms responsible for cell membrane function, such as ion transport through gated channels, antigen-antibody binding, signal transduction, *etc.*

Since the emergence of the RS/Au SAM system, several model membrane architectures supported on metal or semiconductor surfaces have been developed (Figure 1.3). The three main approaches which have been used are: *i*) a phospholipid monolayer spread on a hydrophobic surface (such as a RS/Au SAM), *ii*) a phospholipid bilayer on a hydrophilic surface (XRS/Au SAM where X = OH, CO_2^-,NH_3^+), and *iii*) a covalently-anchored phospholipid bilayer.

The strategy for building model membranes involves mimicking the natural lipid environment of the native protein and the immobilization of the entire system onto the metal (Au) surface which serves as both the support and the signal transducer. The search for suitable lipid membrane mimics has been the workhorse of several research groups and requires a multi-disciplinary approach, based on advanced knowledge in chemistry, biology, biochemistry and physics. The ideal biomimetic material should possess biophysical properties that are as close as possible to that of the original lipid bilayer in terms of its electrical and mechanical (viscosity, fluidity) properties. These biomimetic materials not only provide the protein with an adequate environment in which to function, but also act (in the absence of an electrical stimulus) as an insulator (or effective barrier) for ions and electrons.

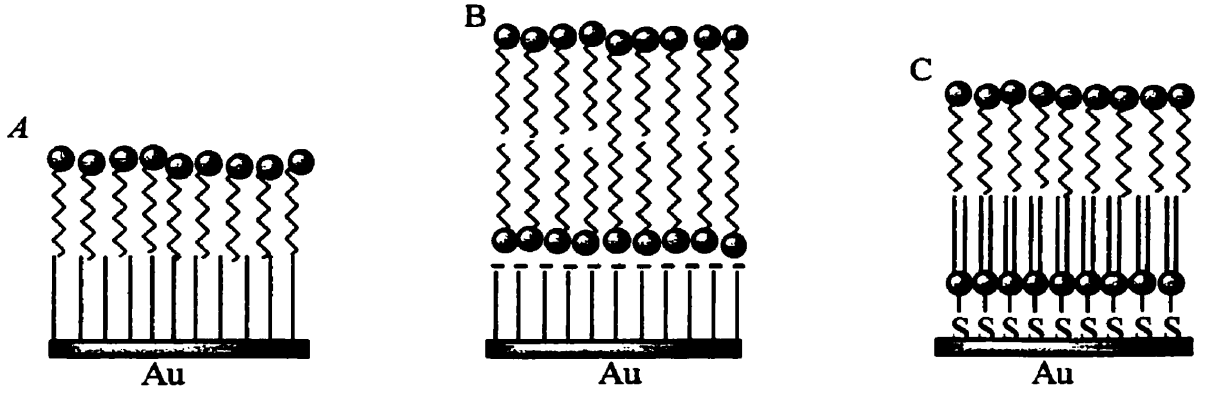

Figure 1.3. Architectures of model membranes. *A)* a phospholipid monolayer spread on a hydrophobic surface (such as a $CH_3(CH_2)_nS$/Au SAM), *B)* a phospholipid bilayer on a hydrophilic surface (*e.g.* $^-OOC(CH_2)_nS$/Au SAM), and *C)* a covalently-anchored phospholipid bilayer. Adapted from Vogel *et al. Biochim. Biophys. Acta* **1998**, *85507*, 319-338.

1.7 SAMs as Building Blocks of Molecular Architectures in Microelectronics

RS/metal SAMs are obvious starting points for fabrication of micro- and nanostructures. Two approaches are generally used to generate systems at the nanometer scale (1 nm = 10 Å): the "top-down" approach and the "bottom-up" approach. The "top-down" approach has been widely used for decades in the fabrication of electronic devices using lithography (photo, electron-beam) techniques. The evolution of the "top-down" approach is likened to that of a sculptor using finer and finer chisels. Lithography techniques are fundamentally limited by the Rayleigh criterion which limits the feature size to $> \lambda/2$. The current state-of-the-art allows one to fabricate structures of *ca.* 200 nm and thus approaches the limit of photolithography. On the other hand, the "bottom-up" approach uses the spontaneous assembly of molecules to create more complex structures. The molecular building blocks are synthetically designed to self-organize into the desired supramolecular architecture. A "bottom-up" process thus creates structures using a bricks-and-mortar methodology rather than the sculptor's "top-down" approach.

SAMs have been proposed for use in microelectronics as ultrathin film resists and masks. However, the density of pinholes (as shown in Figure 1.2) is critical to determining whether this will be practical. Any method developed to both prepare defect-free SAMs and non-destructively assess them will be an important contribution. The determination of the level of defects in a RS/Au SAM is limited by the technique used to probe defects. Molecular defects, as revealed by STM, may not be observed using more macroscopic techniques such as infrared and Raman spectroscopies, contact angle measurements, and electrochemistry. The criterion for establishing a defect-free SAM for electrochemical biosensor applications might not be the same as that required for opto-electronic devices. Thus, the technological applications themselves will determine what kind of defects can be tolerated.

1.8 The Present Work

Although the electrochemical characterization of SAMs on gold has been the topic of many studies, an understanding of how the applied potential affects the SAM structure and insulating properties has not been clearly described. The work presented in this thesis thus focuses on the characterization of the electrical and electrochemical properties of alkylthiol/Au SAMs as a function of the applied d.c. potential. The objectives of this research have been to understand *i*) the transport of *ions* at a SAM/electrolyte interface, *ii*) the kinetics of *electron* transfer across SAMs, and *iii*) the effect of the terminal dipole orientation at the SAM/air interface on the surface potential of the monolayer.

This thesis consists of seven chapters including the present introduction:

Chapter Two is a description of SAMs as insulating materials. Emphasis is placed on how to differentiate between defect-free and defect-laden SAMs using the electrical properties obtained by a.c. impedance spectroscopy.

Chapter Three investigates the dielectric properties of *n*-alkylthiol SAMs as a function of the applied d.c. potential. Ion penetration across SAMs at potential-induced defects is principally revealed using the phase angle in a.c. impedance measurements. The effect of the chainlength on the ionic permeability of $CH_3(CH_2)_nS$/Au SAMs is studied.

In Chapter Four, the ionic SAM permeability is modulated through the chemical nature of the chain end group *X* in $X(CH_2)_{15}S$/Au SAMs (*X* = CH_3, OH, CO_2H and CF_3).

Chapter Five investigates the kinetics of electron transfer at a $CH_3(CH_2)_{15}S$/Au SAM using three different redox couples, *i.e.* $Ru(NH_3)_6^{3+/2+}$, $Fe(CN)_6^{3-/4-}$, and $Co(bpy)_3^{3+/2+}$. The kinetics are observed over a broad range of d.c. potentials, typically ± 150 mV with respect to the reversible half-wave potential of

the probe. The results are analyzed in terms of the variation of the Warburg coefficient as a function of the d.c. potential.

In Chapter Six, the effects of chainlength and end group orientation on the surface potential of $CH_3(CH_2)_nS$/Au SAMs (n = 3 – 19) are investigated using the Kelvin probe technique. Attention is paid to the effect of odd/even alkyl chainlength on the measured surface potential.

Chapter Seven is an overview of the conclusions which can be drawn from the work presented in this thesis. The significant contributions made to original knowledge are noted and suggestions for future work are proposed.

The Appendix contains some of the general principles of a.c. impedance spectroscopy.

References

1) Langmuir, I. *J. Am. Chem. Soc.* **1917**, *39*, 1848-1906.
2) Blodgett, K. B. *J. Am. Chem. Soc.* **1935**, *57*, 1007-1022.
3) Dubois, L. H.; Nuzzo, R. G. *Annu. Rev. Phys. Chem.* **1992**, *43*, 437-463.
4) Ulman, A. *An Introduction to Ultrathin Organic Films from Langmuir - Blodgett to Self-Assembly*; Academic Press: San Diego, 1991.
5) Whitesides, G. M.; Laibinis, P. E. *Langmuir* **1990**, *6*, 87-96.
6) Bain, C. D.; Whitesides, G. M. *Angew. Chem. Int. Ed. Engl.* **1989**, *28*, 506-512.
7) Nuzzo, R. G.; Fusco, F. A.; Allara, D. L. *J. Am. Chem. Soc.* **1987**, *109*, 2358-2368.

8) Porter, M. D.; Bright, T. B.; Allara, D. L.; Chidsey, C. E. D. *J. Am. Chem. Soc.* **1987**, *109*, 3559-3568.

9) Allara, D. L.; Nuzzo, R. G. *Langmuir* **1985**, *1*, 45-52.

10) Allara, D. L.; Nuzzo, R. G. *Langmuir* **1985**, *1*, 52-66.

11) Chidsey, C. E. D.; Bertozzi, C. R.; Putvinski, T. M.; Mujsce, A. M. *J. Am. Chem. Soc.* **1990**, *112*, 4301-4306.

12) Sagiv, J. *J. Am. Chem. Soc.* **1980**, *102*, 92-98.

13) Silberzan, P.; Leger, L.; Ausserre, D.; Benattar, J. *Langmuir* **1991**, *7*, 1647-1651.

14) Wasserman, S. R.; Tao, Y.-T.; Whitesides, G. M. *Langmuir* **1989**, *5*, 1074-1087.

15) Le Grange, J. D.; Markham, J. L.; Kurjian, C. R. *Langmuir* **1993**, *9*, 1749-1753.

16) Maoz, R.; Sagiv, J. *J. Colloid Interface Sci.* **1984**, *100*, 465-496.

17) Gun, J.; Sagiv, J. *J. Colloid Interface Sci.* **1986**, *112*, 457-472.

18) Ogawa, H.; Chihara, T.; Taya, K. *J. Am. Chem. Soc.* **1985**, *107*, 1365-1369.

19) Bigelow, W. C.; Pickett, D. L.; Zisman, W. A. *J. Colloid Interface Sci.* **1946**, *1*, 513-538.

20) Nuzzo, R. G.; Allara, D. L. *J. Am. Chem. Soc.* **1983**, *105*, 4481-4483.

21) Bain, C. D.; Whitesides, G. M. *Science* **1988**, *240*, 62-63.

22) Bain, C. D.; Whitesides, G. M. *J. Am. Chem. Soc.* **1988**, *110*, 3665-3666.

23) Whitesides, G. M.; Gorman, C. B. *Handbook of Surface Imaging and Visualization*; CRC Press:, 1995.

24) Kumar, A.; Biebuyck, H. A.; Abott, N. L.; Whitesides, G. M. *J. Am. Chem. Soc.* **1992**, *114*, 9188-9189.

25) Lee, T. R.; Cary, R. L.; Biebuyck, H. A.; Whitesides, G. M. *Langmuir* **1994**, *10*, 741-749.

26) Creager, S. E.; Clarke, J. *Langmuir* **1994**, *10*, 3675-3683.

27) Lopez, G. P.; Albers, M. W.; Schreiber, S. L.; Carroll, R.; Peralta, E.; Whitesides, G. M. *J. Am. Chem. Soc.* **1993**, *115*, 5877-5878.

28) Singhvi, R.; Kumar, A.; Lopez, G. P.; Stephanopoulos, G. N.; Wang, D. I. C.; Whitesides, G. M.; Ingber, D. E. *Science* **1994**, *264*, 696-698.

29) Delamarche, E.; Sundarabadu, G.; Biebuyck, H. A.; Michel, B.; Gerber, C.; Sigrist, H.; Wolf, H.; Ringsdorf, H.; Xanthopoulos, N.; Mathieu, H. J. *Langmuir* **1996**, *12*, 1997-2006.

30) Bain, C. D.; Troughton, E. B.; Tao, Y. T.; Evall, J.; Whitesides, G. M.; Nuzzo, R. G. *J. Am. Chem. Soc.* **1989**, *111*, 321-335.

31) Bain, C. D.; Withesides, G. M. *J. Am. Chem. Soc.* **1988**, *110*, 5897-5898.

32) Stora, T.; Lakey, J. H.; Vogel, H. *Angew. Chem., Int. Ed. Engl.* **1999**, *38*, 389-392.

33) Steinem, C.; Janshoff, A.; von dem Bruch, K.; Reihs, K.; Goossens, J.; Galla, H.-J. *Bioelectrochem. Bioenerg.* **1998**, *45*, 17-26.

34) Duschl, C.; Liley, M.; Corradin, G.; Vogel, H. *Biophys. J.* **1994**, *67*, 1229-1237.

35) Lang, H.; Duschl, C.; Gratzel, M.; Vogel, H. *Thin Solid Films* **1992**, *210/211*, 818-821.

36) Duschl, C.; Liley, M.; Lang, H.; Ghandi, A.; Zakeeruddin, S. M.; Stahlberg, H.; Dubochet, J.; Nemetz, A.; Knoll, W.; Vogel, H. *Mater. Sci. Eng. C* **1996**, *4*, 7-18.

37) Heyse, S.; Stora, T.; Schmid, E.; lakey, J. H.; Vogel, H. *Biochim. Biophys. Acta* **1998**, *85507*, 319-338.

38) Lang, H.; Duschl, C.; Vogel, H. *Langmuir* **1994**, *10*, 197-210.

39) Stora, T.; Hovius, R.; Dienes, Z.; Pachoud, M.; Vogel, H. *Langmuir* **1997**, *13*, 5211-5214.

40) Flink, S.; Boukamp, B. A.; van den Berg, A.; van Veggel, F. C. J. M.; Reinhoudt, D. N. *J. Am. Chem. Soc.* **1998**, *120*, 4652-4657.

41) Hubbard, A. T.; Strickney, J. L.; Soriaga, M. P.; Chia, V. K. F.; Rosasco, S. D.; Schardt, B. C.; Solumun, T.; Sond, D.; White, J. H.; Wieckowski, A. *J. Electroanal. Chem.* **1984**, *168*, 43-66.

42) Finklea, H. O. *Electrochemistry of Organized Monolayers of Thiols and Related Molecules on Electrodes*; Marcel Dekker: New York, 1996; Vol. 19; Chapter 2.

43) Troughton, E. B.; Bain, C. D.; Whitesides, G. M.; Nuzzo, R. G.; Allara, D. L.; Porter, M. D. *Langmuir* **1988**, *4*, 365-385.

44) Hamelin, A. *J. Electroanal. Chem.* **1985**, *195*, 175-176.

45) Finklea, H. O.; Hanshew, D. D. *J. Electroanal. Chem.* **1993**, *347*, 327-340.

46) Whitesides, G. M.; Laibinis, P. E. *Langmuir* **1990**, *6*, 87-96.

47) Biebuyck, H. A.; Bain, C. D.; Whitesides, G. M. *Langmuir* **1994**, *10*, 1825-1831.

48) Thomas, R. C.; Sun, L.; Crooks, R. M.; Ricco, A. J. *Langmuir* **1991**, *7*, 620-622.

49) Weisshaar, D. E.; Lamp, B. D.; Porter, M. D. *J. Am. Chem. Soc.* **1992**, *114*, 5860-5862.

50) Ron, H.; Rubinstein, I. *J. Am. Chem. Soc.* **1998**, *120*, 13444-13452.

51) Folkers, J. P.; Laibinis, P. E.; Whitesides, G. M. *Langmuir* **1992**, *8*, 1330-1341.

52) Ulman, A. *Chem. Rev.* **1996**, *96*, 1533-1554.

53) Schlenoff, J. B.; Li, M.; Ly, H. *J. Am. Chem. Soc.* **1995**, *117*, 12528-12536.

54) Nuzzo, R. G.; Zegarski, B. R.; Dubois, L. H. *J. Am. Chem. Soc.* **1987**, *109*, 733-740.

55) Nuzzo, R. G.; Dubois, L.; Allara, D. L. *J. Am. Chem. Soc.* **1990**, *112*, 558-569.

56) Sobocinski, R. L.; Bryant, M. A.; Pemberton, J. E. *J. Am. Chem. Soc.* **1990**, *112*, 6177-6183.

57) Bryant, M. A.; Pemberton, J. E. *J. Am. Chem. Soc.* **1991**, *113*, 8284-8293.

58) Bryant, M. A.; Pemberton, J. E. *J. Am . Chem. Soc.* **1991**, *113*, 3629-3637.

59) Laibinis, P. E.; Whitesides, G. M.; Allara, D. L.; Y.-T., T.; Parikh, A. N.; Nuzzo, R. G. *J. Am. Chem. Soc.* **1991**, *113*, 7152-7167.

60) Bain, C. D.; Biebuyck, H. A.; Whitesides, G. M. *Langmuir* **1989**, *5*, 723-727.

61) Camillone III, N.; Chidsey, C. E. D.; Liu, G. Y.; Scoles, G. *J. Chem. Phys.* **1993**, *98*, 4234-4245.

62) Walczak, M. M.; Chung, C.; Stole, S. M.; Widrig, C. A.; Porter, M. D. *J. Am. Chem. Soc.* **1991**, *113*, 2370-2378.

63) Evans, S. D.; Urankar, E.; Ulman, A.; Ferris, N. *J. Am. Chem. Soc.* **1991**, *113*, 4121-4131.

64) Fenter, P.; Eisenberger, P.; Li, J.; Camillone III, N.; Bernasek, S.; Scoles, G.; Ramanarayanan, T. A.; Liang, K. S. *Langmuir* **1991**, *7*, 2013-2016.

65) Camillone III, N.; Eisenberger, P.; Leung, T. Y. B.; Schwartz, P.; Scoles, G.; Poirier, G. E.; Tarlov, M. J. *J. Chem. Phys.* **1994**, *101*, 11031-11036.

66) Chidsey, C. E. D.; Liu, G. Y.; Scoles, G.; Wang, J. *Langmuir* **1990**, *6*, 1804-1806.

67) Fenter, P.; Eberthardt, A.; Eisenberger, P. *Science* **1994**, *266*, 1216-1218.

68) Samant, M. G.; Brown, C. A.; Gordon II, J. G. *Langmuir* **1993**, *9*, 1082-1085.

69) Strong, L.; Whitesides, G. M. *Langmuir* **1988**, *4*, 546-558.

70) Sun, L.; Crooks, R. M. *Langmuir* **1993**, *9*, 1951-1954.

71) Creager, S. E.; Hockett, L. A.; Rowe, G. K. *Langmuir* **1992**, *8*, 854-861.

72) Kim, Y. T.; Bard, A. J. *Langmuir* **1992**, *8*, 1096-1102.

73) Delamarche, E.; Michel, B.; Gerber, C.; Anselmetti, D.; Guntherodt, H.-J.; Wolf, H.; Ringsdorf, H. *Langmuir* **1994**, *10*, 2869-2871.

74) Delamarche, E.; Michel, B.; Kang, H.; Gerber, C. *Langmuir* **1994**, *10*, 4103-4108.

75) Schonenberger, C.; Sondag-Huethorst, J. A. M.; Jorritsma, J.; Fokkink, L. G. J. *Langmuir* **1994**, *10*, 611-614.

76) Stranick, S. J.; Kamma, M. M.; Krom, K. R.; Parick, A. N.; Allara, D. L.; Weiss, P. S. *J. Vac. Sci. Technol. B.* **1994**, *12*, 20004-20007.

77) Stranick, S. J.; Parikh, A. N.; Tao, Y. T.; Allara, D. L.; Weiss, P. S. *J. Phys. Chem.* **1994**, *98*, 7636-7646.

78) Bucher, J. P.; Santesson, L.; Kern, K. *Langmuir* **1994**, *10*, 979-983.

79) Gregory, B. W.; Dluhy, R. A.; Bottomley, L. A. *J. Phys. Chem.* **1994**, *98*, 1010-1021.

80) Sondag-Huethorst, J. A. M.; Schonenberger, C.; Fokkink, L. G. L. *J. Phys. Chem.* **1994**, *98*, 6826-6834.

81) Wolf, H.; Ringsdorf, H.; Delamarche, E.; Takami, T.; Kang, H.; Michel, B.; Gerber, C.; Jaschke, M.; Butt, H.-J.; Bamberg, E. *J. Phys. Chem.* **1995**, *99*, 7102-7107.

82) Allara, D. L.; Atre, S. V.; Elliger, C. A.; Snyder, R. G. *J. Am. Chem. Soc.* **1991**, *113*, 1852-1854.

83) Chidsey, C. E. D.; Loiacono, D. N. *Langmuir* **1990**, *6*, 682-691.

84) Hautman, J.; Bareman, J. P.; Mar, V.; Klein, M. L. *J. Chem. Soc. Faraday Trans.* **1991**, *87*, 2031-2037.

85) Mar, W.; Klein, M. L. *Langmuir* **1994**, *10*, 188-196.

86) Hautman, J.; Klein, M. L. *J. Chem. Phys.* **1990**, *93*, 7483-7492.

87) Nuzzo, R. G.; Korenic, E. M.; Dubois, L. H. *J. Chem. Phys.* **1990**, *93*, 767-773.

88) Pemberton, J. E.; Bryant, M. A.; Sobocinski, R. L.; Joa, S. L. *J. Phys. Chem.* **1992**, *96*, 3776-3782.

89) Nemetz, A.; Fischer, T.; Ulman, A.; Knoll, W. *J. Chem. Phys.* **1993**, *98*, 5912-5919.

90) Dubois, L. H.; Zegarski, B. R.; Nuzzo, R. G. *J. Electron Spectrosc. Relat. Phenom.* **1990**, *54/55*, 1143-1152.

91) Stole, S. M.; Porter, M. D. *Langmuir* **1990**, *6*, 1199-1202.

92) Laibinis, P. E.; Nuzzo, R. G.; Whitesides, G. M. *J. Phys. Chem.* **1992**, *96*, 5097-5105.

93) Anderson, M. R.; Gatin, M. *Langmuir* **1994**, *10*, 1638-1641.

94) Ong, T. H.; Ward, R. N.; Davies, P. B.; Bain, C. D. *J. Am. Chem. Soc.*. **1992**, *114*, 6243-6245.

95) Ong, T. H.; Davies, P. B.; Bain, C. D. *Langmuir* **1993**, *9*, 1836-1845.

96) Delamarche, E.; Michel, B.; Biebuyck, H. A.; Gerber, C. *Adv. Mater.* **1996**, *8*, 719-729.

97) Bard, A. J.; Faulkner, L. R. *Electrochemical Methods: Fundamentals and Applications*; John Wiley & Sons: New York, USA, 1980.

98) Widrig, C. A.; Chung, C.; Porter, M. D. *J. Electroanal. Chem.* **1991**, *310*, 335-359.

99) Miller, C.; Cuendet, P.; Grätzel, M. *J. Phys. Chem.* **1991**, *95*, 877-886.

100) Finklea, H. O.; Avery, S.; Lynch, M.; Furtsch, T. *Langmuir* **1987**, *3*, 409-413.

101) Evans, S. D.; Ulman, A. *Chem. Phys. Lett.* **1990**, *170*, 462-466.

102) Swietlow, A.; Skoog, M.; Johansson, G. *Electroanalysis* **1992**, *4*, 921-928.

103) Sabatini, E.; Rubinstein, I.; Maoz, R.; Sagiv, J. *J. Electroanal. Chem.* **1987**, *219*, 365-371.

104) Sabatini, E.; Rubinstein, I. *J. Phys. Chem.* **1987**, *91*, 6663-6669.

105) Finklea, H. O.; Snider, D. A.; Fedyk, J. *Langmuir* **1990**, *6*, 371-376.

106) Finklea, H. O.; Snider, D. A.; Fedyk, J.; Sabatini, E.; Gafni, Y.; Rubinstein, I. *Langmuir* **1993**, *9*, 3660-3667.

107) Obeng, Y. S.; Laing, M. E.; Freidli, A. C.; Yang, H. C.; Wang, D. N.; Thulstrup, E. W.; Bard, A. J.; Michl, J. *J. Am. Chem. Soc.* **1992**, *114*, 9943-9952.

108) Rodriguez, J. F.; Mebrahtu, T.; Soriaga, M. P. *J. Electroanal. Chem.* **1987**, *233*, 283-289.

109) Rodriguez, J. F.; Soriaga, M. P. *J. Electrochem. Soc.* **1988**, *135*, 616-618.

110) Tadayyoni, M. A.; Gao, P.; Weaver, M. J. *J. Electroanal. Chem.* **1986**, *198*, 125-136.

111) Schultze, J. W.; Dickermann, D. *Surf. Sci.* **1976**, *54*, 489-505.

112) Demoz, A.; Harrison, D. J. *Langmuir* **1993**, *9*, 1046-1050.

113) Slowinski, K.; Chamberlain II, R. V.; Bilewicz, R.; Majda, M. *J. Am. Chem. Soc* **1996**, *118*, 4709-4710.

114) Takehara, K.; Takemura, H.; Ide, Y. *Electrochim. Acta* **1994**, *39*, 817-822.

115) Xu, J.; Li, H.-L.; Zhang, Y. *J. Phys. Chem.* **1993**, *97*, 11497-11500.

116) Becka, A. M.; Miller, C. J. *J. Phys. Chem.* **1993**, *97*, 6233-6239.

117) Becka, A. M.; Miler, C. J. *J. Phys. Chem.* **1992**, *96*, 2657-2668.

118) Miller, C. J.; Grätzel, M. *J. Phys. Chem.* **1991**, *95*, 5225-5233.

119) Doblhofer, J.; Figura, J.; Furhop, J.-H. *Langmuir* **1992**, *8*, 1811-1816.

120) Finklea, H. O.; Ravenscroft, M. S.; Snider, D. A. *Langmuir* **1993**, *9*, 223-227.

121) Finklea, H. O.; Hanshew, D. D. *J. Am. Chem. Soc.* **1992**, *114*, 3173-3181.

122) Chidsey, C. E. D. *Science* **1991**, *251*, 919-922.

123) Collard, D. M.; Fox, M. A. *Langmuir* **1991**, *7*, 1192-1197.

124) Rowe, G. K.; Creager, S. E. *Langmuir* **1991**, *7*, 2307-2312.

125) Hickmann, J. J.; Ofer, D.; Zou, C.; Wrighton, M. S.; Laibinis, P. E.; Whitesides, G. M. *J. Am. Chem. Soc.* **1991**, *113*, 1128-1132.

126) Katz, E.; Itzhak, N.; Willner, I. *Langmuir* **1993**, *9*, 1392-1396.

127) Creager, S. E.; Collard, D. M.; Foxe, M. A. *Langmuir* **1990**, *6*, 1617-1620.

128) Li, T. T.-T.; Weaver, M. J. *J. Am. Chem. Soc.* **1984**, *106*, 6107-6108.

129) Tokuda, K.; Gueshi, T.; Matsuda, H. *J. Electroanal. Chem.* **1979**, *102*, 41-48.

130) Amatore, C.; Savéant, J. M.; Tessier, D. *J. Electroanal. Chem.* **1983**, *147*, 39-51.

131) Badia, A.; Back, R.; Lennox, R. B. *Angew. Chem., Int. Ed. Engl.* **1994**, *33*, 2333-2334.

132) Lipkowski, J. *Modern Aspects of Electrochemistry*; Plenum Press: New York, 1992; Vol. 23.

133) Mann, B.; Kuhn, H. *J. Appl. Phys.* **1971**, *42*, 4398-4405.

134) Collet, J.; Vuillaume, D. *Appl. Phys. Lett.* **1998**, *73*, 2681-2683.

135) Collet, J.; Vuillaume, D.; Bonnier, M.; Bouloussa, O.; Rondelez, F.; Gay, J. M.; Kham, K.; Chevrot, C. *Mat. Res. Soc. Symp. Proc.* **1998**, *488*, 847-852.

136) Collet, J.; Bonnier, M.; Bouloussa, O.; Rondelez, F.; Vuillaume, D. *Microelectron. Eng.* **1997**, *36*, 119-122.

137) Vuillaume, D.; Boulas, C.; Collet, J.; Davidovits, J. V.; Rondelez, F. *Appl. Phys. Lett.* **1996**, *69*, 1646-1648.

138) Boulas, C.; Davidovits, J. V.; Rondelez, F.; Vuillaume, D. *Phys. Rev. Lett.* **1996**, *76*, 4797-4800.

139) Vuillaume, D.; Rondelez, F. *Bull. Soc. Fr. Phys.* **1995**, *102*, 3-6.

140) Vuillaume, D.; Chen, B.; Metzger, R. M. *Langmuir* **1999**, *15*, 4011-4017.

141) Rampi, M. A.; Schueller, O. J. A.; Whitesides, G. M. *Appl. Phys. Lett.* **1998**, *72*, 1781-1783.

142) Tien, H. T. *Bilayer Lipid Membranes (BLM) : Theory and Practice*; Marcel Dekker: New York, 1974.

143) Haag, R.; Rampi, M. A.; Holmlin, R. E.; Whitesides, G. M. *J. Am. Chem. Soc.* **1999**, *121*, 7895-7906.

144) Dhirani, A.-A.; Lin, P. H.; Guyot-Sionnest, P.; Zehner, R. W.; Sita, L. R. *J. Chem. Phys.* **1997**, *106*, 5249-5253.

145) Bumm, L. A.; Arnold, J. J.; Cygan, M. T.; Dunbar, T. D.; Burgin, T. P.; Jones, L. I.; Allara, D. L.; Tour, J. M.; Weiss, P. S. *Science* **1996**, *271*, 1705-1707.

146) Cygan, M. T.; Dunbar, T. D.; Arnold, J. J.; Bumm, L. A.; Shedlock, N. F.; Burgin, T. P.; Jones, L. I.; Allara, D. L.; Tour, J. M.; Weiss, P. S. *J. Am. Chem. Soc.* **1998**, *120*, 2721-2732.

147) Andres, R. P.; Bein, T.; Dorogi, M.; Fenf, S.; Henderson, J. I.; Kubiak, C. P.; Mahoney, W.; Osifchin, R. G.; Reifenberger, R. *Science* **1996**, *272*, 1323-1325.

148) Hickman, J. J.; Ofer, D.; Laibinis, P. E.; Whitesides, G. M.; Wrighton, M. S. *Science* **1991**, *252*, 688-690.

149) Whitesides, G. M.; Mathias, J. P.; Seto, C. T. *Science* **1991**, *254*, 1312-1319.

150) Parikh, A. N.; Allara, D. L. *J. Chem. Phys.* **1992**, *96*, 927-945.

151) Miller, W. J.; Abbott, N. L. *Langmuir* **1997**, *13*, 7106-7114.

152) Gupta, V. K.; Abbott, N. L. *Phys. Rev. E* **1996**, *54*, R4540-R4543.

153) Smith, E. L.; Porter, M. D. *J. Phys. Chem.* **1993**, *97*, 8032-8038.

154) Tao, Y.-T. *J. Am. Chem. Soc.* **1993**, *115*, 4350-4358.

155) Colorado, R., Jr.; Villazana, R. J.; Lee, T. R. *Langmuir* **1998**, *14*, 6337-6340.

156) Wong, S.-S.; Takano, H.; Porter, M. D. *Anal. Chem.* **1998**, *70*, 5209-5212.

Chapter 2

Insulating Properties of SAMs Monitored by Impedance Spectroscopy*

2.1 Introduction

The *ionic* insulating properties of nanometer-scale thick *n*-alkylthiol ($CH_3(CH_2)_nS/Au$, n = 7-15) and related fluorinated self-assembled monolayers (SAMs) chemisorbed on polycrystalline gold are explored here. The dielectric response of these SAMs is probed as a function of the alkyl chainlength, n. A.C. electrochemical impedance spectroscopy (EIS) allows one to test the Helmholtz model (parallel plate capacitor with a dielectric material)[1,2] with SAM-modified electrodes using an appropriate equivalent circuit. If the Helmholtz model is applicable, the SAM will fit an equivalent circuit involving a solution resistance in series with a capacitor. Although many electrochemical studies assume that SAM-modified electrodes do in fact obey the Helmholtz model, there has been no clear evidence presented to date that confirms such an assumption.[3-8] It is important to confirm this because it provides a well-defined diagnostic of the quality of that particular SAM.

The electrical properties of SAMs, as used in electrochemical systems, comprise both *electronic* and *ionic* modes of conduction. Cyclic voltammetry has been used with SAMs to test for electron tunneling, provided a redox center (such as ferrocene) is tethered to the outer part of the SAM.[9-14] Although most of the studies have addressed electronic conduction, ionic conduction may often play a measurable,

* Reproduced with permission form *Langmuir* 2000, *16*, 4222-4228. Copyright 2000, American Chemical Society.

if not major, role in SAM conductivity. Our purpose in this and related studies is to develop the experimental basis for evaluating SAM ionic conductivity.

The *electronic* conductivity across nanometer-scale thick organic monolayers sandwiched between two metal surfaces was first investigated with fatty acids ($CH_3(CH_2)_{n-2}CO_2H$, n = 18-22),[15] and more recently with *n*-alkyltrichlorosilanes ($CH_3(CH_2)_nSiCl_3$, n = 12-18).[16,17] These long alkyl chainlength SAMs immobilized between SiO_2 and Al surfaces (semiconductor/insulator/metal structure) exhibit a very low conductivity, typically 5×10^{-15} Ω^{-1} cm^{-1}. A similar conductivity was reported for Hg-$S(CH_2)_{n\geq 10}CH_3/CH_3(CH_2)_{n\geq 10}S$-Hg structures.[18] Monolayers made of fatty acids, *n*-alkyltrichlorosilanes or *n*-alkylthiols were then shown to be electronic insulators. A contribution from electron tunneling to the measured conductivity, σ, at room temperature was ruled out, as there was no dependence between σ and the SAM thickness.[16-27] The measured conductivities for *n*-alkyltrichlorosilanes and *n*-alkylthiols SAMs were instead attributed to the intrinsic electrical properties the organic monolayers, given that the conductivities are in the same range as that of bulk poly(ethylene) (2×10^{-16} Ω^{-1} cm^{-1}).[28]

These studies of the *electronic* insulating properties of SAMs are important, considering that SAMs could be used as ultra-thin gate insulators in organic field-effect transistors[29] or in molecular electronic devices.[30] SAMs also find applications in biosensors as matrices for the insertion of guest molecules, and more importantly as insulating layers.[31-33] However, the fact that alkylthiol and related SAMs are electronic insulators does not necessarily mean that these SAMs are also *ionic* insulators. As per a recent publication,[34] the presence of ions in the electrolyte considerably lowers the electrical breakdown voltage values of a Hg-$S(CH_2)_{15}CH_3/CH_3(CH_2)_{15}S$-Ag structure, from 3.2 ± 0.5 V in the absence of electrolyte to 1.1 ± 0.3 V in the presence of aqueous 1 mM $LiClO_4$.

We describe the *ionic* insulating properties of *n*-alkylthiol ($CH_3(CH_2)_nS$/Au) SAMs and a fluorinated SAM measured by a.c. EIS in a non-electroactive electrolyte. The effect of chainlength (n = 7-15) of the constituent *n*-alkylthiol on the SAM impedance (Z), capacitance (C), and phase angle (φ) is studied in order to assess

whether SAMs can indeed be viewed as ideal capacitors as per the Helmholtz model.[2] The a.c. EIS work presented here differs from that previous reported because it involves the characterization of SAMs *in the absence* of redox active species.[35-38]

2.2 Experimental Section

Chemicals. Octanethiol (98.5 %), decanethiol (97 %) and dodecanethiol (98 %) were obtained from Aldrich (Milwaukee, USA) and were used as received. Hexadecanethiol was available from previous studies and was synthesized from 1-bromohexadecane (97 %, Aldrich) by standard procedures.[39]

$HS(CH_2)_{15}CH_3$: M.p. 19.5-21 °C; TLC (silica gel, *n*-hexane): R_f = 0.7; ^1H NMR (500 MHz, $CDCl_3$, 25°C): δ 2.52 (q, 2H, CH_2SH), 1.58 (m, 2H CH_2CH_2SH), 1.40 (m, 2H, $CH_2CH_2CH_2SH$), 1.31 (t, 1H, CH_2SH), 1.24 (s, 24H, $(CH_2)_{12}$), 0.87 (t, 3H, CH_3).

Fluorinated ($HS(CH_2)_2(CF_2)_7CF_3$) thiol was obtained from Ciba (Chem Division, Ardsley, New York). The abbreviation CF_3C_9S/Au SAM for monolayers made of $HS(CH_2)_2(CF_2)_7CF_3$ is used for convenience, where the C_9 designation includes 2 CH_2 groups and 7 CF_2 groups.

Potassium hexaferricyanide, potassium hexaferrocyanide and dibasic potassium phosphate were ACS reagent grade (BDH, Montreal, Canada).

Instrumentation. Impedance of SAMs adsorbed onto polycrystalline gold was measured using a conventional 3-electrode electrochemical cell with an EG&G lock-in amplifier (5210) combined to an EG&G PAR 273 potentiostat. Data acquisition was performed using EG&G M398 software. Impedance was measured at 0 V *vs.* Ag/AgCl and was superimposed to a sinusoidal potential modulation of ± 10 mV. The amplitude and phase shift of the resulting current were recorded over a frequency domain spanning five decades (1 Hz to 65 kHz). Fifteen points, equally spaced on a logarithmic scale, were acquired per decade increment in *f*.

All experiments were performed at room temperature. Solutions were purged with nitrogen for 30 minutes prior to measurement. Impedance spectra were transferred to the Zplot/Zview software package (Scribner Associates Inc., NC) and

were fitted to an appropriate electrical equivalent circuit using the Complex Nonlinear Least Squares (CNLS) Immittance Fitting Program.[40] This fitting procedure defines the best set of parameters that minimizes the sum S_m:

$$S_m = \sum \left[w_j' (X_e' - X_{th}')_j^2 + w_j'' (X_e'' - X_{th}'')_j^2 \right] \quad (1)$$

The sum is taken over 1 to m, where m is the total number of data points. X' is the real part of the immittance of the j^{th} point, and X'' is its corresponding imaginary part. Subscripts *"e"* and *"th"* denote the experimental values and the calculated values from the model function. w_j' and w_j'' are the weighting factors associated with the real and imaginary parts of the j^{th} point. The fitting procedure is based on established literature precedent.[40,41]

Cyclic voltammetry experiments were performed with a BAS 100W potentiostat (Bioanalytical Systems Inc, IN) using a Pt counter electrode and a Ag/AgCl reference (3 M NaCl) electrode.

Procedure. Polycrystalline gold electrodes (0.020 cm^2 geometric surface area, Bioanalytical Systems Inc., IN) were hand-polished on microcloth pads (Buehler) with alumina slurries of decreasing particle size (1.0 μm, 0.3 μm and 0.05 μm) and sonicated in ultra pure water in an ultrasonic bath (Branson 1200). The gold surface was then cleaned with freshly prepared *aqua regia* solution (60:30:10 water:HCl:HNO_3). The electrodes were then electrochemically polished in N_2-purged 1 M perchloric acid (HPLC grade, BDH) solution from 0 to + 1.7 V *vs.* Ag/AgCl at a scan rate of 80 mV s^{-1}. Cyclic voltammograms were stable after the second cycle. Electrodes were then rinsed with a copious amount of ultra pure water (18 MΩ cm, Milli-Q Systems) and absolute ethanol (Commercial Alcohols Inc., ON) prior to incubation in N_2-purged 1 mM fresh $CH_3(CH_2)_nSH$ solution in a sealed vial, at room temperature, for 3 to 4 days. The current densities, capacitance and resistance values are reported in terms of the geometric surface area.

In all impedance spectra presented here, symbols represent the experimental raw data and the solid lines are the fitting curves obtained from CNLS data fits. Three different types of impedance plots (φ *vs.* f, $|Z|$ *vs.* f and Z'' *vs.* Z') were used to

visualize the raw data and evaluate the quality of data fitting over the entire frequency domain probed.

2.3 Results and Discussion

The electrochemical polishing of polycrystalline gold electrodes (Figure 2.1) yields electrodes that exhibit highly reproducible cyclic voltammograms. As per literature, gold oxide formation is observed at + 1.1 V to + 1.5 V (*vs.* Ag/AgCl), followed by oxide stripping (+ 0.9 V) on the reverse scan.[4,5,42] The impedance spectra at an applied potential of 0 V (*vs.* Ag/AgCl) in K_2HPO_4 (2 mM to 250 mM, pH 7.7-8.7) can be adequately fitted to an equivalent circuit involving a solution resistance R_s in series with a constant phase element, *CPE* (Figure 2.2). The *CPE* ($Z_{CPE} = A(j\omega)^{-\alpha}$) is a power law-dependent interfacial capacity and accounts for the topological imperfections of the gold surface caused by the different crystal facets and the surface roughness of the electrode. If $\alpha = 1$, the CPE is an ideal capacitor.[41] A small deviation ($\alpha > 0.88$) from 1.0, as observed here, suggests that the gold substrates are adequately smooth for these studies (Table 2.1). The surface roughness as estimated from Cu UPD (under potential deposition) is 1.03 to 1.1. The double layer capacitance of a gold electrode cleaned in this fashion is ~ 16 $\mu F\ cm^{-2}$, in agreement with potential step experiments for polycrystalline gold in 10 mM phosphate buffer.[43] The experimental impedance spectrum and the corresponding CNLS fit of a freshly prepared gold electrode are shown in Figure 2.3. The CNLS data fit (solid line) corresponds to the situation where $\alpha = 0.920$ ($C_{dl} = 16.4 \pm 0.16\ \mu F\ cm^{-2}$ and $R_s = 7.0 \pm 0.04\ \Omega\ cm^2$), while the dashed line is a simulation using $\alpha = 1$ and maintaining R_s and C_{dl} constant.

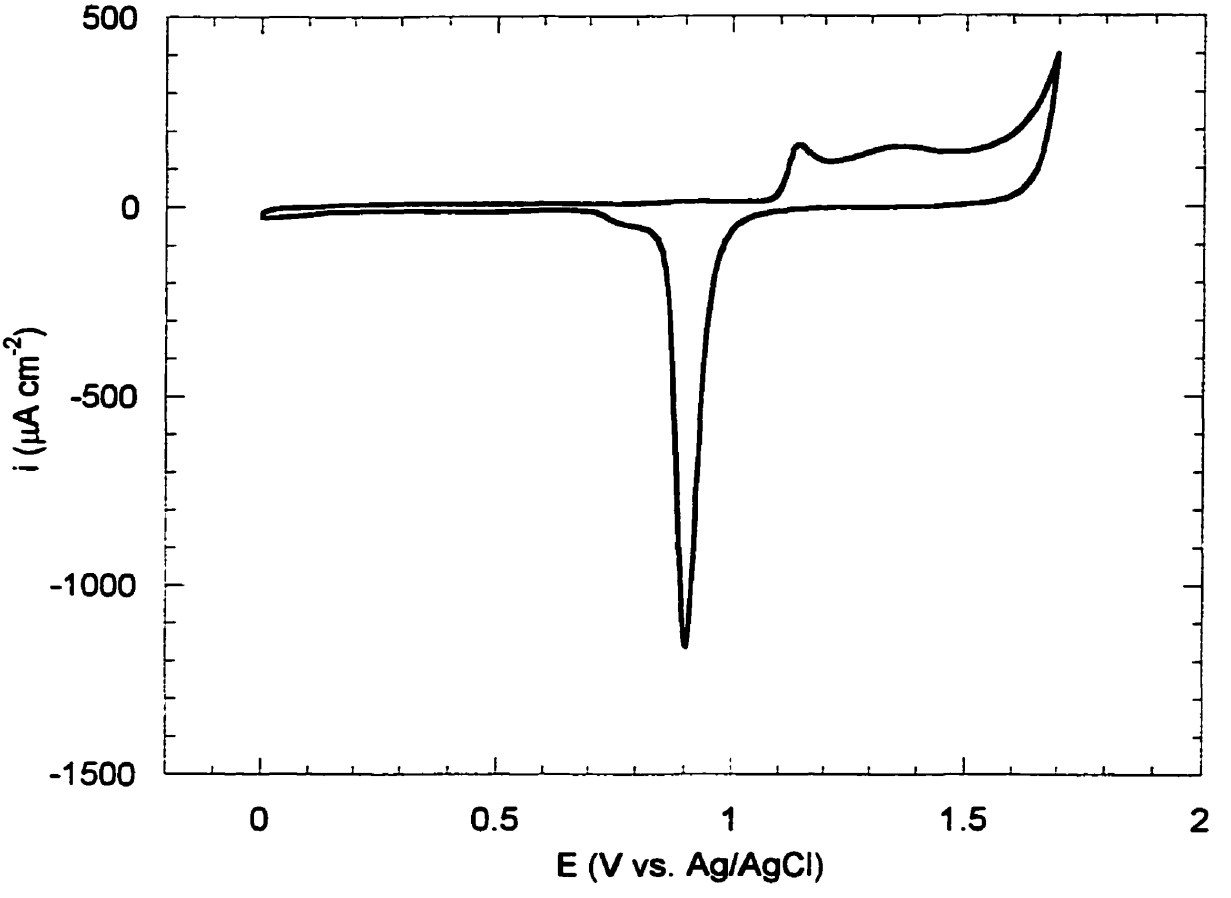

Figure 2.1. Typical cyclic voltammogram (5th sweep) of a polycrystalline bare gold electrode in 1 M $HClO_4$ at 80 mV s^{-1}, from 0 V to + 1.7 V (*vs.* Ag/AgCl).

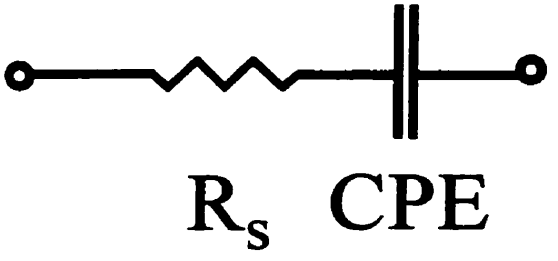

Figure 2.2. Equivalent circuit used for CNLS data fits of bare gold electrodes, $CH_3(CH_2)_nS/Au$ (n = 7-15) SAMs, and a CF_3C_9S/Au SAM at 0 V (*vs.* Ag/AgCl) when $\varphi_{1Hz} \geq 88°$. R_s is the solution resistance, and the constant phase element (*CPE*) accounts for either the Au double layer capacitance or the SAM capacitance. .

$[K_2HPO_4]$ mM	R_s Ω cm^2	C_{dl} μF cm^{-2}	α
Bare polycrystalline gold			
2	184 ± 4	20.6 ± 0.16	0.886 ± 0.002
10	27 ± 0.12	15.6 ± 0.15	0.926 ± 0.002
20	15 ± 0.08	17.8 ± 0.15	0.913 ± 0.001
30	10 ± 0.06	17.5 ± 0.15	0.916 ± 0.001
40	8.1 ± 0.06	17.0 ± 0.16	0.917 ± 0.002
50	7.0 ± 0.04	16.4 ± 0.16	0.920 ± 0.002
100	4.0 ± 0.04	17.5 ± 0.20	0.916 ± 0.002
150	3.0 ± 0.06	17.2 ± 0.28	0.919 ± 0.002
200	2.5 ± 0.04	17.2 ± 0.27	0.920 ± 0.002
250	2.2 ± 0.02	16.6 ± 0.24	0.925 ± 0.002

Table 2.1. CNLS fitting parameters for a bare polycrystalline gold electrode immersed in K_2HPO_4 at 0 V *vs.* Ag/AgCl. Electrolyte concentration is varied from 2 mM to 250 mM. The equivalent circuit used is shown in Figure 2.2.

Theoretically, $CH_3(CH_2)_nS$/Au SAMs and fluorinated CF_3C_9S/Au SAMs obey the Helmholtz ideal capacitor model when the phase angle at 1 Hz (φ_{1Hz}) is 90°. A φ = 90° over the measured frequency domain (1 Hz to 65 kHz) means that current leakage does not occur at defect sites and that one has an ideal dielectric material.[41] 1 Hz is chosen as a suitable evaluation frequency, given that diffusion-related phenomena occur in this time domain.[44] In practical terms, a SAM whose $\varphi \geq 88°$ in the low-to-medium frequency range (1 Hz $< f <$ 10^3 Hz) is viewed as a pure capacitor. At high frequency (10 kHz $< f <$ 65 kHz), the total impedance is dominated by the solution resistance. A SAM that behaves as an ideal capacitor has the gold metal surface acting as one capacitor plate and the physisorbed ions at the SAM/electrolyte interface acting as the other capacitor plate. The intervening dielectric material is made of the polymethylene chains. A SAM that exhibits $\varphi_{1Hz} < \sim 87°$ behaves like a capacitor contaminated by a resistive component associated with current leakage at defect sites.

The formation of SAMs can be followed by monitoring the change in the phase angle and the capacitance after various incubation times of a freshly prepared gold electrode in a thiol solution (1mM in ethanol). The SAM-coated electrode was thoroughly rinsed with ethanol and water both before and after each measurement in electrolyte. The impedance spectra were acquired *ex-situ* and run in 50 mM K_2HPO_4, pH 7.0. As observed in Figure 2.3, the phase angle in the low frequency range increases as the incubation time increases. A minimum of 40 h incubation in the thiol solution is necessary to achieve a $\varphi_{1Hz} \geq 88°$ for n = 11. The change in capacitance (ΔC) between 1 h to 38.5 h is 14 % (1.37 to 1.20 μF cm^{-2}), whereas $\Delta\varphi_{1Hz}$ is 28 % (from 68.9 to 88.5°). This later parameter is more sensitive in revealing the insulating character of a SAM. A $\varphi_{1Hz} \geq 88°$ can be used as a reliable diagnostic to assess the ionic insulating character of a SAM.

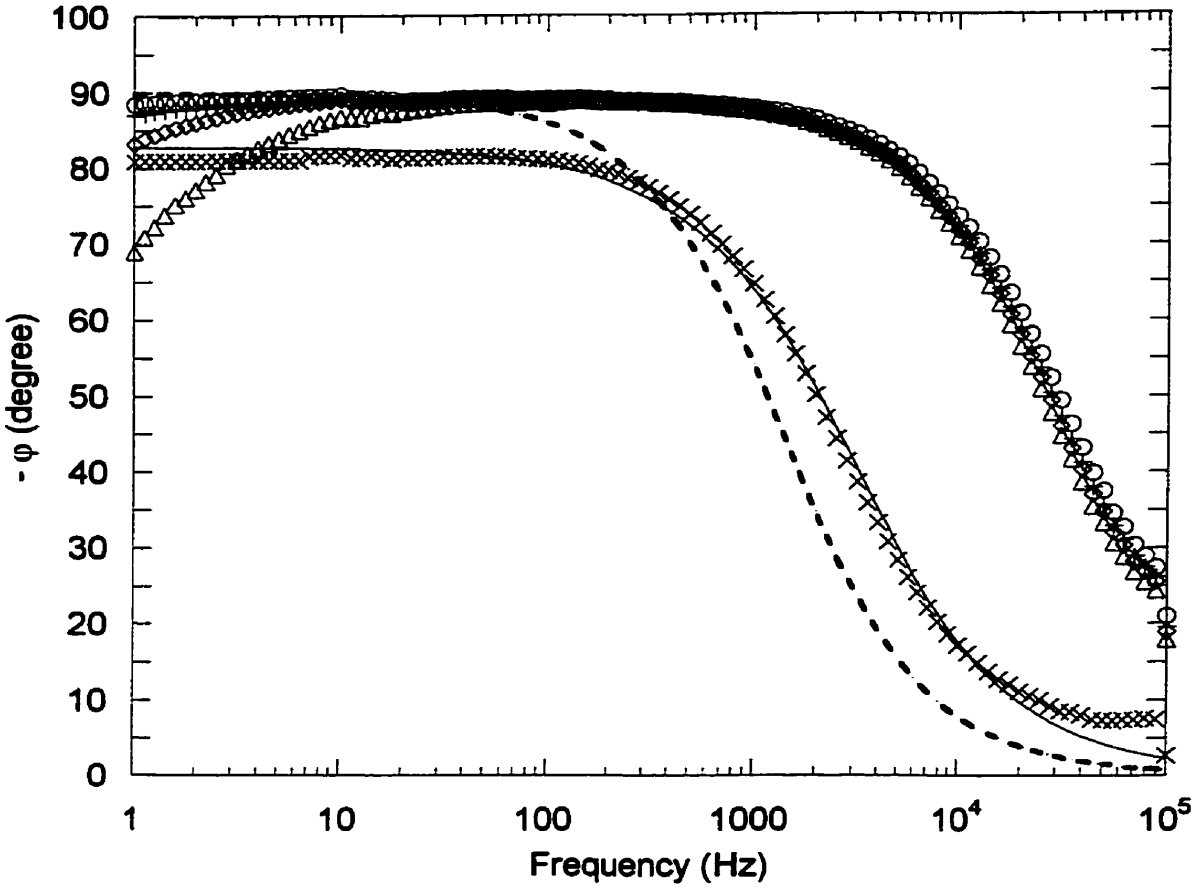

Figure 2.3. Impedance spectra of a $CH_3(CH_2)_{11}S$/Au SAM acquired after various incubation times in the thiol solution. The spectra were run *ex-situ* at 0 V (*vs.* Ag/AgCl) in 50 mM K_2HPO_4, pH 7.0. Each spectrum represents an incubation time: 1 h (Δ), 15.5 h (◊), 22.5 h (+), and 38.5 h (o). When φ_{1Hz} is ≥ 88°, the SAM is considered to be effectively defect-free (see text). The bare gold in 50 mM K_2HPO_4, pH 7.0 at 0 V (*vs.* Ag/AgCl) is given as (×). The solid line is the CNLS data fit using the equivalent circuit in Figure 2.2 ($R_s = 7 \pm 0.06\ \Omega\ cm^2$, $C_{dl} = 16 \pm 0.2\ \mu F\ cm^{-2}$, $\alpha = 0.920 \pm 0.002$). The dashed line is obtained from a simulation using $\alpha = 1.0$, while keeping R_s and C_{dl} constant.

The timescales for SAM formation (typically 24 h to 72 h) are in the range of those previously reported using other *ex-situ* techniques (contact-angle and ellipsometry)[45] and *in-situ* methods such as SHG,[46,47] QCM,[48] and SPR.[49] Bard and coworkers have shown by scanning electrochemical microscopy (SECM) that while 90 % surface coverage for n = 15 is reached very rapidly (< 5 min.), a slow defect healing process (> hours) follows, leading to a more compact film. Only if this follow-on incubation process is used can one hope to achieve a defect-free SAM.[50]

To put these SAM preparations into the more common context of electron transfer kinetics, a $CH_3(CH_2)_{15}S$/Au SAM as prepared here clearly attenuates the electron transfer process with comparison to the response of a film-free, freshly cleaned electrode, as per previous reports (Figure 2.4).[3,4,7,35,50-52] Also, the cyclic voltammograms, obtained in the absence of the redox active species, of a bare gold electrode (dashed line) and a SAM-coated electrode (solid line) are presented. The charging current measured on a defect-free SAM-coated electrode is greatly attenuated and is independent of the applied potential, as per literature reports.[6] The interfacial capacity of a $CH_3(CH_2)_{15}S$/Au SAM determined from the cyclic voltammogram is *ca.* 1.2 $\mu F\ cm^{-2}$, using the current value and the experimental scan rate.

2.3.1 Effect of the Alkyl Chainlength on SAM Interfacial Properties

$CH_3(CH_2)_nS$/Au (n = 7-15) and CF_3C_9S/Au SAMs exhibit a φ_{1Hz} of ≥ 88° (Figure 2.5a). At 0 V (*vs.* Ag/AgCl), these SAMs are *ionic* insulators and they are well described by the Helmholtz ideal capacitor model. This observation is also valid for potentials between + 0.4 V and – 0.2 V. A detailed potential dependence study (from + 0.4 V to – 0.5 V *vs.* Ag/AgCl) of the electrochemical properties of alkylthiol SAMs (n = 7-15) is described elsewhere.[53]

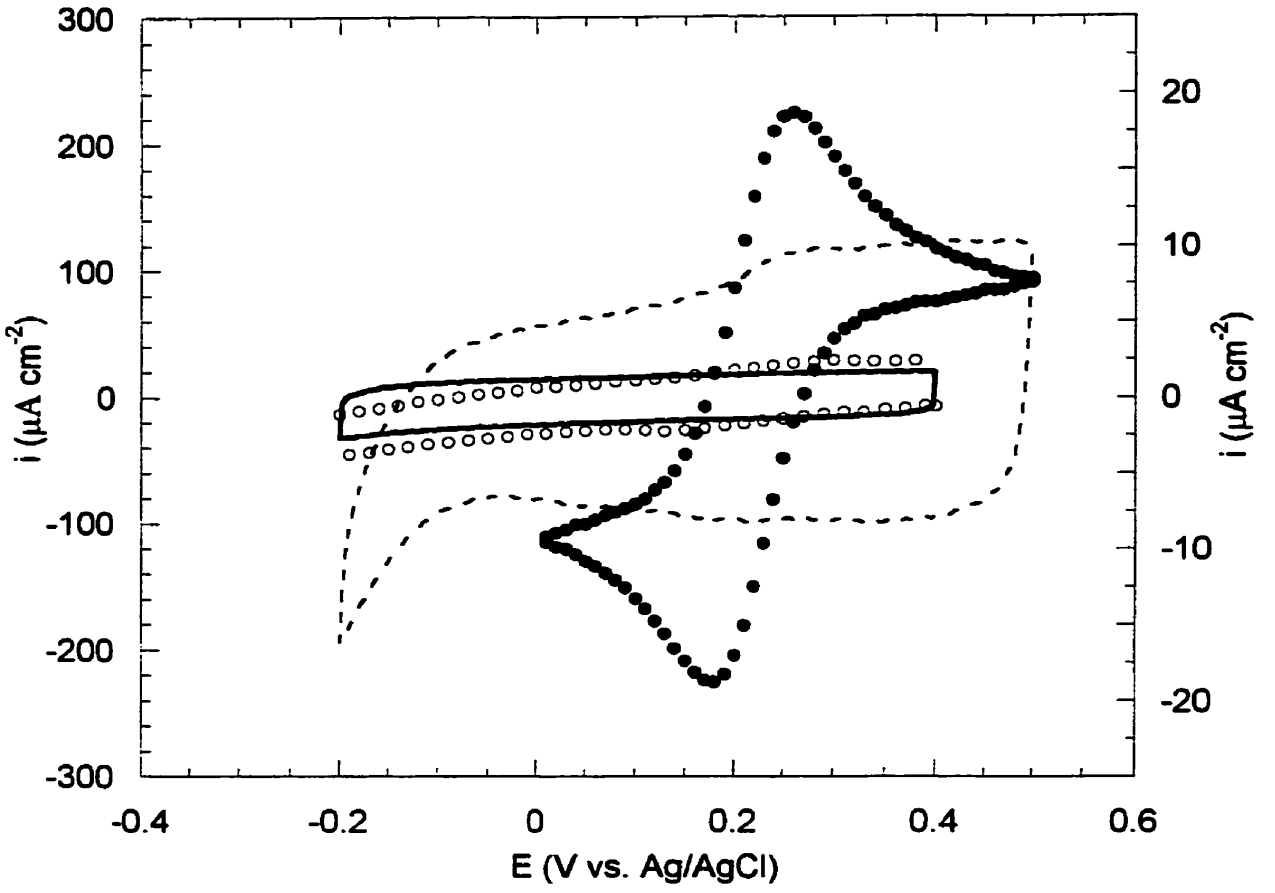

Figure 2.4. Cyclic voltammograms of a freshly prepared bare Au electrode (left *y*-axis) in 50 mM K_2HPO_4 only (dashed line, 1 V s^{-1}) and in 5 mM $Fe(CN)_6^{3-/4-}$ (equimolar concentration) in 50 mM K_2HPO_4 (•, 0.05 V s^{-1}); of a $CH_3(CH_2)_{15}S$/Au SAM (right *y*-axis) in 50 mM K_2HPO_4 only (solid line, 1 V s^{-1}) and in 5 mM $Fe(CN)_6^{3-/4-}$ (equimolar concentration) in 50 mM K_2HPO_4 (o, 1 V s^{-1}).

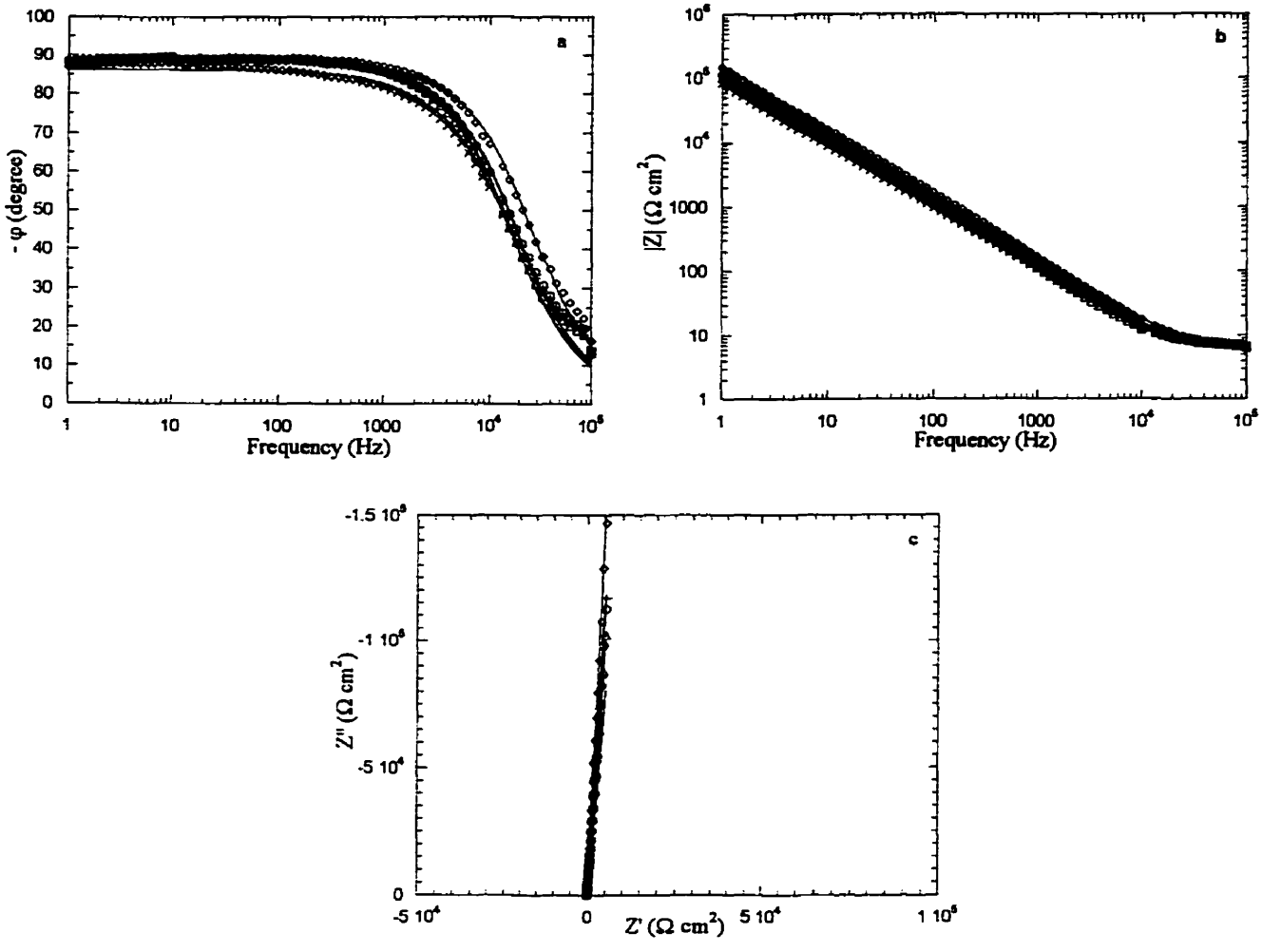

Figure 2.5. *a)* Bode phase plot, *b)* Bode plot, and *c)* Nyquist plot for $CH_3(CH_2)_nS$/Au SAMs, $n = 7$ (Δ), $n = 9$ (+), $n = 11$ (O), $n = 15$ (◊), and for the CF_3C_9S/Au SAM (×). Impedance spectra were acquired at 0 V *vs.* Ag/AgCl in 50 mM K_2HPO_4, pH 7.0. Symbols are the experimental data and solid lines result from CNLS data fits using the equivalent circuit in Figure 2.2. Fitting parameters are listed in Table 2.2.

Little variation in $|Z|$ is observed as the chainlength is increased from $n = 7$ to 15 (Figure 2.5b). At 1 Hz $< f <$ 1 kHz, the slope in Bode plots (log $|Z|$ *vs.* log f) is -1 for each chainlength, typical of a purely capacitive behavior. The high value of $|Z|$ at 1 Hz ($10^5\ \Omega\ cm^2$) reveals the insulating character of these SAMs. By comparison, the impedance at 1 Hz of supported phospholipid bilayer membranes is $10^6\ \Omega\ cm^2$.[54] At high frequencies, $|Z|$ becomes independent of f, the measured impedance being dominated by the solution resistance.

The corresponding Nyquist plots (Z'' *vs.* Z') of $CH_3(CH_2)_nS$/Au (n = 7-15) SAMs and CF_3C_9S/Au SAMs exhibit a nearly vertical line parallel to the y-axis over the entire frequency domain studied (1 Hz to 65 kHz), typical of a pure capacitor (Figure 2.5c). These data imply that ion transport in the SAM is not occurring over the timescale of the experiment and consequently SAMs are ionic insulators under these conditions.

The equivalent circuit that best fits the experimental data for all the SAMs studied here involves a solution resistance (R_s) in series with a constant phase element, *CPE* (Figure 2.2). The capacitance values in 50 mM K_2HPO_4 pH 7.0 thus obtained are $1.68 \pm 0.02\ \mu F\ cm^{-2}$ for $n = 7$, $1.55 \pm 0.01\ \mu F\ cm^{-2}$ for $n = 9$, $1.24 \pm 0.03\ \mu F\ cm^{-2}$ for $n = 11$, and $1.11 \pm 0.01\ \mu F\ cm^{-2}$ for $n = 15$ (Table 2.2). These values are in excellent agreement with those previously reported in the literature for RS/Au SAMs.[44,55-57] SAMs of short chainlength (n = 10) have been previously characterized by a.c. EIS (1 Hz – 100 kHz) in the absence of redox species. A $CH_3(CH_2)_9S$/Au(111) SAM was shown to be impermeable to ions ($C_{dl} = 1.61 \pm 0.09\ \mu F\ cm^{-2}$ in 0.01 M $NaClO_4$) at the potential of zero charge of Au(111) (*i.e.* + 0.27 V *vs.* Ag/AgCl).[44] The capacitance of a Au/SAM interface (1.1 to 2.3 $\mu F\ cm^{-2}$) is approximately one order of magnitude smaller than that of a Au/electrolyte interface ($\sim 16\ \mu F\ cm^{-2}$) (Tables 2.1 and 2.2).

$[K_2HPO_4]$	R_s	CPE	α
mM	Ω cm^2	μF cm^{-2}	
$CH_3(CH_2)_7S$/Au SAM			
2	106 ± 0.8	2.28 ± 0.04	0.987 ± 0.003
10	28 ± 0.4	2.20 ± 0.04	0.989 ± 0.003
20	16 ± 0.2	1.81 ± 0.02	0.985 ± 0.002
30	11 ± 0.1	1.83 ± 0.02	0.984 ± 0.002
40	8 ± 0.1	1.78 ± 0.02	0.986 ± 0.002
50	7 ± 0.08	1.68 ± 0.02	0.985 ± 0.001
$CH_3(CH_2)_9S$/Au SAM			
2	110 ± 0.8	1.66 ± 0.02	0.988 ± 0.002
10	27 ± 0.4	1.67 ± 0.04	0.988 ± 0.001
20	15 ± 0.08	1.60 ± 0.02	0.986 ± 0.001
30	11 ± 0.08	1.59 ± 0.01	0.986 ± 0.001
40	9 ± 0.1	1.59 ± 0.02	0.984 ± 0.001
50	7 ± 0.04	1.55 ± 0.01	0.984 ± 0.001
$CH_3(CH_2)_{11}S$/Au SAM			
2	118 ± 0.4	1.36 ± 0.01	0.985 ± 0.001
10	28 ± 0.4	1.35 ± 0.02	0.983 ± 0.001
20	16 ± 0.1	1.29 ± 0.01	0.988 ± 0.001
30	11 ± 0.1	1.26 ± 0.01	0.989 ± 0.001
40	9 ± 0.08	1.26 ± 0.01	0.988 ± 0.001
50	7 ± 0.2	1.24 ± 0.03	0.989 ± 0.001
$CH_3(CH_2)_{15}S$/Au SAM			
2	105 ± 0.3	1.29 ± 0.01	0.986 ± 0.001
10	28 ± 0.2	1.21 ± 0.01	0.987 ± 0.001
20	15 ± 0.1	1.17 ± 0.01	0.980 ± 0.001
30	10 ± 0.06	1.14 ± 0.01	0.989 ± 0.001
40	8 ± 0.06	1.12 ± 0.01	0.988 ± 0.001
50	7 ± 0.04	1.11 ± 0.01	0.988 ± 0.001
CF_3C_9S/Au SAM			
2	86 ± 0.4	2.14 ± 0.02	0.984 ± 0.001
10	28 ± 0.1	1.93 ± 0.01	0.979 ± 0.001
20	15 ± 0.08	1.84 ± 0.01	0.976 ± 0.001
30	11 ± 0.06	1.83 ± 0.01	0.977 ± 0.001
40	9 ± 0.06	2.03 ± 0.01	0.963 ± 0.001
50	7 ± 0.06	2.19 ± 0.02	0.958 ± 0.001

Table 2.2. CNLS fitting parameters for $CH_3(CH_2)_nS$/Au SAMs (n = 7-15) and the CF_3C_9S/Au SAM as a function of $[K_2HPO_4]$. The equivalent circuit used is shown in Figure 2.2.

2.3.2 Effect of the Electrolyte Concentration on SAM Insulating Properties

The phase angle at $f < 10^3$ Hz for $CH_3(CH_2)_nS$/Au (n = 7 and 15) SAMs remains constant at ≥ 88° as the electrolyte concentration is increased from 2 mM to 50 mM (Figure 2.6). The same trend is observed for n = 9 and 11, and for the CF_3C_9S/Au SAM. The impedance spectra obtained for all of the SAMs studied here can only be fitted using the equivalent circuit described above (Figure 2.2). The fitting parameters are given in Table 2.2. The origin of the small deviations between the fits and the experimental data in the high frequencies (> 3×10^4 Hz) is not known presently. The relationship between φ and the electrolyte concentration further demonstrates that these SAMs are virtually defect-free, given that a change in the electrolyte concentration has no impact on the ionic insulating properties. As expected, there is a linear relationship ($r^2 > 0.999$) between the solution resistance R_s and the electrolyte concentration for bare gold electrodes, $CH_3(CH_2)_nS$/Au (n = 7-15) SAMs and CF_3C_9S/Au SAMs.[44]

The SAM capacitance values are relatively insensitive to the electrolyte concentration for n = 7-15 (Figure 2.7). This, combined with the observation that φ_{1Hz} ≥ 88° (Figure 2.6) is a good indication that SAMs are truly impermeable to K^+, HPO_4^{2-}, and $H_2PO_4^-$ ions. However, for the fluorinated SAM, the capacitance goes through a minimum. As yet unexplained, this change can not however be due to ion permeation into the SAM, since φ_{1Hz} remains constant at 89°.

A linear relationship between C^{-1} and the total number of carbon atoms n in the chain is found, as predicted by the Helmholtz theory model ($C^{-1} = d/\varepsilon\varepsilon_o A$).[58] The correlation is best when [K_2HPO_4] ≥ 30 mM. The slope (averaged over 30 mM to 50 mM) is 0.044 cm^2 μF^{-1} per CH_2 with an intercept of 0.2 cm^2 μF^{-1} (average r^2 = 0.970). The dielectric constant ε is 3.0, assuming a chain tilt of 30° from the surface normal. A slope of 0.055 cm^2 μF^{-1} per CH_2 (ε = 2.2) and an intercept of 0.1 cm^2 μF^{-1} were obtained for $CH_3(CH_2)_nS$/Au SAMs in 1 M KCl, $HClO_4$ or NaF.[51]

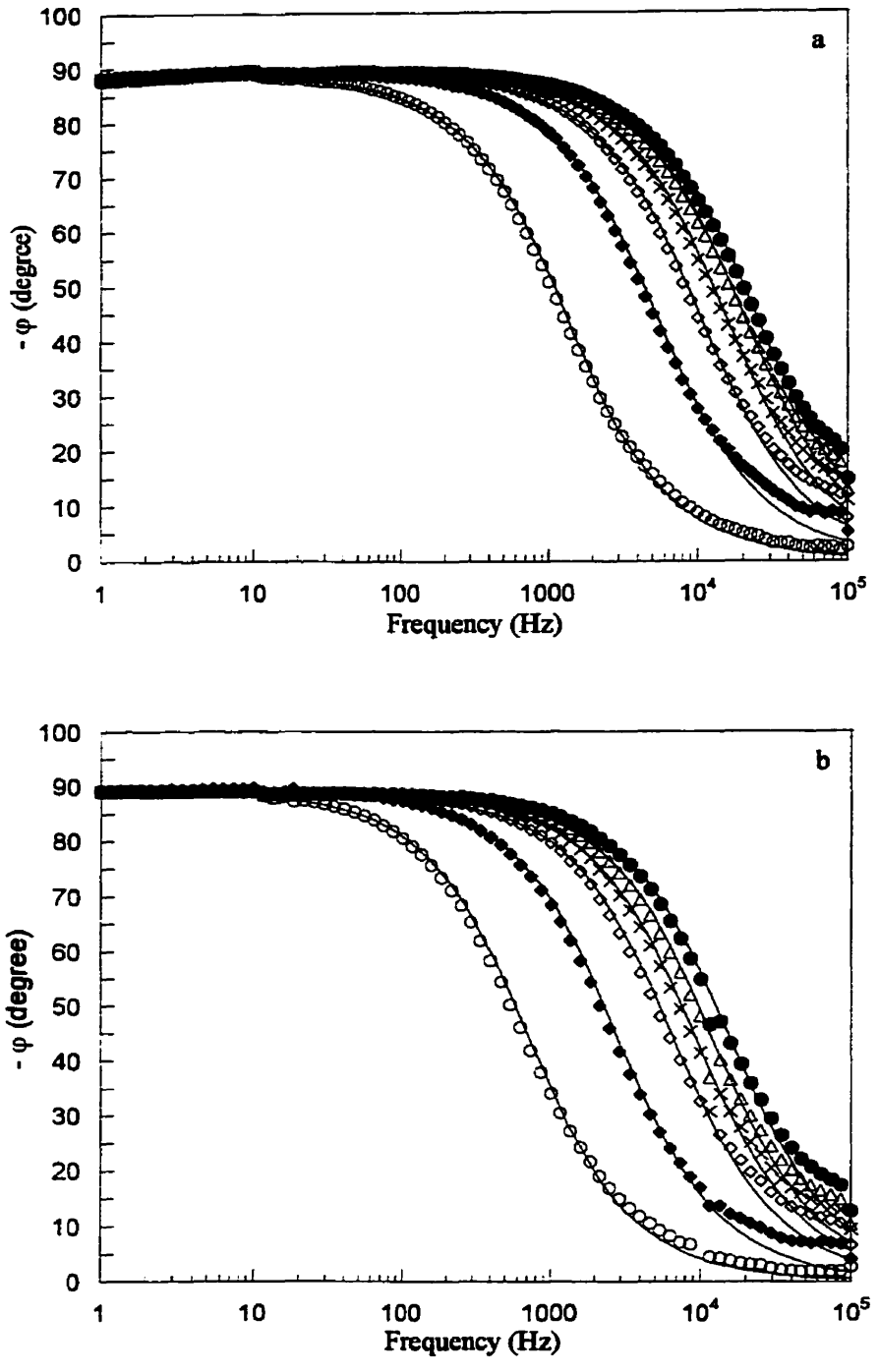

Figure 2.6. Bode phase plots for $CH_3(CH_2)_nS$/Au SAMs at various electrolyte concentrations for *a) n* = 15 and *b) n* = 7. [K_2HPO_4] = 2 mM (o), 10 mM (♦), 20 mM (◊), 30 mM (x), 40 mM (Δ), and 50 mM (•). Symbols are the experimental data and solid lines result from CNLS data fits using the equivalent circuit in Figure 2.2. Fitting parameters are shown in Table 2.2.

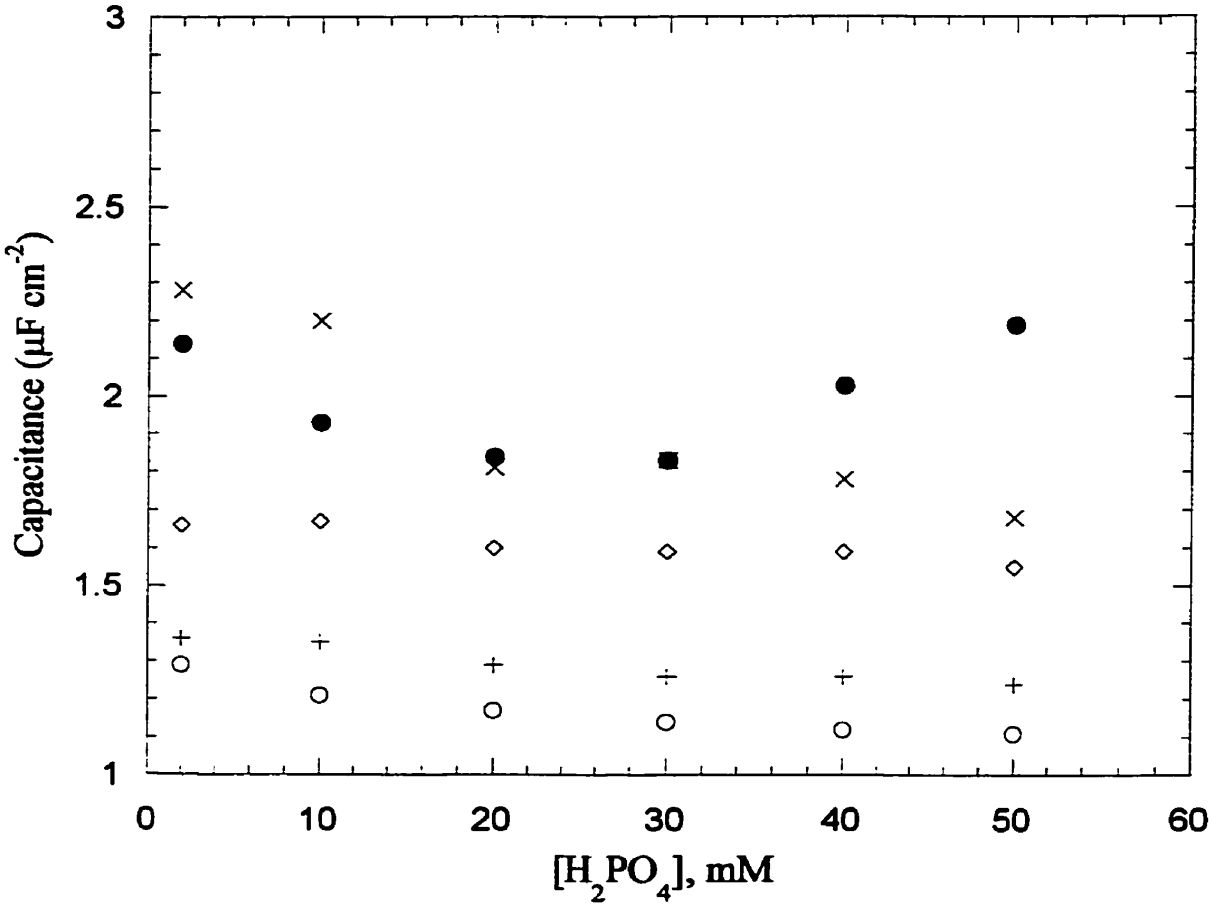

Figure 2.7. Effect of the electrolyte concentration on SAM capacitance at 0 V *vs.* Ag/AgCl. $CH_3(CH_2)_nS$/Au SAMs: n = 7 (×), n = 9 (◊), n = 11 (+), n = 15 (○); and CF_3C_9S/Au SAM (●).

It is important to note that interlab comparisons of these types of data can be problematic since the measured capacitance can be affected by the nature of the substrate (single crystal *vs.* polycrystalline), and by different cleaning and preparation conditions. The literature examples which we use for comparison purposes are believed to be fully formed SAMs.

2.3.3 Dispersion of the Complex Dielectric Constant with Frequency

The ionic insulating properties of thin films can also be characterized in terms of how the complex dielectric constant $|\varepsilon|$ varies with frequency.[59-61] The complex dielectric constant $|\varepsilon|$ is defined as:

$$|\varepsilon| = \varepsilon' - j\varepsilon'' \qquad (2)$$

where $j^2 = -1$, ε' and ε'' are the real and the imaginary components of the complex dielectric "constant" ε. Although dielectric spectroscopy (*i.e.* $|\varepsilon|$ *vs.* f) is not commonly used in assessing SAM properties, it can reveal interesting features in the low frequency domain that are not otherwise visualized in either the Nyquist plots or Bode plots. Dielectric spectroscopy has been useful in assessing phospholipid bilayer membrane properties[59] and the internal structure of biological cells in terms of ion permeation in the lipid phase.[60,61] The complex dielectric constant $|\varepsilon|$ is not necessarily "constant" over the entire frequency domain, and therefore the term "constant" does not apply to all cases.

The dielectric spectra of $CH_3(CH_2)_nS/Au$ (n = 7-15) SAMs do not show dispersion in $|\varepsilon|$ with f between 1 and 10^4 Hz, consistent with these SAMs being impermeable to ions at 0 V *vs.* Ag/AgCl (Figure 2.8). The independence of $|\varepsilon|$ with f is noted over the range of potentials between + 0.4 V and – 0.2 V for all chainlengths.

The CF_3C_9S/Au SAM has a greater value of $|\varepsilon|$ (1.4–fold) than the corresponding CH_3C_9S/Au SAM, reflecting the higher polarizability of the C-F bond compared to the C-H bond. The dispersion in $|\varepsilon|$ with f is negligible in this case as well, further establishing that the SAM is impermeable to the electrolyte.

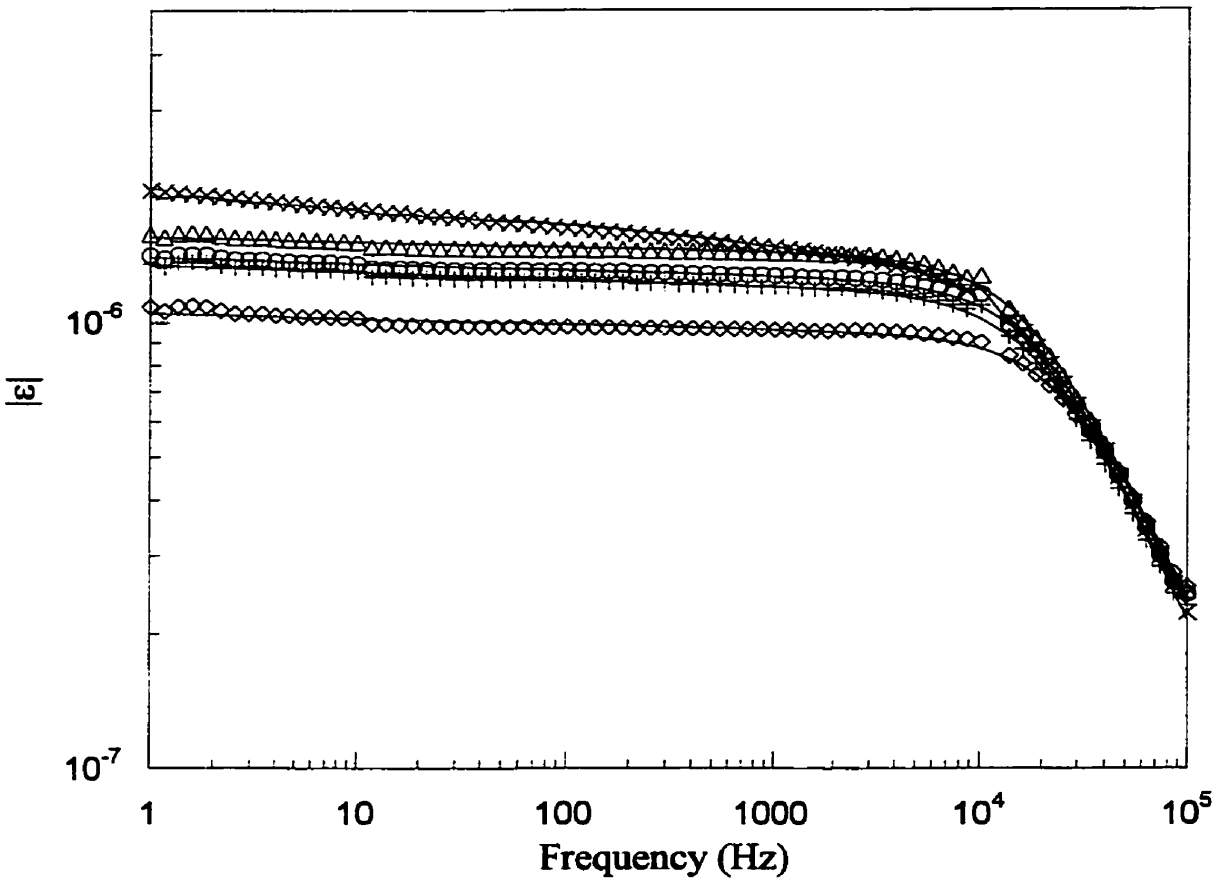

Figure 2.8. Dielectric spectra of $CH_3(CH_2)_nS$/Au SAMs for n = 15 (◊), n = 11 (O), n = 9 (+), n = 7 (Δ), and for the CF_3C_9S/Au SAM (×). Symbols are the experimental data and solid lines result from CNLS data fits using the equivalent circuit in Figure 2.2.

2.4 Conclusions and Overview

A.C. EIS spectroscopy of $CH_3(CH_2)_nS/Au$ (n = 7-15) SAMs and a CF_3C_9S/Au SAM shows that in the absence of a redox couple, SAMs prepared *via* prolonged passive incubation are adequately described by the Helmholtz ideal capacitor model. These SAMs of nanometer-level thickness lead to a dielectric layer with a $|Z|$ of 10^5 Ω cm^2 at 1 Hz. The phase angle at an ion diffusion-related frequency (1 Hz) of $CH_3(CH_2)_nS/Au$ (n = 7-15) and CF_3C_9S/Au SAMs is constant at ~ 88-89°, consistent with this entire range of SAMs being excellent *ionic* insulators.

A number of recent studies have shown that SAMs are *electronic* insulators.[16-18,34] The study presented here show that *n*-alkylthiol SAMs are also *ionic* insulators, provided they are poised at moderate potentials. Long alkyl chainlength SAMs may thus be effective as insulating barriers in electrochemical sensor configurations.

Several important implications of these results are apparent. Firstly, a.c. EIS allows one to readily assess whether a SAM is completely, or close to being, defect-free. If SAMs are to go beyond being the subject of fundamental studies of interfacial chemistry and electrochemistry to being components in reliable technologies, one must be able to prepare them in a reliable manner. Accessible assessment procedures often have practical drawbacks. They can be damaging (gold oxide formation), perturbing (redox couple in solution), too low resolution (capacitance), or too high resolution (AFM and STM) to be of practical utility. The a.c. EIS technique described here, on the other hand, provides a rapid and non-damaging assessment of SAM quality. A φ *vs.* f plot is not affected by true (*vs.* geometric) area differences

Secondly, many potential applications of SAMs in devices (sensor, actuator, current rectifier) depend on the SAM responding to a stimulus (electrical, chemical, thermal) in a predictable way. The initial state of the SAM must be similar from sample to sample for this stimulus-response cycle to be usable. The a.c. EIS protocol described here may be a suitable starting point in this regard.

Finally, a.c. EIS is very useful in assessing RS/Au SAMs before they are taken into complex mechanistic studies. This is advantageous because mechanistic

electron transfer studies ultimately rely on knowing whether a SAM is defect-free or not. Prolonged incubation of the gold substrate in the RSH solution is necessary to prepare a highly insulating SAM. Experiments that modulate SAM electrical properties are currently being addressed in our laboratory.

References

1) Helmholtz, H. *Ann. Phys.* **1879**, *7*, 337-382.
2) Halliday, D.; Resnick, R. *Physics*; Wiley: New York, 1978.
3) Becka, A. M.; Miller, C. J. *J. Phys. Chem.* **1993**, *97*, 6233-6239.
4) Chidsey, C. E. D.; Loiacono, D. N. *Langmuir* **1990**, *6*, 682-691.
5) Finklea, H. O.; Avery, S.; Lynch, M.; Furtsch, T. *Langmuir* **1987**, *3*, 409-413.
6) Finklea, H. O. *Electrochemistry of Organized Monolayers of Thiols and Related Molecules on Electrodes*; Marcel Dekker: New York, 1996; Vol. 19; Chapter 2.
7) Miller, C. J.; Grätzel, M. *J. Phys. Chem.* **1991**, *95*, 5225-5233.
8) Miller, C.; Cuendet, P.; Grätzel, M. *J. Phys. Chem.* **1991**, *95*, 877-886.
9) Alleman, K. S.; Weber, K.; Creager, S. E. *J. Phys. Chem.* **1996**, *100*, 17050-17058.
10) Richardson, J. N.; Peck, S. R.; Curtin, L. S.; Tender, L. M.; Terrill, R. H.; Carter, M. T.; Murray, R. W.; Rowe, G. K.; Creager, S. E. *J. Phys. Chem.* **1995**, *99*, 766-772.
11) Chidsey, C. E. D.; Bertozzi, C. R.; Putvinski, T. M.; Mujsce, A. M. *J. Am. Chem. Soc.* **1990**, *112*, 4301-4306.
12) Chidsey, C. E. D. *Science* **1991**, *251*, 919-922.
13) Weber, K.; Creager, S. E. *Anal. Chem.* **1994**, *66*, 3164-3172.
14) Smalley, J. F.; Feldberg, S. W.; Chidsey, C. E. D.; Linford, M. R.; Newton, M. D.; Liu, Y.-P. *J. Phys. Chem.* **1995**, *99*, 13141-13149.
15) Mann, B.; Kuhn, H. *J. Appl. Phys.* **1971**, *42*, 4398-4405.

16) Boulas, C.; Davidovits, J. V.; Rondelez, F.; Vuillaume, D. *Phys. Rev. Lett.* **1996**, *76*, 4797-4800.

17) Vuillaume, D.; Boulas, C.; Collet, J.; Davidovits, J. V.; Rondelez, F. *Appl. Phys. Lett.* **1996**, *69*, 1646-1648.

18) Rampi, M. A.; Schueller, O. J. A.; Whitesides, G. M. *Appl. Phys. Lett.* **1998**, *72*, 1781-1783.

19) Polymeropoulos, E. E.; Sagiv, J. *J. Chem. Phys.* **1978**, *69*, 1836-1847.

20) Collet, J.; Vuillaume, D.; Bonnier, M.; Bouloussa, O.; Rondelez, F.; Gay, J. M.; Kham, K.; Chevrot, C. *Mat. Res. Soc. Symp. Proc.* **1998**, *488*, 847-852.

21) Vuillaume, D. *Mat. Res. Soc. Symp. Proc.* **1997**, *446*, 79-90.

22) Boulas, C.; Davidovits, J. V.; Rondelez, F.; Vuillaume, D. *Microelec. Eng.* **1995**, *28*, 217-220.

23) Vuillaume, D.; Rondelez, F. *Bull. Soc. Fr. Phys.* **1995**, *102*, 3-6.

24) Vuillaume, D.; Rondelez, F. *Mat. Res. Soc. Symp. Proc.* **1994**, *328*, 203-208.

25) Vuillaume, D.; Fontaine, P.; Collet, J.; Deresmes, D.; Garet, M.; Rondelez, F. *Microelectron. Eng.* **1993**, *22*, 101-104.

26) Fontaine, P.; Goguenheim, D.; Deresmes, D.; Vuillaume, D.; Garet, M.; Rondelez, F. *Appl. Phys. Lett.* **1993**, *62*, 2256-2258.

27) Collet, J.; Bonnier, M.; Bouloussa, O.; Rondelez, F.; Vuillaume, D. *Microelectron. Eng.* **1997**, *36*, 119-122.

28) Brandrup, J.; Immergut, E. H. *Polymer Handbook*; 3rd ed.; Wiley: New York, 1989, Section V.

29) Collet, J.; Vuillaume, D. *Appl. Phys. Lett.* **1998**, *73*, 2681-2683.

30) Allara, D. L.; Dunbar, T. D.; Weiss, P. S.; Bumm, L. A.; Cygan, M. T.; Tour, J. M.; Reinerth, W. A.; Yao, Y.; Kozaki, M.; Jones II., L. *Ann. N. Y. Acad. Sci.* **1998**, *852*, 349-370.

31) Gritsch, S.; Nollert, P.; Jahnig, F.; Sackmann, E. *Langmuir* **1998**, *14*, 3118-3125.

32) Raguse, B.; Braach-Maksvytis, V.; Cornell, B. A.; King, L. G.; Osman, P. D. J.; Pace, R. J.; Wieczorek, L. *Langmuir* **1998**, *14*, 648-659.

33) Stelzle, M.; Weissmuller, G.; Sackmann, E. *J. Phys. Chem.* **1993**, *97*, 2974-2981.

34) Haag, R.; Rampi, M. A.; Holmlin, R. E.; Whitesides, G. M. *J. Am. Chem. Soc.* **1999**, *121*, 7895-7906.

35) Janek, R. P.; Fawcett, W. R.; Ulman, A. *Langmuir* **1998**, *14*, 3011-3018.

36) Sabatini, E.; Rubinstein, I. *J. Phys. Chem.* **1987**, *91*, 6663-6669.

37) Sabatini, E.; Rubinstein, I.; Maoz, R.; Sagiv, J. *J. Electroanal. Chem.* **1987**, *219*, 365-371.

38) Finklea, H. O.; Snider, D. A.; Fedyk, J.; Sabatini, E.; Gafni, Y.; Rubinstein, I. *Langmuir* **1993**, *9*, 3660-3667.

39) Furniss, B. S.; Hannaford, A. J.; Rogers, V.; Smith, P. W. G.; Tatchell, A. R. *Vogel's Textbook of Practical Organic Chemistry*; 4th ed.; Longman: New York, 1978.

40) Macdonald, J. R. *Complex Nonlinear Least Squares Immittance Fitting Program, LEVM 7.0*; Macdonald, J. R., Ed.: Department of Physics and Astronomy, University of North Carolina, Chapel Hill, NC., 1990.

41) Macdonald, J. R. *Impedance Spectroscopy*; Wiley: New York, 1987.

42) Burke, L. D.; Nugent, P. F. *Gold Bull.* **1997**, *30*, 43-53.

43) Swietlow, A.; Skoog, M.; Johansson, G. *Electroanalysis* **1992**, *4*, 921-928.

44) Janek, R. P.; Fawcett, W. R.; Ulman, A. *J. Phys. Chem. B* **1997**, *101*, 8550-8558.

45) Bain, C. D.; Troughton, E. B.; Tao, Y. T.; Evall, J.; Whitesides, G. M.; Nuzzo, R. G. *J. Am. Chem. Soc.* **1989**, *111*, 321-335.

46) Jung, C.; Dannenberger, O.; Xu, Y.; Buck, M.; Grunze, M. *Langmuir* **1998**, *14*, 1103-1107.

47) Dannenberger, O.; Buck, M.; Grunze, M. *J. Phys. Chem. B* **1999**, *103*, 2202-2213.

48) Pan, W.; Durning, C. J.; Turro, N. J. *Langmuir* **1996**, *12*, 4469-4473.

49) Peterlinz, K. A.; Georgiadis, R. *Langmuir* **1996**, *12*, 4731-4740.

50) Forouzan, F.; Bard, A. J.; Mirkin, M. V. *Isr. J. Chem.* **1997**, *37*, 155-164.

51) Porter, M. D.; Bright, T. B.; Allara, D. L.; Chidsey, C. E. D. *J. Am. Chem. Soc.* **1987**, *109*, 3559-3568.

52) Sabatini, E.; Cohen-Boulakia, J.; Bruening, M.; Rubinstein, I. *Langmuir* **1993**, *9*, 2974-2981.

53) Boubour, E.; Lennox, R. B. *Submitted to J. Phys. Chem. B* **2000**.

54) Steinem, C.; Janshoff, A.; von dem Bruch, K.; Reihs, K.; Goossens, J.; Galla, H.-J. *Bioelectrochem. Bioenerg.* **1998**, *45*, 17-26.

55) Sondag-Huethorst, J. A. M.; Fokkink, L. G. L. *Langmuir* **1992**, *8*, 2560-2566.

56) Sondag-Huethorst, J. A. M.; Fokkink, L. G. L. *J. Electroanal. Chem.* **1994**, *367*, 49-57.

57) Sondag-Huethorst, J. A. M.; Fokkink, L. G. L. *Langmuir* **1995**, *11*, 2237-2241.

58) Bard, A. J.; Faulkner, L. R. *Electrochemical Methods: Fundamentals and Applications*; John Wiley & Sons: New York, USA, 1980.

59) Coster, H. G. L.; Chilcott, T. C.; Coster, A. C. F. *Bioelectrochem. Bioenerg.* **1996**, *40*, 79-98.

60) Schmukler, R. E. *Mat. Res. Soc. Symp. Proc.* **1996**, *411*, 45-56.

61) Asami, K.; Yonezawa, T.; Wakamatsu, H.; Koyanagi, N. *Bioelectrochem. Bioenerg.* **1996**, *40*, 141-145.

Chapter 3

Ion Penetration into *n*-Alkylthiol SAMs Monitored by Impedance Spectroscopy*

3.1 Introduction

Self-assembled monolayers (SAMs) are of great interest since they allow one to deliberately derivatize metal (Au, Pt, Cu, Ag, Hg) and semiconductor (Si, Ge, GaAs, CdSe, CdS, InP, $MoSe_2$, and MoS_2) substrates with a chemically well-defined organic ultrathin film, in a relatively facile and reliable manner. The applications of SAMs include work function modulation of metals and semiconductors,[1-7] nano-FETs[8,9] and biosensors construction.[10-13] SAMs are also ideal components in impedimetric sensors, given that they may be used to directly detect a specific binding event.[14]

n-Alkylthiol SAMs ($CH_3(CH_2)_nS$/Au) SAMs have been particularly well studied using a number of bulk and surface sensitive techniques. These include contact angle, ellipsometry, FT-IR and Raman spectroscopies, surface plasmon resonance, He diffraction, XPS, SHG, X-ray diffraction, UHV-STM, AFM, TPD (temperature programmed desorption), and electrochemistry.[15] Issues such as the presence and size of pinhole defects,[16-19] phase transitions,[20] and domain formation have been of particular interest as they relate to the quality of the film.

Only a limited number of studies have considered $CH_3(CH_2)_nS$/Au SAMs as models of supported lipid membranes (s-BLMs), despite the obvious structural

* Reproduced with permission from *J. Phys. Chem. B.*, submitted for publication. Unpublished work, copyright 2000 American Chemical Society.

parallels. The permeability properties of s-BLMs and black lipid membranes (BLMs) under applied electric fields are of importance because they themselves are excellent models of cell membranes. These artificial phospholipid membrane-based systems provide detailed information about diffusion coefficients and membrane conductance as a function of the applied electric field, as well as details about ion and water translocation in the membrane. While most s-BLM and BLM studies use d.c. electrochemical techniques, a.c. impedance spectroscopy has provided a better understanding of how transmembrane ion transport is modulated by ion carriers or peptide channels.[13,21-33]

A tentative link between lipid membranes and $CH_3(CH_2)_nS$/Au SAMs was revealed in our earlier work, where $CH_3(CH_2)_nS$/Au SAMs exhibit the same phase transition temperatures as the phospholipid membranes of equivalent chainlength. Using $Fe(CN)_6^{3-/4-}$ as a permeability probe, it was shown that SAMs can mimic phospholipid membranes in regards to their permeability features.[20]

In this study, we have undertaken to define the relationship between the alkyl chainlength of SAMs and their permeability properties using a.c. impedance spectroscopy in the absence of an electrochemical redox couple. We wish to probe how an applied d.c. voltage (between + 0.4 V and – 0.5 V *vs.* Ag/AgCl) modulates alkylthiol SAMs structure. Reductive electrodesorption of alkanethiol chains is observed at much more reductive potentials (~ –1 V to – 1.4 V for n = 7-15) than the working potential window used in this study.[34-40] We also wish to explore parallels between $CH_3(CH_2)_nS$/Au systems and previous BLM and s-BLM reports.[12,22,24-26,31,41,42] The broad timescale spanned by a.c. impedance spectroscopy (microseconds to seconds) makes it possible to unambiguously relate, with some confidence, changes in the dielectric properties of SAMs to molecular mechanisms. The effect of a transmembrane electrical potential on *n*-alkylthiol SAMs of various chainlengths (n = 7-15) will be discussed in terms of electrochemical stability, permeability to electrolyte ions, and variation in the SAM microstructure.

3.2 Experimental Section

Instrumentation. Electrochemical Impedance Spectroscopy (EIS) measurements were obtained in a conventional 3-electrode electrochemical cell with an EG&G lock-in amplifier (5210) combined to an EG&G PAR 273 potentiostat/galvanostat. The counter electrode was a platinum mesh (Aldrich) and the reference electrode was a Ag/AgCl electrode (3 M NaCl, Bioanalytical Systems Inc., IN). Data acquisition was performed using EG&G M398 software. A sinusoidal potential modulation of ± 10 mV amplitude was superimposed on a fixed d.c. potential. The amplitude and the phase shift of the resulting current were recorded at each frequency (15 points per decade equally spaced on a log scale).

The effect of the applied potential on SAMs permeability is investigated from + 0.4 V to – 0.5 V in 0.1 V steps. The time duration of each experiment is 30 min. The impedance data were then transferred to the Zplot/Zview software package (Scribner Associates Inc., NC) and were fitted to an electrical equivalent circuit using the Complex Nonlinear Least Square (CNLS) Immittance Fitting Program.[43] The equivalent circuit provides an electrical analog of chemical/physical processes probed by a.c. EIS.[44] On each impedance graph, symbols represent the raw experimental data and the solid lines result from CNLS data fits. The electrolyte resistance, R_s, is 300 ± 25 Ω (for an electrolyte of 50 mM K_2HPO_4, pH 7.0). A Teflon cover was used to close the electrochemical cell and to position the three electrodes in a reproducible manner, minimizing experiment to experiment variation.

Chemicals. Octanethiol (98.5 %), decanethiol (97 %) and dodecanethiol (98 %) were purchased from Aldrich (Milwaukee, USA) and were used as received. Hexadecanethiol was available from previous studies and was synthesized from 1-bromohexadecane (97 % Aldrich) by standard procedures.[45]

$HS(CH_2)_{15}CH_3$: M.p. 19.5-21°C; TLC (silica gel, *n*-hexane): R_f = 0.7; ^1H NMR (500 MHz, $CDCl_3$, 25°C): δ 2.52 (q, 2H, CH_2SH), 1.58 (m, 2H CH_2CH_2SH), 1.40 (m, 2H, $CH_2CH_2CH_2SH$), 1.31 (t, 1H, CH_2SH), 1.24 (s, 24H, $(CH_2)_{12}$), 0.87 (t, 3H, CH_3).

Dibasic potassium phosphate was ACS reagent grade (BDH, Montreal, Canada).

Procedure. Polycrystalline gold electrodes (0.020 cm^2 geometric surface area) were purchased from Bioanalytical Systems Inc. (West Lafayette, IN) and were mechanically hand polished on microcloth pads (Buehler) with alumina slurries (Buehler) of decreasing particle size (1.0 μm, 0.3 μm and 0.05 μm). The polished electrodes were sonicated in ultra pure water (Milli-Q water system, 18 MΩ cm) in an ultrasonic bath (Branson 1200) for 2 minutes. The electrodes were then immediately cleaned with freshly prepared *aqua regia* solution (60:30:10 H_2O:HCl:HNO_3). This step was immediately followed by the electrochemical polishing of the gold surface between 0 and + 1.7 V (*vs.* Ag/AgCl) at 80 mV s^{-1} in N_2-purged 1 M perchloric acid (HPLC grade, BDH). The electrodes were then thoroughly rinsed with ultra pure water and absolute ethanol (Commercial Alcohols Inc., Canada) prior to incubation in a N_2-purged 1 mM $CH_3(CH_2)_nSH$ solution, at room temperature, in sealed vials. The electrodes were incubated for a minimum of 72 hours. Prior to each measurement, the SAM coated electrodes were rinsed with a copious amount of absolute ethanol followed by ultra pure water. Impedance spectra were obtained at room temperature after a stable open circuit potential was reached.

Data Analysis. Special care must be taken when analyzing impedance spectra, particularly with biological tissues, living cells, and membrane models such as SAMs.[46] Data interpretation from impedance spectra can depend upon the way the data are represented, where two main types of representations are often used. An Argand diagram plots the imaginary component of a parameter (impedance Z, capacitance C, or the dielectric constant ε) *vs.* its real component. A Bode diagram plots the modulus of a given parameter ($|Z|$ or $|C|$) or the phase angle (φ) as a function of the frequency, f. The graphical interpretation of the raw data can further influence modeling of the experimental results. For example, ion-diffusion processes occur in the low frequency domain ($\leq \sim 10^2$ Hz); they are thus more apparent in Bode phase plots (φ *vs.* f) than in Argand diagrams (Z'' *vs.* Z') or in $|Z|$ *vs.* f. A comparison of these three representations also assists in judging the validity of data fitting over the entire experimental frequency domain probed.

3.3 Results and Discussion

$CH_3(CH_2)_nS$/Au SAMs reported in this study were first analyzed by a.c. EIS at a benign d.c. potential (*i.e.* non-altering to the SAM)[47] in 50 mM K_2HPO_4 at pH 7.0. $CH_3(CH_2)_nS$/Au SAMs behave as excellent capacitors at + 0.4 V (*vs.* Ag/AgCl), exhibiting a phase angle $\varphi \geq 88°$ at 1 Hz $< f <$ 10^3 Hz (cross symbols in Figure 3.1a). From an electrical circuit perspective, a pure capacitor (in absence of leakage current) has a phase angle $\varphi = 90°$ over the entire frequency domain. On the other hand, $\varphi =$ 0° for a pure resistor.[44] SAMs are practically defect-free when $\varphi \geq 88°$ in the medium-to-low frequency region ($1 \leq f \leq \sim 10^3$ Hz).[47] The lowest observation frequency in this study is 1 Hz because when $f <$ 1 Hz, the data acquisition can take minutes and the electrochemical response may no longer be linear. Since very slow frequency sweeps (mHz range) correspond to long observation periods (~ 15 minutes), conducting a.c. experiments in the mHz range effectively corresponds to performing a d.c. experiment.

3.3.1 Effect of d.c. Potential on the Phase Angle and SAM Capacitance

The effect of an applied d.c. potential, V_{appl}, at either – 0.4 V or – 0.5 V (*vs.* Ag/AgCl) on a $CH_3(CH_2)_{15}S$/Au SAM is shown in Figure 3.1. Raw data (symbols) and CNLS simulations (solid lines) are displayed using three different impedance representations (Figures 3.1a-c). When $V_{appl} >$ – 0.4 V (*i.e.* from – 0.3 V to + 0.4 V), the phase angle remains ≥ 88° (cross symbols), even in the lowest frequency domain probed (1 Hz $\leq f \leq$ 50 Hz). Therefore, at – 0.3 V $\leq V_{appl} \leq$ + 0.4 V, the data can be fitted to the Helmholtz parallel plate capacitor model,[48,49] whose equivalent circuit involves a solution resistance in series with a constant phase element, *CPE* (Figure 3.2a).[47] The *CPE* corresponds to the SAM capacitance and its exponent α relates to the surface roughness.[50] The exponent α is ~ 0.98 at all potentials, establishing that the SAM/electrolyte interface is reasonably smooth (column 3 in Table 3.1).[44,50]

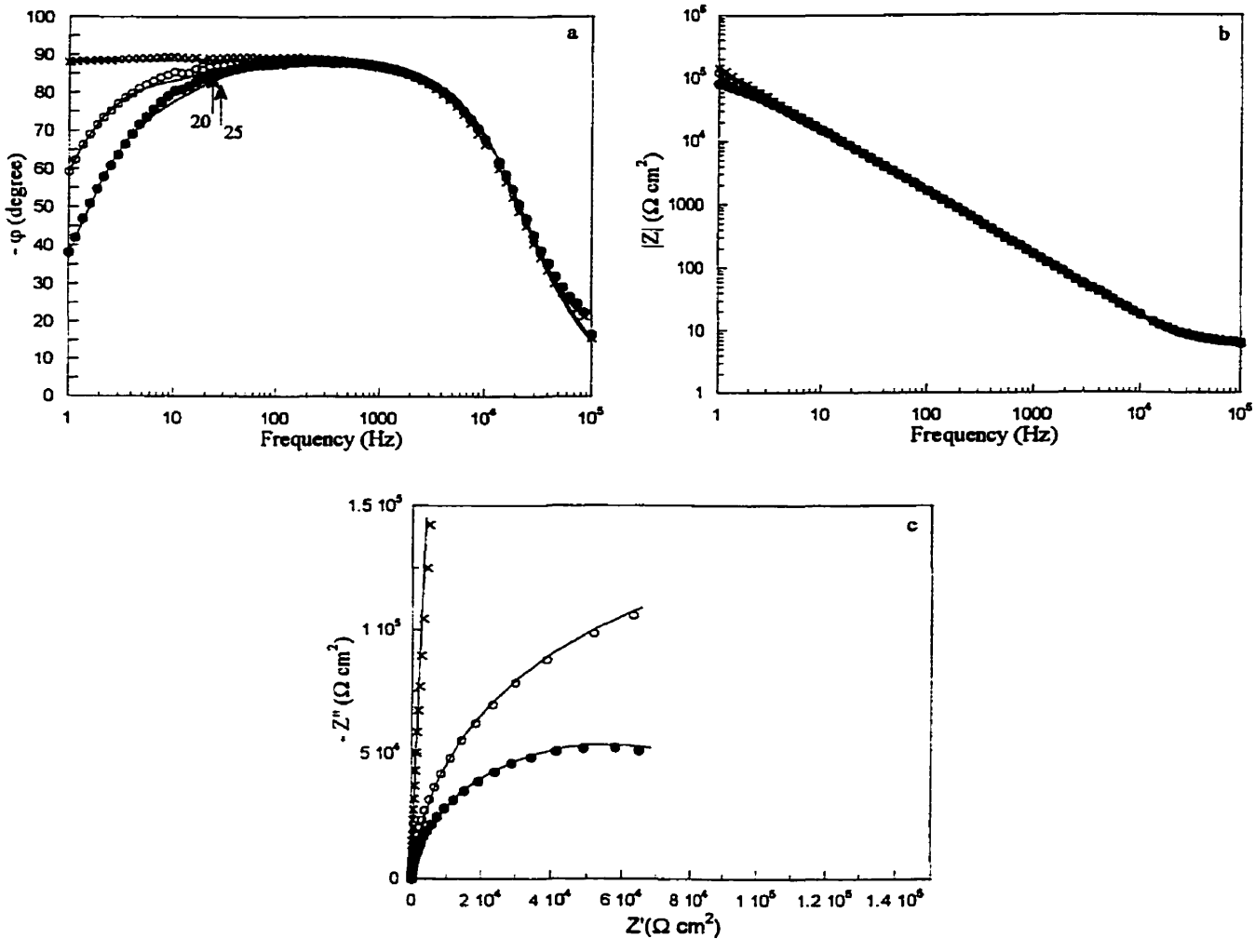

Figure 3.1 *a)* Bode phase plot, *b)* Bode plot, and *c)* Nyquist plot for a $CH_3(CH_2)_{15}S$/Au SAM from + 0.4 V (*vs.* Ag/AgCl) to – 0. 3 V (x), at – 0.4 V (o) and – 0.5 V (•) in 50 mM K_2HPO_4, pH 7.0. Symbols are the experimental data points and solid lines result from CNLS data fits, according to the equivalent circuit shown in Figure 3.2b. The numbers in *a)* correspond to the relaxation frequency, $\underline{\nu_d}$, tabulated in Table 3.1.

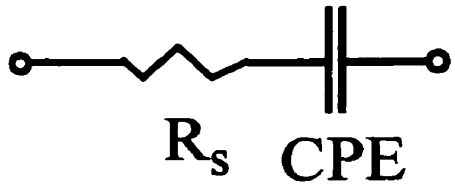

2 a

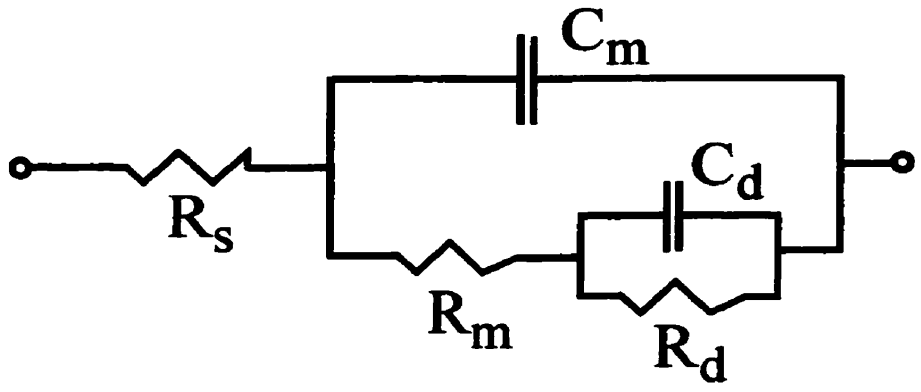

2 b

Figure 3.2 Equivalent circuits for *a)* a defect-free $CH_3(CH_2)_nS$/Au SAM (*i.e.* at $V_{appl} > V_c$) and *b)* a SAM presenting potential-induced defects at $V_{appl} \leq V_c$. R_s is the solution resistance (350 ± 25 Ω). The *CPE* (Constant Phase Element) and C_m represent the SAM capacitance. In *b)*, R_m is the SAM resistance. C_d and R_d account for the deliberately formed defects induced at potentials more cathodic than V_c (*i.e.* $V_{appl} \leq V_c$).

Equivalent circuit 2a			*Equivalent circuit 2b*				
E	*CPE*	α	C_m	R_m	C_d	R_d	ν_d
V	μF cm^{-2}		μF cm^{-2}	kΩ cm^2	nF	MΩ	Hz
$CH_3(CH_2)_7S$/Au SAM							
0.4	1.80±0.06	0.986±0.005					
0.3	1.70±0.02	0.984±0.001					
0.2	1.61±0.02	0.989±0.002					
0.1	1.50±0.10	1.000±0.009					
0	1.59±0.02	0.989±0.002					
− 0.2			1.46±0.01	92±31	2.9±0.5	97±53	3.6±1.9
− 0.3			1.46±0.02	48±10	4.6±0.5	16±1.5	15±1.5
− 0.4			1.46±0.01	48±8	6.9±1.0	5±0.3	33±4.8
− 0.5			1.46±0.02	15±3	6.2±1.2	2±0.4	100±20
$CH_3(CH_2)_9S$/Au SAM							
0.4	1.67±0.05	0.976±0.004					
0.3	1.55±0.02	0.975±0.001					
0.2	1.41±0.08	0.989±0.008					
0.1	1.40±0.02	0.985±0.002					
0	1.28±0.09	1.000±0.010					
− 0.1	1.28±0.08	1.000±0.009					
− 0.2	1.36±0.02	0.986±0.002					
− 0.3			1.20±0.01	50±12	2.8±0.4	53±13	6.6±1.6
− 0.4			1.20±0.01	50±12	4.1±0.5	11±0.8	20±2.4
− 0.5			1.24±0.01	56±4	6.2±0.5	7±0.2	25±2.0

Table 3.1 Fitting parameters obtained for defect-free SAMs (Figure 3.2a, *CPE* and α) and potential-induced defects $CH_3(CH_2)_nS$/Au (n = 7 and 9) SAMs (Figure 3.2b, C_m, R_m, C_d, R_d, and relaxation frequency ν_d).

Equivalent circuit 2a			*Equivalent circuit 2b*				
E	*CPE*	α	C_m	R_m	C_d	R_d	ν_d
V	μF cm^{-2}		μF cm^{-2}	kΩ cm^2	nF	MΩ	Hz
$CH_3(CH_2)_{11}S$/Au SAM							
0.4	1.44±0.01	0.987±0.001					
0.3	1.42±0.01	0.988±0.001					
0.2	1.42±0.01	0.987±0.001					
0.1	1.43±0.01	0.986±0.001					
0	1.44±0.01	0.986±0.001					
− 0.1	1.43±0.01	0.986±0.001					
− 0.2	1.43±0.01	0.986±0.001					
− 0.3			1.27±0.01	54±11	2.44±0.23	28±2.3	15±1.4
− 0.4			1.27±0.01	36±6.6	3.59±0.42	7.3±0.4	33±3.9
− 0.5			1.27±0.01	14±2.3	3.30±0.28	3.9±0.1	78±6.6
$CH_3(CH_2)_{15}S$/Au SAM							
0.4	1.07±0.03	0.970±0.004					
0.3	1.09±0.01	0.988±0.001					
0.2	1.08±0.01	0.893±0.002					
0.1	1.07±0.01	0.981±0.002					
0	1.01±0.08	1.000±0.010					
− 0.1	1.03±0.06	0.996±0.008					
− 0.2	1.05±0.13	1.000±0.012					
− 0.3	1.11±0.01	0.983±0.002					
− 0.4			0.95±0.01	79±12	5.2±0.8	9±0.7	20±3.1
− 0.5			0.96±0.01	52±5	12±2.2	3±0.2	25±4.5

* ν_d = dielectric frequency = $(C_d R_d)^{-1}$. Values for C_d and R_d are not normalized for the electrode surface area.

Table 3.1 (cont'd) n = 11 and 15.

At – 0.4 V for n = 15 and beyond, φ in the low frequency domain deviates from 88° (Figure 3.1a). This decrease in φ occurs when $V_{appl} \leq -0.3$ V for n = 11 (Figure 3.3a) and $V_{appl} \leq -0.2$ V for n = 7 (Figure 3.4a), and is more accentuated as the applied potential becomes increasingly cathodic. These results demonstrate that for each chainlength n, the SAM no longer behaves as a pure capacitor once a particular potential is exceeded. We refer to this experimental potential as the critical potential (V_c). An equivalent circuit different from Figure 3.2a is necessary if one is to obtain an adequate fit to the data at $V_{appl} \leq V_c$ (Figure 3.2b). The fit to the equivalent circuit 2b at $V_{appl} \leq V_c$ is excellent in all frequency regions, except for small deviations from the experimental data in the 5 - 30 Hz range. Attempts to improve the fit by introducing a *CPE* instead of C_m did not give better results. The physical interpretation of each of the components (C_m, R_m, C_d, and R_d) is presented later in the discussion.

The electrochemical signal change associated with $V_{appl} \leq V_c$ in the low frequency domain for n = 7-15 is also observed in Bode impedance plots, $|Z|$ *vs.* f (Figures 3.1b, 3.3b, and 3.4b), but not as prominently as in the Bode phase plots, φ *vs.* f (Figures 3.1a, 3.3a, and 3.4a). The corresponding Nyquist plots Z'' *vs.* Z' (Figures 3.1c, 3.3c, and 3.4c) also demonstrate that V_{appl} affects the interfacial properties of SAMs. For example, at – 0.5 V (n = 15), the data deviate significantly from the vertical line observed at $V_{appl} > -0.3$ V (cross symbols).

The critical potential V_c is determined from the interpolation of the phase angle at 1 Hz (φ_{1Hz}) *vs.* V_{appl}, and corresponds to the potential where φ_{1Hz} deviates significantly from 88°. V_c depends on the alkyl chainlength and ranges from – 0.35 V *vs.* Ag/AgCl (n = 15) to – 0.25 V (n = 11) and to – 0.15 V (n = 7). We believe the changes in the electrochemical responses at $V_{appl} \leq V_c$ are associated with molecular changes within the SAM or at the SAM/electrolyte interface, or both. The range of potentials over which the SAMs undergo changes depends on the SAM thickness, and V_c corresponds to the onset of film perturbation.

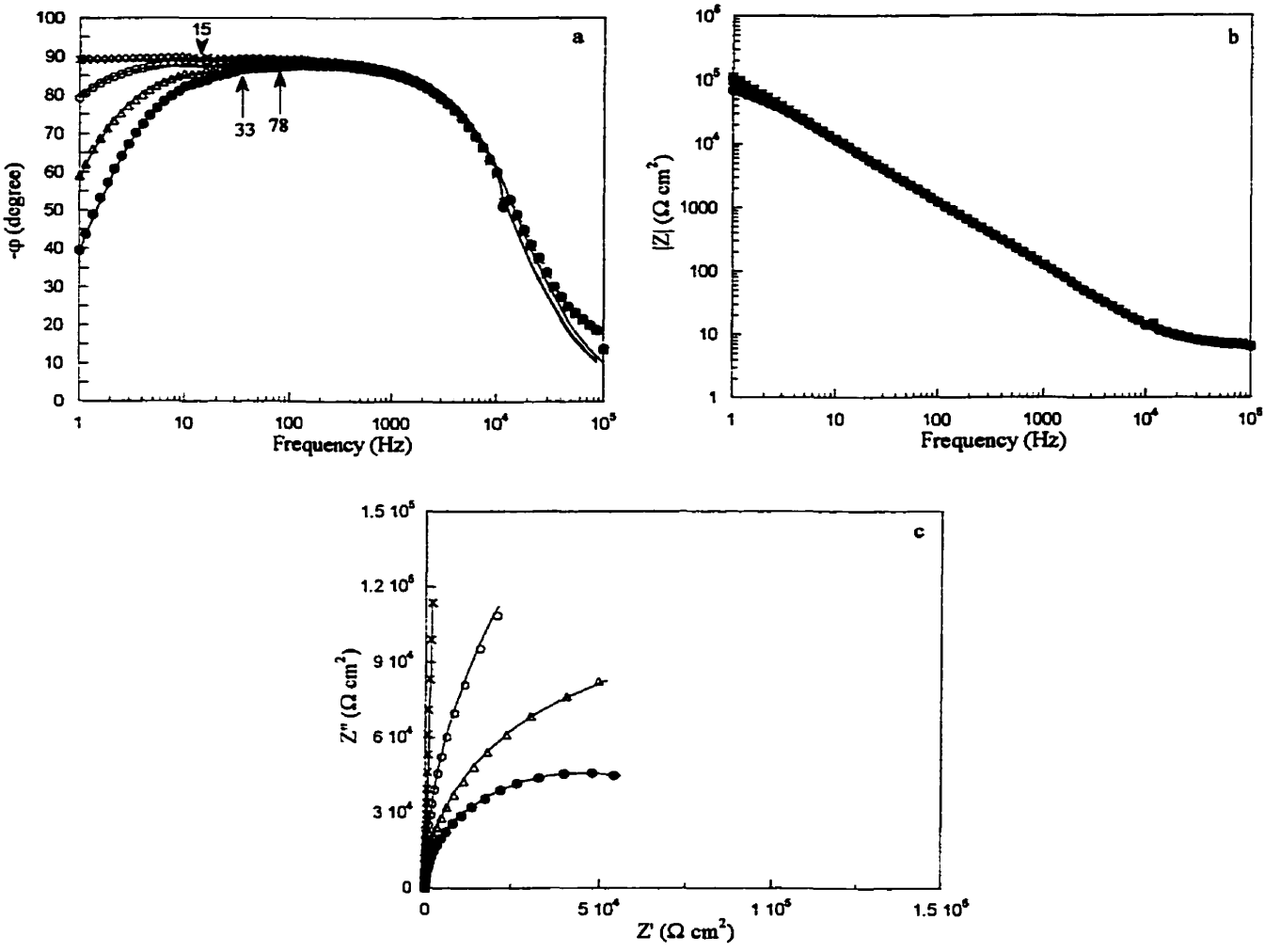

Figure 3.3 *a)* Bode phase plot, *b)* Bode plot, and *c)* Nyquist plot for a $CH_3(CH_2)_{11}S$/Au SAM from + 0.4 V (*vs.* Ag/AgCl) to – 0.2 V (x), at – 0.3 V (o), – 0.4 V (Δ) and – 0.5 V (•) in 50 mM K_2HPO_4, pH 7.0. Symbols are the experimental data and solid lines result from CNLS fits according to the equivalent circuit shown in Figure 3.2b. The numbers in *a)* correspond to the relaxation frequency, ν_d, tabulated in Table 3.1.

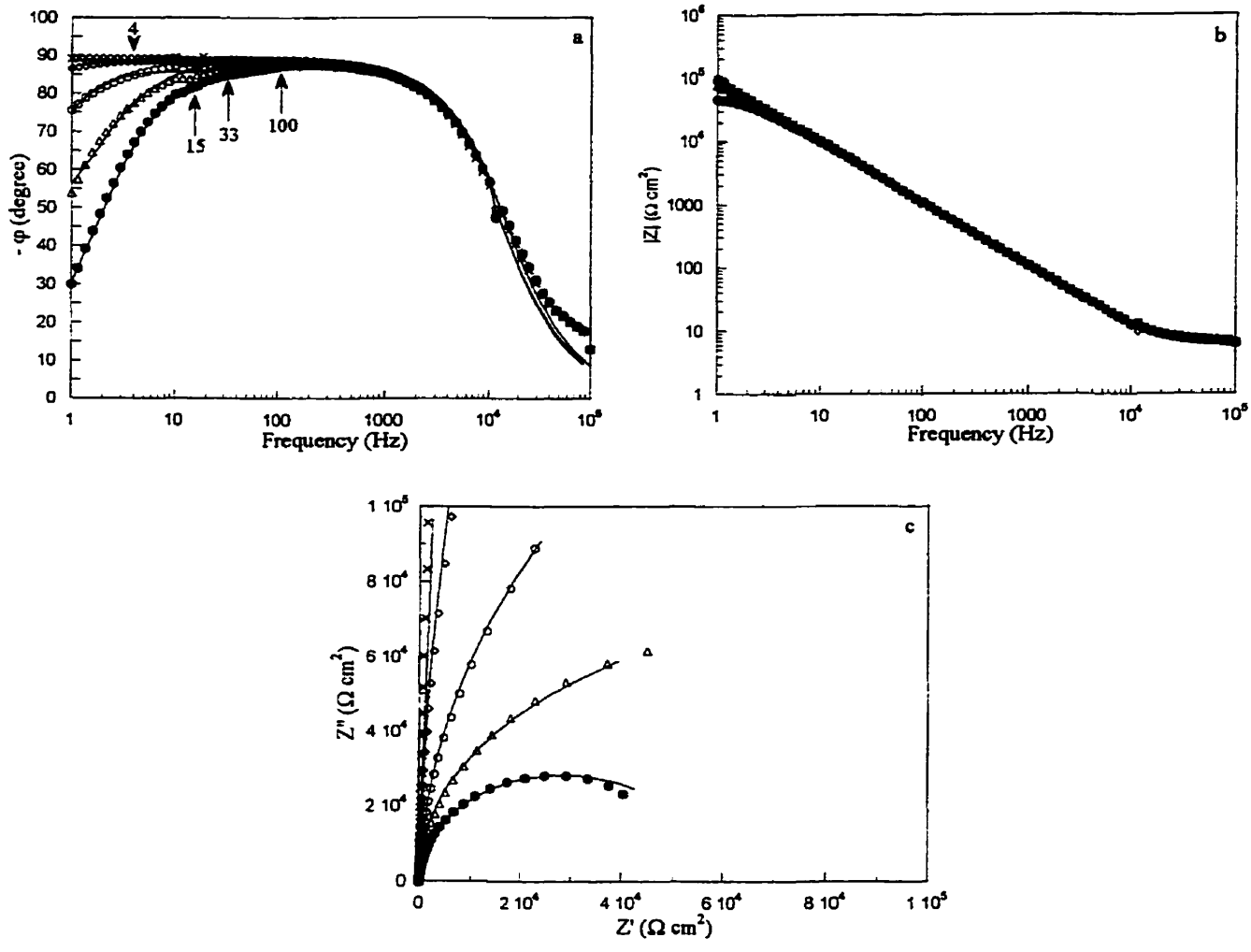

Figure 3.4 *a)* Bode phase plot, *b)* Bode plot, and *c)* Nyquist plot for a $CH_3(CH_2)_7S$/Au SAM from + 0.4 V (V *vs.* Ag/AgCl) to – 0.1 V (x), at – 0.2 V (◊), – 0.3 V (o), – 0.4 V (Δ), and – 0.5 V (•) in 50 mM K_2HPO_4, pH 7.0. Symbols are the experimental data and solid lines result from CNLS data fits according to the equivalent circuit shown in Figure 3.2b. The numbers in *a)* correspond to the relaxation frequency, ν_d, tabulated in Table 3.1.

A recent AFM/electrochemical study showed that a CH_3CH_2S/Au SAM undergoes a transformation at – 0.08 V (*vs.* Ag/AgCl). This is unrelated to the reductive desorption process which occurs at – 0.27 V for this chainlength.[51] This film transformation involves the formation of small islands and is reversible when the electrode is polarized to more positive potentials, typically + 0.2 V. We believe that longer alkyl chains SAMs studied here are subjected to a similar process. V_c is apparently linked to a film transformation and can effectively be probed by a.c. EIS. We show below that this film transformation is strongly associated with the formation of potential-induced defects in *n*-alkylthiol SAMs and that these disruptions are not completely reversible.

The equivalent circuit in Figure 3.2b is used for $CH_3(CH_2)_nS$/Au SAMs (n = 7-15) when $V_{appl} \leq V_c$ and yields a good fit (solid lines) to the experimental data (symbols) (Figures 3.1, 3.3, and 3.4). This equivalent circuit is also appropriate in describing corrosion processes in polymer-coated metals,[52] water up-take during polymer degradation,[53] oxygen diffusion into *n*-alkylthiol SAMs adsorbed onto copper,[54] and Cs^+ selective transport in s-BLMs doped with Gramicidin D.[22] The CNLS fit provides also the value of each component (C_m, R_m, C_d, and R_d) in the equivalent circuit (Table 3.1). The SAM capacitance (C_m) is not affected by the applied potential over the range of + 0.4 V to – 0.5 V (*vs.* Ag/AgCl), as per cyclic voltammetry studies.[55-60] The other parameters (R_m, C_d and R_d) do however vary with V_{appl}.

The SAM resistance, R_m, reflects the ion/water migration within the SAM. R_m is affected by the formation or enhancement of defects and gradually decreases as V_{appl} becomes increasingly cathodic. R_d describes the ease of moving an ion from the interface to the SAM,[31,33] given that R_d in lipid membrane studies is a phase transfer resistance associated with the transport of ions from the solution into the membrane. As the applied electric field increases in magnitude, the energy required for ion transfer into the SAM decreases, leading to a substantial decrease in R_d. The capacitance of defects, C_d, reflects the ability of the SAM to store ions. C_d increases when V_{appl} is polarized at increasingly cathodic potentials.

The nature of the dependences of R_m, R_d, and C_d on V_{appl} indicates that the electric field induces molecular changes at the SAM/electrolyte interface and facilitates the permeation of water molecules and/or ions into the film. These experimental results do not however allow one to explicitly describe the sort of "defect" that has been formed. Extreme descriptions might include pores or holes. For BLMs, these sites of facilitated diffusion are believed to be microscopic regions of high-to-medium dielectric constants that permit ion transport across the bilayer.[61]

It is important to emphasize that the critical potential, V_c, described here is clearly not due to the cathodic electrodesorption of the individual $CH_3(CH_2)_nS$ chains from the gold substrate. Table 3.2 summarizes the literature reductive electrodesorption potentials (E_p) of alkanethiols adsorbed onto both Au single crystals and polycrystalline Au. E_p is chainlength dependent and ranges from – 0.73 V ($n = 2$) to – 1.35 V (n = 17). Clearly, the values of the electrodesorption potentials are considerably more cathodic than V_c values reported here. The variation in E_p[62] has been suggested to arise from *i)* the decrease in solubility of the desorbed molecule as n increases,[35,39] *ii)* a dependence of the potential gradient across the SAM on n,[34] and *iii)* a chainlength dependence of the SAM permeability towards the electrolyte.[63] This later possibility, which has not yet been thoroughly investigated, would suggest that the hydrocarbon chainlength controls the ease with which ions can be partitioned into the SAM. From that perspective, the critical potential (V_c) observed by a.c. impedance spectroscopy can most probably be viewed as a precursor to the electrodesorption process observed in the – 1.1 to –1.4 V region.

3.3.2 Timescale of Processes in SAMs

The timescale of chemical and electrochemical processes is a key factor in the electrochemical characterization of SAMs. The electrical subcircuit (C_d in parallel to R_d) accounts for the SAM modification induced by the d.c. applied voltage at $V_{appl} \leq V_c$, while the main circuit accounts for the properties of the intact SAM (Figure 3.2b).

Chainlength, *n* $CH_3(CH_2)_nS/Au$	E_p V *vs.* Ag/AgCl	Experimental Conditions	Reference
2	– 0.73	0.5 M KOH, Au(111)	[a]
3	– 0.80	0.1 M $KClO_4$/KOH, pH 10.5	[b]
	– 0.89	0.5 M KOH, polycrystalline Au	[c]
5	– 1.05	0.5M KOH, polycrystalline Au	[d]
7	– 0.96	0.5M KOH, polycrystalline Au	[c]
8	– 1.00	0.1 M $KClO_4$/KOH, pH 10.5	[b]
	– 0.96	0.1 M KOH, Au(111)	[e]
	– 1.00	0.1 M KOH, Au(111)	[f]
10	– 1.07	0.5 M KOH, Au(111)	[a]
13	– 1.10	0.10 M KOH, Au(111)	[g]
15	– 1.11	0.1 M $KClO_4$/KOH, pH 10.5	[b]
	– 1.06	0.5 M KOH, quasi-Au(111)	[h]
17	– 1.35	0.5M KOH, polycrystalline Au	[d]

[a]Imabayashi, S.-I.; Iida, M.; Hobara, D.; Feng, Z. Q.; Niki, K.; Kakiuchi, T. *J. Electroanal. Chem.* **1997**, *428*, 33-38. [b]Yang, D.-F.; Wilde, C. P.; Morin, M. *Langmuir* **1997**, *13*, 243-249. [c]Walczak, M. M.; Alves, C. A.; Lamp, B. D.; Porter, M. D. *J. Electroanal. Chem.* **1995**, *396*, 103-114. [d]Widrig, C. A.; Chung, C.; Porter, M. D. *J. Electroanal. Chem.* **1991**, *310*, 335-359. [e]Yang, D.-F.; Al-Maznai, H.; Morin, M. *J. Phys. Chem. B.* **1997**, *101*, 1158-1166. [f]Yang, D.-F.; Wilde, C. P.; Morin, M. *Langmuir* **1996**, *12*, 6570-6577. [g]Badia, A.; Arnold, S.; Scheumann, V.; Zizlsperger, M.; Mack, J.; Jung, G.; Knoll, W. *Sensors and Actuators B* **1999**, *54*, 145-165. [h]Nishizawa, M.; Sunagawa, T.; Yoneyama, H. *J. Electroanal. Chem.* **1997**, *436*, 213-218.

Table 3.2 Literature cathodic electrodesorption potentials (E_p) of $CH_3(CH_2)_nS/Au$ SAMs. These E_p values were obtained from cyclic voltammetry studies in alkaline solution.

The product $(R_dC_d)^{-1}$ yields the dielectric relaxation frequency, ν_d. ν_d has been used in the experimental characterization of polymers and ion-selective membranes and describes the rate at which a film can be charged (and discharged) by ions originating from the electrolyte. The relaxation frequency ν_d here is found to be strongly potential dependent and is (modestly) thickness dependent (Table 3.1). At − 0.5 V (*i.e.* at $V_{appl} < V_c$), where defects are created in $CH_3(CH_2)_nS/Au$ (n = 7-15) SAMs, ν_d varies between 4 and 100 Hz. These values are similar to those previously reported for 4'-hydroxy-4-mercaptobiphenyl and ω-hydroxydecanethiol SAMs (1-10 Hz).[64]

The value of the relaxation frequency, ν_d, calculated using the equivalent circuit in Figure 3.2b can also be directly estimated from the Bode phase plots (φ *vs.* f). The onset of the decrease of φ, from 88-89° at $f < \sim 100$ Hz (shown by arrows in Figures 3.1a-4a), to smaller values is at about the same relaxation frequency values calculated from CNLS data fits (Table 3.1). No specific features can however be observed at ν_d in the other types of impedance plots ($|Z|$ *vs.* f or Z'' *vs.* Z'). The behavior of φ over a wide frequency domain thus provides a unique and direct tool for the characterization of SAMs, and shows that important information can be obtained without resorting to an equivalent circuit analysis. The relaxation frequency ν_d is only obtained when $V_{appl} \leq V_c$ and corresponds to the SAM having a contaminating resistive component associated with the formation of defects.

It is important to note that the time during which a SAM is poised at $V_{appl} \leq V_c$ could be important. Many electrochemical studies of SAMs use relative to very fast potential cycling and potential limits which greatly exceed the V_c values determined here. We do not know as yet what the relationship between the extent of damage and the residence time in the $V_{appl} \leq V_c$ region is. This issue is currently under investigation.

3.3.3 Reversibility of the Potential-Induced Defects

As described, V_{appl} alters the SAM/electrolyte interface in a chainlength dependent fashion. The changes observed in φ, R_m, C_d, R_d and ν_d at $V_{appl} \leq V_c$ are

consistent with the size and/or the number of the local defects becoming more and more pronounced as V_{appl} increases in magnitude.

The reversibility of the potential-induced perturbation was studied by returning each SAM (n = 7-15) to 0 V immediately after the polarization at – 0.5 V (*vs.* Ag/AgCl). Plots of φ *vs.* f obtained at – 0.5 V (Figure 3.5, open symbols) and subsequently at 0 V (filled symbols) suggest that the d.c. potential induces changes which are partially reversible since φ_{1Hz} returns to a large extent (> 81°) to its maximum value (≥ 88°). This is a good indication that $CH_3(CH_2)_nS$/Au SAMs are substantially but not completely restored to their initial electrical function. The potential excursion to $V_{appl} < V_c$ causes the SAM capacitance, C_m, to increase 8-fold (from 1.46 μF cm^{-2} at – 0.5 V to 11.7 μF cm^{-2}) for n = 7 and 7-fold (from 1.24 μF cm^{-2} at – 0.5 V to 9.3 μF cm^{-2}) for n = 9. The change in C_m is negligible however for n = 11 (from 1.27 to 1.28 μF cm^{-2}) and for n =15 (from 0.96 μF cm^{-2} to 0.99 μF cm^{-2}). Small irreversible changes in the SAM structure but permanent ion insertion into the SAM at $V_{appl} \leq V_c$ are consistent with these changes in C_m. Ion insertion is clearly more pronounced for $n \leq 9$.

3.4 Conclusions and Overview

Detailed a.c. impedance spectroscopy measurements reveal unique electrochemical properties of *n*-alkylthiols SAMs formed on polycrystalline gold surfaces. Of particular note here is that a hitherto unreported change in these SAMs is detectable using a.c. EIS. This change is potential induced. At potentials more anodic than the critical potential (V_c), SAMs (n = 7-15) are ionic insulators. A SAM transformation is observed at applied potentials more cathodic than V_c and is associated with the formation of potential-induced defects. These defects render the SAM permeable to electrolyte ions and/or water at $V_{appl} < V_c$. For *n*-alkylthiol SAMs (n = 7-15), V_c is chainlength dependent and occurs between – 0.15 and – 0.35 V *vs.* Ag/AgCl, potentials distant from the Faradaic reaction due to the reductive thiol electrodesorption.

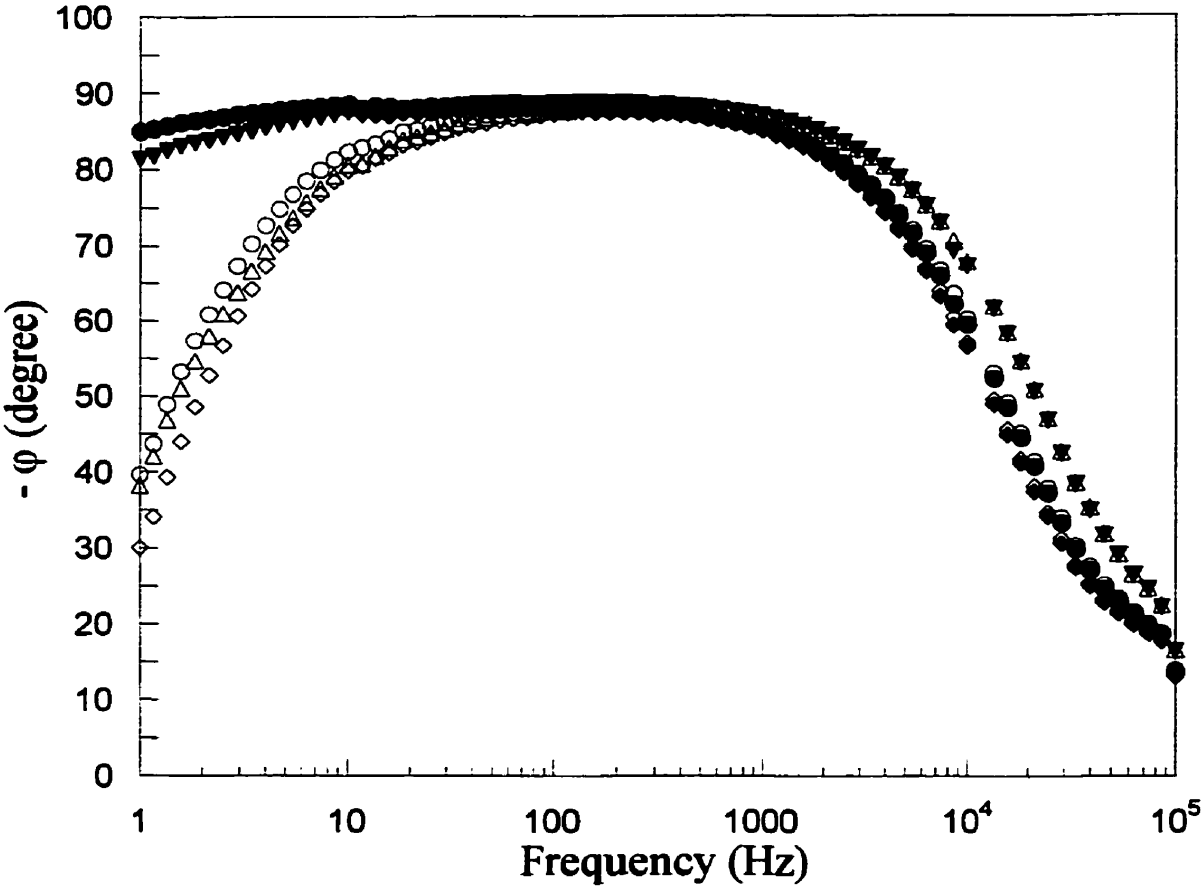

Figure 3.5 Investigation of the reversibility of potential-induced defects for $CH_3(CH_2)_nS$/Au SAMs for n = 7 (◊), n = 11 (o), and n = 15 (Δ) at − 0.5 V (open symbols) followed by d.c. polarization at 0 V (filled symbols). For defect-free SAMs, the phase angle at $f < \sim 30$ Hz remains ≥88°.

The chainlength dependence of V_c is consistent with the change being related to the electrical breakdown experienced by thin organic films and lipid membranes in particular. An awareness of the sensitivity of a SAM to potential-induced structural changes is particularly important given that many electrochemistry/redox probe studies (unknowingly) traverse V_c during measurement.

A detailed analysis of an appropriate equivalent circuit at various applied d.c. potentials leads to a relationship between each electrical component and the microstructural/molecular changes at the interface and/or inside the SAM. At $V_{appl} \leq V_c$, Bode phase plots (φ *vs.* f) access the relaxation frequency ν_d of ion diffusion-related phenomena in $CH_3(CH_2)_nS$/Au SAMs, where ν_d is typically between 4 Hz and 100 Hz. The potential-induced defects are not completely reversible over the timescale of these experiments.

The a.c. EIS experiment provides a unique view of SAMs including the observation of structural transition. It is particularly powerful because it is capable of deconvoluting the electrical properties of the system from electrode kinetics. Our ongoing work involves further characterization of the SAM change noted here and how it affects SAM performance.

References

1) Evans, S. D.; Ulman, A. *Chem. Phys. Lett.* **1990**, *170*, 462-466.

2) Cohen, R.; Bastide, S.; Cahen, D.; Libman, J.; Shanzer, A.; Rosenwaks, Y. *Opt. Mater.* **1998**, *9*, 394-400.

3) Campbell, I. H.; Rubin, S.; Zawodzinski, T. A.; Kress, J. D.; Martin, R. L.; Smith, D. L.; Barashkov, N. N.; Ferraris, J. P. *Phys. Rev. B* **1996**, *54*, R14321-R14324.

4) Janata, J.; Josowicz, M. *Anal. Chem.* **1997**, *69*, 293A-296A.

5) Novotny, V. J.; Karis, T. E. *Appl. Phys. Lett.* **1997**, *71*, 52-54.

6) Zenou, N.; Zelichenok, A.; Yitzchaik, S.; Cohen, R.; Cahen, D. *ACS Symp. Ser.* **1998**, *695*, 57-66.

7) Zehner, R. W.; Parsons, B. F.; Hsung, R. P.; Sita, L. R. *Langmuir* **1999**, *15*, 1121-1127.

8) Collet, J.; Vuillaume, D. *Appl. Phys. Lett.* **1998**, *73*, 2681-2683.

9) Vuillaume, D.; Fontaine, P.; Collet, J.; Deresmes, D.; Garet, M.; Rondelez, F. *Microelectron. Eng.* **1993**, *22*, 101-104.

10) Stora, T.; Lakey, J. H.; Vogel, H. *Angew. Chem., Int. Ed. Engl.* **1999**, *38*, 389-392.

11) Terrettaz, S.; Stora, T.; Duschl, C.; Vogel, H. *Langmuir* **1993**, *9*, 1361-1369.

12) Stelzle, M.; Weissmuller, G.; Sackmann, E. *J. Phys. Chem.* **1993**, *97*, 2974-2981.

13) Raguse, B.; Braach-Maksvytis, V.; Cornell, B. A.; King, L. G.; Osman, P. D. J.; Pace, R. J.; Wieczorek, L. *Langmuir* **1998**, *14*, 648-659.

14) Gafni, Y.; Weizman, H.; Libman, J.; Shanzer, A.; Rubinstein, I. *Chem. Eur. J.* **1996**, *2*, 759-766.

15) Finklea, H. O. *Electrochemistry of Organized Monolayers of Thiols and Related Molecules on Electrodes*; Marcel Dekker: New York, 1996; Vol. 19; Chapter 2.

16) Finklea, H. O.; Snider, D. A.; Fedyk, J.; Sabatini, E.; Gafni, Y.; Rubinstein, I. *Langmuir* **1993**, *9*, 3660-3667.

17) Amatore, C.; Savéant, J. M.; Tessier, D. *J. Electroanal. Chem.* **1983**, *147*, 39-51.

18) Nahir, T. M.; Bowden, E. F. *Electrochim. Acta* **1994**, *39*, 2347-2352.

19) Sluyters-Rehbach, M.; Sluyters, J. H. *Sine wave methods in the study of electrode process*; Marcel Dekker:, 1970; Vol. 4.

20) Badia, A.; Back, R.; Lennox, R. B. *Angew. Chem., Int. Ed. Engl.* **1994**, *33*, 2333-2334.

21) Alonso-Romanowski, S.; Gassa, L. M.; Vilche, J. R. *Electrochim. Acta* **1995**, *40*, 1561-1567.

22) Steinem, C.; Janshoff, A.; Ulrich, W.-P.; Sieber, M.; Galla, H.-J. *Biochim. Biophys. Acta* **1996**, *1279*, 169-180.

23) Gassa, L. M.; Vallejo, A. E.; Alonso-Romanowski, S.; Vilche, J. R. *Bioelectrochem. Bioenerg.* **1997**, *42*, 187-192.

24) Steinem, S.; Janshoff, A.; Wegener, J.; Ulrich, W.-P.; Willenbrink, W.; Sieber, M.; Galla, H.-J. *Biosens. Bioelectron.* **1997**, *12*, 787-808.

25) Gritsch, S.; Nollert, P.; Jahnig, F.; Sackmann, E. *Langmuir* **1998**, *14*, 3118-3125.

26) Steinem, C.; Janshoff, A.; von dem Bruch, K.; Reihs, K.; Goossens, J.; Galla, H.-J. *Bioelectrochem. Bioenerg.* **1998**, *45*, 17-26.

27) de Levie, R.; Seidah, N. G.; Larkin, D. *J. Electroanal. Chem.* **1974**, *49*, 153-159.

28) de Levie, R. *J. Electroanal. Chem.* **1975**, *58*, 203-216.

29) de Levie, R. *Adv. Chem. Phys.* **1978**, *37*, 99-137.

30) Ding, L.; Li, J.; Wang, E.; Dong, S. *Thin Solid Films* **1997**, *293*, 153-158.

31) Steinem, C.; Janshoff, A.; Galla, H.-J.; Sieber, M. *Bioelectrochem. Bioenerg.* **1997**, *42*, 213-220.

32) Schulze, K.-D. *Chem. Phys.* **1998**, *238*, 495-505.

33) Vallejo, A. E.; Gervasi, C. A.; Gassa, L. M. *Bioelectrochem. Bioenerg.* **1998**, *47*, 343-348.

34) Walczak, M. M.; Alves, C. A.; Lamp, B. D.; Porter, M. D. *J. Electroanal. Chem.* **1995**, *396*, 103-114.

35) Yang, D.-F.; Wilde, C. P.; Morin, M. *Langmuir* **1997**, *13*, 243-249.

36) Yang, D.-F.; Al-Maznai, H.; Morin, M. *J. Phys. Chem. B.* **1997**, *101*, 1158-1166.

37) Yang, D.-F.; Wilde, C. P.; Morin, M. *Langmuir* **1996**, *12*, 6570-6577.

38) Imabayashi, S.-I.; Iida, M.; Hobara, D.; Feng, Z. Q.; Niki, K.; Kakiuchi, T. *J. Electroanal. Chem.* **1997**, *428*, 33-38.

39) Badia, A.; Arnold, S.; Scheumann, V.; Zizlsperger, M.; Mack, J.; Jung, G.; Knoll, W. *Sens. Actuators B* **1999**, *54*, 145-165.

40) Nishizawa, M.; Sunagawa, T.; Yoneyama, H. *J. Electroanal. Chem.* **1997**, *436*, 213-218.

41) Lang, H.; Duschl, C.; Vogel, H. *Langmuir* **1994**, *10*, 197-210.

42) Zha, F. F.; Coster, H. G. L.; Fane, A. G. *J. Membrane Sci.* **1994**, *93*, 255-271.

43) Macdonald, J. R. *Complex Nonlinear Least Squares Immittance Fitting Program, LEVM 7.0*; Macdonald, J. R., Ed.: Department of Physics and Astronomy, University of North Carolina, Chapel Hill, NC., 1990.

44) Macdonald, J. R. *Impedance Spectroscopy*; Wiley: New York, 1987.

45) Furniss, B. S.; Hannaford, A. J.; Rogers, V.; Smith, P. W. G.; Tatchell, A. R. *Vogel's Textbook of Practical Organic Chemistry*; 4th ed.; Longman: New York, 1978.

46) McAdams, E. T.; Jossinet, J. *Physiol. Meas.* **1995**, *16*, A1-A13.

47) Boubour, E.; Lennox, R. B. *Langmuir. In press* **2000**.

48) Helmholtz, H. *Ann. Phys.* **1879**, *7*, 337-382.

49) Halliday, D.; Resnick, R. *Physics*; Wiley: New York, 1978.

50) Piela, B.; Wrona, P. K. *J. Electroanal. Chem.* **1995**, *388*, 69-79.

51) Hagenstrom, H.; Schneeweiss, M. A.; Kolb, D. M. *Langmuir* **1999**, *15*, 2435-2443.

52) Mansfeld, F. *Electrochim. Acta* **1993**, *38*, 1891-1897.

53) Mitton, D. B.; Latanasion, R. M.; Bellucci, F. *J. Electrochem. Soc.* **1996**, *143*, 3307-3316.

54) Jennings, G. K.; Munro, J. C.; Yong, T.-H.; Laibinis, P. E. *Langmuir* **1998**, *14*, 6130-6139.

55) Sondag-Huethorst, J. A. M.; Fokkink, L. G. L. *Langmuir* **1992**, *8*, 2560-2566.

56) Sondag-Huethorst, J. A. M.; Fokkink, L. G. L. *J. Electroanal. Chem.* **1994**, *367*, 49-57.

57) Sondag-Huethorst, J. A. M.; Fokkink, L. G. L. *Langmuir* **1995**, *11*, 2237-2241.

58) Porter, M. D.; Bright, T. B.; Allara, D. L.; Chidsey, C. E. D. *J. Am. Chem. Soc.* **1987**, *109*, 3559-3568.

59) Becka, A. M.; Miller, C. J. *J. Phys. Chem.* **1993**, *97*, 6233-6239.

60) Swietlow, A.; Skoog, M.; Johansson, G. *Electroanalysis* **1992**, *4*, 921-928.

61) Miyamoto, V. K.; Thompson, T. E. *J. Colloid Interf. Sci.* **1967**, *25*, 16-25.

62) Widrig, C. A.; Chung, C.; Porter, M. D. *J. Electroanal. Chem.* **1991**, *310*, 335-359.

63) Yang, D.-F.; Wilde, C. P.; Morin, M. *Langmuir* **1997**, *13*, 243-249.

64) Janek, R. P.; Fawcett, W. R.; Ulman, A. *J. Phys. Chem. B* **1997**, *101*, 8550-8558.

Chapter 4

The Dependence of ω-Functionalized SAMs Stability on Applied Potential Monitored by A.C. Impedance Spectroscopy*

4.1 Introduction

The manner in which an applied potential affects the interfacial properties of ω-functionalized self-assembled monolayers (SAMs) is rarely discussed in the extensive SAM literature, even though many SAM studies use broad potential windows (> ± 0.5 V *vs.* Ag/AgCl) in cyclic voltammetry experiments.[1-6] In previous studies, we have described how a.c. EIS can be used to monitor the electrochemical stability of *n*-alkylthiol SAMs of various chainlengths ($CH_3(CH_2)_nSH$, n = 7-15) as a function of potential (V_{appl}) in the absence of a redox active species.[7,8] *n*-Alkylthiols SAMs were shown to be impermeable to electrolyte and are therefore ionic insulators at the sub-microscopic scale, provided that the $CH_3(CH_2)_nS$/Au SAM electrode is poised only at moderate potentials (– 0.15 V < V_{appl} < + 0.4 V, *vs.* Ag/AgCl). Under these potential conditions, *n*-alkylthiol SAMs adhere to the Helmholtz ideal capacitor model and fit a simple equivalent circuit involving a solution resistance in series with a capacitor (I in Figure 4.1).[9,10] Values of the phase angle, φ, of ≥ 88° at 1 Hz < f < 50 Hz indicate that a given SAM is an ionic insulator.

$CH_3(CH_2)_nS$/Au SAMs are transformed from being pure ionic insulators to being leaky once a critical potential, V_c, is exceeded.[7] Significant changes in both the

* Reproduced with permission from *Langmuir*, submitted for publication. Unpublished work, copyright 2000 American Chemical Society.

φ_{1Hz} and the SAM resistance are observed when $V_{appl} \leq V_c$, *i.e.* at potentials more cathodic than V_c. These changes suggest that potential-induced defects which cause ion and water diffusion are formed in the SAM. When V_{appl} becomes increasingly more cathodic than V_c, the density of defects increases and the SAM resistance decreases. For $X = CH_3$, the value of V_c is chainlength dependent and varies from – 0.15 V *vs.* Ag/AgCl (n = 7) to – 0.35 V (n = 15). The potential-induced defects formed in $CH_3(CH_2)_nS$/Au SAMs are not completely reversible.

The equivalent circuit that best describes $CH_3(CH_2)_nS$/Au SAMs bearing potential-induced defects (II in Figure 4.1) is the same as that used to describe ion/solvent uptake into polymer-coated metal electrodes and polymer degradation studies,[11,12] oxygen diffusion in SAMs,[13] and Cs^+ transport in supported bilayer lipid membranes doped with Gramicidin D.[14]

A number of studies have shown that SAMs form robust structures due to the contribution from the Au-S bond, interchain van der Waals forces and headgroup interactions.[15] The presence of the terminal functional group X at the outer surface affects the polarity and the wettability of SAMs, rendering the surface hydrophilic with X = OH or CO_2H, and hydrophobic with CH_3 or CF_3.[1,16,17] For X = OH and CO_2H, the impact of H-bonding on the SAM structure is not, however, well described.[18] Electrochemical studies show that the hydrogen bond network stabilizes the SAM,[3] whereas contact angle measurements for X = OH show that the chain end undergoes a time-dependent reorganization.[19]

In this study, we expand upon our earlier methodology developed for *n*-alkylthiol SAMs and investigate the ionic permeability of $X(CH_2)_nS$/Au SAMs (X = CH_3, OH, CO_2H) and of a fluorinated ($HS(CH_2)_2(CF_2)_7CF_3$) thiol SAM, all measured in the absence of a redox active species.[20] The variation in the terminal functional group reveals how the chemical composition of the SAM/electrolyte interface plays an important role in the penetration of ions into the hydrocarbon SAM region.

4.2 Experimental Section

Materials. Hexadecanethiol was synthesized from 1-bromohexadecane (97 %, Aldrich) by standard procedures and was available from previous studies.[21] $HS(CH_2)_{15}CH_3$: m.p. 19.5-21 °C; TLC (silica gel, *n*-hexane): $R_f = 0.7$; ^1H NMR (500 MHz, $CDCl_3$): δ 2.52 (q, 2H, CH_2SH), 1.58 (m, 2H CH_2CH_2SH), 1.40 (m, 2H, $CH_2CH_2CH_2SH$), 1.31 (t, 1H, CH_2SH), 1.24 (s, 24H, $(CH_2)_{12}$), 0.87 (t, 3H, CH_3).

16-Hydroxyhexadecanethiol was synthesized from 1,16-hexadecanediol (≥ 98 %, Fluka) following the procedure reported by Becka and Miller.[3]
$HS(CH_2)_{15}CH_2OH$: m.p. 52.5-54 °C; TLC (silica gel, 12:88 (w/w) ethyl acetate:chloroform): $R_f = 0.5$; ^1H NMR (500 MHz, $CDCl_3$): δ 3.62 (t, 2H, CH_2OH), 2.56 (q, 2H, CH_2SH), 1.55 (m, 4H, CH_2CH_2SH, CH_2CH_2OH), 1.31 (t, 1H, CH_2SH), 1.28 (s, 24H, $(CH_2)_{12}$).

16-Mercaptohexadecanoic acid was synthesized from 16-bromohexadecanoic acid which in turn was obtained by refluxing 16-hydroxydecanoic acid (98 %, Aldrich) for two days in a 1:1 mixture of 48 % HBr and glacial acetic acid. 16-Bromohexadecanoic acid (m.p. 70-71 °C) was dissolved in 95 % ethanol with one equivalent of thiourea (Aldrich 99%), and refluxed for 6 hours. The resulting thiouronium salt was hydrolyzed with three equivalents of NaOH by refluxing under a positive nitrogen atmosphere for three hours. Recrystallization from hexanes yielded pure 16-mercaptohexadecanoic acid.
$HS(CH_2)_{15}CO_2H$: m.p. 61-62 °C; ^1H NMR (500 MHz, $CDCl_3$): δ 2.45 (q, 2H, CH_2SH), 2.28 (t, 2H, CH_2CO_2H), 1.55 (m, 4H, CH_2CH_2SH, $CH_2CH_2CO_2H$), 1.25 (t, 1H, CH2S*H*), 1.20 (s, 22H, $(CH_2)_{11}$).

Fluorinated thiol $HS(CH_2)_2(CF_2)_7CF_3$ was obtained from Ciba (Chem Division, Ardsley, New York). The abbreviation CF_3C_9S/Au SAM for monolayers made of $HS(CH_2)_2(CF_2)_7CF_3$ is used for convenience throughout this report.

Dibasic potassium phosphate (ACS grade) was from BDH (Toronto, Canada). The counter electrode was a platinum mesh (Aldrich) and the reference electrode was a Ag/AgCl electrode (3 M NaCl, Bioanalytical Systems Inc., IN).

Procedure. Polycrystalline gold electrodes of 0.020 cm^2 geometric surface area (Bioanalytical Systems Inc., West Lafayette, IN) were mechanically hand polished on microcloth pads (Buehler) with alumina slurries (Buehler) of decreasing particle size (1.0 μm, 0.3 μm and 0.05 μm). The polished electrodes were sonicated in ultra pure water (Milli-Q water system, MA, 18 MΩ cm) in an ultrasonic bath (Branson 1200) for 2 minutes and copiously rinsed with ultra pure water. The electrodes were immediately cleaned with freshly prepared *aqua regia* solution (60:30:10 water:HCl:HNO_3). This step was immediately followed by the electrochemical polishing of the gold surface in degassed 1 M perchloric acid (HPLC grade, BDH) between 0 and + 1.7 V (*vs.* Ag/AgCl) at 80 mV s^{-1}. The electrodes were then thoroughly rinsed with ultra pure water and absolute ethanol (Commercial Alcohols Inc., Canada) prior to incubation in N_2-purged 1 mM $X(CH_2)_nSH$ solution, at room temperature, in sealed vials. The electrodes were incubated for a minimum of 3 days. Prior to each measurement, the SAM coated electrodes were thoroughly rinsed with absolute ethanol followed by ultra pure water. Impedance spectra were obtained at room temperature after a stable open circuit potential was reached. A Teflon cover was used to close the electrochemical cell to position the 3 electrodes in the same manner, minimizing variation from experiment to experiment.

Instrumentation. Impedance measurements were obtained in a conventional 3-electrode electrochemical cell with an EG&G lock-in amplifier (5210) combined to an EG&G PAR 273 potentiostat/galvanostat. Data acquisition was performed using EG&G M398 software. A sinusoidal potential modulation of ± 10 mV amplitude was superimposed on a d.c. potential. The amplitude and the phase shift of the resulting current were recorded at each frequency from 65 kHz to 1 Hz. Fifteen points, equally spaced on a logarithmic scale, were acquired per decade increment in frequency (f).

A $X(CH_2)_nS$/Au SAM is first assessed at + 0.4 V *vs.* Ag/AgCl for its ability to block ion access to the gold surface.[8] This applied potential does not cause changes in either the electrical or electrochemical properties of the SAM. Once a given SAM is shown to be highly impermeable to ions ($\varphi_{1Hz} \geq 88°$) at all electrolyte concentrations (2-50 mM), it is subjected to increasingly cathodic d.c. potentials

(from + 0.4 V to – 0.5 V *vs.* Ag/AgCl) applied in a succession of 0.1 V steps. Impedance data were then transferred to the Zplot/Zview software package (Scribner Associates Inc., NC) and were fitted to an appropriate electrical equivalent circuit using the Complex Nonlinear Least Square (CNLS) Immittance Fitting Program.[22] The symbols on each impedance plot represent the experimental data and the solid lines are the CNLS fits.

4.3 Results and Discussion

This study is focused on how the critical potential (V_c) of ω-functionalized $X(CH_2)_nS$/Au SAMs depends on the chemical speciation of the terminal group (X = CH_3, CF_3, OH, CO_2H). This critical potential (V_c) can be determined for any SAM, where V_c corresponds to the potential at which the Helmholtz ideal capacitor model (equivalent circuit I in Figure 4.1) inadequately describes the experimental data at a given V_{appl}.[8] V_c has been shown to be a transition potential between two structural states of the SAM. The SAM starts in a state which is impermeable to ions when V_{appl} is more anodic than V_c ($V_{appl} > V_c$), and is then transformed to a state which is permeable to ions when V_{appl} is equal to or more cathodic than V_c ($V_{appl} \leq V_c$). Defects are formed when $V_{appl} \leq V_c$ and these are believed to lead to the ion permeability.[7]

$CH_3(CH_2)_nS$/Au SAMs (n = 7-15) prepared in the manner used here fit the Helmholtz ideal capacitor behavior at V_{appl} = + 0.4 V (*vs.* Ag/AgCl) and are ionic insulators at potentials more anodic than V_c.[7,8] The ionic insulating properties of SAMs measured by a.c. EIS are best revealed in Bode phase plots (φ *vs.* f) where φ is defined as $\tan^{-1}(-Z''/Z')$.[23] From an electrical viewpoint, purely capacitive behavior (in the absence of a leakage current) exhibits φ = 90° over the entire frequency domain, while purely resistive behavior exhibits φ = 0°.[23] A SAM is deemed defect-free for practical purposes when $\varphi \geq$ 88° over the 1 Hz - 50 Hz range.[8]

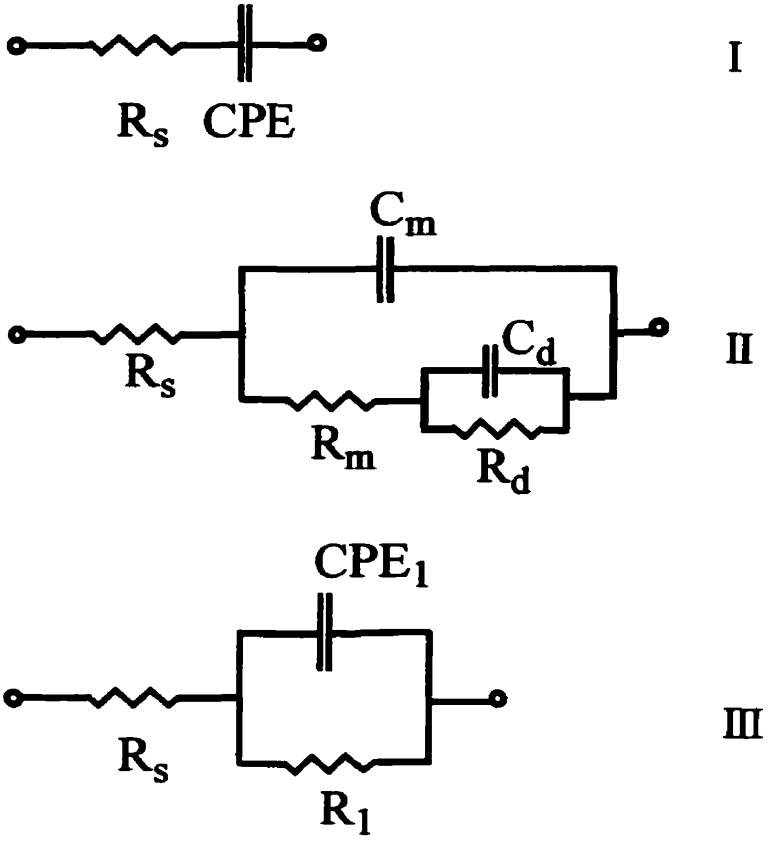

Figure 4.1 Equivalent circuits of a defect-free SAM at V_{appl} more anodic than V_c ($V_{appl} > V_c$) (I), and of SAMs with deliberately formed defects at $V_{appl} \leq V_c$ (II) and (III). Use of equivalent circuit II or III depends on the chemical nature of the functional group ($X = CH_3$, OH, CO_2H or CF_3). R_s is the solution resistance, C_d and R_d are the capacitance and resistance of defects respectively. The SAM capacitance is noted as *CPE*, C_m or CPE_1. R_m and R_1 take into account the presence of ions and/or water into the defect-laden SAMs.

Bode phase plots at + 0.4 V (*vs.* Ag/AgCl) of a $CH_3(CH_2)_{15}S$/Au SAM (Figure 4.2a), a $HO(CH_2)_{16}S$/Au SAM (4.2b), and of a CF_3C_9S/Au SAM (4.2d) are presented over a range of electrolyte concentrations ($[K_2HPO_4]$ = 2-50 mM). The displacement of the Bode phase curves to higher frequencies (*i.e.* at $f > 10^3$ Hz) is associated with the lowering of the solution resistance as the electrolyte concentration is increased. For X = OH, CH_3 and CF_3, φ_{1Hz} is ~ 88-89° at + 0.4 V *vs.* Ag/AgCl, demonstrating that these SAMs are effectively defect-free. These SAMs can be fitted to a simple equivalent circuit involving a solution resistance (R_s) in series with a constant phase element, *CPE*, over the entire range of electrolyte concentrations (equivalent circuit I in Figure 4.1, solid lines in 4.2a, b, d, and Table 4.1). The *CPE* accounts for the SAM capacitance, where the SAM capacitance in 50 mM K_2HPO_4 at V_{appl} = + 0.4 V (*vs.* Ag/AgCl) is 1.11 ± 0.01 μF cm^{-2} for $X = CH_3$ and 1.65 ± 0.01 μF cm^{-2} for X = OH. The OH group dipole at the interface can account for the increase in the capacitance of ω-functionalized SAMs compared to $CH_3(CH_2)_{15}S$/Au SAMs.[24,25] The capacitance of the fluorinated CF_3C_9S/Au SAM is 2.19 ± 0.02 μF cm^{-2}, a value greater than that of the corresponding $CH_3(CH_2)_9S$/Au SAM (1.55 ± 0.01 μF cm^{-2}).[7] For all of these SAMs, the capacitance values remain reasonably constant (3 % < Δ *CPE* < 15 %) as the electrolyte concentration is increased. As expected, the solution resistance R_s has a linear dependence ($r > 0.999$) on the electrolyte concentration.[26]

For $X = CO_2H$, φ at 1 Hz < f < 50 Hz is ~ 85°, as opposed to ≥ 88° observed for the other SAMs studied here (Figure 4.2c). Nonetheless, the minimal equivalent circuit that best fits the experimental data for $X = CO_2H$ is the same as for $X = CH_3$, OH and CF_3 (equivalent circuit I, solid lines in Figure 4.2c, and Table 4.1). This probably reflects the fact that although the $-CO_2H/CO_2^-$ group alters the SAM/electrolyte interface by introducing a hydrogen bond and/or ion pair network, it does not affect the alkyl chain region so markedly so as to cause fundamentally different electrical properties.

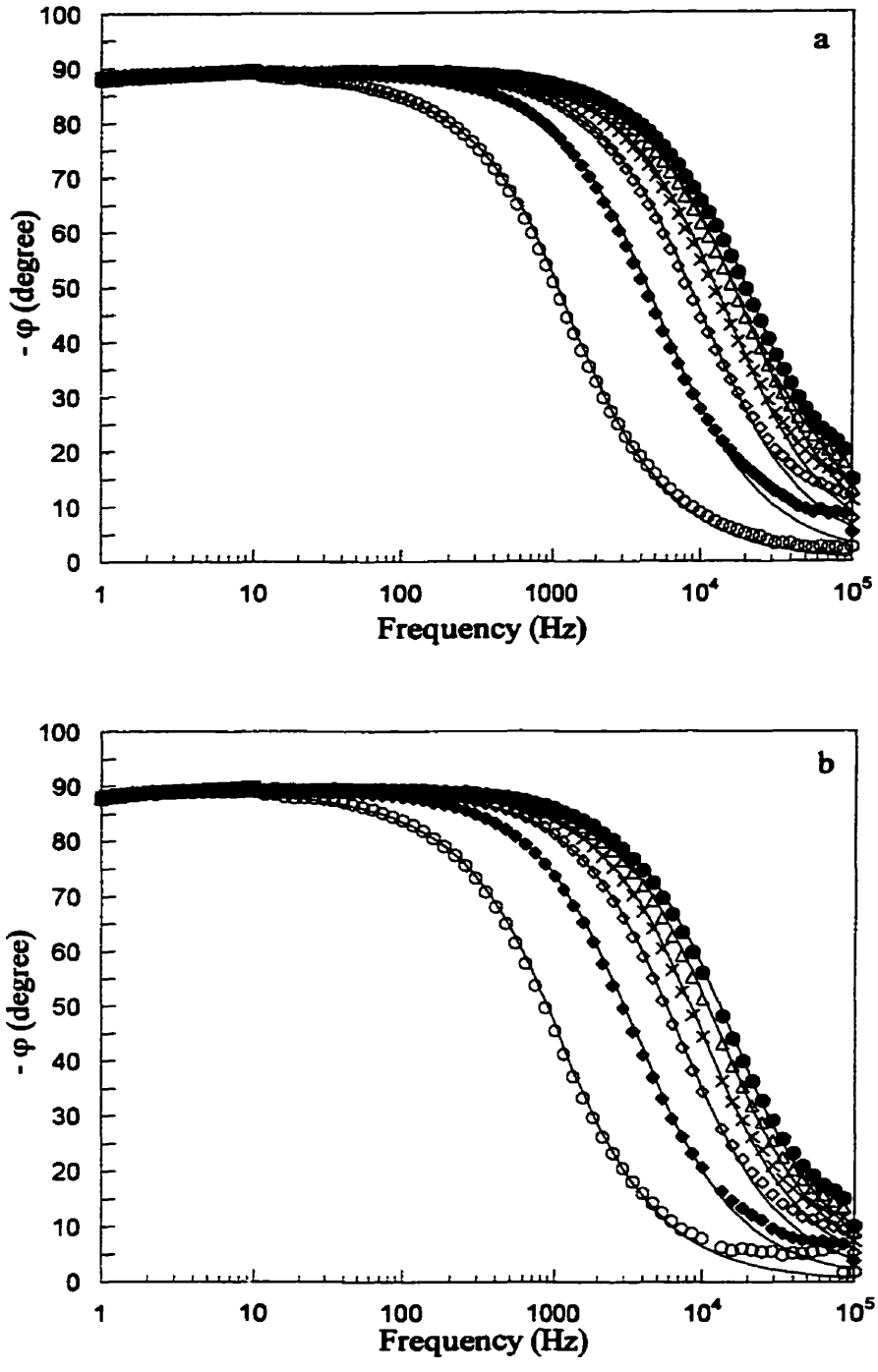

Figure 4.2 Bode phase plots of SAMs at various electrolyte (K_2HPO_4) concentrations at + 0.4 V (*vs.* Ag/AgCl): *a)* $CH_3(CH_2)_{15}S$/Au and *b)* $HO(CH_2)_{16}S$/Au at [K_2HPO_4] = 2mM (O), 10 mM (♦), 20 mM (◊), 30 mM (x), 40 mM (Δ), and 50 mM (•). Symbols are experimental data and solid lines result from CNLS data fits, according to the equivalent circuit I. Fitting parameters are listed in Table 4.1.

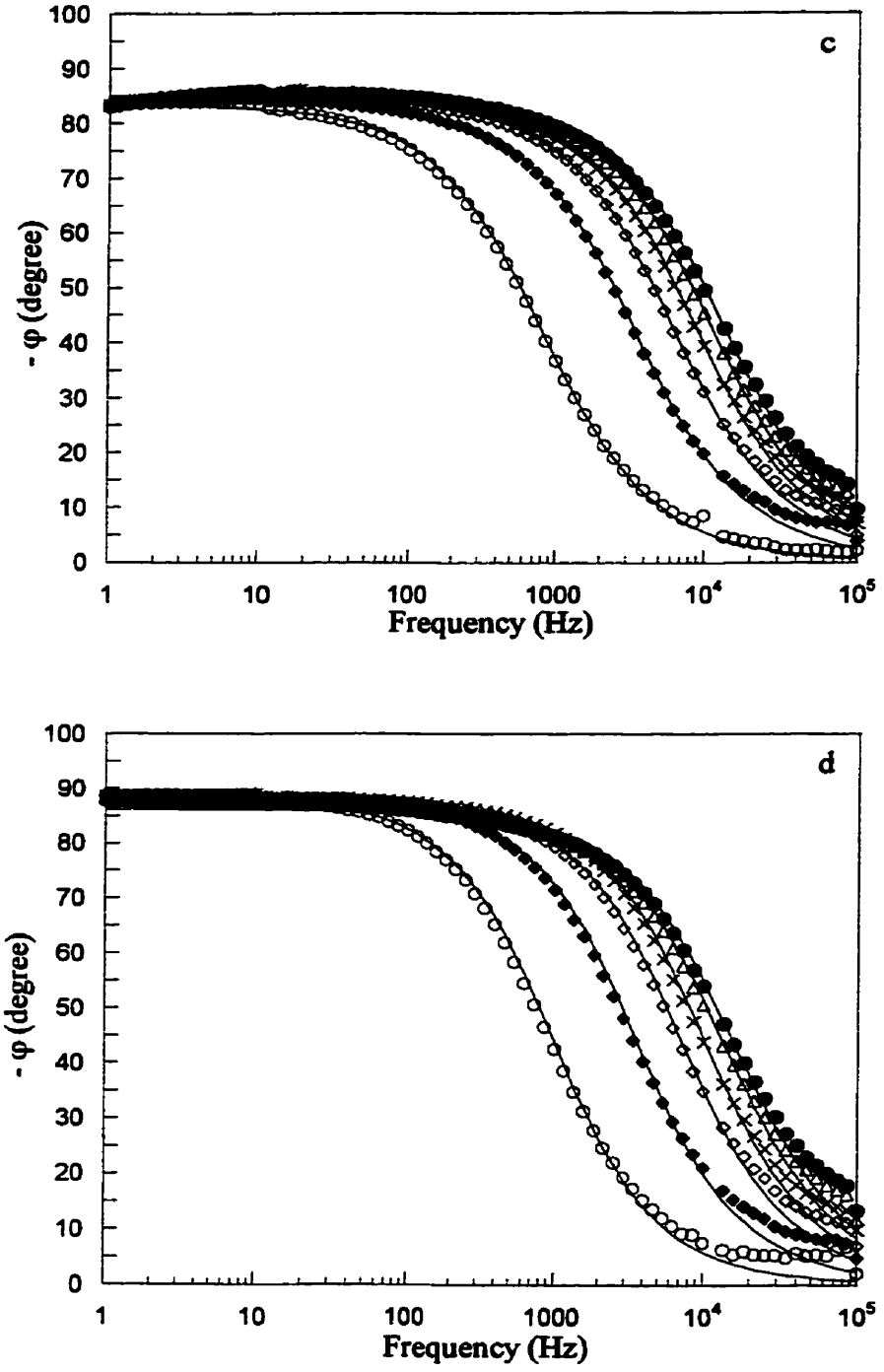

Figure 4.2 (cont'd) *c)* $HO_2C(CH_2)_{15}S/Au$, and *d)* CF_3C_9S/Au SAM.

$[K_2HPO_4]$ mM	R_s Ω cm^2	*CPE* μF cm^{-2}	α
$CH_3(CH_2)_{15}S$/Au SAM			
2	105±0.3	1.29±0.01	0.986±0.001
10	28±0.2	1.21±0.01	0.987±0.001
20	15±0.1	1.17±0.01	0.980±0.001
30	10±0.06	1.14±0.01	0.989±0.001
40	8±0.06	1.12±0.01	0.988±0.001
50	7±0.04	1.11±0.01	0.988±0.001
$HO(CH_2)_{16}S$/Au SAM			
2	95±0.9	1.70±0.03	0.986±0.003
10	26±1	1.63±0.08	0.997±0.001
20	15±0.1	1.66±0.02	0.992±0.001
30	10±0.08	1.66±0.02	0.992±0.001
40	8±0.06	1.66±0.01	0.993±0.001
50	7±0.06	1.65±0.01	0.993±0.001
$HO_2C(CH_2)_{15}S$/Au SAM			
2	106±0.4	3.34±0.03	0.928±0.001
10	26±0.4	3.34±0.06	0.934±0.003
20	15±0.08	3.32±0.02	0.934±0.001
30	10±0.06	3.30±0.02	0.941±0.001
40	8±0.04	3.25±0.02	0.944±0.001
50	7±0.04	3.33±0.02	0.944±0.001
CF_3C_9S/Au SAM			
2	86±0.4	2.14±0.02	0.984±0.001
10	28±0.1	1.93±0.01	0.979±0.001
20	15±0.08	1.84±0.01	0.976±0.001
30	11±0.06	1.83±0.01	0.977±0.001
40	9±0.06	2.03±0.01	0.963±0.001
50	7±0.06	2.19±0.02	0.958±0.001

Table 4.1 CNLS fitting parameters of defect-free $X(CH_2)_nS$/Au and CF_3C_9S/Au SAMs at + 0.4 V (*vs.* Ag/AgCl), at various electrolyte concentrations. The equivalent circuit (I, Figure 4.1) is composed of a solution resistance (R_s) in series with a constant phase element (*CPE*, α).

4.3.1 Determination of the SAM Critical Potential, V_c

As a reference point, and for the purpose of this discussion, the effect of the applied potential on a $CH_3(CH_2)_{15}S$/Au SAM is shown in Figure 4.3.[7] The relevant impedance data are presented in three different formats: the Bode phase plot (φ *vs.* f, 4.3a), Bode plot ($|Z|$ *vs.* f, 4.3b), and Nyquist plot (Z'' *vs.* Z', 4.3c). Between + 0.4 V and – 0.3 V *vs.* Ag/AgCl, φ *vs.* f curves for a $CH_3(CH_2)_{15}S$/Au SAM are superimposable and are characteristic of ideal capacitive behavior given that $\varphi_{1Hz} \geq 88°$ at 1 Hz - 10^3 Hz. For clarity, only the curve + 0.4 V is presented in Figure 4.3a (open circles). Within the potential window of + 0.4 V to – 0.3 V (*vs.* Ag/AgCl), the $CH_3(CH_2)_{15}S$/Au SAM is an ionic insulator and the impedance data fit equivalent circuit I (Figure 4.1).

The critical potential V_c is identified in the Bode phase plot as the potential where φ_{1Hz} deviates markedly from 88°. Interpolation of φ_{1Hz} *vs.* V_{appl} for the $CH_3(CH_2)_{15}S$/Au SAM data yields $V_c \approx -0.35$ V *vs.* Ag/AgCl. Formation of potential-induced defects at $V_{appl} \leq V_c$ (*i.e.* at potentials more cathodic than V_c) leads to ion permeation/diffusion across the SAM. It is evident from the significant decrease in φ at $f < \sim 50$ Hz that the SAM permeability increases as V_{appl} becomes increasingly cathodic from V_c (open diamonds and filled circles in Figure 4.3a). The electrochemical signal changes associated with the formation of potential-induced defects in SAMs are best visualized in φ *vs.* f plots. However, $|Z|$ *vs.* f (3b) and Z'' *vs.* Z' plots (3c) are also displayed since they are more commonly used in the literature to assess thin film properties. It is noteworthy that only the Bode phase plot (φ *vs.* f) provides a distinctive indication that there are substantial changes in the film when V_c is exceeded. The permeability of a $CH_3(CH_2)_{15}S$/Au SAM clearly can be modulated by varying the d.c. applied potential, in a manner only recently described.[7]

The permeability of a $CH_3(CH_2)_{15}S$/Au SAM at potentials beyond V_c (– 0.4 V and – 0.5 V) is well described by equivalent circuit II (Figure 4.1 and solid lines in Figure 4.3). A detailed interpretation of each electrical component (C_m, R_m, C_d, and R_d) is possible (Table 4.2).[7]

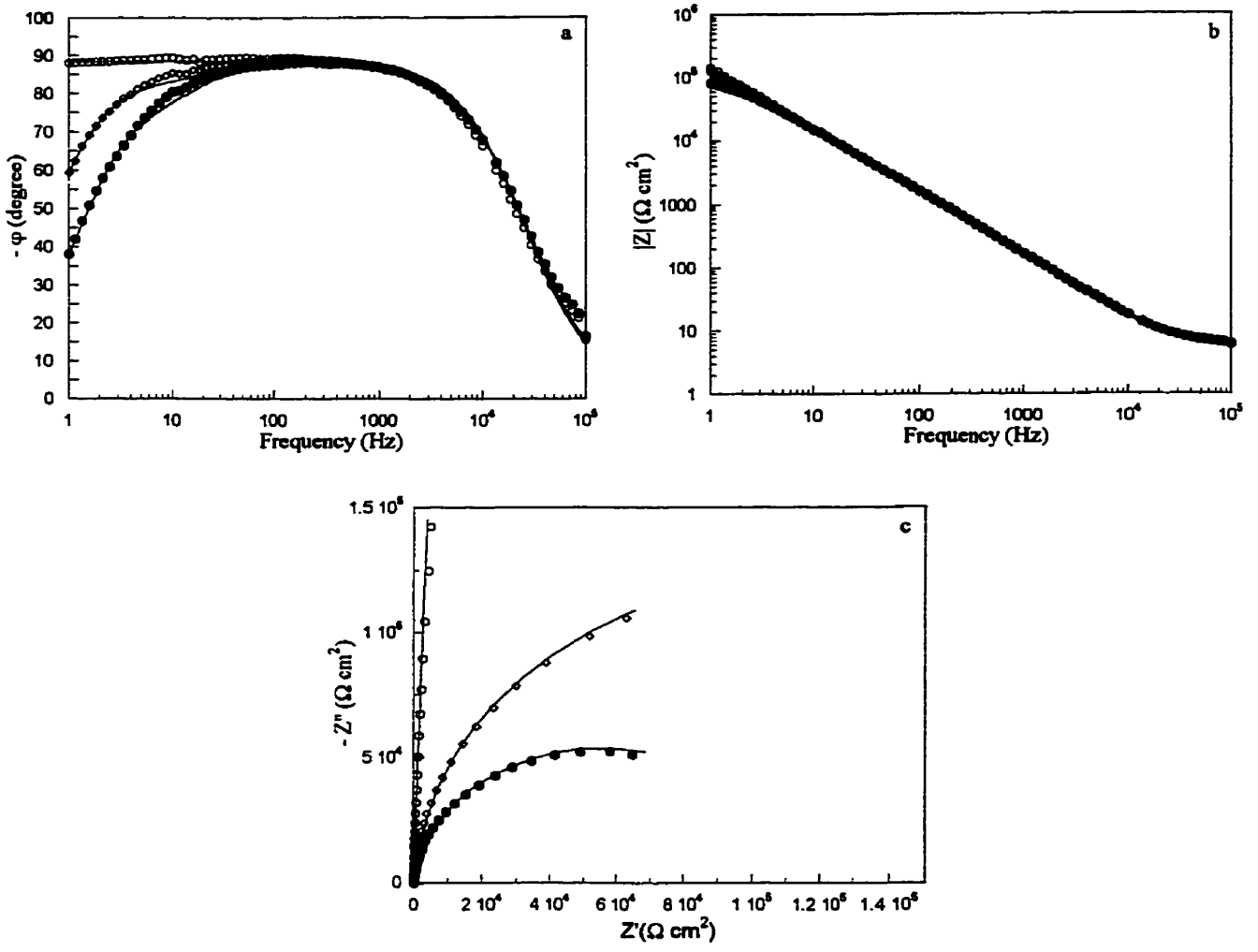

Figure 4.3 *a)* Bode phase plot, *b)* Bode plot, and *c)* Nyquist plot of a $CH_3(CH_2)_{15}S$/Au SAM from + 0.4 V (*vs.* Ag/AgCl) to – 0.3 V(o), at – 0.4 V (◊) and – 0.5 V (•), in 50 mM K_2HPO_4 at pH 7.0. Symbols are experimental data and solid lines result from CNLS data fits. Equivalent circuit I is used at potentials more anodic than V_c ($V_{appl} > V_c$) while II is used when $V_{appl} \leq V_c$. The fitting parameters are listed in Table 4.2.

E V	*CPE* μF cm^{-2}	α	C_m μF cm^{-2}	R_m kΩ cm^2	C_d nF	R_d MΩ	ν_d* Hz
$CH_3(CH_2)_{15}S$/Au SAM							
0.4	1.07±0.03	0.970±0.004					
0.3	1.09±0.01	0.988±0.001					
0.2	1.08±0.01	0.893±0.002					
0.1	1.07±0.01	0.981±0.002					
0	1.01±0.08	1.000±0.010					
− 0.1	1.03±0.06	0.996±0.008					
− 0.2	1.05±0.13	1.000±0.012					
− 0.3	1.11±0.01	0.983±0.002					
− 0.4			0.95±0.01	79±12	5.2±0.8	9±0.7	20±3.1
− 0.5			0.96±0.01	52±5	12±2.2	3±0.2	25±4.5
$HO(CH_2)_{16}S$/Au SAM							
0.4	1.65±0.01	0.993±0.001					
0.3	1.66±0.01	0.992±0.001					
0.2			1.55±0.01	170±46	2.6±0.4	48±10	8 ±1.5
0.1			1.55±0.01	170±37	3.4±0.5	28±4	10±1.5
0			1.55±0.01	135±27	3.9±0.6	19±2	13±2.0
− 0.1			1.55±0.01	110±22	4.1±0.7	16±2	14±2.4
− 0.2			1.55±0.01	110±22	5.2±1.1	11±1	18±3.8
− 0.3			1.55±0.01	66±8	10±2.2	4±0.4	25±5.5
− 0.4			1.56±0.01	40±4	21±5.6	1±0.1	48±13

* $\nu_d = (C_d R_d)^{-1}$. Values for C_d and R_d are not normalized for the electrode surface area.

Table 4.2 Effect of V_{appl} on the interfacial properties of $CH_3(CH_2)_{15}S$/Au and $HO(CH_2)_{16}S$/Au SAMs. Columns 2 (*CPE*) and 3 (α) correspond to the equivalent circuit I ($V_{appl} > V_c$). Columns 4-8 correspond to the equivalent circuit II ($V_{appl} \leq V_c$).

C_m denotes the SAM capacitance; it remains relatively constant at all V_{appl}. R_m is related to the movement of ions and/or water within the SAM. As expected, R_m decreases as V_{appl} becomes increasingly cathodic, most probably due to the appearance of hydrophilic "defects", "pores", or "channels" structures in the SAM. C_d and R_d are both associated with defects formed at $V_{appl} \leq V_c$, and each varies as the size and/or number of defects is increased. C_d increases and R_d decreases as V_{appl} is brought to more cathodic potentials, because ions and/or water can now be stored in the SAM.

As in the case of $CH_3(CH_2)_nS$/Au SAMs, potential-induced defects causing ion penetration can also be deliberately created in both ω-functionalized SAMs (X = OH and CO_2H) and in the CF_3C_9S/Au SAM. For a $HO(CH_2)_{16}S$/Au SAM, φ_{1Hz} is ≅ 89° at both + 0.3 V and + 0.4 V (*vs.* Ag/AgCl), consistent with these SAMs being ionic insulators in their as-prepared form (Figure 4.4). However, at $V_{appl} \leq$ + 0.2 V, φ at 1 Hz < f < 50 Hz is << 89°. V_c is estimated to be + 0.25 V (*vs.* Ag/AgCl) from an interpolation of the φ_{1Hz} *vs.* V_{appl} curve. φ_{1Hz} ranges from 84° (+ 0.2 V) to 20° (– 0.5 V). V_c for X = OH is ~ 0.6 V more anodic than for $X = CH_3$ (*i.e.* – 0.35 V) which in simple energy terms is very large. These results clearly show that ion diffusion/migration at these hydrophilic interfaces is likely to occur given that one is usually operating beyond V_c during cyclic voltammetry experiments in the X = OH SAM.

The experimental data fit equivalent circuit II at $V_{appl} \leq V_c$ for both $X = CH_3$ (solid lines in Figure 4.3) and X = OH (solid lines in Figure 4.4). In both cases, the SAM capacitance, C_m, does not vary with V_{appl}, whereas R_m, R_d and C_d do (Table 4.2). From V_c to – 0.5 V, R_m decreases more significantly for X = OH (4-fold) than for X = CH_3 (1.5-fold), demonstrating that a larger ion flux is triggered in the $HO(CH_2)_{16}S$/Au SAM. From V_c to – 0.5 V, the capacitance of the defects, C_d, increases by 8-fold for X = OH compared to only 2-fold for $X = CH_3$. This reflects the greater capability of the OH-terminated SAM to store ions and/or water.

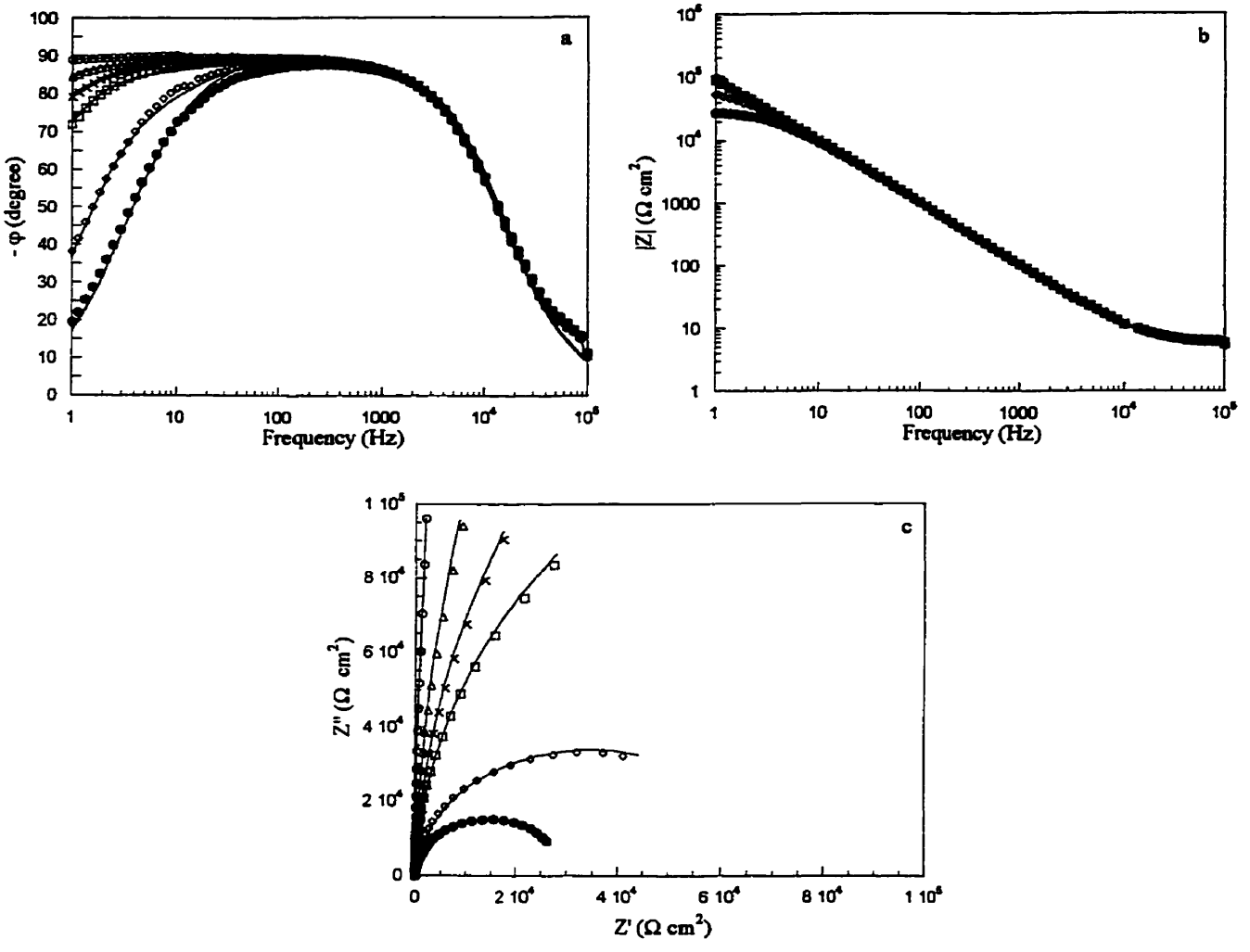

Figure 4.4 *a)* Bode phase plot, *b)* Bode plot, and *c)* Nyquist plot of a $HO(CH_2)_{16}S$/Au SAM from + 0.4 V (*vs.* Ag/AgCl) to + 0.3 V(o), at + 0.2 V (Δ), 0 V (x), – 0.2 V (□), – 0.4 V (◊), and – 0.5 V (•) in 50 mM K_2HPO_4 at pH 7.0. Symbols are experimental data and solid lines result from CNLS data fits. Equivalent circuit I is used at potentials more anodic than V_c ($V_{appl} > V_c$) while II is used when $V_{appl} \leq V_c$. The fitting parameters are listed in Table 4.2.

The value of the relaxation frequency ν_d (at $V_{appl} \leq V_c$), defined by $(C_dR_d)^{-1}$, ranges from 20 Hz to 50 Hz for both X = OH and CH_3 (Table 4.2). ν_d values calculated in Table 4.2 also correspond to the onset of the decrease of φ from 88-89° in φ *vs.* f plots. This generally occurs at $f \leq 50$ Hz.[7] The small values of ν_d suggest that ν_d is associated with a process whose activation barrier is relatively high. This is reasonable, given that ion transport energetics into the lipid phase, estimated using the Born charging equation, can be as high as 255 kJ mol^{-1} for K^+ in $CH_3(CH_2)_nS$/Au SAMs for example.[27] Since ν_d values increase as V_{appl} becomes increasingly cathodic from V_c, the electric field at $V_{appl} \leq V_c$ appears to facilitate ion penetration by lowering the energy barrier in the SAM itself.

In the case of $HO_2C(CH_2)_{15}S$/Au SAMs, φ *vs.* f curves are superimposable from + 0.4 V to + 0.2 V (*vs.* Ag/AgCl). Only the data at + 0.4 V is shown (open circles in Figure 4.5). As previously noticed, φ is ~ 85° at 1 Hz < f < 50 Hz. This SAM is clearly an ionic insulator given that the experimental data successfully fit equivalent circuit (I), involving a solution resistance in series with a *CPE* (solid lines in Figure 4.5). $V_c \cong$ + 0.15 V (*vs.* Ag/AgCl) for $X = CO_2H$, as estimated from Bode phase plots, and is similar to that obtained for X = OH (+ 0.25 V). φ_{1Hz} is 78° at + 0.1 V and falls off to 28° at – 0.5 V. The SAM capacitance is 3 to 3.3 μF cm^{-2} throughout the potential region + 0.4 V to – 0.5 V *vs.* Ag/AgCl (Table 4.3). The equivalent circuit used to describe defect-laden $HO_2C(CH_2)_{15}S$/Au SAMs at $V_{appl} \leq V_c$ (equivalent circuit III, solid lines in Figure 4.5) differs from the one used for both X = CH_3 and X = OH, as the C_dR_d subcircuit in this case is not used. CPE_1 is the SAM capacitance. The leakage current that originates from potential-induced defects leads to a modulation in R_1. From V_c (+ 0.15 V) to – 0.5 V (*vs.* Ag/AgCl), R_1 decreases by 20-fold while CPE_1 only changes slightly (Table 4.3).

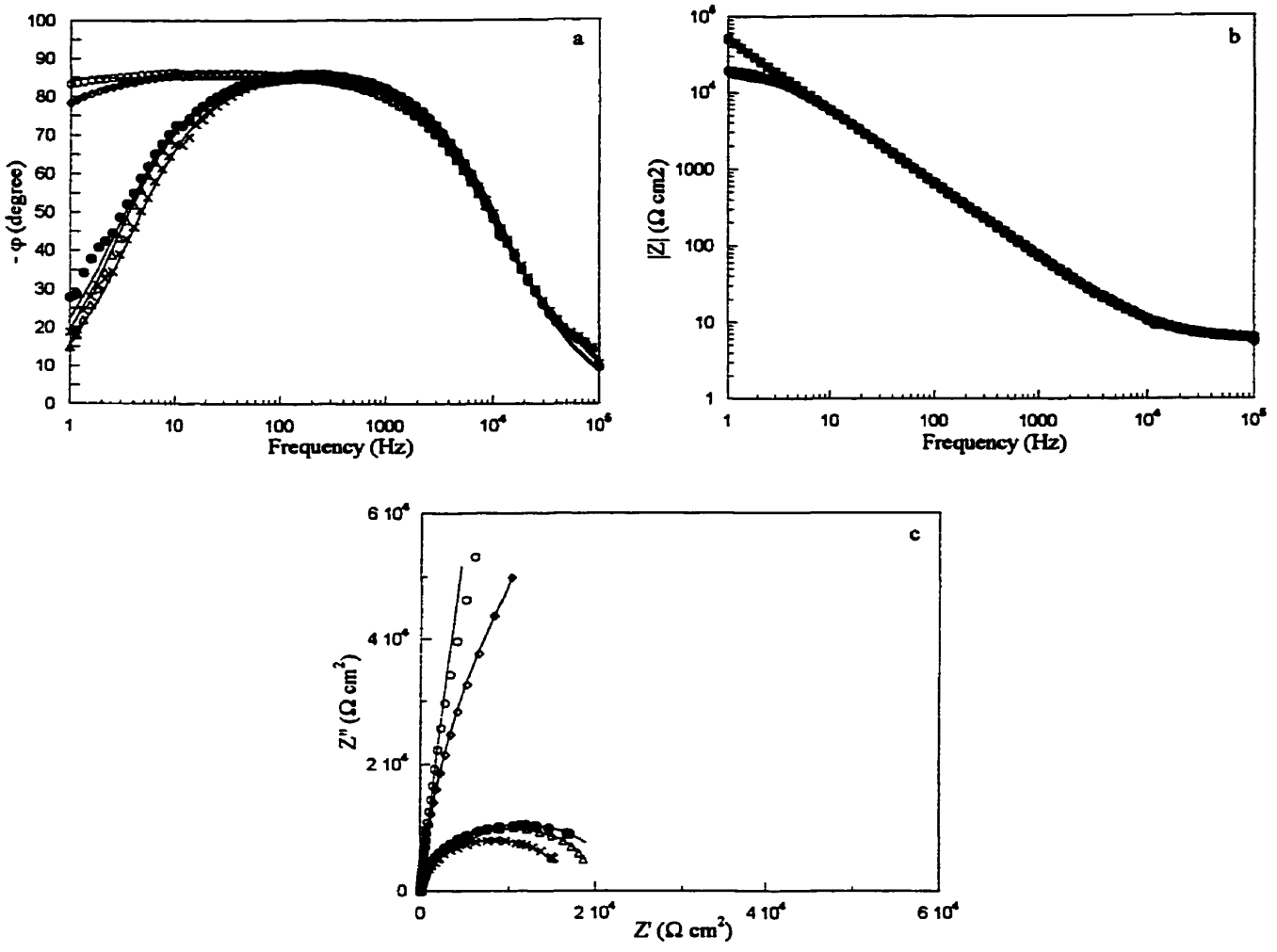

Figure 4.5 *a)* Bode phase plot, *b)* Bode plot, and *c)* Nyquist plot of a $HO_2C(CH_2)_{15}S$/Au SAM from + 0.4 V (*vs.* Ag/AgCl) to + 0.2 V (o), at + 0.1 (◊), – 0.1 V (Δ), – 0.3 V (x), and – 0.5 V (•) in 50 mM K_2HPO_4 at pH 7.0. Symbols are experimental data and solid lines result from CNLS data fits. Equivalent circuit I is used at potentials more anodic than V_c ($V_{appl} > V_c$) while III is used at $V_{appl} \leq V_c$. The fitting parameters are listed in Table 4.3.

E V	*CPE* μF cm^{-2}	α	CPE_1 μF cm^{-2}	α_1	R_1* MΩ
$HO_2C(CH_2)_{15}S$/Au SAM					
0.4	3.40±0.02	0.943±0.001			
0.3	3.30±0.02	0.949±0.001			
0.2	3.34±0.02	0.949±0.001			
0.1			3.39±0.02	0.949±0.001	21.2±2.2
0			3.39±0.02	0.951±0.001	4.06±0.01
− 0.1			3.09±0.04	0.960±0.001	1.05±0.01
− 0.2			3.02±0.03	0.960±0.001	0.89±0.01
− 0.3			2.93±0.03	0.959±0.002	0.85±0.01
− 0.4			2.97±0.04	0.958±0.001	1.18±0.01
− 0.5			3.12±0.05	0.956±0.002	1.12±0.02
CF_3C_9S/Au SAM					
0.4	1.92±0.01	0.964±0.001			
0.3	1.95±0.01	0.962±0.001			
0.2	2.00±0.01	0.961±0.001			
0.1	2.07±0.02	0.960±0.001			
0	2.13±0.02	0.958±0.001			
− 0.1	2.17±0.02	0.959±0.001			
− 0.2	2.25±0.02	0.958±0.001			
− 0.3			2.39±0.02	0.954±0.001	150±87
− 0.4			2.48±0.02	0.953±0.001	2.66±0.04
− 0.5			2.77±0.04	0.943±0.002	0.74±0.08

* Values for R_1 are not normalized for the electrode surface area.

Table 4.3 Effect of V_{appl} on the interfacial properties of $HO_2C(CH_2)_{15}S$/Au and CF_3C_9S/Au SAMs. Columns 2 (*CPE*) and 3 (α) correspond to the equivalent circuit I ($V_{appl} > V_c$). Columns 4-6 correspond to the equivalent circuit III ($V_{appl} \leq V_c$).

The behavior of the CF_3C_9S/Au SAM (Figure 4.6) is similar to the corresponding methyl $CH_3(CH_2)_9S$/Au SAM.[8] Both have V_c of – 0.25 V (*vs.* Ag/AgCl) (Table 4.3). At $V_c < V_{appl} \leq +0.4$ V, φ_{1Hz} remains constant at ~ 88° in the medium-to-low frequency region, consistent with this film being an ionic insulator (open circles). Both the CF_3/electrolyte and CH_3/electrolyte interfaces are of comparable hydrophobicity, as confirmed by contact angle measurements with water (118° for $X = CF_3$ and 113° for $X = CH_3$).[1] This is reasonable, given that the bulk dielectric constants of polyethylene and poly(tetrafluoroethylene) are also very similar (2.28 and 2.1, respectively).[28] The equivalent circuit used to fit the data at $V_{appl} \leq V_c$ for $X = CF_3$ involves a *CPE* (SAM capacitance) in parallel to a resistance R_1 (equivalent circuit III and solid lines in Figure 4.6). R_1 and φ_{1Hz} both decrease markedly as V_{appl} becomes increasingly cathodic, the former goes from 150 MΩ (– 0.3 V) to 140 kΩ (– 0. 5 V) and the latter from 83° to 15°.

The dependence of V_c on X shows that ion penetration in SAMs is triggered more readily for X = OH or CO_2H than for either $X = CH_3$ or CF_3. This can be explained by the hydrophilic character of the SAM/electrolyte interface and by the nature of the permanent dipole layer at the chain terminus. Cyclic voltammetry studies of the unsymmetrical dialkyl sulfide $CH_3(CH_2)_mS(CH_2)_nCO_2H$ SAMs showed that the capacitive current is considerably higher when $n > m$, *i.e.* when the SAM/electrolyte interface is mainly composed of hydrophilic terminal groups.[29] This effect, attributed to the greater permeability of SAMs that have a hydrophilic interface, is supported by the measurements made here.

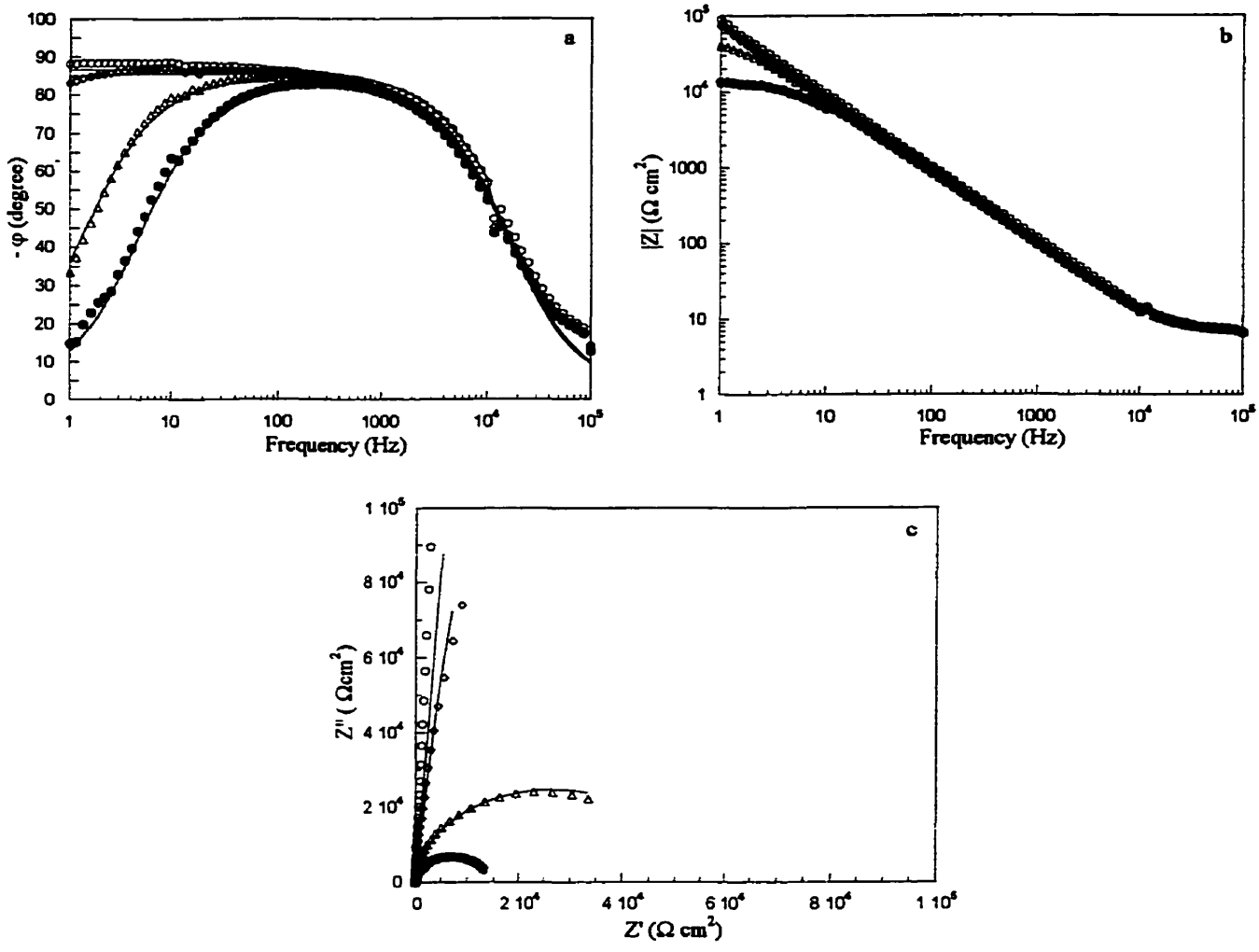

Figure 4.6 *a)* Bode phase plot, *b)* Bode plot, and *c)* Nyquist plot of a CF_3C_9S/Au SAM from + 0.4 V (*vs.* Ag/AgCl) to – 0.2 V (o), at – 0.3 V (◊), – 0.4 V (Δ), and – 0.5 V (•) in 50 mM K_2HPO_4 at pH 7.0. Symbols are experimental data and solid lines result from CNLS data fits. Equivalent circuit I is used at potentials more anodic than V_c ($V_{appl} > V_c$) while III is used when $V_{appl} \leq V_c$. The fitting parameters are listed in Table 4.3.

4.3.2 Variation of the Complex Dielectric Constant with Frequency

The complex dielectric constant $|\varepsilon|$, plotted as a function of frequency, has been used to study ion permeation into phospholipid bilayers.[30-32] $|\varepsilon|$ *vs.* f relationships are of interest for materials of very low conductivity,[23] such as SAMs, as they emphasize phenomena in the low frequency region where diffusion-related phenomena occur.

As a reference point, the dielectric spectrum for $X = CH_3$ ($n = 15$) at + 0.4 V (*vs.* Ag/AgCl) is shown in Figure 4.7 (open circles). In the high frequency region (10^4 Hz $< f < 10^5$ Hz), the impedance signal is dominated by the solution resistance. In the low-to-medium frequency region (1 Hz $< f < 10^3$ Hz), there is no variation of $|\varepsilon|$ with f at + 0.4 V. Evidently, ion penetration into $CH_3(CH_2)_nS$/Au SAMs at + 0.4 V (*vs.* Ag/AgCl) does not occur. When X = OH, there is again no evidence for ion penetration at + 0.4 V (open diamonds). For $X = CO_2H$, however, $|\varepsilon|$ increases slightly over most of the frequency domain probed, reflecting the complicated nature of this SAM/electrolyte interface (open triangles). Overall, $|\varepsilon|$ is larger as the functional group varies from $X = CH_3$, OH, and CO_2H. This trend reflects the nature of the terminal dipole, as was noted already in the discussion of the SAM capacitance values.

When $V_{appl} \leq V_c$ however (*i.e.* − 0.5 V, filled symbols), $|\varepsilon|$ markedly increases at $f < 20$ Hz for $X = CH_3$, OH, and CO_2H. This sharp increase in $|\varepsilon|$ in the low frequency domain is consistent with the accumulation of ions into the low dielectric hydrocarbon region of these SAMs. Ion penetration in potential-induced defects formed at $V_{appl} \leq V_c$ can thus be readily visualized in both φ *vs.* f plots and $|\varepsilon|$ *vs.* f plots.

4.3.3 Reversibility of Potential-Induced Defects

As demonstrated, $X(CH_2)_nS$/Au SAMs are affected to different extents by V_{appl}. The chemical nature of the terminal group (X) (and n) control V_c. The most stable films are obtained with $X = CH_3$ ($V_c = -0.35$ V *vs.* Ag/AgCl for $n = 15$) and with $X = CF_3$ ($V_c = -0.25$ V). SAMs ($n = 15$) with hydrophilic interfaces are clearly

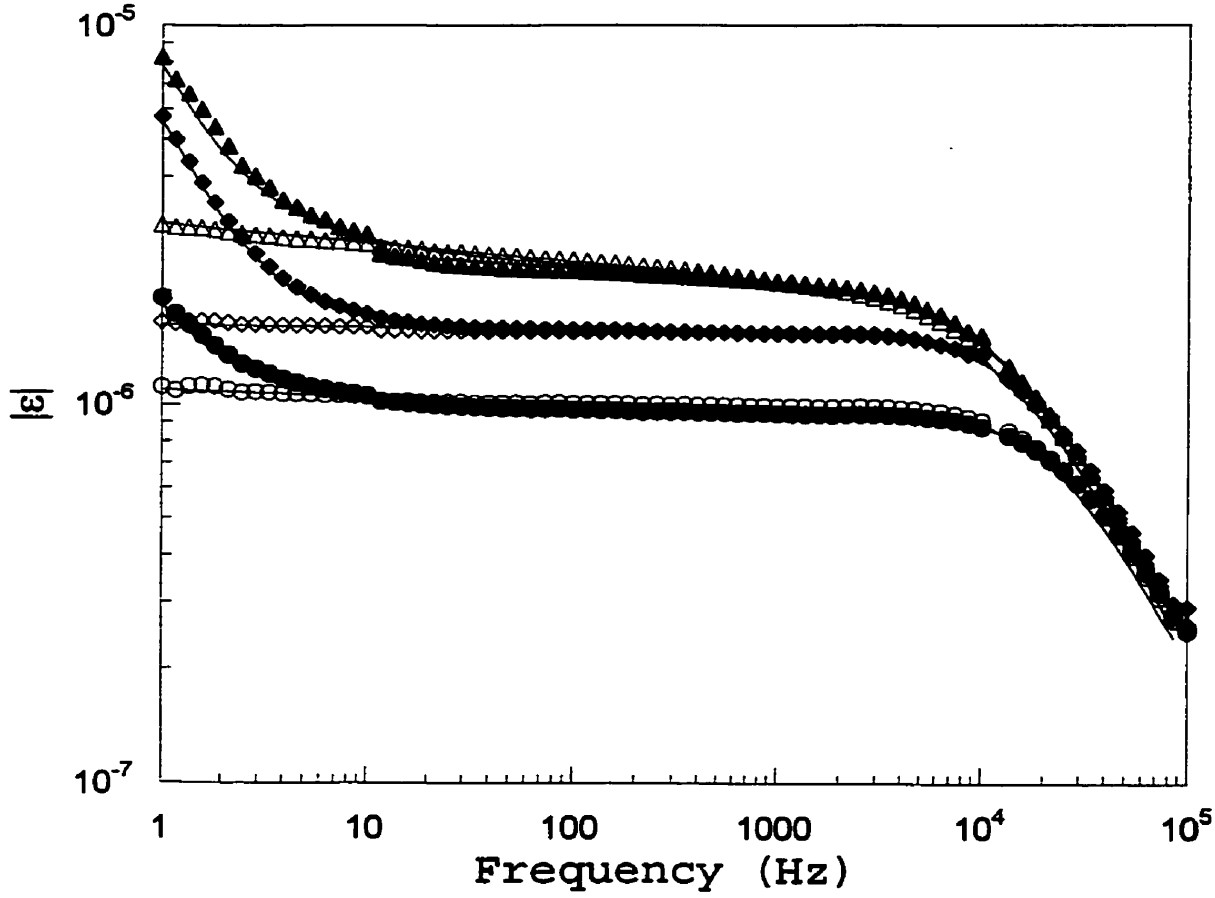

Figure 4.7 Dispersion of the complex dielectric constant $|\varepsilon|$ with frequency of a $CH_3(CH_2)_{15}S$/Au SAM at + 0.4 V (*vs.* Ag/AgCl) (o) and – 0.5 V (•); of a $HO(CH_2)_{16}S$/Au SAM at + 0.4 V (◊) and – 0.5 V (♦); and of a $HO_2(CH_2)C_{15}S$/Au SAM at + 0.4 V (Δ) and – 0. 5 V (▲).

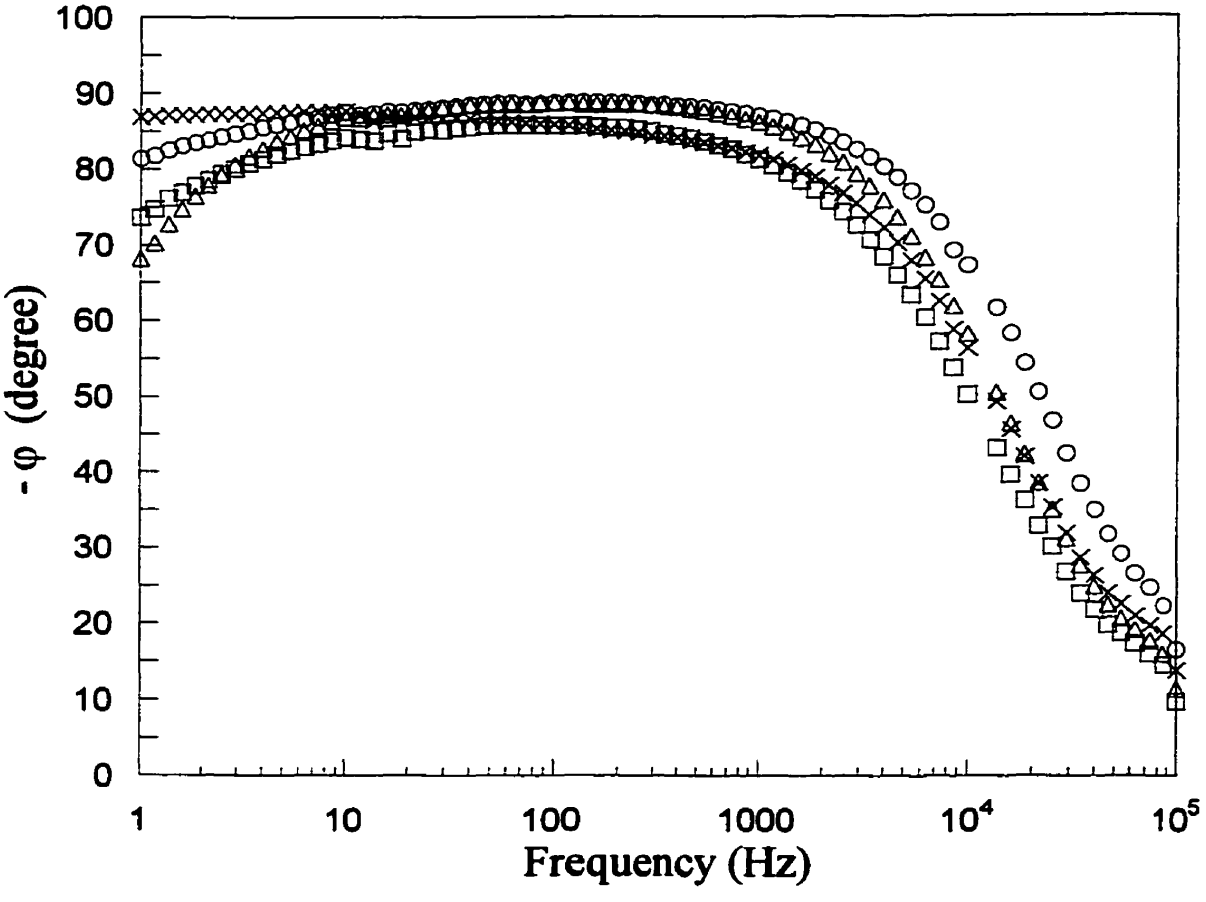

Figure 4.8 Investigation of the reversibility of potential-induced defects in SAMs observed as the variation of φ as a function of frequency, after the polarization at –0.5 V (*vs.* Ag/AgCl). Curves at 0 V (*vs.* Ag/AgCl) are shown for $CH_3(CH_2)_{15}S$/Au (o) and CF_3C_9S/Au (x) SAMs and at + 0.3 V for $HO(CH_2)_{16}S$/Au (Δ) and $HO_2C(CH_2)_{15}S$/Au (□) SAMs.

less stable as they have more anodic V_c values: + 0.15 V for $X = CO_2H$ and + 0.25 V for $X = OH$. A question that arises is whether the potential-induced defects created at – 0.5 V are reversible in these ω-functionalized SAMs.

$CH_3(CH_2)_nS/Au$ (n = 7-15) SAMs that are subjected to V_{appl} = – 0.5 V (*vs.* Ag/AgCl) recover their original electrochemical characteristics to a large extent once V_{appl} is returned to 0 V (Figure 4.8).[8] This is evident in the Bode phase plots where a substantial, albeit incomplete, recovery in φ_{1Hz} occurs. For n = 7 - 15, φ_{1Hz} ranges from 30 - 60° at – 0.5 V and reverts to 81 - 85° once they are returned to 0 V.

For the hydrophilic SAM/electrolyte interfaces (X = OH or CO_2H), the reversibility of potential-induced defects is measured at + 0.3 V, *i.e.* at V_{appl} slightly more anodic than V_c. φ_{1Hz} at – 0.5 V is 19° for X = OH and 28° for CO_2H. On returning to + 0.3 V, φ_{1Hz} only increases to 68° for X = OH and 74° for $X = CO_2H$ (Figure 4.8). The hydrophilic interfaces are clearly more affected by the formation of potential-induced defects than are hydrophobic interfaces. Either the reorganization of the film which occurs at $V_{appl} > V_c$ is more extensive when the terminal group is polar, or the kinetics of return to the organized state is slow because water, ions, and the polar group become trapped within the SAM. Potential excursions beyond V_c, with the attendant perturbation may serve to accelerate the process described previously where a folding back of the polar group into the SAM, occurs over long periods.[33]

4.4 Conclusions and Overview

A variation in the critical potential (V_c) as a function of chainlength noted in n-alkylthiol SAMs[7] is also observed when the chemical speciation of the chain end group is varied ($X = CH_3$, OH, and CO_2H with n = 15). V_c values as determined here by impedance spectroscopy are well within the commonly used operating window (from + 0.5 V to – 0.5 V *vs.* Ag/AgCl) in many cyclic voltammetry studies of RS/Au SAMs.[1-6] $X(CH_2)_nS/Au$ SAMs undergo some type of an ill defined structural transformation when V_{appl} exceeds V_c. Of note is the fact that these V_c values are

located well within the 'window of stability' for these SAMs. The 'window of stability' in fact commonly refers to the potential window where neither reductive nor oxidative Faradaic chemistry of RS/Au linkage occurs. The results described here however alert one to the fact that stability indeed has different degrees and that the potential induced-transformation characterized here has profound effects on the electrical and electrochemical properties of a SAM.

The immobilization of highly resistive SAMs on conductors followed by the insertion of membrane receptors, peptides or DNA strands is a key step in the design of impedimetric biosensors.[34-36] The ω-functionalized SAMs clearly fail as ionic insulators at potentials more cathodic than V_c. Moreover, the SAM resistance can actually be modulated by V_{appl}. Caution must therefore be exercised in making conclusions about SAM structures and properties if the SAM is taken beyond V_c during either the preparation or measurement process. The hysteresis in the electrochemical properties of potential-perturbed, polar terminated SAMs is considerably more significant than for methyl terminated SAMs so that return to the 'window of stability' does not ensure that the SAM is returned to its highly resistive state.

References

1) Chidsey, C. E. D.; Loiacono, D. N. *Langmuir* **1990**, *6*, 682-691.

2) Porter, M. D.; Bright, T. B.; Allara, D. L.; Chidsey, C. E. D. *J. Am. Chem. Soc.* **1987**, *109*, 3559-3568.

3) Miller, C.; Cuendet, P.; Grätzel, M. *J. Phys. Chem.* **1991**, *95*, 877-886.

4) Becka, A. M.; Miller, C. J. *J. Phys. Chem.* **1993**, *97*, 6233-6239.

5) Chailapakul, O.; Crooks, R. M. *Langmuir* **1995**, *11*, 1329-1340.

6) Chailapakul, O.; Crooks, R. M. *Langmuir* **1993**, *9*, 884-888.

7) Boubour, E.; Lennox, R. B. *Submitted to J. Phys. Chem. B* **2000**.

8) Boubour, E.; Lennox, R. B. *Langmuir. In press* **2000**.

9) Helmholtz, H. *Ann. Phys.* **1879**, *7*, 337-382.

10) Halliday, D.; Resnick, R. *Physics*; Wiley: New York, 1978.

11) Mansfeld, F. *Electrochim. Acta* **1993**, *38*, 1891-1897.

12) Mitton, D. B.; Latanasion, R. M.; Bellucci, F. *J. Electrochem. Soc.* **1996**, *143*, 3307-3316.

13) Jennings, G. K.; Munro, J. C.; Yong, T.-H.; Laibinis, P. E. *Langmuir* **1998**, *14*, 6130-6139.

14) Steinem, C.; Janshoff, A.; Ulrich, W.-P.; Sieber, M.; Galla, H.-J. *Biochim. Biophys. Acta* **1996**, *1279*, 169-180.

15) Ulman, A. *An Introduction to Ultrathin Organic Films from Langmuir - Blodgett to Self-Assembly*; Academic Press: San Diego, 1991.

16) Troughton, E. B.; Bain, C. D.; Whitesides, G. M.; Nuzzo, R. G.; Allara, D. L.; Porter, M. D. *Langmuir* **1988**, *4*, 365-385.

17) Bain, C. D.; Troughton, E. B.; Tao, Y. T.; Evall, J.; Whitesides, G. M.; Nuzzo, R. G. *J. Am. Chem. Soc.* **1989**, *111*, 321-335.

18) Nuzzo, R. G.; Dubois, L.; Allara, D. L. *J. Am. Chem. Soc.* **1990**, *112*, 558-569.

19) Evans, S. D.; Urankar, E.; Ulman, A.; Ferris, N. *J. Am. Chem. Soc.* **1991**, *113*, 4121-4131.

20) A recent study showed that in the presence of 1 mM $Fe(CN)_6^{3-/4-}$, a $CH_3(CH_2)_9S$/Au SAM is only electrochemically stable between – 0.2 V and + 1 V (*vs.* Ag/AgCl). Beulen, M.W.J; Kastenberg, M.I.; van Veggel F.C.J.M.; Reinhoudt, D.N. *Langmuir* **1998**, *14*, 7463-7467.

21) Furniss, B. S.; Hannaford, A. J.; Rogers, V.; Smith, P. W. G.; Tatchell, A. R. *Vogel's Textbook of Practical Organic Chemistry*; 4th ed.; Longman: New York, 1978.

22) Macdonald, J. R. *Complex Nonlinear Least Squares Immittance Fitting Program, LEVM 7.0*; Macdonald, J. R., Ed.: Department of Physics and Astronomy, University of North Carolina, Chapel Hill, NC., 1990.

23) Macdonald, J. R. *Impedance Spectroscopy*; Wiley: New York, 1987.

24) Sondag-Huethorst, J. A. M.; Fokkink, L. G. L. *Langmuir* **1995**, *11*, 2237-2241.

25) Swietlow, A.; Skoog, M.; Johansson, G. *Electroanalysis* **1992**, *4*, 921-928.

26) Janek, R. P.; Fawcett, W. R.; Ulman, A. *J. Phys. Chem. B* **1997**, *101*, 8550-8558.

27) Parsegian, A. *Nature* **1969**, *221*, 844-846.

28) Brandrup, J.; Immergut, E. H. *Polymer Handbook*; 3rd ed.; Wiley: New York, 1989, Section V.

29) Zhang, M.; Anderson, M. R. *Langmuir* **1994**, *10*, 2807-2813.

30) Note that the data are presented here as a function of f, not ω (= 2πf), as is more commonly presented in the literature.

31) Karolis, C.; Coster, H. G. L.; Chilcott, T. C.; Barrow, K. D. *Biochim. Biophys. Acta* **1998**, *1368*, 247-255.

32) Coster, H. G. L.; Chilcott, T. C.; Coster, A. C. F. *Bioelectrochem. Bioenerg.* **1996**, *40*, 79-98.

33) Evans, S. D.; Sharma, R.; Ulman, A. *Langmuir* **1991**, *7*, 156-161.

34) Stora, T.; Lakey, J. H.; Vogel, H. *Angew. Chem., Int. Ed. Engl.* **1999**, *38*, 389-392.

35) Sackmann, E. *Science* **1996**, *271*, 43-48.

36) Steinem, C.; Janshoff, A.; Galla, H.-J.; Sieber, M. *Bioelectrochem. Bioenerg.* **1997**, *42*, 213-220.

Chapter 5

Kinetics of Electron Transfer at Self-Assembled Monolayers Probed by a.c. Impedance Spectroscopy*

5.1 Introduction

Both *ion* transport and *electron* transfer across the bilayer membrane are essential to cell survival. Self-assembled monolayers (SAMs) are an interesting class of materials, as they appear to mimic the phospholipid bilayer in terms of their permeability profile.[1] *Ion* transport through SAMs probed by a.c. impedance spectroscopy has been explored in our previous work.[2,3] It is the objective here to describe the *electron* transfer across SAMs at SAM-coated electrodes.

Interfacial electron transfer reactions across SAMs chemisorbed on gold surfaces have been explored primarily by cyclic voltammetry[4-13] and a.c. impedance spectroscopy at a fixed d.c. potential *(i.e.* at the half-wave potential of the redox couple).[14-21] The mechanism by which the electrons are transferred from the redox species to the electrode surface through the SAM is difficult to ascertain and is clearly dependent upon the state of the film. Several mechanisms have been proposed so far to explain the heterogeneous electron transfer reaction. Among these are electron tunneling through the dielectric media constituted of the alkylthiol chains,[9,22-25]

* This chapter is to be submitted to *J. Phys. Chem. B.* in an adapted form where the theory presentation will be incorporated in an appendix to the paper. The submitted manuscript will otherwise be identical to the text presented here.

direct electron transfer at pinholes in SAMs,[11,14-16,18,21,26] and permeation of the redox couple within the hydrocarbon phase of the SAM.[1,10,27]

A difficulty in comparing the data between cyclic voltammetry (CV) and a.c. electrochemical impedance spectroscopy (a.c. EIS) in terms of SAM integrity stems from the fact that while CV scans a broad potential range, a.c. EIS is usually performed at a fixed d.c. potential, *i.e.* that of the redox couple half-wave potential ($E^r_{1/2}$). Kinetic parameters (rate constant and diffusion coefficient) have been previously determined from a.c. impedance spectroscopy at $E^r_{1/2}$ using deliberately perforated SAM-coated electrodes to form microarray electrodes (*i.e.* small active sites embedded in the SAM insulating plane).[14,15,21] In this approach, it is assumed that the electron transfer only occurs at the pinhole sites (with pinhole radii of *ca.* 0.1 to 10 μm and pinhole separations of 1-100 μm), where the redox couple is directly exposed to the bare gold electrode. The experimental data has been analyzed using the model developed by Matsuda[28] and Amatore[29] for microarray electrodes. In this model, the non-linear diffusion phenomena at small pinholes lead to a mathematical model which is equivalent to that of a CEC (Chemical-Electrochemical-Chemical) mechanism. Deviations of the experimental data from this model were attributable to the non-uniformity in the pore size and distribution of the pinholes.[15]

The *potential dependence* ($E^r_{1/2}$ ± 100 mV) of electrode reactions probed by a.c. impedance spectroscopy gives crucial information about the kinetics and mechanism of electron transfer, as pioneered by Sluyters-Rehbach and Sluyters.[30-32] σ - E plots (Warburg coefficient as a function of the applied potential) have been used as a diagnostic of the mechanism of electron transfer (*i.e.* CE, CEC, EC, *etc.*) at self-assembled monolayers.[30] The reduction of Tl^+ ions through Gramicidin channels embedded in self-assembled phospholipid monolayers on Hg follows a CEC (Chemical-Electrochemical-Chemical) mechanism, as assessed by σ - E plots.

The study of the potential dependence of the reduction of several redox couples at a $CH_3(CH_2)_{15}S$/Au SAM by a.c. impedance is presented here and is compared to the corresponding cyclic voltammograms. The redox couples

investigated are: $Fe(CN)_6^{3-/4-}$, $Ru(NH_3)_6^{3+/2+}$ and $Co(bpy)_3^{3+/2+}$. The $Fe(CN)_6^{3-/4-}$ and $Ru(NH_3)_6^{3+/2+}$ are routinely used by the SAM community to assess SAM integrity and properties. They both undergo simple outer-sphere electron transfer reactions at bare gold electrode but their heterogeneous rate constant are significantly different. The choice of redox couples was also based on their contrasting hydrophobic/hydrophilic character and size. The electrochemical response of each of these redox couples is probed at several d.c. potentials centered about $E^r_{1/2}$ ($\sim \pm 150$ mV) in 25 mV steps at a bare gold electrode and at SAM/Au electrodes. σ - E plots are used as diagnosis of electron transfer mechanisms based on theoretical models developed by Sluyters-Rehbach and Sluyters for reversible electron transfer reaction,[32] irreversible electron transfer reaction,[30,33,34] and CE mechanism.[35]

5.2 Theory

5.2.1 The Randles Equivalent Circuit

The Randles equivalent circuit describes electrode behavior when both charge transfer (R_{ct}) processes and diffusion controlled phenomena (Z_W) occur (Figure 5.1). This equivalent circuit widely applies to the impedance of electrochemical systems undergoing heterogeneous electron transfer reactions.[32,36] In the Randles circuit, R_s is the solution resistance, C_{dl} is the double layer capacitance, R_{ct} is the charge transfer resistance, and Z_W is a mass transfer term associated with the diffusion of redox species to the electrode surface (typically observed at low frequencies). The real and imaginary components of the Randles circuit are given as:

$$Z'_{Randles} = R_s + \frac{R_{ct} + \sigma\omega^{-1/2}}{(C_{dl}\sigma\omega^{1/2} + 1)^2 + \omega^2 C_{dl}^2 (R_{ct} + \sigma\omega^{-1/2})^2} \quad (1)$$

and

$$Z''_{Randles} = \frac{\omega C_{dl}(R_{ct} + \sigma\omega^{-1/2})^2 + \sigma\omega^{-1/2}(\omega^{1/2} C_{dl}\sigma + 1)}{(C_{dl}\sigma\omega^{1/2} + 1)^2 + \omega^2 C_{dl}^2 (R_{ct} + \sigma\omega^{-1/2})^2} \quad (2)$$

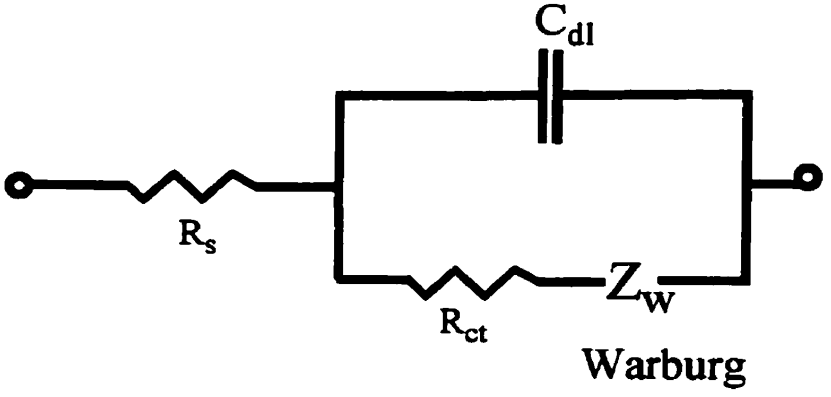

Figure 5.1 Randles Equivalent Circuit.

where

$$Z_W = \sigma\omega^{-1/2}(1-j) \tag{3}$$

Expressions describing the dependence of σ and R_{ct} with applied d.c. potential depend on the mechanism of electron transfer involved.[31,32] Mechanisms that involve more than a simple reversible electron transfer (such as when a preceding or a following chemical reaction is coupled to the electron transfer step) can still be fitted to the Randles equations when a linear relationship between the faradaic impedance (Z_f' or Z_f'') and $\omega^{-1/2}$ is verified.[30,37] From this perspective, the Randles equivalent circuit can be successfully applied to a wide variety of mechanisms where an electron transfer (E) is coupled to a chemical reaction (C), as has been reported by Sluyters-Rehbach and Sluyters.

5.2.2 Simple Reversible Electron Transfer

The simplest electron transfer reaction occurs when the electron transfer step (faradaic reaction) is not coupled to a chemical reaction. It can be formulated as:

$$O + n\,e^- \underset{}{\overset{k_{sh}}{\longleftrightarrow}} R \tag{4}$$

where k_{sh} is the standard heterogeneous rate constant of the charge transfer reaction. The reversible half-wave potential is:

$$E_{1/2}^r = E_o + \frac{RT}{nF}\ln(a_r/a_o) \tag{5}$$

The expressions for the potential dependence of the Warburg coefficient (σ) and the charge transfer resistance (R_{ct}) are:[32]

$$(\sigma)_{rev} = \sigma_m \cosh^2\left[\frac{nF}{2RT}\left(E - E_{1/2}^r\right)\right] \tag{6}$$

$$(R_{ct})_{rev} = \frac{RT}{n^2F^2k_{sh}^a}\frac{e^{\beta\Psi} + (a_r/a_o)e^{-\alpha\Psi}}{C_o^* + (a_r/a_o)C_r^*} \tag{7}$$

where R, T, n, and F have their usual meaning and $a_i = D_i/\delta_i k_{sh}^a$ (with $i = O$ or R). For simplification purposes, we can consider $a_r = a_o$ and $\alpha = \beta$. Therefore $E_o = E_{1/2}^r$, and

$$(R_{ct})_{rev} = \frac{RT}{n^2F^2k_{sh}^a}\frac{e^{\alpha\psi} + e^{-\alpha\psi}}{C^*} \tag{8}$$

The Warburg coefficient σ is the slope of Z_f' (or Z_f^*) *vs.* $\omega^{-1/2}$. A plot of σ and R_{ct} as a function of the applied potential E gives a symmetrical function with a minimum value in both σ and R_{ct} at $E_{1/2}^r$. The diffusion coefficient D of the electroactive species and the heterogeneous rate constant k_{sh} of the faradaic reaction can be obtained from σ_m and R_{ct}, where:

$$\sigma_m = \frac{2RT}{n^2F^2C^*\sqrt{2}\sqrt{D}} \tag{9}$$

$$(R_{ct})_m = \frac{RT}{n^2F^2k_{sh}C^*} \tag{10}$$

These equations are valid under the conditions where *i)* there is no reactant adsorption at the electrode, *ii)* the Butler-Volmer equation is applicable and *iii)* the mass transfer only takes place by diffusion. The model for a simple reversible reaction can be tested for the reduction of $Fe(CN)_6^{3-}$ and $Co(bpy)_3^{3+}$ on a bare gold electrode, as shown below.

5.2.3 CE Mechanism

When a chemical reaction is coupled to the electron transfer step, several scenarios are possible. The CE mechanism is fairly simple as it involves a chemical step (homogeneous reaction) which precedes the electron transfer step. The CE mechanism can be depicted as shown in Figure 5.2 and is formulated as:

$$O_{sol} \overset{K}{\rightleftharpoons} O_{SAM} + n\,e^- \overset{k_{sh}}{\longleftrightarrow} R_{SAM} \tag{11}$$

where $K(=k_1/k_2)$ is the equilibrium constant of the (preceding) chemical reaction. When k_{sh} is small (*i.e.* $k_{sh} \ll \omega_{min}$), the chemical reaction is rate limiting and the expression for σ as a function of applied potential E is given by:[35]

$$(\sigma)_{CE} = \frac{RT}{n^2F^2C_p^*(2D_o)^{1/2}}\frac{K+1}{K}\left[e^{\psi} + L + 1 + Le^{-\psi}\right] \tag{12}$$

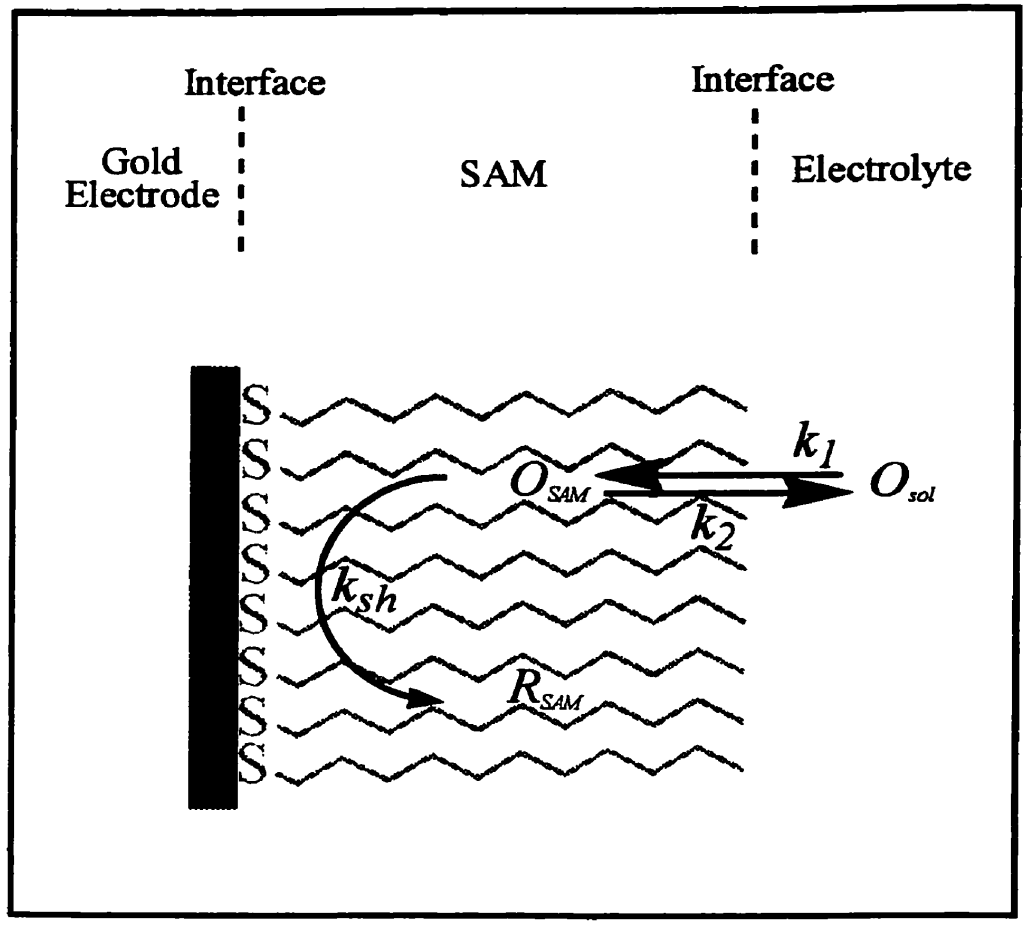

Figure 5.2 Schematic representation of a CE mechanism (chemical reaction followed by electron transfer) at a SAM-coated electrode.

where

$$\psi = \frac{nF}{RT}(E - E^r_{1/2}) \tag{13}$$

and L represents the influence of the chemical reaction. L is always less than 1 for a CE mechanism and is defined by Jacq's reaction layer treatment for the mass transfer for a first-order reaction.[38] The parameter σ can be obtained at various potentials around $E^r_{1/2}$ from the slope of Z'_f *vs.* $\omega^{-1/2}$, after subtraction of R_s and C_{dl} from the total impedance.[32] The minimum in the σ - E plot is given by:

$$(\sigma_m)_{CE} = \frac{RT}{n^2F^2C^*_p(2D_o)^{1/2}}\frac{K+1}{K}\left(1+L^{1/2}\right)^2 \tag{14}$$

$$(E_m)_{CE} = E^r_{1/2} + \left(\frac{RT}{nF}\right)\ln L^{1/2} \tag{15}$$

The measured half-wave potential $(E_{1/2})_{CE}$ for a CE mechanism is:

$$(E_{1/2})_{CE} = E^r_{1/2} + \frac{RT}{nF}\ln L \tag{16}$$

σ - E simulations for a CE mechanism using eq (12), taking typical literature values for D_o (10^{-6} cm^2 s^{-1}) and C^*_p (10^{-3} M), as a function of L (< 1) and K and are shown in Figure 5.3. The σ - E curves obtained for the CE mechanism (eq 12) are compared with the σ - E curves expected for a simple electron transfer (eq 6). From Figure 5.3, it can be seen that E_m values for the CE mechanism are shifted negatively with respect to the reversible half-wave potential $(E - E^r_{1/2} = 0)$ and positively with respect to $E_{1/2}$; and that σ_m is greater than that for a reversible electron transfer. The kinetic parameter k_{sh} is not apparent in eq 14, but is actually buried in the L factor, together with K.

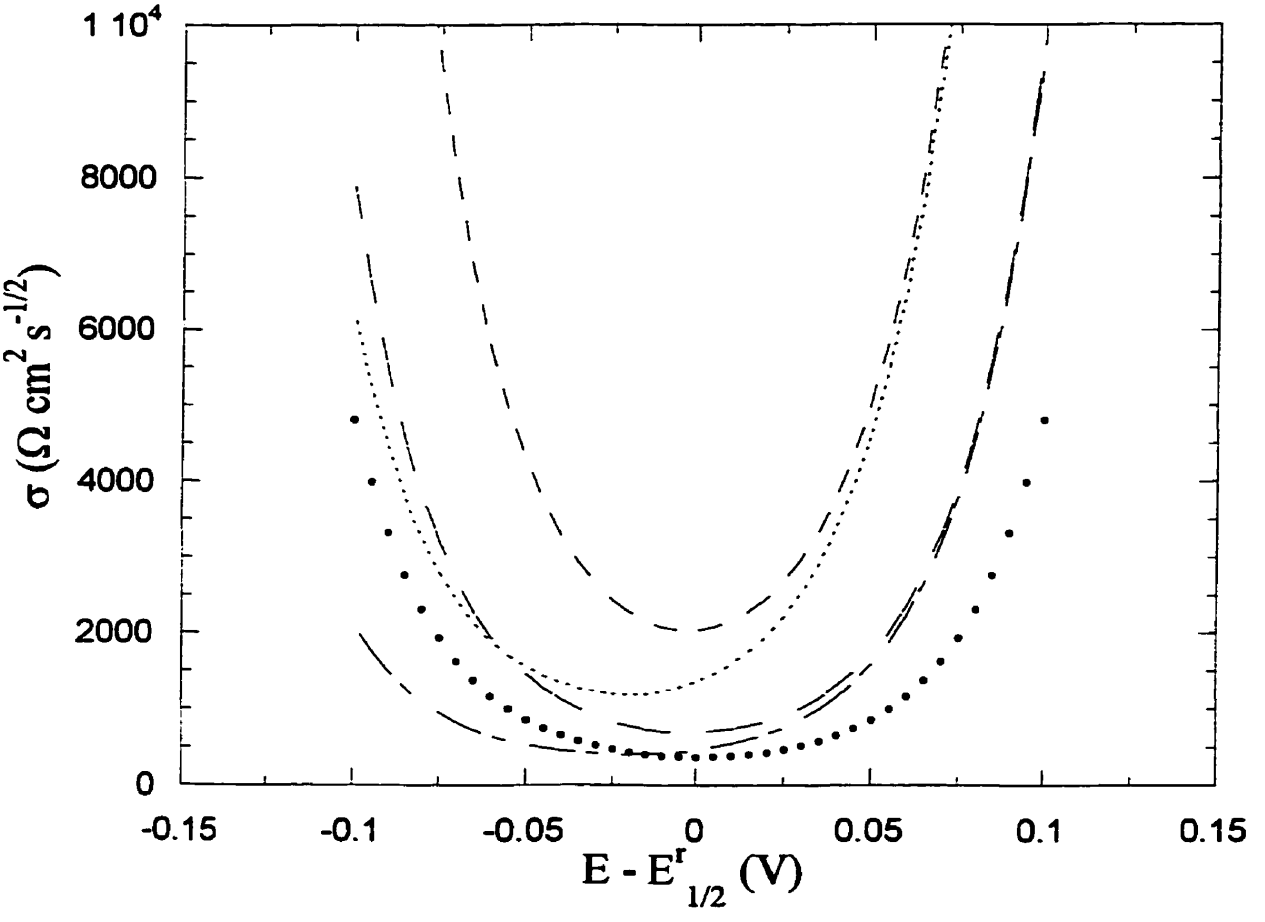

Figure 5.3 Warburg coefficient (σ) as a function of applied potential for the CE mechanism calculated with eq 12, $n = 1$, $D_o = 10^{-6}$ cm^2 s^{-1}, $C_p^* = 10^{-3}$ M; $L = 0.2$ and $K = 0.5$ (—), $L = 0.2$ and $K = 50$ (– – –), $L = 0.8$ and $K = 0.5$ (– –), $L = 0.8$ and $K = 50$ (– – –). The dotted line corresponds to a simple electron transfer calculated using eq. 6 with $C^* = 10^{-3}$ M and $D = 10^{-6}$ cm^2 s^{-1}.

5.2.4 Irreversible Electron Transfer

For an irreversible electron transfer, where $E - E^{r}_{1/2} >> 0$ and $k_{sh}e^{\psi}$ is small, σ and R_{ct} can be expressed as follows,[30]

$$(\sigma)_{irrev} = \frac{RT}{n^2F^2C^{*}_{r}(2D_r)^{1/2}} \frac{\delta_r / D_r + 1/(k_{sh}e^{\psi})}{(1-\alpha)/(k_{sh}e^{\psi})} \quad (17)$$

$$(R_{ct})_{irrev} = \frac{RT}{n^2F^2C^{*}_{r}} \frac{\delta_r / D_r + 1/(k_{sh}e^{\psi})}{1-\alpha} \quad (18)$$

The equations corresponding to the cases where *i)* $(E - E^{r}_{1/2}) >> 0$ and $k_{sh}e^{\psi}$ large, *ii)* $(E - E^{r}_{1/2}) << 0$ and k_{sh} small, and *iii)* $(E - E^{r}_{1/2}) << 0$ and k_{sh} large have also been derived.[30] Figure 5.4 shows some σ - E curves for the irreversible electron transfer obtained from eq 17 (using typical literature values for C^{*}_{r}= 10^{-3} M, D_r= 10^{-6} cm^2 s^{-1}, and k_{sh}= 10^{-3} cm s^{-1}) as a function of δ_r / D_r and (1 − α). From Figure 5.4, the quotient δ_r / D_r affects the shape of the anodic arm, while (1 − α) shifts the σ - E curve along the y-axis.

5.3 Experimental Section

Instrumentation. Electrochemical Impedance Spectroscopy (EIS) measurements were obtained in a conventional 3-electrode electrochemical cell with a Solartron 1286 Potentiostat combined with a Solartron 1255 Frequency Response Analyzer. All measurements were conducted at room temperature in a Faraday cage. The counter electrode was a platinum mesh (Aldrich) and the reference electrode was a Ag/AgCl electrode (3 M NaCl, Bioanalytical Systems Inc., IN). Data acquisition was performed using Zplot/Zview software. A sinusoidal potential modulation of ± 10 mV amplitude was superimposed on a fixed d.c. potential. The amplitude and the phase shift of the resulting current were recorded at each frequency, from 65 kHz to 100 mHz. All measurements are reported with respect to the geometrical area. Cyclic voltammograms were obtained with a BAS 100A potentiostat.

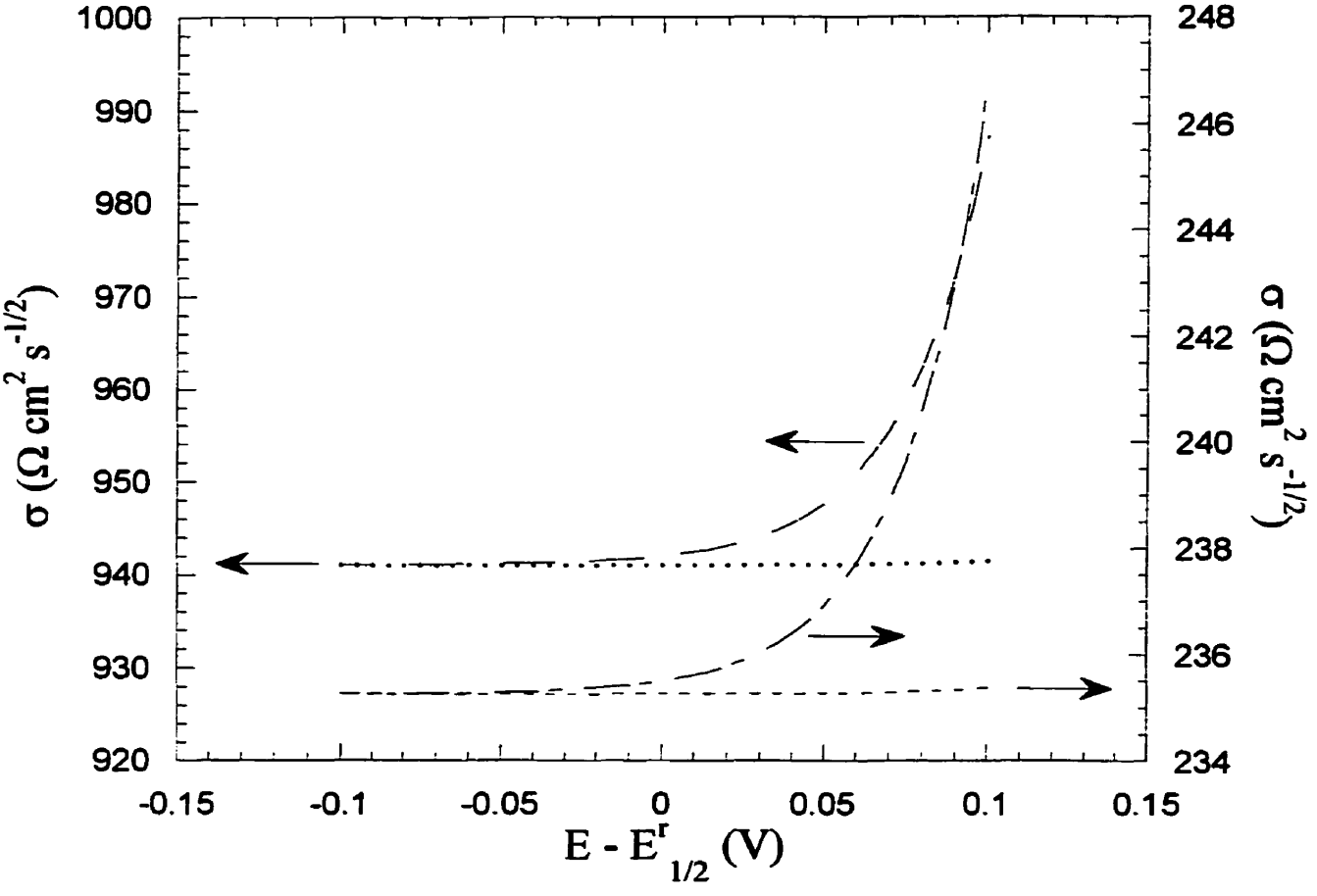

Figure 5.4 Warburg coefficient (σ) as a function of applied potential for the irreversible electron transfer calculated with eq 17, $n = 1$, $D_r = 10^{-6}$ cm^2 s^{-1}, $C_r^* = 10^{-3}$ M, $k_{sh} = 10^{-3}$ cm s^{-1}; $\delta_r / D_r = 10^{-2}$ s and $(1 - \alpha) = 0.8$ (---), $\delta_r / D_r = 10^{-2}$ s and $(1 - \alpha) = 0.2$ (...), $\delta_r / D_r = 1$ s and $(1 - \alpha) = 0.8$ (— — —), $\delta_r / D_r = 1$ s and $(1 - \alpha) = 0.2$ (— — —).

The effect of the d.c. applied potential on the electrochemical response of bare gold electrodes and of $CH_3(CH_2)_{15}S$/Au SAMs in the presence of the redox couples ($Ru(NH_3)_6^{3+}$, $Fe(CN)_6^{3-/4-}$ and $Co(bpy)_3^{3+}$) solubilized (5 mM) in the electrolyte (50 mM K_2HPO_4, pH 7.0) is investigated from ~ + 0.15 V to ~ – 0.15 V in 0.25 V steps with respect to the reversible half-wave potential ($E^r_{1/2}$). The impedance data were then fitted to an electrical equivalent circuit using the Complex Nonlinear Least Square (CNLS) Immittance Fitting Program.[39]

Chemicals. Hexadecanethiol was available from previous studies and was synthesized from 1-bromohexadecane (97 % Aldrich) by standard procedures.[40,41]

$HS(CH_2)_{15}CH_3$: M.p. 19.5-21°C; TLC (silica gel, *n*-hexane): R_f = 0.7; ^1H NMR (500 MHz, $CDCl_3$, 25°C): δ 2.52 (q, 2H, CH_2SH), 1.58 (m, 2H CH_2CH_2SH), 1.40 (m, 2H, $CH_2CH_2CH_2SH$), 1.31 (t, 1H, CH_2SH), 1.24 (s, 24H, $(CH_2)_{12}$), 0.87 (t, 3H, CH_3).

Dibasic potassium phosphate, potassium ferrocyanide and potassium ferricyanide were obtained from BDH (Montreal, Canada). Hexaammineruthenium (III) chloride was bought from Aldrich (Milwaukee).

$Co(bpy)_3(ClO_4)_3.3H_2O$ (bpy = bipyridine) was synthesized following the procedure of Nyholm *et al.*[42] The identity and purity of the synthesized complex were confirmed by ^1H NMR and UV-visible spectroscopy.

Water (18 MΩ cm) was obtained from a Milli-Q water system (Bedford, MA).

Procedure. Gold electrodes (1 cm^2 geometric surface area) were prepared by thermal evaporation of 95 nm of gold on freshly cleaved mica. The substrates were then annealed under a nitrogen atmosphere in an oven at 650 °C for one minute. $CH_3(CH_2)_{15}S$/Au SAMs were prepared by alkythiol adsorption from 1 mM solution in pure ethanol, at room temperature, in sealed vials. The incubation time was typically of 3 days. The quality of the monolayer obtained was tested by a.c impedance spectroscopy in the absence of the redox probe, as previously described.[43] A SAM is assessed to be defect-free when the resulting impedance spectrum obtained in the absence of a redox couple can be fitted to a capacitor in series with a solution resistance. Typically, a phase angle of ≥ 88° at 1 Hz is obtained, consistent with the

samples adhering to the Helmholtz model.[44,45] Measurements performed by either a.c. impedance spectroscopy or cyclic voltammetry in the presence of a redox probe were performed only after this criterion was met.

5.4 Results and Analysis

The reversible half-wave potential ($E^r_{1/2}$) of each redox couple was determined by cyclic voltammetry at bare gold electrodes in supporting electrolyte (Figure 5.5a). The $E^r_{1/2}$ values are + 0.225 V (*vs.* Ag/AgCl) for $Fe(CN)_6^{3-/4-}$, + 0.100V for $Co(bpy)_3^{3+/2+}$, and – 0.185 V for $Ru(NH_3)_6^{3+/2+}$.

The presence of the SAM at the gold surface considerably reduces the current density, as per many previous reports.[10,13,46] From Figure 5.5b, it appears that the blocking of the faradaic current is virtually complete for $Fe(CN)_6^{3-/4-}$ at overpotentials of either ± 200 mV with respect to the half-wave potential (+ 0.225 V). This is not, however, the case for either $Ru(NH_3)_6^{3+/2+}$ or $Co(bpy)_3^{3+/2+}$, where a significant increase in the current density is observed near $E^r_{1/2}$ and at increasingly reductive potentials. The presence of such a "tail" has also been observed for $Ru(NH_3)_6^{3+/2+}$ with a $CH_3(CH_2)_{17}S$/Au SAM[4] and also with ω-functionalized SAMs.[10,26] The shape of the tail is different from the sigmoidal shape characteristic of an electron transfer reaction at pinhole sites.[15] The mechanism of electron transfer cannot however readily be elucidated by cyclic voltammetry since the effects of the solution resistance, the double layer charging, and the ion diffusion cannot be independently isolated.

This interesting observation led us to perform a.c. impedance spectroscopy measurements at several fixed d.c. potentials. A potential window of ± 150 mV about $E^r_{1/2}$ was chosen, sweeping in the cathodic direction. The applied d.c. potential never exceeded the critical potential (– 0.4 V *vs.* Ag/AgCl for a $CH_3(CH_2)_{15}S$/Au SAM) at which defects begin to become formed.[2]

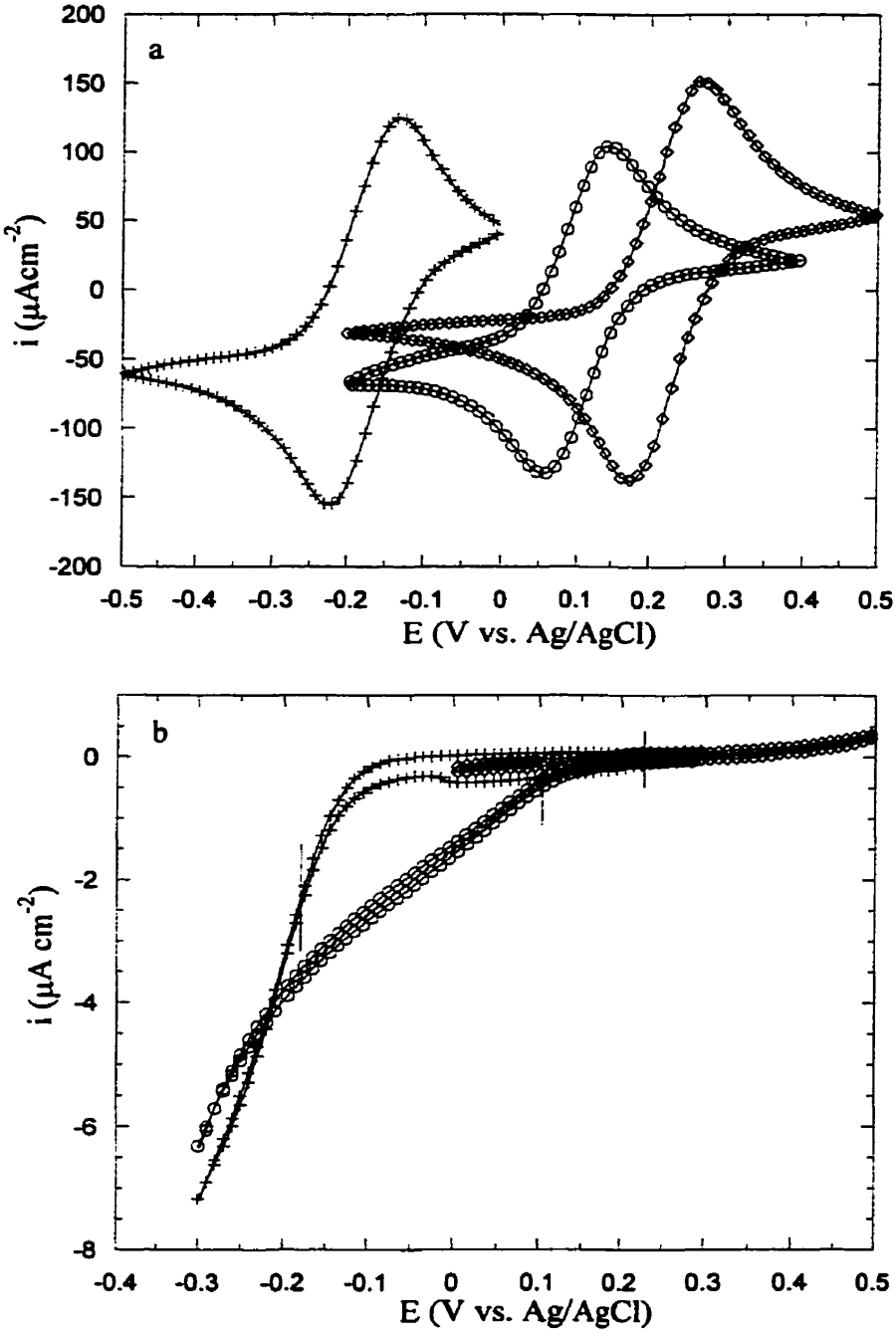

Figure 5.5 Cyclic voltamogramms *a)* on bare gold electrodes at 5 mV s^{-1}, and *b)* at $CH_3(CH_2)_{15}S$/Au SAMs at 50 mV s^{-1} in 5 mM of redox couple solubilized in 50 mM K_2HPO_4, pH 7.0 (the vertical bar represents the reversible half-wave potential of each redox couple). Each cyclic voltammogram corresponds to a freshly prepared SAM. $Ru(NH_3)_6^{3+}$ (+), $Co(bpy)_3^{3+}$ (o), and $Fe(CN)_6^{3-}$ (◊).

These defects are believed to provide a direct conduit for ion penetration from the aqueous phase into the hydrophobic part of the SAM.

5.4.1 A.C. Impedance Response at $E^r_{1/2}$ at Bare Gold and SAM-Coated Electrodes

The electrochemical response of the three redox couples at a bare gold electrode and a $CH_3(CH_2)_{15}S$/Au SAM were studied at their respective half-wave potentials by a.c. impedance spectroscopy (Figure 5.6 a-d). The kinetics of electron transfer at $E^r_{1/2}$ at bare gold are in the same order of magnitude for both $Fe(CN)_6^{3-/4-}$ (R_{ct} = 32 Ω cm^2) and $Co(bpy)_3^{3+/2+}$ (R_{ct} = 25 Ω cm^2). The heterogeneous electron transfer rate constant for $Ru(NH_3)_6^{3+/2+}$ is so large that no semi-circle is observed in the Nyquist plot ($R_{ct} \rightarrow 0$).[14]

In the presence of a SAM, the R_{ct} values (as extrapolated from the semi-circle to the *x*-axis) increase by more than two orders of magnitude compared to those obtained at a bare gold electrode (Figure 5.6). The value of the charge transfer resistance R_{ct} (as obtained from CNLS fits) of the three probes at SAM-coated electrodes at $E^r_{1/2}$ are substantially different: 104 Ω cm^2 for $Ru(NH_3)_6^{3+}$; 4 kΩ cm^2 for $Co(bpy)_3^{3+}$, and 62 kΩ cm^2 for $Fe(CN)_6^{3-/4-}$. The R_{ct} value has an inverse dependence on C^* (bulk concentration) and k_{sh} (eq 10). If one assumes that the heterogeneous rate constant at a SAM-coated electrode is that of bare gold, the ratio of C^*_{bare}/C^{app}_{SAM} gives 160 for $Co(bpy)_3^{3+/2+}$, 1940 for $Fe(CN)_6^{3-/4-}$ and 3470 for $Ru(NH_3)_6^{3+/2+}$. These ratios show that the penetration of the redox probe from the electrolyte to the electrode through the hydrophobic SAM is more restricted in the case of the hydrophilic Ru complex than for the hydrophobic Co complex.

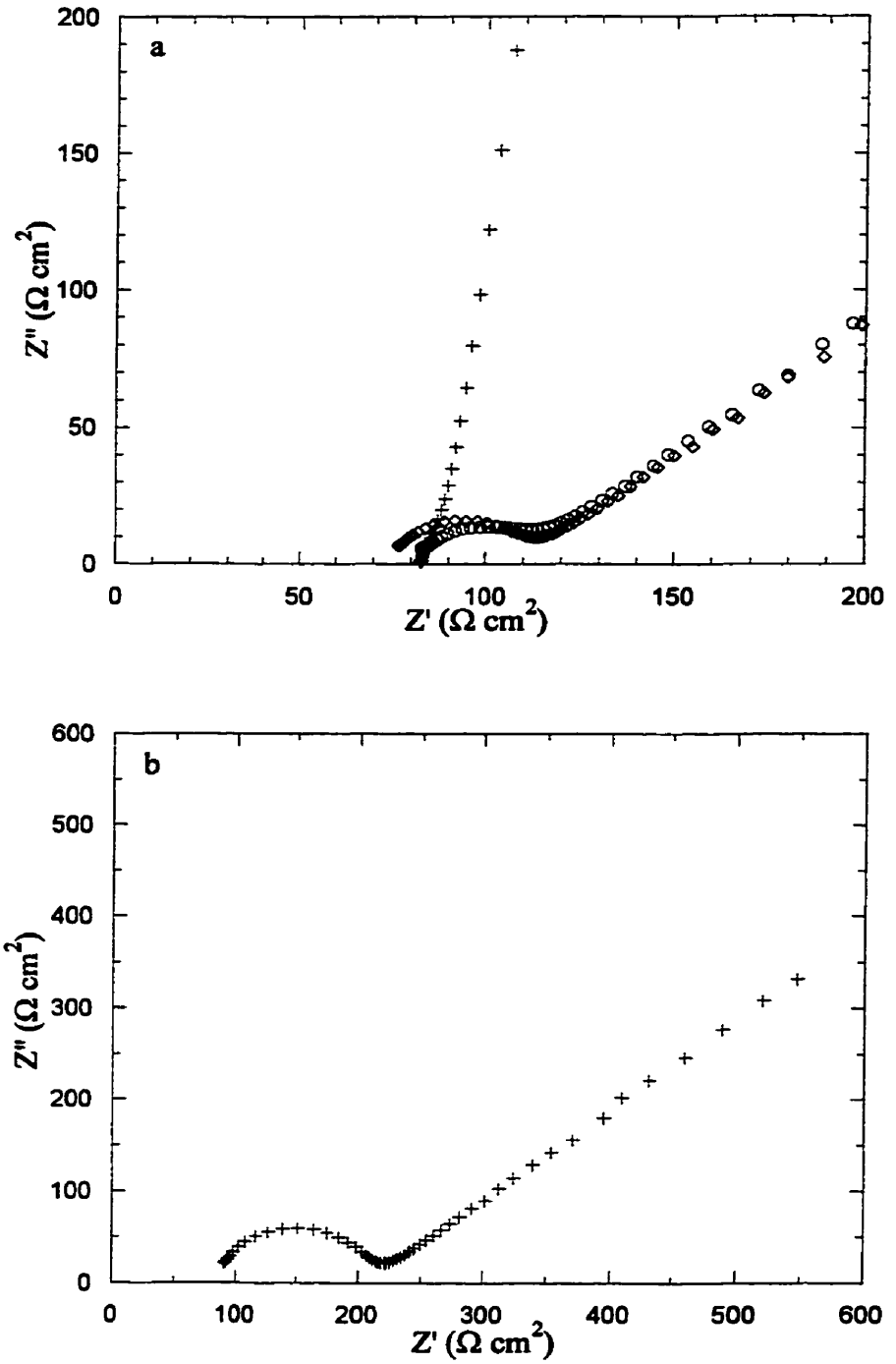

Figure 5.6 Nyquist plots at the reversible half-wave potential, $E^r_{1/2}$, at *a)* a bare gold electrode, and *b)* a $CH_3(CH_2)_{15}S$/Au SAM in the presence of 5 mM $Ru(NH_3)_6^{3+}$ (–0.185 V *vs.* Ag/AgCl) in 50 mM K_2HPO_4, pH 7.0. Each spectrum corresponds to an independent measurement.

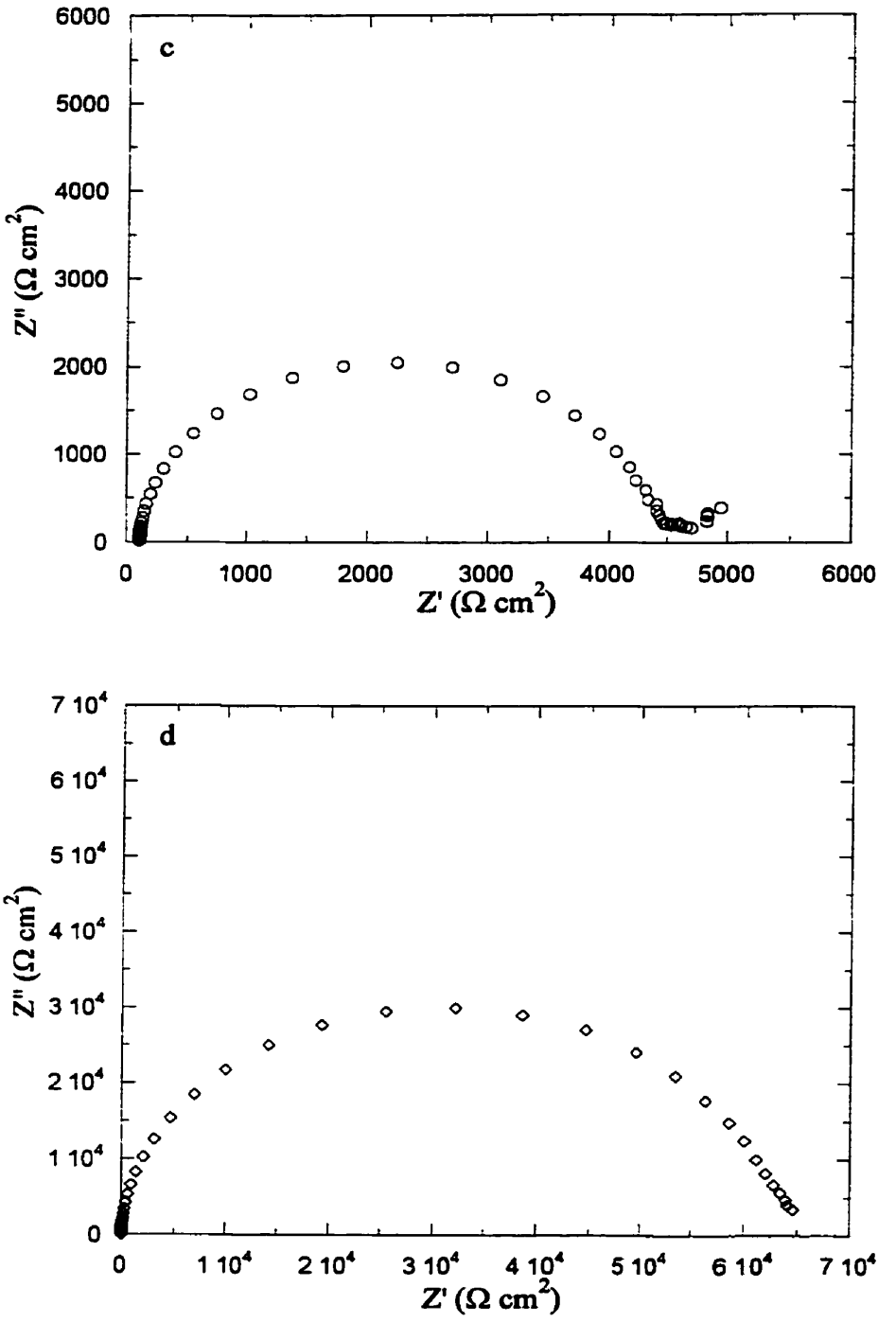

Figure 5.6 (cont'd) *c)* a $CH_3(CH_2)_{15}S$/Au SAM in the presence of 5 mM $Co(bpy)_3^{3+}$ (+ 0.100 V), and *d)* a $CH_3(CH_2)_{15}S$/Au SAM in the presence 5 mM $Fe(CN)_6^{3-/4-}$ (+ 0.225 V) (equimolar concentration).

5.4.2 The Randles Hypothesis

The effect of the d.c. applied potential (E) at both bare gold electrodes and $CH_3(CH_2)_{15}S$/Au SAM electrodes with $Ru(NH_3)_6^{3+}$, $Fe(CN)_6^{3-/4-}$, and $Co(bpy)_3^{3+}$ was studied at ~ ± 150 mV with respect to $E^r_{1/2}$. Except for $Fe(CN)_6^{3-/4-}$ at $CH_3(CH_2)_{15}S$/Au SAM ($R_{ct} \rightarrow \infty$) and $Ru(NH_3)_6^{3+/2+}$ at bare gold ($R_{ct} \rightarrow 0$), the other four systems allow the experimental data to be successfully fitted to a Randles equivalent circuit over all potentials studied. The values of the circuit elements are compiled in Table 5.1. The capacitance of the $CH_3(CH_2)_{15}S$/Au SAMs (0.9 to 1 μF cm^{-2}) is 15 to 20 times smaller than that of the bare gold surface and is independent of both the applied potential and the chemical nature of the redox couple.

As mentioned in section 2, the σ - E analysis is applicable when the electrochemical system under study *i)* fits the Randles equivalent circuit and *ii)* meets the Randles condition (linear $Z'_f - \omega^{-1/2}$ relationship). The solid lines in Figure 5.7 represent fits of the experimental data to the Randles equation. $Z'_f - \omega^{-1/2}$ plots yield straight lines of slope σ. Electron transfer kinetics at a bare gold electrode in the presence of $Ru(NH_3)_6^{3+}$ and at a $CH_3(CH_2)_{15}S$/Au SAM in the presence of $Fe(CN)_6^{3-/4-}$ cannot thus be analyzed in terms of σ - E kinetics.

5.4.3 Reversible Electron Transfer

The kinetics of electron transfer of redox couples of moderate k_{sh} on a bare gold surface can be described in terms of a reversible electron transfer reaction. The σ - E plots for both $Co(bpy)_3^{3+}$ and $Fe(CN)_6^{3-/4-}$ are shown in Figure 5.8. There is a good correlation between the experimental results and the simulated curves (dashed lines) for a simple electron transfer reaction (eq 6). The minima in σ - E occur at $E = E^r_{1/2}$. For $Co(bpy)_3^{3+}$, the diffusion coefficient D_o and the heterogeneous rate constant k_{sh}, obtained from eq 9 and 10, are: $D_o = 5.0 \times 10^{-7}$ cm^2 s^{-1} and $k_{sh} = 2.2 \times 10^{-3}$ cm s^{-1}. For $Fe(CN)_6^{3-/4-}$, $D_o = 7.8 \times 10^{-7}$ cm^2 s^{-1} and $k_{sh} = 3.1 \times 10^{-3}$ cm s^{-1}.

E (mV)	η (mV)	R_s (Ω)	C_{dl} (μF cm^{-2})	R_{ct} (Ω cm^2)	Z_w (Ω cm^2)
Bare Au electrode + 5 mM $Co(Bpy)_3^{3+}$					
+ 200	+ 100	86 ± 0.7	52 ± 1	122 ± 8	4984 ± 60
+ 150	+ 50	84 ± 0.5	38 ± 1	38 ± 0.8	1008 ± 8
+ 100	0	83 ± 0.3	27 ± 0.4	25 ± 0.4	481 ± 3
+ 50	− 50	84 ± 0.3 2	6 ± 0.7	34 ± 0.5	1071 ± 5
0	− 100	85 ± 0.4	23 ± 0.5	65 ± 3	5472 ± 25
Bare Au electrode + 5 mM $Fe(CN)_6^{4-/3-}$					
+ 300	+ 75	79 ± 0.4	17 ± 0.4	47 ± 0.7	2063 ± 8
+ 250	+ 25	80 ± 0.4 1	8 ± 0.6	26 ± 0.4	497 ± 2
+ 225	0	77 ± 0.3	13 ± 0.4	32 ± 0.4	380 ± 3
+ 200	− 25	77 ± 0.4	13 ± 0.3	48 ± 0.5	442 ± 5
+ 150	− 75	78 ± 0.5	13 ± 0.1	177 ± 1	1576 ± 14
+ 100	− 125	78 ± 0.4	12 ± 0.1	832 ± 109	198 ± 85
$CH_3C_{15}S$/Au SAM + 5 mM $Co(bpy)_3^{3+}$					
+ 200	+ 100	111 ± 1	0.94 ± 0.01	9991 ± 86	8170 ± 285
+ 150	+ 50	112 ± 1	0.95 ± 0.01	5716 ± 34	2372 ± 576
+ 100	0	112 ± 1	0.95 ± 0.01	4228 ± 26	1774 ± 129
+ 50	− 50	112 ± 1	0.96 ± 0.01	3391 ± 22	1649 ± 122
0	− 100	112 ± 1	0.96 ± 0.01	2784 ± 19	1578 ± 109
− 50	− 150	113 ± 1	0.97 ± 0.01	2431 ± 17	1671 ± 115
$CH_3C_{15}S$/Au SAM + 5 mM $Fe(CN)_6^{4-/3-}$					
+ 350	+ 125	81 ± 3	0.98 ± 0.02	19920 ± 299	none
+ 300	+ 75	85 ± 1	0.97 ± 0.01	35624 ± 224	none
+ 250	+ 25	86± 1	0.98 ± 0.01	54117 ± 471	none
+ 200	− 25	86 ± 1	0.97 ± 0.01	61912 ± 763	none
+ 100	− 125	85 ± 1	0.97 ± 0.01	31032 ± 125	none
$CH_3C_{15}S$/Au SAM + 5 mM $Ru(NH_3)_6^{3+}$					
− 50	+ 135	90 ± 1	0.99 ± 0.01	2925 ± 12	14628 ± 117
− 100	+ 85	89 ± 1	0.98 ± 0.06	711 ± 3	2363 ± 28
− 150	+ 35	88 ± 1	0.95 ± 0.01	214 ± 1	566 ± 10
− 200	− 15	86 ± 1	0.87 ± 0.02	105 ± 1	405 ± 8
− 225	− 40	87 ± 1	0.95 ± 0.02	99 ± 1	691 ± 4
− 250	− 65	88 ± 1	0.96 ± 0.02	120 ± 1	1643 ± 10
− 275	− 90	89 ± 1	1.00 ± 0.01	167 ± 1	2818 ± 20
− 300	− 115	89 ± 1	1.03 ± 0.01	268 ± 2	6304 ± 44
− 325	− 140	90 ± 1	1.06 ± 0.01	477 ± 4	13667 ± 86

Table 5.1 CNLS regression results.

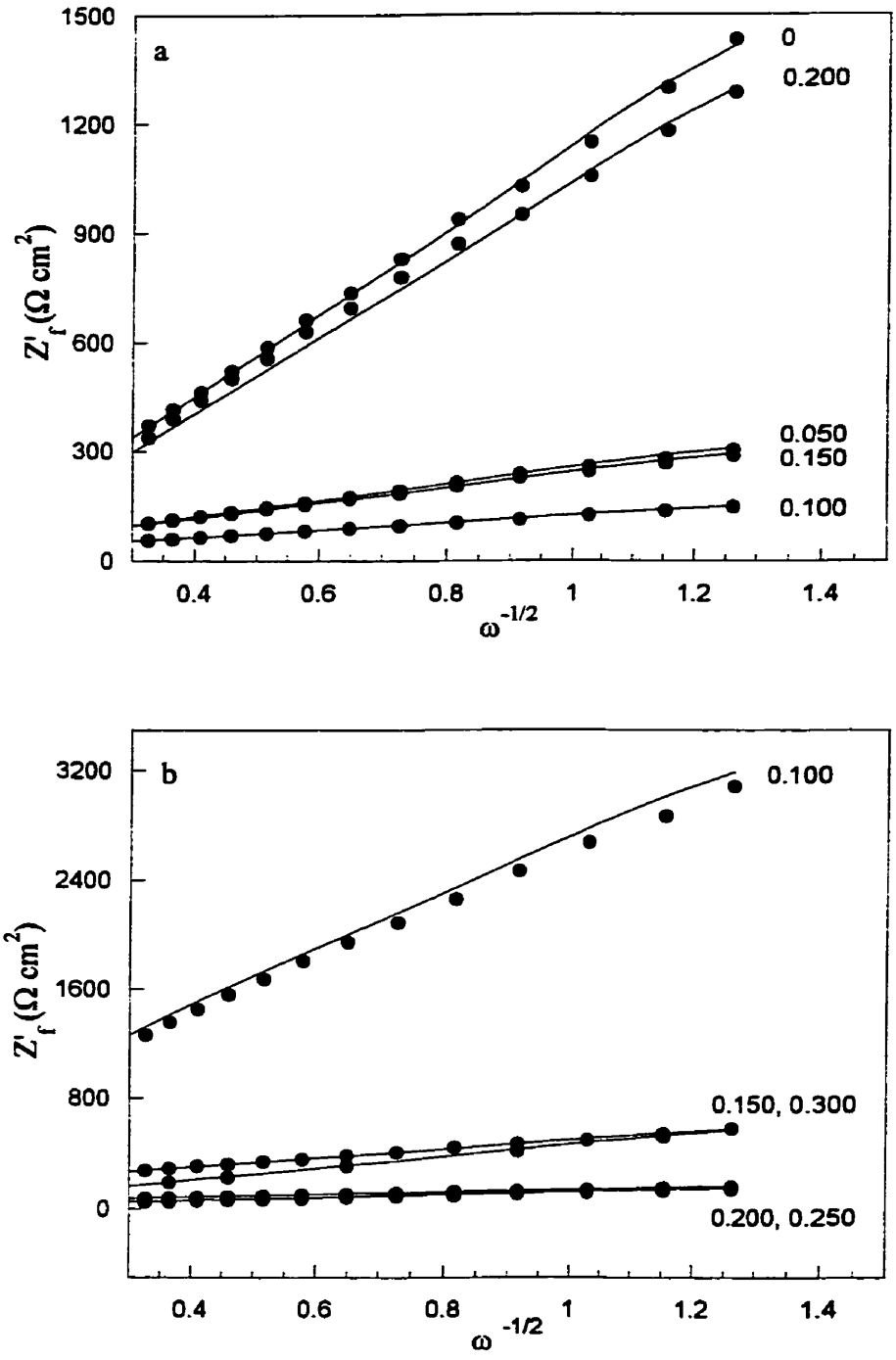

Figure 5.7 Real faradaic impedance (Z'_f) as a function of $\omega^{-1/2}$ for the electrochemical systems at various applied potentials, typically ± 150 mV with respect to $E^r_{1/2}$. The solid lines represent the results fitted to the Randles equation. The numbers correspond to the applied d.c. potential, E (in V *vs.* Ag/AgCl). *a)* Bare Au + 5 mM $Co(bpy)_3^{3+}$, *b)* Bare Au + 5 mM $Fe(CN)_6^{3-/4-}$.

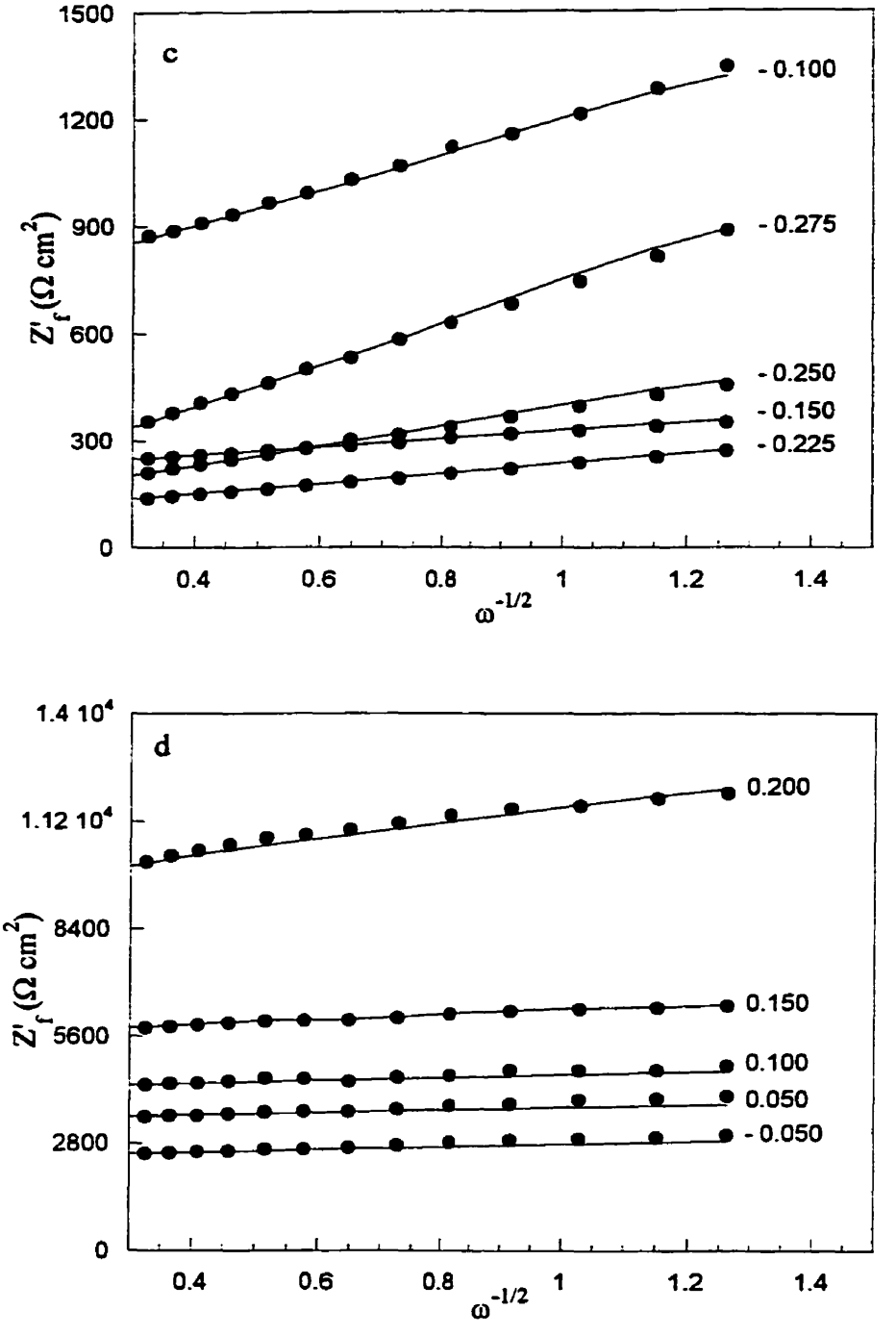

Figure 5.7 (cont'd) *c)* $CH_3(CH_2)_{15}S$/Au SAM + 5 mM $Ru(NH_3)_6^{3+}$, and *d)* $CH_3(CH_2)_{15}S$/Au SAM + 5 mM $Co(bpy)_3^{3+}$.

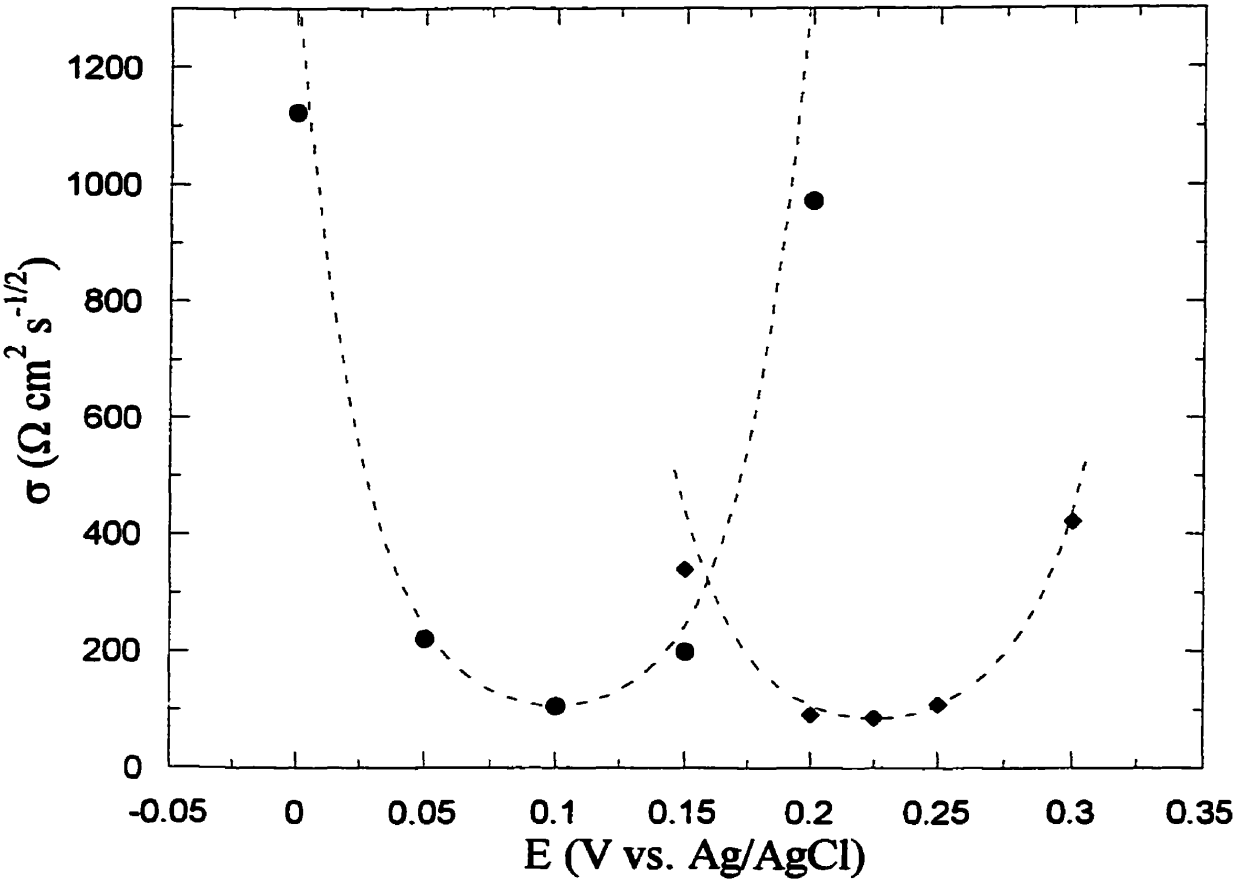

Figure 5.8 Warburg coefficient σ as a function of applied potential E for (•) the reduction of $Co(bpy)_3^{3+}$ (5mM in 50 mM K_2HPO_4) and (♦) $Fe(CN)_6^{3-/4-}$ (5mM, equimolar concentration, in 50 mM K_2HPO_4) on a bare gold electrode. The lines represent curves calculated using eq 6 for a simple one electron transfer (---): D_o = 5.0×10^{-7} cm^2 s^{-1}, $E^r_{1/2} = +0.100$ V (*vs.* Ag/AgCl) for $Co(bpy)_3^{3+}$, and $D_o = 7.8 \times 10^{-7}$ cm^2 s^{-1}, $E^r_{1/2} = +0.225$ V for $Fe(CN)_6^{3-/4-}$.

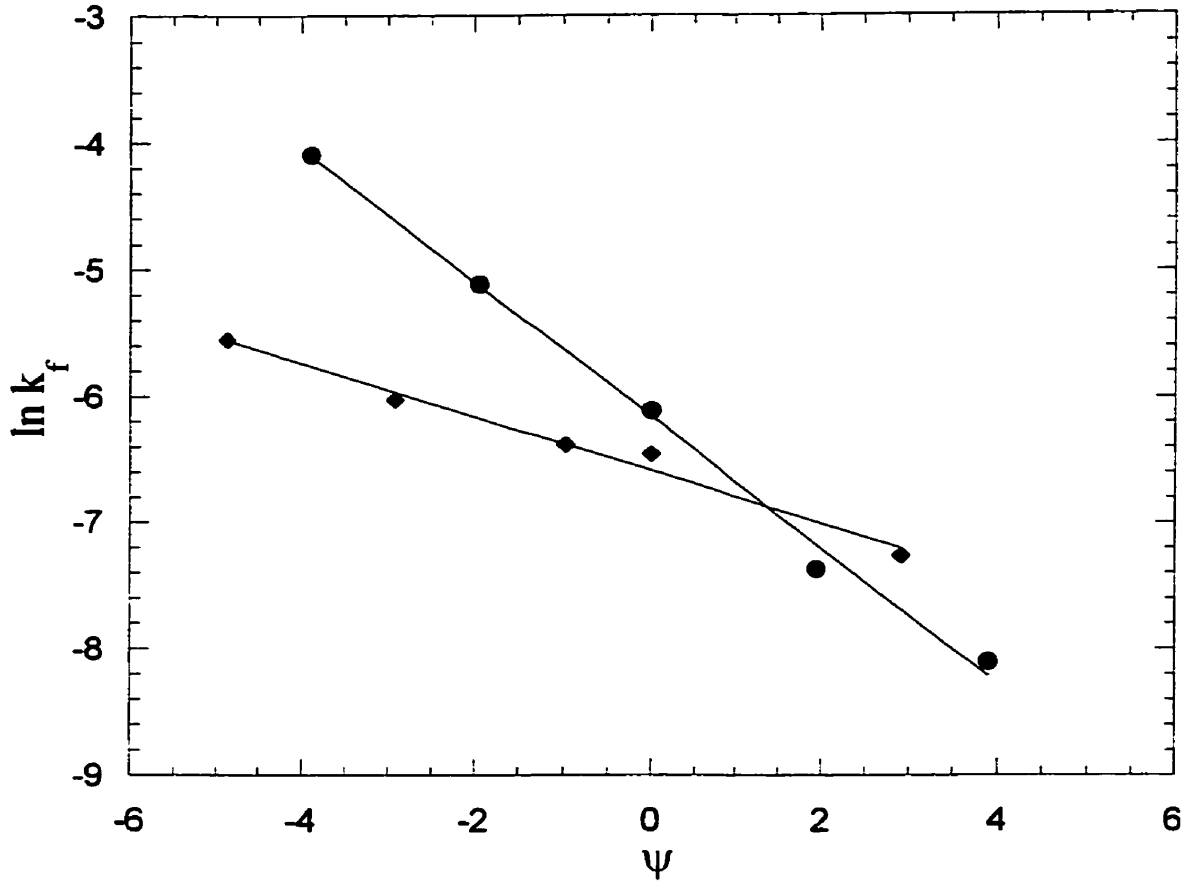

Figure 5.9 Potential dependence of the forward rate constant k_f (eq 19 and 20) for the faradaic reaction on a bare gold electrode obtained from the values of σ and R_{ct} at a given potential. D_o = 5.0 × 10^{-7} cm^2 s^{-1}, $E^r_{1/2}$ = + 0.100 V (*vs.* Ag/AgCl) for $Co(bpy)_3^{3+}$ (•), and D_o = 7.8 × 10^{-7} cm^2 s^{-1}, $E^r_{1/2}$ = + 0.225 V for $Fe(CN)_6^{3-/4-}$ (♦). The line results from the linear regression (r^2 = 0.995 for $Co(bpy)_3^{3+}$, and r^2 = 0.985 for $Fe(CN)_6^{3-/4-}$). The k_f values for $Ru(NH_3)_6^{3+}$ cannot be obtained since $R_{ct} \rightarrow 0$.

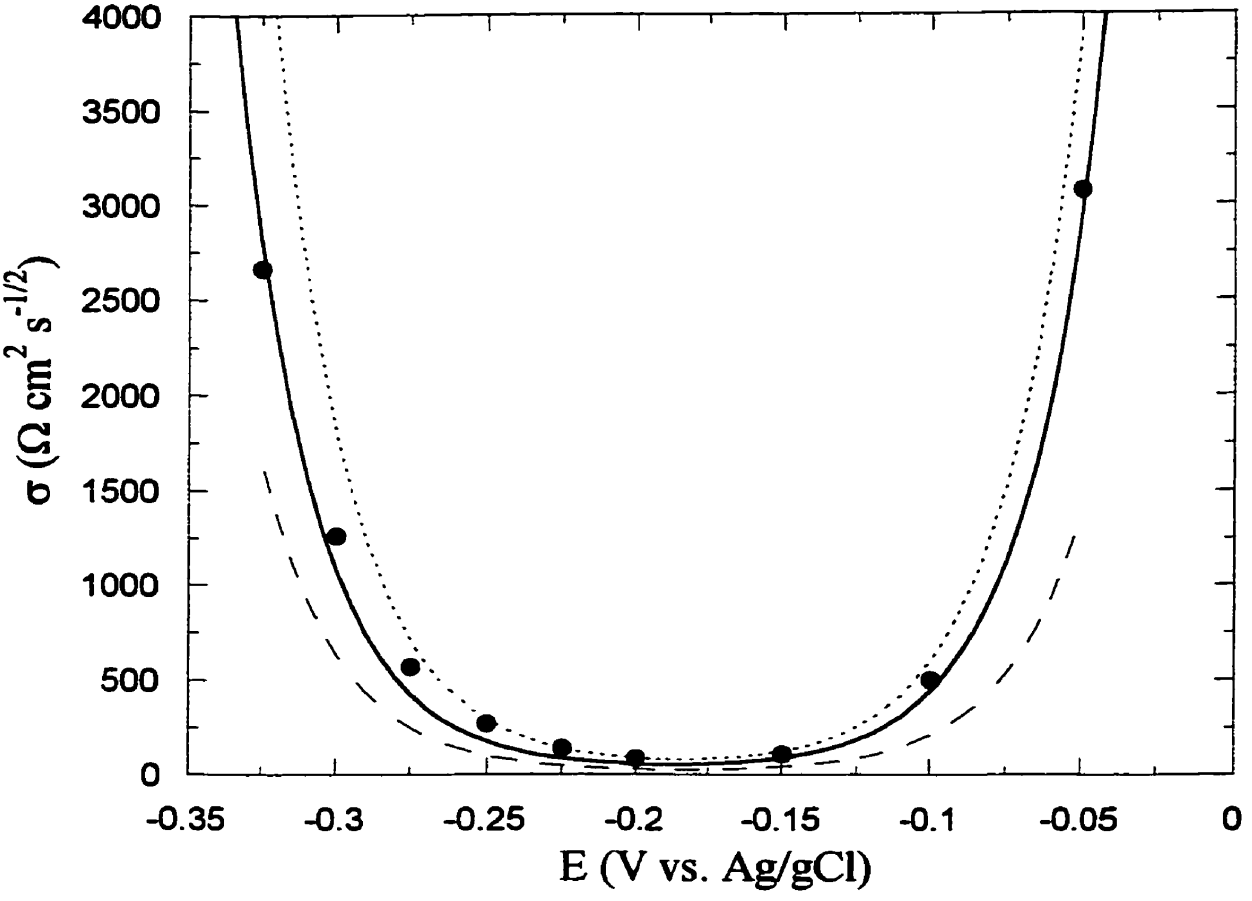

Figure 5.10 Warburg coefficient σ as a function of applied potential E for the reduction of $Ru(NH_3)_6^{3+}$ (5 mM in 50 mM K_2HPO_4) at a $CH_3(CH_2)_{15}S$/Au SAM. The dots are experimental data points. The lines represent calculated curves: with eq 12 for the CE mechanism and $D_o = 7.1 \times 10^{-6}$ cm^2 s^{-1}, $K = 16$, $L = 0.8$, and $E^r_{1/2} = -0.185$ V (*vs.* Ag/AgCl) (—); with eq 6 for a simple electron transfer and $D_o = 7.1 \times 10^{-6}$ cm^2 s^{-1}, $E^r_{1/2} = -0.185$ V (- - -), and $D_o = 2.8 \times 10^{-6}$ cm^2 s^{-1}, $E^r_{1/2} = -0.185$ V (---).

The potential dependence of k_f (for a one-electron reaction) assuming Butler-Volmer kinetics is given by:[47-49]

$$k_f = k_{sh} e^{-\alpha\psi} \qquad (19)$$

where k_f can be determined at each potential from the values of σ and R_{ct} according to:[30]

$$k_f = \left(\frac{1}{e^{\psi}+1}\right)\left(\frac{\sqrt{2D_o\sigma}}{R_{ct}}\right) \qquad (20)$$

As expected from eq. 19, $\ln k_f - \psi$ plots lead to a straight line from which α (slope) and k_{sh} (y-intercept) can be determined (Figure 5.9). For $Co(bpy)_3^{3+}$, $k_{sh} = 2.1 \times 10^{-3}$ cm s^{-1} and $\alpha = 0.5$; the k_{sh} values obtained using eq 10 (2.2×10^{-3} cm s^{-1}) and 19 are thus in excellent agreement with one another. However, for $Fe(CN)_6^{3-/4-}$, eq 10 yields a k_{sh} of 3.1×10^{-3}, whereas eq 19 yields a k_{sh} of 1.4×10^{-3} cm s^{-1} and $\alpha = 0.2$.

5.4.4 CE Mechanism

The reduction of $Ru(NH_3)_6^{3+}$ at a $CH_3(CH_2)_{15}S$/Au SAM is adequately described by the Randles equivalent circuit at all applied potentials, *i.e.* ~ $E^r_{1/2} \pm 150$ mV (*vs.* Ag/AgCl) (Figure 5.7c). The experimental σ - E curve is better described by a CE mechanism (solid line) rather than a simple reversible electron transfer (Figure 5.10). The solid line in Figure 5.10 is the best fit of the experimental data to the CE mechanism (eq 12), using a literature value for $D_o = 7.1 \times 10^{-6}$ cm^2 s^{-1},[50] and taking $L = 0.8$ and $K = 16$. The dotted line corresponds to a simple electron transfer (eq 6) using $D_o = 2.8 \times 10^{-6}$ cm^2 s^{-1} (as obtained from σ_m at bare gold, eq 9) and $E^r_{1/2} = -0.185$ V *vs.* Ag/AgCl. The dashed line results also from a simple electron transfer (eq 6) with $D_o = 7.1 \times 10^{-6}$ cm^2 s^{-1} (literature value) and $E^r_{1/2} = -0.185$ V *vs.* Ag/AgCl. The shape of the experimental σ-E curve gives crucial indications on the type of electron transfer mechanism that is taking place at the SAM-coated electrode. Evidence for a mechanism different from a simple reversible electron transfer arise

from the shape of the σ -E curve. The shape of the σ-E curve (Figure 5.10) is different from that of a simple electron transfer as it is not symmetrical about its minimum value and is not a purely exponential function. It is observable (although not striking) that the left arm ($E < E^r_{1/2}$) of the simulated CE curve is displaced to a greater extent towards reductive overpotentials than is the right arm ($E > E^r_{1/2}$) towards greater anodic overpotentials. In a CE mechanism (contrary to a simple electron transfer reaction), the position of the cathodic arm can be moved by varying the K parameter. There is a good correlation between the fit (solid line, K = 16) and the experimental data (dots), meaning that a CE mechanism as described in section 2 is operative. The sensitivity of the simulated CE curves is such that the errors in K and L are within 10 to 15 % of fitting values.

It is of interest is to test whether the experimental σ - E plot (Figure 5.10) allows one to differentiate between a CE mechanism and a CEC mechanism. The CEC mechanism can be formulated as:

$$O_{sol} \overset{K_a}{\rightleftharpoons} O_{SAM} + n\,e^- \overset{k_{sh}}{\longleftrightarrow} R_{SAM} \overset{K_b}{\rightleftharpoons} R_{sol} \qquad (21)$$

The expression for σ corresponding to a CEC mechanism is given by:[51]

$$(\sigma)_{CEC} = \frac{RT}{n^2F^2C_o^*(2D_o)^{1/2}}\left[\frac{K_a}{K_a+1}\left(\frac{L_a}{L_b}e^{-\psi}+1\right)+\frac{K_b}{K_b+1}\left(\frac{L_a}{L_b}+e^{\psi}\right)\right] \qquad (22)$$

L_a and L_b can adopt values either smaller or greater than 1, whereas $L < 1$ in a CE mechanism (section 2). Assuming $K_a = K_b$ in eq 22, the σ - E curve is shifted negatively with respect to $E^r_{1/2}$ when L_a/L_b < 1 and positively when L_a/L_b > 1. Because the experimental σ - E curve is shifted negatively with respect to $E^r_{1/2}$ (Figure 5.10), we cannot formally differentiate between a CE and a CEC mechanism. K_a and K_b affect the σ - E curve independently (eq 22). Increasing values of K_a displace the cathodic arm ($E < E^r_{1/2}$) towards the center $(\sigma_m)_{CE}$ (*i.e* leads to higher slopes) while increasing values of K_b displace the anodic arm ($E > E^r_{1/2}$)

towards $(\sigma_m)_{CE}$. This effect is more apparent at large overpotentials. From Figure 5.10, the CE simulation curve (solid line) accommodates all the experimental data (dots), including data at large cathodic and anodic overpotentials. This suggests that there is no need, in fact, to include a chemical step following the electrochemical step, as it would necessarily displace the position of the anodic arm of the $\sigma - E$ fit (solid line). The reduction of $Ru(NH_3)_6^{3+}$ at a $CH_3(CH_2)_{15}S$/Au SAM thus appears to be most adequately described in terms of CE mechanism (eq 11 and 12), rather than either E or CEC mechanisms.

5.4.5 Irreversible Electron Transfer

The potential dependence of the Warburg coefficient for the reduction of $Co(bpy)_3^{3+}$ at a $CH_3(CH_2)_{15}S$/Au SAM is shown in Figure 5.11. The experimental data can be fitted to an irreversible electron transfer reaction (solid line, eq 17). The D_r and k_{sh} values used in the simulation are those obtained for the reduction of $Co(bpy)_3^{3+}$ on a bare gold electrode. The quotient δ_r / D_r (= 20) and α (0.9) were obtained by iterative fits to the experimental data, recognizing that these two parameters independently affect the $\sigma - E$ plot (section 2). The errors in δ_r / D_r and α is within 10 % of the fitting values.

5.5 Discussion

5.5.1 Electron Transfer at a Bare Gold Electrode

$Fe(CN)_6^{3-/4-}$ (in 50 mM K_2HPO_4) has a k_{sh} of 3.1×10^{-3} cm s^{-1} on a gold surface as determined from a $\sigma - E$ plot. This value is greater than that obtained from the $\ln k_f - \psi$ plot (1.4×10^{-3} cm s^{-1}). However, both values are approximately one order of magnitude smaller than the literature values reported in 0.5 M KCl (3.7×10^{-2} cm s^{-1})[21] and in 0.5 M $NaClO_4$ (~ 1.0×10^{-2} cm s^{-1}).[18]

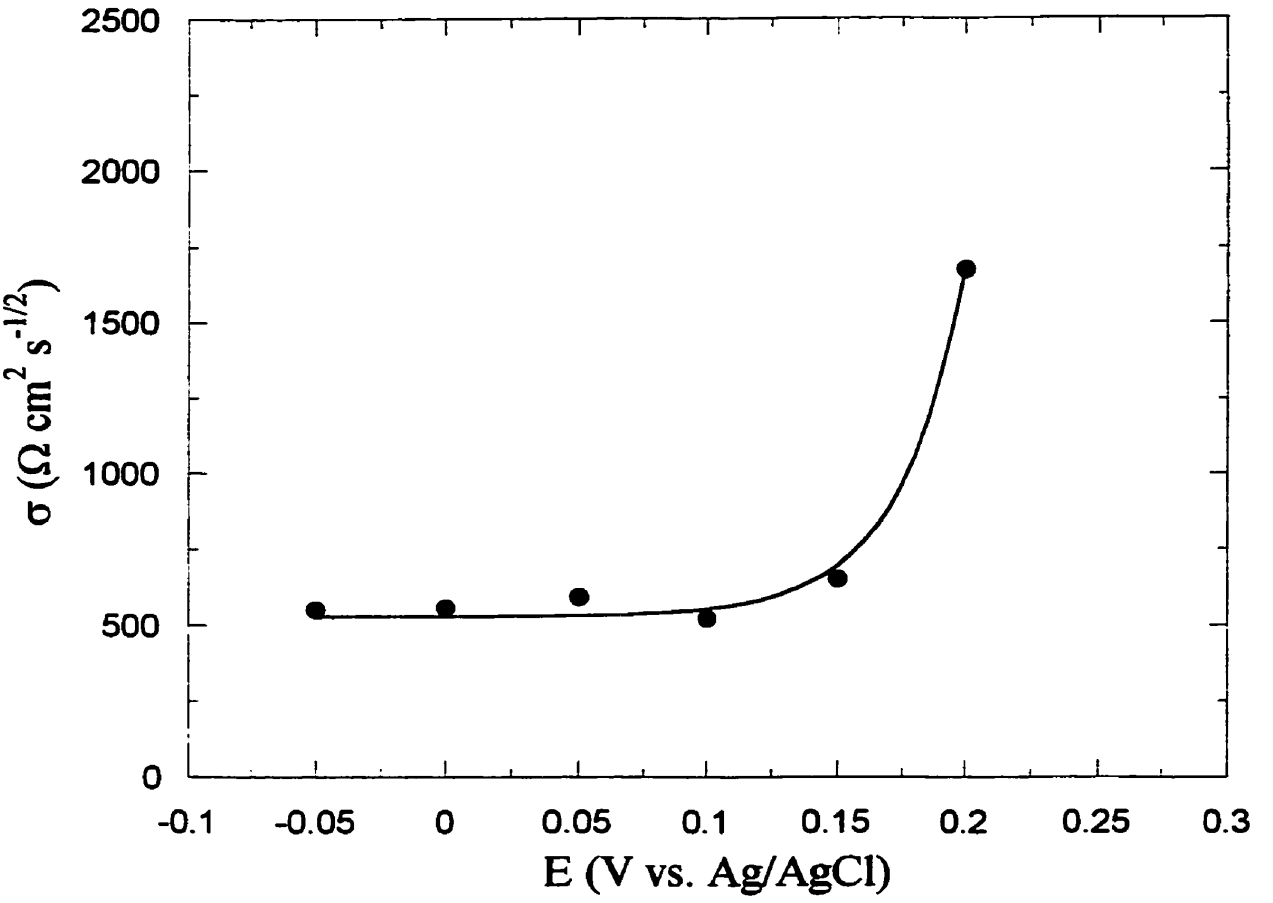

Figure 5.11 Warburg coefficient σ as a function of applied potential E for the reduction of $Co(bpy)_3^{3+}$ (5 mM in 50 mM K_2HPO_4) at a $CH_3(CH_2)_{15}S$/Au SAM. The dots are experimental data points. The line represents the calculated curve obtained with eq 17 for an irreversible electron transfer mechanism, $D_r = 5.0 \times 10^{-7}$ cm^2 s^{-1}, $k_{sh} = 2.1 \times 10^{-3}$ cm s^{-1}, $E^r_{1/2} = +0.100$ V (*vs.* Ag/AgCl), $\delta_r / D_r = 20$ and $\alpha = 0.9$.

It is however well-established that $Fe(CN)_6^{3-/4-}$ kinetics are sensitive to the nature and concentration of the supporting electrolyte.[52] Alkali metal cations promote the reaction in the order $Li^+ < Na^+ < K^+ \sim Cs^+$, and k_{sh} is inversely dependent upon the cation concentration over the 0.1 M to 10 M range. The lower concentration of the supporting electrolyte used in this study (50 mM K_2HPO_4) may contribute to the discrepancy between the k_{sh} values obtained here and the literature values. The α value of 0.2 (from $\ln k_f - \psi$ plot) for $Fe(CN)_6^{3-/4-}$ indicates that the kinetics are inadequately described by Butler-Volmer kinetics.

The kinetics of the $Co(bpy)_3^{3+/2+}$ couple, on the other hand, are well behaved ($\alpha = 0.5$). The k_{sh} is 2.2×10^{-3} cm s^{-1}, as determined from both the σ-E and the $\ln k_f - \psi$ plots.

5.5.2 Electron transfer at a $CH_3(CH_2)_{15}S$/Au SAM

The σ - E characteristics of the reduction of $Ru(NH_3)_6^{3+}$ at a pinhole-free $CH_3(CH_2)_{15}S$/Au electrode establish that a CE (chemical-electrochemical) process is operative. This is particularly interesting as it sheds new light on the role played by SAMs in electrode kinetics. The precise nature of the chemical step preceding the electron transfer cannot however be readily identified. The most appropriate analogy is to a very recent study by Nelson and co-workers.[51] A CEC mechanism has been shown to be effective in lipid monolayer-coated electrodes which have been deliberately perforated with peptide (Gramicidin D) channels. The preceding chemical reaction in this case is believed to be either the translocation of the Tl^+ cations into the channels or the desolvation of the Tl^+ ion prior to electron transfer. The nature of the following reaction (*i.e.* the second C step) in this system has not yet been determined.

The heterogeneous rate constant k_{sh} for the reduction of $Ru(NH_3)_6^{3+}$ at a $CH_3(CH_2)_{15}S$/Au SAM is not directly accessible from the σ - E plot, as it is part of the parameter L. Since it is readily apparent that the presence of the SAM considerably reduces the kinetics of electron transfer (Figure 5.6), there are (at least) four different possible origins of the chemical step in the CE mechanism:

i) ion pairing and/or desolvation of the redox couple,

ii) transfer of the redox molecule from the aqueous phase into the organic phase, as in a partitioning process,

iii) a combination of both *i)* and *ii)*,

iv) the surface area available for electron transfer is greatly reduced by the SAM and electron transfer occurs only at defects and/or pinhole sites.

Each interpretation would lead to a decrease in the apparent value of k_{sh} by either reducing the effective concentration of the redox probe at the gold surface or by considerably diminishing the effective area available for the electron transfer (eq 10). Case *iv)* is applicable when ion channels[51] or pinholes are present in the SAM,[14,15,21] forming favorable paths for presenting the redox couple directly to the electrode surface. However, the impedance results presented here and elsewhere[2,43] clearly establish that the SAMs used in this study are pinhole-free prior to the redox couple being introduced. Case *iv)* is therefore not considered to be relevant here. It is most likely that the chemical step in the CE mechanism is due to a preceding chemical reaction or process.

There are two limiting descriptions of the mechanism of electron transfer in the SAM literature: *via* pinholes[11,14,15,21,26] or *via* electron tunneling across the full width of the SAM.[25,53,54] The pinhole-mediated process is unlikely here and the tunneling process does not readily accommodate a prior chemical step. We cannot yet resolve all the mechanistic details but an intermediate mechanism involving a permeation process is consistent with cases *i)*, *ii)*, and *iii)*. This permeation process does not necessarily exclude a tunneling process. One can envisage a situation where electrons can tunnel across a SAM once the redox probe has partitioned and traveled in the SAM to a distance sufficiently close for efficient electron transfer to occur.

We find that the mechanism of electron transfer of $Fe(CN)_6^{3-/4-}$ across defect-free SAMs cannot be elucidated from the potential dependence of σ, since the Randles equivalent circuit is not applicable (as no diffusion process is observed in the low frequency range, Figure 5.6). This has also been observed in a previous report.[18]

The R_{ct} values obtained with $Fe(CN)_6^{3-/4-}$ are considerably larger than for either $Ru(NH_3)_6^{3+/2+}$ or $Co(bpy)_3^{3-/2+}$ (Table 5.1). The large R_{ct} values with $Fe(CN)_6^{3-/4-}$ may be the result of high energy process such as desolvation. $Fe(CN)_6^{3-}$ and $Fe(CN)_6^{4-}$ are both highly solvated (and hydrophilic). Moreover, the difference in solvation number is large between the two redox ions.[55] Born solvation theory[56] allows one to estimate the energy, U, required to transfer a redox molecule from the aqueous phase into the organic (SAM) phase, where:

$$U = \frac{(ze)^2}{8\pi\varepsilon_o r}\left(\frac{1}{\varepsilon_m} - \frac{1}{\varepsilon_{aq}}\right) \qquad (23)$$

The valence of the ion is z, e is the electronic charge, r is the ionic radius, and ε_o is the permittivity of free space (8.85×10^{-14} F cm^{-1}). Using $\varepsilon_m \approx 2$ and $\varepsilon_{aq} \approx 80$, and assuming an ionic radius of 4.1 Å for $Fe(CN)_6^{4-}$ and 3.3 Å for $Ru(NH_3)_6^{3+}$,[57] the transfer of non-solvated $Fe(CN)_6^{4-}$ from the aqueous electrolyte into the low dielectric media of the SAM requires about twice the energy than does non-solvated $Ru(NH_3)_6^{3+}$. Of course, these differences can be greatly magnified (or attenuated) if the charge and effective radii are differentially modulated. Also, a change in the hydrophobicity of the SAM/electrolyte interface affects the electron transfer kinetics, as observed in cyclic voltammetry studies. For example, the reduction of $Fe(CN)_6^{3-}$ at a methyl-terminated SAM is more than 20 times slower than at a hydroxylated SAM.[7]

5.6 Conclusions

The kinetics of electron transfer at *defect-free* SAM-coated electrodes as a function of the d.c. applied potential is reported using a.c. impedance spectroscopy. Experimental and simulated σ - E (Warburg coefficient as a function of the applied potential) curves are extremely valuable tools in determining the mechanism of electron transfer and the kinetic parameters at SAM-coated electrodes. The σ - E analysis is only applicable when the experimental data fit the Randles equivalent circuit and a linear $Z_f' - \omega^{1/2}$ relationship is satisfied.

The study of the mechanism of electron transfer was conducted at a $CH_3(CH_2)_{15}S$/Au SAM with three redox couples $Ru(NH_3)_6^{3+/2+}$, $Fe(CN)_6^{3-/4-}$, and $Co(bpy)_3^{3+/2}$ in 25 mV steps about $E^r_{1/2} \pm \sim 150$ mV. Fits of the experimental σ - E data to simulations at $CH_3(CH_2)_{15}S$/Au SAMs reveal that the electron transfer significantly depends on the nature of the redox couple. The differences in the heterogeneous rate constants of the three redox probes cannot in themselves account for the observed differences in the electron transfer kinetics.

At $CH_3(CH_2)_{15}S$/Au SAMs, the electron transfer is irreversible in the case of $Co(bpy)_3^{3+/2+}$ and proceeds *via* a CE mechanism with $Ru(NH_3)_6^{3+/2+}$. The chemical step in the CE mechanism observed with $Ru(NH_3)_6^{3+}$ appears to be a complex process and likely involves desolvation of the redox couple and/or partitioning of the redox couple in the hydrocarbon region of the SAM prior to the reduction step. Although it is the most frequently used probe in SAM electrochemical studies, the properties of the $Fe(CN)_6^{3-/4-}$ couple is particularly complex in the presence of the SAM. The results of this study reveal the complexity in predicting the performance of SAMs as electronic barriers using redox carriers. More investigations involving the effects of chainlength n, chain end group X, concentration of the redox probe C^*, and temperature on the σ - E curve will allow one to better understand the factors that govern the kinetics of interfacial electron transfer at SAM-coated electrodes.

References

1) Badia, A.; Back, R.; Lennox, R. B. *Angew. Chem., Int. Ed. Engl.* **1994**, *33*, 2333-2334.

2) Boubour, E.; Lennox, R. B. *Submitted to J. Phys. Chem. B* **2000**.

3) Boubour, E.; Lennox, R. B. *In preparation* **2000**.

4) Krysinski, P.; Brzostowska-Smolska, M. *J. Electroanal. Chem.* **1997**, *424*, 61-67.

5) Chen, J.; Saghi-Szabo, G.; Tossell, J. A.; Miller, C. J. *J. Am. Chem. Soc.* **1996**, *118*, 680-684.

6) Chailapakul, O.; Crooks, R. M. *Langmuir* **1993**, *9*, 884-888.

7) Becka, A. M.; Miller, C. J. *J. Phys. Chem.* **1993**, *97*, 6233-6239.

8) Miller, C. J.; Grätzel, M. *J. Phys. Chem.* **1991**, *95*, 5225-5233.

9) Miller, C.; Cuendet, P.; Grätzel, M. *J. Phys. Chem.* **1991**, *95*, 877-886.

10) Chidsey, C. E. D.; Loiacono, D. N. *Langmuir* **1990**, *6*, 682-691.

11) Finklea, H. O.; Avery, S.; Lynch, M.; Furtsch, T. *Langmuir* **1987**, *3*, 409-413.

12) Finklea, H. O.; Robinson, L. R.; Blackburn, A.; Richter, B. *Langmuir* **1986**, *2*, 239-244.

13) Porter, M. D.; Bright, T. B.; Allara, D. L.; Chidsey, C. E. D. *J. Am. Chem. Soc.* **1987**, *109*, 3559-3568.

14) Sabatini, E.; Rubinstein, I. *J. Phys. Chem.* **1987**, *91*, 6663-6669.

15) Finklea, H. O.; Snider, D. A.; Fedyk, J.; Sabatini, E.; Gafni, Y.; Rubinstein, I. *Langmuir* **1993**, *9*, 3660-3667.

16) Sabatini, E.; Cohen-Boulakia, J.; Bruening, M.; Rubinstein, I. *Langmuir* **1993**, *9*, 2974-2981.

17) Nahir, T. M.; Bowden, E. F. *Electrochim. Acta* **1994**, *39*, 2347-2352.

18) Janek, R. P.; Fawcett, W. R.; Ulman, A. *Langmuir* **1998**, *14*, 3011-3018.

19) Beulen, M. W. J.; Kastenberg, M. I.; M., v. V. F. C. J.; Reinhoudt, D. N. *Langmuir* **1998**, *14*, 7463-7467.

20) Song, S.; Clark, R. A.; Bowden, E. F.; Tarlov, M. J. *J. Phys. Chem.* **1993**, *97*, 6564-6572.

21) Sabatini, E.; Rubinstein, I.; Maoz, R.; Sagiv, J. *J. Electroanal. Chem.* **1987**, *219*, 365-371.

22) Slowinski, K.; Chamberlain II, R. V.; Bilewicz, R.; Majda, M. *J. Am. Chem. Soc* **1996**, *118*, 4709-4710.

23) Xu, J.; Li, H.-L.; Zhang, Y. *J. Phys. Chem.* **1993**, *97*, 11497-11500.

24) Becka, A. M.; Miler, C. J. *J. Phys. Chem.* **1992**, *96*, 2657-2668.

25) Chidsey, C. E. D. *Science* **1991**, *251*, 919-922.

26) Finklea, H. O.; Snider, D. A.; Fedyk, J. *Langmuir* **1990**, *6*, 371-376.

27) Doblhofer, J.; Figura, J.; Furhop, J.-H. *Langmuir* **1992**, *8*, 1811-1816.

28) Tokuda, K.; Gueshi, T.; Matsuda, H. *J. Electroanal. Chem.* **1979**, *102*, 41-48.

29) Amatore, C.; Savéant, J. M.; Tessier, D. *J. Electroanal. Chem.* **1983**, *147*, 39-51.

30) Sluyters, J. H.; Sluyters-Rehbach, M. *Comprehensive Treatise of Electrochemistry*; Plenum Press: New York, 1984; Vol. 9.

31) Sluyters, J. H.; Sluyters-Rehbach, M. *Comprehensive Chemical Kinetics*; Elsevier: Amsterdam, 1986; Vol. 26.

32) Sluyters-Rehbach, M.; Sluyters, J. H. *Sine wave methods in the study of electrode process*; Marcel Dekker:, 1970; Vol. 4.

33) Timmer, B.; Sluyters-Rehbach, M.; Sluyters, J. H. *J. Electroanal. Chem.* **1967**, *14*, 169-180.

34) Timmer, B.; Sluyters-Rehbach, M.; Sluyters, J. H. *J. Electroanal. Chem.* **1967**, *14*, 181-191.

35) Sluyters-Rehbach, M.; Sluyters, J. H. *J. Electroanal. Chem.* **1970**, *26*, 237-257.

36) Randles, J. E. B. *Disc. Faraday Soc.* **1947**, *1*, 11-19.

37) Rueda, M. *Research in Chemical Kinetics*; Blackwell Science: Oxford, 1997; Vol. 4.

38) Jacq, J. *Electrochim. Acta* **1967**, *12*, 1-20.

39) Macdonald, J. R. *Complex Nonlinear Least Squares Immittance Fitting Program, LEVM 7.0*; Macdonald, J. R., Ed.: Department of Physics and Astronomy, University of North Carolina, Chapel Hill, NC., 1990.

40) Furniss, B. S.; Hannaford, A. J.; Rogers, V.; Smith, P. W. G.; Tatchell, A. R. *Vogel's Textbook of Practical Organic Chemistry*; 4th ed.; Longman: New York, 1978.

41) Badia, A. *Structure and Dynamics in Self-Assembled Monolayers*; Badia, A., Ed.; McGill University: Montreal, 1996.

42) Burstall, F. H.; Nyholm, R. S. *J. Chem. Soc.* **1952**, *Part III*, 3570-3579.

43) Boubour, E.; Lennox, R. B. *Langmuir. In press* **2000**.

44) Helmholtz, H. *Ann. Phys.* **1879**, *7*, 337-382.

45) Halliday, D.; Resnick, R. *Physics*; Wiley: New York, 1978.

46) Forouzan, F.; Bard, A. J.; Mirkin, M. V. *Isr. J. Chem.* **1997**, *37*, 155-164.

47) Bard, A. J.; Faulkner, L. R. *Electrochemical Methods: Fundamentals and Applications*; John Wiley & Sons: New York, USA, 1980.

48) Butler, J. A. V. *Trans. Faraday Soc.* **1924**, *19*, 729-733.

49) Erdey-Gruz, T.; Volmer, M. *Z. Physik. Chem.* **1930**, *150A*, 203.

50) Licht, S.; Cammarata, V.; Wrigthon, M. S. *J. Phys. Chem.* **1990**, *94*, 6133-6140.

51) Rueda, M.; Navarro, I.; Ramirez, G.; Prieto, F.; Prado, C.; Nelson, A. *Langmuir* **1999**, *15*, 3672-3678.

52) Peter, L. M.; Durr, W.; Bindra, P.; Gerischer, H. *J. Electroanal. Chem.* **1976**, *71*, 31-50.

53) Finklea, H. O.; Hanshew, D. D. *J. Am. Chem. Soc.* **1992**, *114*, 3173-3181.

54) Haran, A.; Waldeck, D. H.; Naaman, R.; Moons, E.; Cahen, D. *Science* **1994**, *263*, 948-950.

55) Noftle, R. E.; Pletcher, D. *J. Electroanal. Chem.* **1990**, *293*, 273-277.

56) Born, M. *Z. Phys.* **1920**, *1*, 45-48.

57) Lappin, A. G. *Redox Mechanisms in Inorganic Chemistry*; Ellis Horwood: London, 1994.

Chapter 6

Surface Potential Measurements of *n*-Alkylthiol/Au SAMs

6.1 Introduction

The Kelvin probe technique has been used to measure the surface potential (also referred to as the contact potential difference) of organic thin films at the air/water interface (phospholipid monolayers and related systems) and to characterize the electric properties of metals and semiconductors. In the latter surfaces, the measured surface potential is related to the work function of the materials. For measurements carried out at the air/water interface, the surface potential is due to the surface dipole moments of the organic film and oriented water molecules.

In the Kelvin probe method, the sample, such as a SAM-coated gold surface is placed close ($d_o \sim 1$ mm) to the metal probe (Figure 6.1). A sinusoidally modulated vibration is applied to the probe at a frequency ω with an amplitude of vibration a, such that the plate separation d varies with time t according to:[1,2]

$$d(t) = d_o + a\sin\omega t \tag{1}$$

The vibrating probe and the sample constitute the two halves of a parallel plate capacitor and the SAM is the intermediary dielectric medium. The capacitance C of this parallel plate capacitor is given by the Helmholtz equation:[3,4]

$$C = \frac{\varepsilon_m \varepsilon_o A}{d} \tag{2}$$

where ε_m is the permittivity of the dielectric, ε_o is the permittivity of free space, and A is the surface area of the probe.

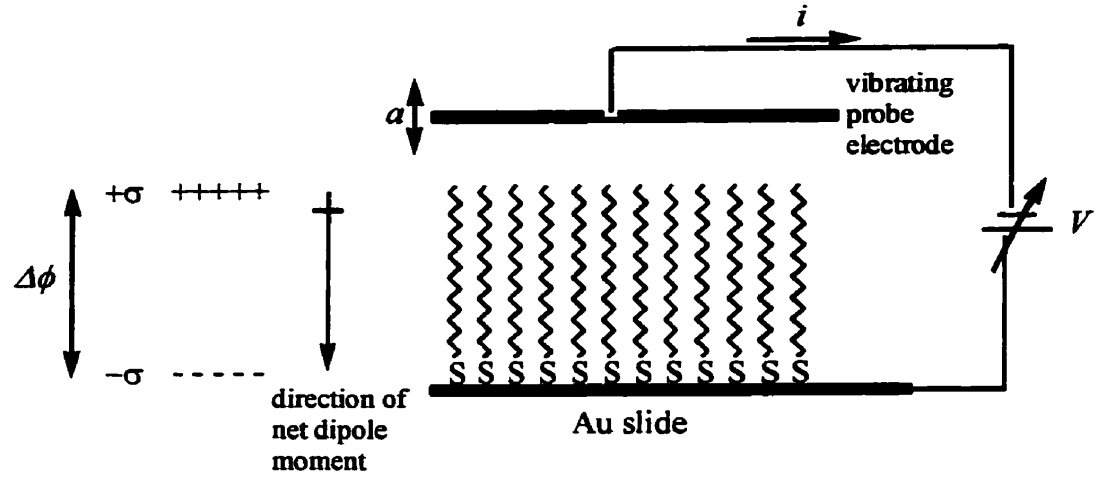

Figure 6.1. Schematic diagram illustrating the Kelvin probe device for measuring the surface potential ($\Delta\phi$) of a C_nS/Au SAM sample ($C_n = CH_3(CH_2)_{n-1}$). The device consists of the vibrating probe electrode made of an inert metal (Au, Pt, oxidized Ta or W) and the sample surface. A two-layer capacitor model describes the distribution of dipoles in C_nS/Au SAMs. The whole device is called the Kelvin probe in honor of Lord Kelvin who first introduced the vibrating condenser method to measure small electric currents (Kelvin, L. *Philos. Mag.* **1898**, *46*, 82-120).

The probe vibration produces a periodic fluctuation in C, resulting in the flow of an alternating current i in the external circuit such that:

$$i(t) = \frac{dQ}{dt} = -\varepsilon_o \varepsilon_m A \Delta V \frac{a\omega \cos(\omega t)}{[d_o + a\sin(\omega t)]^2} \tag{3}$$

where Q is the charge of the capacitor, ΔV is the voltage applied to the capacitor, d_o is the distance between the sample and the probe at rest and ω is the frequency of vibration (typically 60-120 Hz). This a.c. current i is converted to a voltage (using a high impedance preamplifier) which is then entirely compensated by an externally applied potential. The external potential required to null the voltage difference between the vibrating metal probe and the sample surface is the surface potential difference $\Delta\phi$.

Little work has been done on metal adsorbed organic films, even though Kelvin probe studies of Langmuir films have shown that surface potential measurements allow one to study the orientation of the dipole moments of monolayers. The newly developed scanning Kelvin probe microscope (derived from the atomic force microscope) has increased the interest in this technique for mapping the local dipole orientation with a lateral resolution of several tens of nanometers.[5-12]

SAMs are interesting systems for carrying out surface potential investigations as the sulfur anchor and the chain van der Waals interactions may serve to orient the dipole of the chain's end groups. The SAM itself can be envisaged as being composed of layers of dipoles associated with the $Au^{\delta+}$-$S^{\delta-}$ interface and the SAM/air interface (Figure 6.1). The orientation of these two dipole layers is likely to be in opposite direction. This description is an adaptation of a model used by Demchak and Fort used for amphiphilic monolayers at the air/water interface.[13,14] In simple terms, the expected surface potential difference due to a molecular dipole layer can be derived from Gauss' law:[15,16]

$$\Delta\phi = N\left(\frac{\mu_{\perp m}}{\varepsilon_o \varepsilon_m} + \frac{\mu_{Au-S}}{\varepsilon_o \varepsilon_{Au-S}}\right) \tag{4}$$

where N is the areal density of the molecules ($\sim 5 \times 10^{14}$ molecules cm^{-2}), $\mu_{\perp m}$ is the component of the dipole moment (of the anchored molecules) normal to the surface, μ_{Au-S} is the apparent dipole moment of the $Au^{\delta+}$-$S^{\delta-}$ bond, and ε_m is the dielectric constant of the SAM. As a first approximation, a linear relationship between the surface potential $\Delta\phi$ and the chainlength is expected if μ_{Au-S}, ε_{Au-S}, and $\mu_{\perp m}$ remain constant, but ε_m varies continuously with chainlength.[14] Evans and Ulman reported that the surface potential $\Delta\phi$ of *n*-alkylthiol/Au SAMs does indeed increase linearly with chainlength ($6 \leq n \leq 22$).[14] The Kelvin probe technique has not however been directly used to investigate the orientation of the terminal functional group in these SAMs, even though other surface analytical techniques have shown that these act as oriented surface dipoles which can strongly influence SAM interfacial properties.[17-22]

This chapter reports a Kelvin probe study of SAMs on polycrystalline gold formed from odd- and even-numbered carbon alkylthiols of varying chainlengths ($4 \leq C_n \leq 20$). The effects of the alkyl chainlength and methyl terminal group orientation on the measured surface potential are discussed in terms of the SAM structure and dielectric properties.

6.2 Experimental Section

Chemicals 1-Butanethiol (99 %), 1-pentanethiol (98 %), 1-hexanethiol (95 %), 1-octanethiol (97 %), 1-nonanethiol (95 %), 1-decanethiol (96 %), 1-dodecanethiol (98 %), and 1-octadecanethiol (98 %) were obtained from Aldrich (Milwaukee, USA). 1-Heptanethiol (97 %) and 1-tetradecanethiol (98 %) were obtained from Lancaster (Windham, NH) and Fluka (Buchs, Switzerland) respectively. Commercially available chemicals were used as received, except 1-octadecanethiol which was triply recrystallized from ethanol before use. 1-Pentadecanethiol, 1-hexadecanethiol, 1-heptadecanethiol, 1-nonadecanethiol, and 1-eicosanethiol were available from previous studies[23] and were synthesized by conversion of the corresponding aliphatic alcohol (Fluka, purum) to the alkylbromide

by refluxing with 48 % HBr, prior to reaction with thiourea following standard procedures.[24] The purity of the synthesized molecules was monitored by ^{1}H and ^{13}C NMR spectroscopy, thin layer chromatography, mass spectrometry, and melting point determination using differential scanning calorimetry.[23]

Instrumentation The surface potential was recorded using a vibrating plate capacitor device (KSV SP). The vibrating probe (platinum plate) oscillates at a frequency of 80 - 120 Hz. The measuring range of the device is ± 10 V with an accuracy of ± 5 mV. The sample was placed at a distance of about 1 mm from the vibrating probe and electrically connected to it. The whole device was grounded *via* the sample. The surface potential was recorded after a stable signal was obtained (typically 2 to 3 minutes). A freshly cleaned bare gold surface was used as a reference to zero the surface potential meter. The reported surface potential values thus correspond to the surface potential difference between the C_nS/Au SAM and the bare gold reference substrate, that is $\Delta\phi = \phi_{sample} - \phi_{reference}$. n refers to the ***total number of carbon atoms*** in a given SAM, ***including the methyl terminal group***. The surface potential value reported for each SAM is the average of three independent measurements taken on five different SAM-coated samples prepared under the same conditions. All measurements were carried out at 20-22 °C in ambient atmosphere with a relative humidity of ~ 16-22 %.

Monolayer preparation Commercially available polycrystalline gold slides (3 cm^2 geometric surface area, EMF, NY) consisting of 1000 Å of thermally evaporated gold and 50 Å of titanium on glass were cleaned by sonicating in a boiling solution of 50:50 ethanol:chloroform in an ultrasonic bath (Branson 1200). This procedure was repeated twice. The substrates were then thoroughly rinsed with anhydrous ethanol followed by Millipore water (18 MΩ cm, Milli-Q Systems). Traces of organic residues were removed from the gold surface by cleaning with piranha solution (3:1 H_2SO_4:H_2O_2, *extreme caution* must be taken when working with piranha solution since it reacts violently with organic materials). The cleaned slides were finally rinsed with a copious amount of Millipore water and anhydrous ethanol. The slides were immediately incubated in a freshly prepared 1 mM C_nSH solution (N_2 purged ethanol) in a sealed vial, at room temperature, for 3 to 4 days.

6.3 Results and Discussion

As had been previously reported, the surface potential $\Delta\phi$ of C_nS/Au SAMs was found to increase linearly with chainlength for $n > 6$ (Figure 6.2). We measured a total change in the surface potential of ~ 0.6 V on going from 7 carbons to 20 carbons, compared to ~ 0.2 V reported by Evans and Ulman ($n = 6 - 22$). While the measured surface potential in our measurements is constant with chainlength for short chains ($4 \leq n \leq 6$), no upper limit was observed for chainlengths up to 20 carbons. The most striking feature of our results is the systematic 122 mV difference observed between (n) odd-numbered SAMs and the corresponding ($n+1$) even-numbered SAMs. While this odd/even effect in the SAM Kelvin probe experiments has not been previously observed, an odd/even effect on SAM surface properties has been reported with other surface-sensitive techniques.[17-21]

Grazing angle infrared spectroscopy studies indicated early on that the terminal CH_3 orientation is different for SAMs formed from odd- and even-carbon alkylthiolates on predominantly Au(111).[25] This effect is manifested as a modulation of the intensities of the C-H stretching modes of the terminal methyl groups (Figure 6.3). In an even-numbered chainlength, the intensities of the symmetric and antisymmetric CH_3 stretching bands are approximately equal, but for odd-numbered chainlengths, the antisymmetric band intensity is significantly stronger than that of the symmetric band. Since the vibration modes perpendicular to the surface contribute to a greater extent to the measured signal, this suggests that the transition dipole orientation of the terminal methyl group is closer to being perpendicular to the surface for even chains than for odd chains. Furthermore, this would only be observable if the chains have a preferred orientation, that is, they are tilted away from the surface normal at a fixed angle and are in a predominantly *all-trans* configuration.

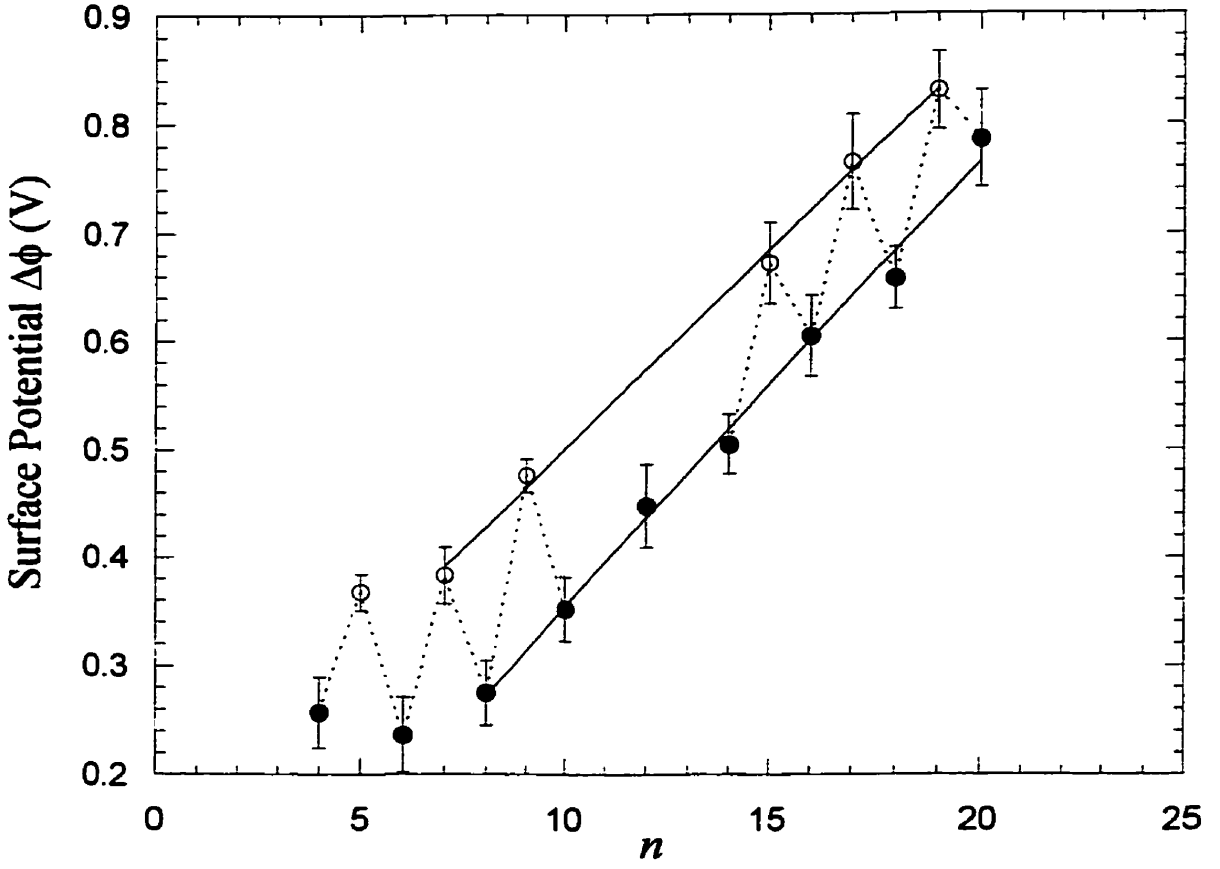

Figure 6.2. Variation of the surface potential $\Delta\phi$ for C_nS/Au SAM (C_n=$CH_3(CH_2)_{n-1}$) with chainlength n, where n is the total number of carbons, methyl group included, in the alkyl chain. The reported surface potential value corresponds to the difference between the surface potential of a SAM-coated gold sample and that of bare gold. When n is even, the slope is 39 (± 1.4) mV per CH_2 unit (r = 0.9963), and when n is odd, the slope is 37 (± 6.6) mV per CH_2 (r = 0.9986). $\Delta\phi$ is greater by 122 (± 43) mV for odd-numbered SAMs than for even-numbered SAMs.

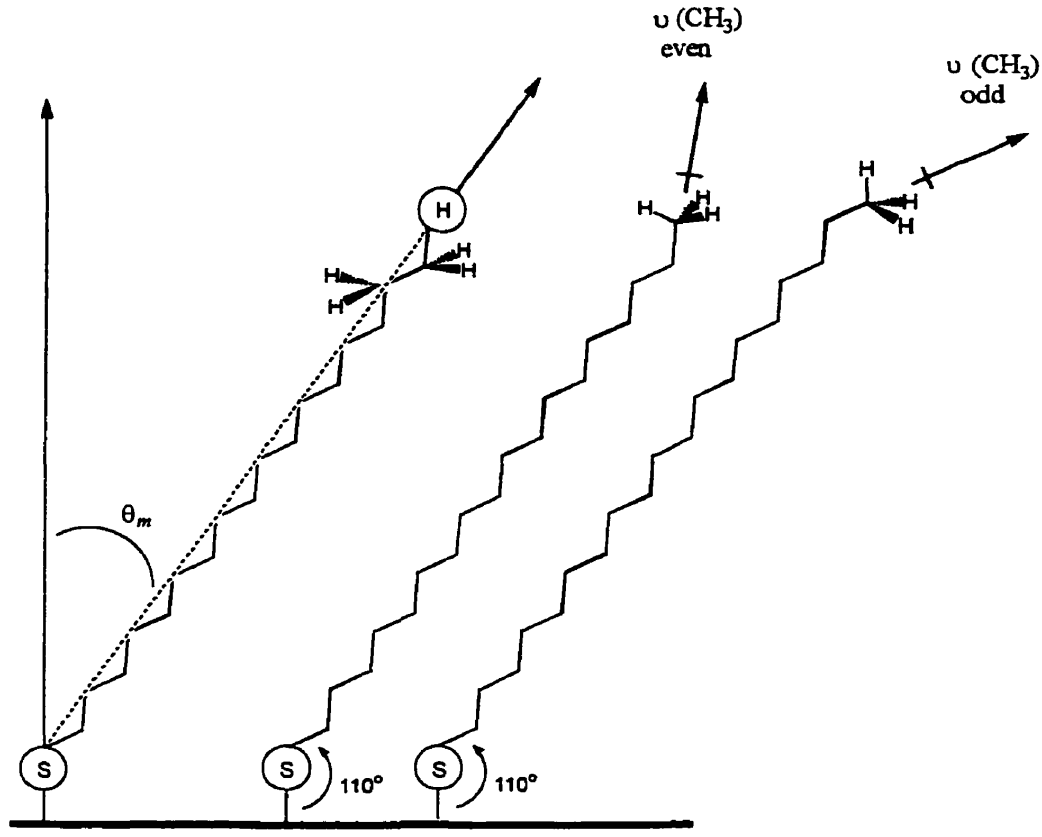

Figure 6.3. Schematic representation of the orientation of the terminal methyl group in C_nS/Au SAMs as a function of n. The transition dipole moment is canted by ~ 53° relative to the surface normal when n is odd, and by only 26° when n is even.[17,25,26]

Subsequent studies showed that the orientation of the terminal functional groups can influence the SAM interfacial properties such as wettability and adhesion. For example, contact angle measurements of C_n/polycrystalline Au SAMs ($5 \leq n \leq 16$) show that the advancing contact angles of hexadecane (θ_a^{HD}) are systematically *greater* by ~ 2-4° when n is *even* than when n is *odd*.[18-21] Application of the Lifshitz theory[27,28] and Young's equation to the experimental contact angle (θ_a - n) data shows that there is a difference of ~ 1 mJ m^{-2} in the work of adhesion ($W_{SAM\text{-}HD}$) between odd- and even-numbered monolayers, with $W_{SAM\text{-}HD}$ being larger for even SAMs.[18] This observed odd-even parity can be explained by the increased wettability of methylene *vs.* methyl groups exposed at the SAM/HD interface (Figure 6.3). An interesting possibility was presented such that the wettability of SAMs by fluids results from a combination of both the orientation of the methyl end groups and the SAM-mediated van der Waals forces acting between the gold substrate and the fluid.

Finally, a recent atomic force microscopy study also detected differences in the frictional properties which were correlated with the orientation of the terminal methyl groups in odd and even chain alkylthiol SAMs (n = 14–15, n = 15-16, and n = 16-17).[17] The trend observed in these friction force measurements is consistent with the descriptions of the methyl group orientation (Figure 6.3) suggested by the wettabilities.

If the orientation of the methyl net dipole moment is the same as the transition dipole moment probe by surface IR, one would expect the surface potential of even-numbered chains to be greater than that of odd chains. We observe the opposite trend. All our measurements were carried out in ambient atmosphere with a relative humidity of 16 to 22 % and we thus suspect that physisorbed water molecules on the SAM surface play an important role in the measurements. Since the methyl group orientation in SAMs is known to strongly influence the orientation or alignment of adsorbates such as nematic liquid crystals,[18] it is possible that the odd-even trend observed here reflects a difference in the orientation of the dipole of physisorbed water molecules.

The odd-even effect gives rise to two separate linear regions of similar slope in the $\Delta\phi$ - n plot given in Figure 6.2. A linear regression analysis of the surface potential values gives a slope of 39 ± 1 mV per CH_2 when n is even and 37 ± 7 mV per CH_2 when n is odd. By contrast, a slope of 9.3 mV per CH_2 unit was found for C_nS/polycrystalline Au SAMs by and Evans and Ulman. Although this value is comparable to that obtained for monolayers of straight chain alcohols ($16 \leq n \leq 22$) at the air/water interface (8.9 mV per CH_2),[29] significantly higher values have been reported for fatty acid Langmuir monolayers (28 mV per CH_2)[30] and for C_nS SAMs on chromium (23 mV per CH_2).[31]

The precise significance of the $\Delta\phi$ - n slope is not yet fully resolved. If one applies the 2-layer model (Figure 6.2) proposed by Evans and Ulman, which considers $\frac{\mu_{Au-S}}{\varepsilon_{Au-S}}$ as constant (eq 4),[13,32,33] an increase in $\Delta\phi$ with n would imply that either, or both, μ_m and ε_m vary as n is increased. However, for an all-trans C-C bond configuration, additional CH_2 units would not be expected to greatly affect the dipole of the alkyl chain, μ_m (eq 4).[14] Thus, a variation in the contribution of the SAM dielectric constant (ε_m) to $\Delta\phi$ might explain the trend observed in Figure 6.2.[14] Using the measured surface potential values and eq 4, a non-linear variation of the ε_m of C_nS/Au from ~ 5 for n = 8 to ~ 3 for n = 18 has been estimated.[14] However, surface plasmon resonance spectroscopy measurements (using two wavelengths or two solvents) that allow the film thickness and dielectric constant to be determined independently of one another indicate that the SAM ε_m remains constant at a value of 2.10 for n = 8, 12, 16, and 18.[34] Obviously, the net dipole moment measured by the Kelvin probe technique must be sensitive to other factors, such as the chain tilt angle, screening of the $Au^{\delta+}$-$S^{\delta-}$ by the alkyl chains, and the *gauche* bond population. Since the dielectric constant of the Au-S bond (ε_{Au-S}), and the dipole moments (μ_{Au-S}, and $\mu_{\perp m}$) have not been *independently* measured, their weighted contribution to the observed surface potential remains to be addressed.

6.4 Conclusions

Kelvin probe studies of *n*-alkylthiol SAMs ($4 \leq n \leq 20$) on polycrystalline gold establish that the measured surface potential is sensitive to the alkylthiol chain length and to whether there is an even or odd number of carbons. Modulation of the surface potential by the terminal methyl group is manifested as a larger $\Delta\phi$ (122 mV) for odd-numbered SAMs compared to even-numbered SAMs. This odd/even effect has been previously observed in studies using surface infrared spectroscopy, contact angle measurements, and friction force microscopy. This present study paves the way for the investigation of the SAM surface potential on a tens of nanometer scale by the newly developed scanning Kelvin probe microscopy technique.

References

1) Mignolet, J. C. P. *J. Chem. Soc., Disc. Faraday. Soc.* **1950**, *8*, 326-329.
2) Christmann, K. *Introduction to Surface Physical Chemistry*; Springer-Verlag: New York, 1991.
3) Helmholtz, H. *Ann. Phys.* **1879**, *7*, 337-382.
4) Halliday, D.; Resnick, R. *Physics*; Wiley: New York, 1978.
5) Martin, Y.; Williams, C. C.; Wickramasinghe, H. K. *J. Appl. Phys.* **1987**, *61*, 4723-4729.
6) Weaver, J. M. R.; Abraham, D. W. *J. Vac. Sci. Technol. B* **1991**, *9*, 1559-1561.
7) Lu, J.; Guggisberg, M.; Luthi, R.; Kubon, M.; Scandella, L.; Gerber, C.; Meyer, E.; Guntherodt, H. J. *J. Appl. Phys. A* **1998**, *66*, 273-275.
8) Kikukawa, A.; Hosaka, S.; Imura, R. *Rev. Sci. Instrum.* **1996**, *67*, 1463-1467.
9) Jacobs, H. O.; Knapp, H. F.; Muller, S.; Stemmer, A. *Ultramicroscopy* **1997**, *69*, 39-49.

10) Bohmisch, M.; Burmeister, F.; Rettenberger, A.; Zimmermann, J.; Boneberg, J.; Leiderer, P. *J. Phys. Chem. B* **1997**, *101*, 10162-10165.

11) Yasutake, M.; Aoki, D.; Fujihara, M. *Thin Solid Films* **1996**, *273-283*, 279-283.

12) Cheran, L.-E.; Liess, H.-D.; Thompson, M. *Analyst* **1999**, *124*, 961-970.

13) Demchak, R. J.; Fort, T. J. J. *J. Colloid and Interface Sci.* **1974**, *46*, 191-202.

14) Evans, S. D.; Ulman, A. *Chem. Phys. Lett.* **1990**, *170*, 462-466.

15) Campbell, I. H.; Rubin, S.; Zawodzinski, T. A.; Kress, J. D.; Martin, R. L.; Smith, D. L.; Barashkov, N. N.; Ferraris, J. P. *Phys. Rev. B* **1996**, *54*, R14321-R14324.

16) Zehner, R. W.; Parsons, B. F.; Hsung, R. P.; Sita, L. R. *Langmuir* **1999**, *15*, 1121-1127.

17) Wong, S.-S.; Takano, H.; Porter, M. D. *Anal. Chem.* **1998**, *70*, 5209-5212.

18) Gupta, V. K.; Abbott, N. L. *Phys. Rev. E* **1996**, *54*, R4540-R4543.

19) Miller, W. J.; Abbott, N. L. *Langmuir* **1997**, *13*, 7106-7114.

20) Graupe, M.; Takenaga, M.; Koini, T.; Colorado, R. J.; Lee, T. R. *J. Am. Chem. Soc.* **1999**, *121*, 3222-3223.

21) Colorado, R., Jr.; Villazana, R. J.; Lee, T. R. *Langmuir* **1998**, *14*, 6337-6340.

22) Tao, Y.-T.; Lee, M.-T. *Thin Solid Films* **1994**, *244*, 810-814.

23) Badia, A. *Ph.D. Thesis*; Badia, A., Ed.; McGill University: Montreal, 1996.

24) Furniss, B. S.; Hannaford, A. J.; Rogers, V.; Smith, P. W. G.; Tatchell, A. R. *Vogel's Textbook of Practical Organic Chemistry*; 4th ed.; Longman: New York, 1978.

25) Nuzzo, R. G.; Dubois, L.; Allara, D. L. *J. Am. Chem. Soc.* **1990**, *112*, 558-569.

26) Parikh, A. N.; Allara, D. L. *J. Chem. Phys.* **1992**, *96*, 927-945.

27) Landau, L. D.; Lifshitz, E. M. *Electrodynamics of Continuous Media*; Pergamon Press: New York, 1960.

28) Israelachvili, J. *Intermolecular and Surface Forces*; Academic Press: San Diego, 1992.

29) Kuchhal, Y. K.; Katti, S. S.; Biswas, A. B. *J. Colloid Interface Sci.* **1974**, *49*, 48-56.

30) Harkins, W. D.; Fisher, E. K. *J. Chem. Phys.* **1933**, *1*, 852-862.

31) Martin, P. J.; Bornog, B. J. *J. Phys. Chem.* **1968**, *72*, 4172-4175.

32) Vogel, V.; Mobius, D. *Thin Solid Films* **1988**, *159*, 73-81.

33) Oliviera, J., O. N.; Taylor, M. D.; Lewis, T. J.; Salvagno, S.; Stirling, C. J. M. *J. Chem. Soc. Faraday Trans. 1* **1989**, *85*, 1009-1018.

34) Peterlinz, K. A.; Georgiadis, R. *Langmuir* **1996**, *12*, 4731-4740.

Chapter 7

Conclusions, Contributions to Original Knowledge, And Ideas for Continued Research

7.1 Overview and Conclusions

The electrical and electrochemical properties of self-assembled monolayers (SAMs) at gold surfaces have been investigated through *i) ion* transport and *ii) electron* transfer at $X(CH_2)_nS/Au$ SAMs using cyclic voltammetry and a.c. impedance spectroscopy. The effect of the alkyl chainlength n and terminal endgroup X on *ion* transport (K^+, HPO_4^{2-}, $H_2PO_4^-$) into the SAM hydrocarbon region is explored in detail with n = 7-15 and X = CH_3, OH, CO_2H, and with a partially fluorinated $CF_3(CF_2)_7(CH_2)_2S/Au$ SAM. The kinetics of *electron* transfer from a water soluble redox couple through the SAM is explored with $Ru(NH_3)_6^{3+/2+}$, $Fe(CN)_6^{3-/4-}$ and $Co(bpy)_3^{3+/2+}$ using a.c. impedance spectroscopy and by modulating the d.c. potential. Finally, the effect of the orientation of the methyl end-group dipoles on the surface potential of n-alkylthiol SAMs ($3 \leq n \leq 19$) is probed using the Kelvin probe technique.

The ionic insulating properties of $CH_3(CH_2)_nS/Au$ SAMs (n = 7-15) have been addressed in Chapter 2. SAMs are indeed insulators ($|Z| = 10^5\ \Omega\ cm^2$) under well-defined monolayer preparation conditions, and obey the Helmholtz ideal capacitor (parallel plate capacitor with a dielectric medium). This is manifested in a.c. impedance spectroscopy as a phase angle $\geq 88°$ at an ion-diffusion related frequency (*i.e.* 1 Hz). SAMs (n = 7-15) are impermeable to ions, independent of the electrolyte

concentration ($[K_2HPO_4]$ = 2-50 mM) at moderate d.c. potentials (typically 0 to + 0.4 V *vs.* Ag/AgCl).

A transformation from an insulating state to an ionic conducting state in *n*-alkylthiol/Au SAMs has been identified. The ionic permeability of *n*-alkylthiol SAMs (n = 7-15) can in fact be modulated by varying the applied potential, as shown in Chapter 3. When a critical potential (V_c) is reached or exceeded, SAMs are no longer ionic insulators. The critical potential is a transition potential between an insulating state to a (relatively low) ionic conducting state and translates (at $f < 50$ Hz) into a decrease of the phase angle from ~ 88-89° to considerably lower values. V_c is chainlength dependent and becomes more cathodic as the alkyl chain is increased. V_c is – 0.15 V (*vs.* Ag/AgCl) for n = 7, – 0.25 V for n = 9, 11, and – 0.35 V for n = 15. SAM ionic permeability may arise from a film transformation and/or electrical film breakdown upon applied potential, and is unlikely to be caused by the reductive thiol desorption, as it happens at considerably more cathodic potentials (~ – 1 V *vs* Ag/AgCl). The relaxation frequency of trans-SAM ion migration (4 - 100 Hz) can be calculated from fitting of the impedance data to an appropriate equivalent circuit and can also be estimated from Bode phase plots.

The SAM ionic permeability can also be modulated by varying the chain end group functionality. This effect is clearly observed at $X(CH_2)_{15}S$/Au SAMs with X = CH_3, OH, and CO_2H and at a partially fluorinated $CF_3(CF_2)_7(CH_2)_2S$/Au SAM, as demonstrated in Chapter 4. The critical potential V_c, where ion penetration into the SAM is activated, can be understood in terms of the hydrophilic/hydrophobic character of the SAM/electrolyte. For hydrophilic interfaces, V_c is + 0.25 V (*vs.* Ag/AgCl) for X = OH and + 0.15 V for $X = CO_2H$. V_c is substantially more cathodic for the hydrophobic interface, where V_c = – 0.35 V for $X = CH_3$. For the fluorinated SAM, V_c is – 0.25 V. A hydrophilic SAM/electrolyte interface, rather than a hydrophobic one, is more readily transformed by applied potential into a state which favors ion/water penetration into the SAM.

The kinetics of electron transfer of water soluble redox couples at bare gold and at $CH_3(CH_2)_{15}S$/Au SAMs has been elucidated by analyzing a.c. impedance

responses at various d.c. potentials centered about the reversible half-wave potential of the redox couple (Chapter 5). The three systems under study ($Ru(NH_3)_6^{3+/2+}$, $Fe(CN)_6^{3-/4-}$, and $Co(bpy)_3^{3+/2+}$) show distinctly different kinetic behavior as shown by their σ - E curves (Warburg coefficient as a function of the applied potential). The pre-requisites for use of σ - E curve in kinetic studies is that the system adheres to the Randles equivalent circuit and that there is a linear $Z_f' - \omega^{-1/2}$ relationship. These pre-requisites are met for all systems studied except for $Ru(NH_3)_6^{3+/2+}$ at bare gold (as $R_{ct} \rightarrow 0$) and $Fe(CN)_6^{3-/4-}$ at a $CH_3(CH_2)_{15}S$/Au SAM (as $R_{ct} \rightarrow \infty$). Fittings of the experimental σ - E curves to theoretical curves at bare gold for $Fe(CN)_6^{3-/4-}$ and $Co(bpy)_3^{3+/2+}$ show that the electron transfer is reversible. The diffusion coefficient and the heterogeneous rate constant at bare gold are accessible from either the minimum of the σ - E curve or the Butler-Volmer equation ($\ln k_f$ *vs.* E). However, the kinetics of electron transfer at a SAM-coated electrode differs for each probe. Fitting of the σ - E curve to theoretical curves shows that the electron transfer at a $CH_3(CH_2)_{15}S$/Au SAM is irreversible in the case of $Co(bpy)_3^{3+/2+}$. For $Ru(NH_3)_6^{3+/2+}$, the electron transfer proceeds *via* a CE (chemical-electrochemical) mechanism. The preceding chemical step is most likely a process associated with desolvation of the redox probe and/or permeation of the redox probe to the SAM hydrocarbon region. The kinetics for $Fe(CN)_6^{3-/4-}$ are complex at a SAM-coated electrode and σ - E assessment is not possible. The very hydrophilic nature of this couple, and the known large solvation difference between the two forms is the likely source of this complexity.

The effect of the orientation of the terminal methyl group on the SAM surface potential has been addressed in Chapter 6 using the Kelvin probe technique. The surface potential $\Delta\phi$ of C_nS/Au ($C_n = CH_3(CH_2)_{n-1}$, $4 \leq n \leq 20$) SAMs is chainlength sensitive. $\Delta\phi$ varies linearly with n when $n \geq 7$. The data can be interpreted using the two-layer capacitor model, considering the SAM as being made up of two dipole sheets. The $Au^{\delta+}$-$S^{\delta-}$ interface can be viewed as one sheet and the SAM/air interface as the other. The $\Delta\phi$ - n data clearly shows an alternating effect in the values of the

surface potential at all n, where $\Delta\phi$ is systematically greater by 122 mV for SAMs made of odd-numbered alkylthiols. The slope when n = odd number is 37 ± 7 mV and is 39 ± 1 mV when n is even. The modulation of the SAM surface potential is believed to arise from the influence of the net orientation of the methyl dipole. It is also suggested that the measured surface potentials $\Delta\phi$ under ambient atmospheric conditions may result from the effect of the methyl dipole orientation on adsorbed water molecules (or contaminants).

This thesis describes some of the important factors that govern ion transport and electron transfer kinetics at self-assembled *n*-alkIthiol/Au monolayers. The electrical properties of SAMs can be modulated by varying the d.c. applied potential. The kinetics of electron transfer through the SAM hydrocarbon region are complicated and confirms that the description of SAMs as a "hydrocarbon slab" is too limited.

7.2 Contributions to Original Knowledge

The use of a.c. impedance spectroscopy with variation of the d.c. potential about the reversible half-wave potential is a novel approach to the study of self-assembled monolayers at metal surfaces. A diagnostic based on the phase angle of the impedance at low frequency (typically 1 Hz) which allows one to differentiate between an ionic insulator ($\geq 88°$) and a leaky insulator ($< 88°$) is presented for the first time. This thesis clearly establishes that SAM ionic permeability *i)* varies with chainlength and chain end group, and *ii)* can be tuned by the d.c. potential. A critical potential V_c is identified which corresponds to the potential where defects are formed. These potential-induced defects trigger ion penetration from the electrolyte to the hydrocarbon SAM region and are formed at potentials ranging from + 0.25 V *vs.* Ag/AgCl to – 0.35 V. These critical potentials have not been previously identified and these studies therefore shed light on the electrical stability of SAM. It gives a more precise picture of the SAM stability than the more commonly used 'window of stability' which refers to the potential range over which neither reductive nor

oxidative faradaic chemistry of the RS/Au linkage occurs (~ from – 1 V to + 0.9 V *vs.* Ag/AgCl).

Kinetics of electron transfer at SAM-coated electrodes using a.c. impedance spectroscopy over a wide range of d.c. potential ($E^r_{1/2}$ ± 150 mV) is presented here. Data analysis of the σ - E (Warburg coefficient as a function of the applied potential) curves for three redox couples ($Fe(CN)_6^{3-/4-}$, $Ru(NH_3)_6^{3+/2+}$ and $Co(bpy)_3^{3+/2+}$) at bare gold allows one to extract kinetics parameters such as the diffusion coefficient and the heterogeneous rate constant. The kinetic analysis of these redox couples at a defect-free SAM, by fitting the experimental σ - E curve to theoretical models, has been very efficient in providing a better understanding on the mechanism of electron transfer. An alternative mechanism to electron tunneling is proposed for $Ru(NH_3)_6^{3+/2+}$. Kinetic analysis based on σ - E curves reveal that the electron transfer proceeds *via* a CE mechanism for $Ru(NH_3)_6^{3+/2+}$ and is irreversible in the case of $Co(bpy)_3^{3+/2+}$. These studies demonstrate the usefulness of a.c. impedance spectroscopy (at d.c. potentials about $E^r_{1/2}$) as an efficient tool for the elucidation of mechanisms of electron transfer at ultrathin films.

This thesis contains the first demonstration of an the odd/even effect on the surface potential of C_nS/Au SAMs ($C_n = CH_3(CH_2)_{n-1}$) as probed by the Kelvin probe technique. The orientation of the terminal end group dipole relative to the surface normal induces a systematic difference in the surface potential of C_nS/Au SAMs ($4 \leq n \leq 20$). SAMs made of odd-numbered alkylthiols exhibit a surface potential 122 mV higher than SAMs made of even-numbered. The odd/even effect on the SAM surface properties has also been reported in the literature by surface infrared spectroscopy, contact angle measurements, and friction force measurements.

7.3 Ideas for Continued Research

i) X-ray diffraction studies of thiol SAMs at gold single crystal surfaces (as opposed to polycrystalline surfaces) have established that the chain packing density is determined by the Au-S epitaxy. For example, the RS/Au(110) SAM has an 8 % less dense surface packing than RS/Au(111). By contrast, the RS packing density on a Au(100) surface is 20 % greater than for RS/Au(111) SAMs. A greater chain packing density will likely affect the critical potential of SAMs at which potential-induced defects are formed. Thus, the effect of the Au-S epitaxy on the critical potential of SAMs should be investigated. These experiments will serve to elucidate the role of the underlying substrate on the SAM electrical properties.

ii) The effect of the Au-S epitaxy on the surface potential of SAMs should also be investigated. This will allow one to pin down factors that contribute to the surface potential of RS/Au SAMs.

iii) Measurements of the surface potential of SAMs at the microscopic scale using a scanning Kelvin probe microscope should also be investigated, as this equipment is now commercially available. Measurement of the local surface potential could become an efficient "imaging" tool of features which possess similar topologies.

iv) The study of electron transfer at SAM-coated electrode using a.c. impedance spectroscopy at $E^{r}_{1/2} \pm \sim 150$ mV has tremendous potential. Theoretical σ - E curves for many different types of mechanism of electron transfer are available in the literature (Sluyters-Rehbach and Rehbach work). Experiments involving a combination of various redox couples and SAM/electrolyte interfaces should be investigated. The choice of the redox couple can be made based on the differences in the heterogeneous rate constant, charge, size, hydrophobic/hydrophilic character. The hydrophilic/hydrophobic character

and the charge of the SAM/electrolyte interface can be easily modulated by an appropriate choice of the RS molecules, *i.e.* $X = CH_3$, OH, CO_2H, CO_2^-, NH_2, NH_3^+, CN, PO_4^{2-}, *etc.* Judicious choice of the SAM/electrolyte interface and redox couple will provide us with an incomparable understanding of the factors that govern the interfacial electron transfer at SAM-coated electrodes. These studies should lead to the identification of the preceding (and following) chemical step in multistep mechanisms (CE, EC, CEC, *etc.*).

v) Alkylthiol monolayers with pendant redox centers (such as ferrocene) are particularly attractive systems since an electron tunneling mechanism, either through bond or through space, has been proposed for these systems. The σ-E curve in RS/Au SAMs with tethered redox centers is expected to correspond to that of a simple electron transfer, and a.c. impedance studies would be appropriate to confirm this. If a more complex mechanism is operative, the σ-E curves may help to classify the nature of the complexity.

Appendix

General Principles on A.C. Impedance Spectroscopy

When a sinusoidal alternating voltage perturbation, $E(t)$, is applied to a linear system, the current response, $I(t)$, will also be sinusoidal with the same angular frequency ω ($\omega = 2\pi f$), but with a phase shift φ:

$$E(t) = \Delta E = E_m \sin(\omega t) \quad (1)$$

$$I(t) = \Delta I = I_m \sin(\omega t + \varphi) \quad (2)$$

φ is the phase difference between the applied voltage and the measured current and is 0° for a resistor and 90° for a capacitor. The electrical response $I(t)$ reflects the different time constants of the relaxation processes which are taking place in the measured system. ΔE is the amplitude of the perturbing (a.c.) voltage and is typically 10 mV.

The modulus of the cell impedance is defined by:

$$|Z| = E_m / I_m \quad (3)$$

and the real (Z') and imaginary (Z'') components are:

$$Z' = (E_m / I_m)\cos\varphi \quad (4)$$

$$Z'' = (I_m / E_m)\cos(-\varphi) \tag{5}$$

From these definitions, the phase angle, φ, can be expressed as:

$$\varphi = \cot(-\frac{Z''}{Z'}) \tag{6}$$

and the modulus of the total impedance is:

$$|Z| = \sqrt{(Z')^2 + (Z'')^2} \tag{7}$$

In general, Z is frequency dependent and can be measured over a wide range of frequency, typically from 10^{-3} Hz to 10^6 Hz. The resulting Z *vs.* f ($= \omega/2\pi$) curve allows one to derive information about the electrical properties of the system under study.[1,2] A physical interpretation (in terms of physical chemistry concepts) of impedance data usually requires the use of an equivalent electrical circuit that adequately fits the experimental data over the entire frequency range probed. Equivalent circuits are composed of basic electrical components, such as resistors, condensers and inductors (only at very high frequencies), placed in series or in parallel to one another. One must keep in mind that often more than one equivalent circuit can fit a given experimental Z *vs.* f curve. It is therefore recommended to use the simplest equivalent circuit that best fits the experimental data. The impedance equations for some simple circuit elements are:

For a resistor R	$Z = R$	$Z' = R$	$Z'' = 0$
For a capacitor C	$Z = \frac{1}{i\omega C}$	$Z' = 0$	$Z'' = \frac{1}{\omega C}$
For an inductor L	$Z = i\omega L$	$Z' = 0$	$Z'' = \omega L$

More sophisticated elements have been frequently used in equivalent circuits to better reflect the physical meaning at electrode surfaces. The most widely used of these are the constant phase element (*CPE*) and the Warburg element (*W*).

A *CPE* is often used in place of a capacitor to compensate for the non-homogeneity of the material/electrolyte interface. For example, the *CPE* is used in the case of porous or rough surfaces and is given as:

$$Z_{CPE} = A(j\omega)^{-\alpha} \tag{8}$$

where $0 < \alpha < 1$. If $\alpha = 1$, the expression of the *CPE* is identical to that of a capacitor *C*.

The Warburg element *W* is a kind of resistance to mass transfer and is given by:

$$Z_W' = Z_W'' = \sigma\omega^{-1/2} \tag{9}$$

where σ is referred to as the Warburg coefficient.

An inert electrode/electrolyte interface is frequently modeled by an equivalent circuit consisting of a resistance R_s (the solution resistance) in series with a capacitor C_{dl} (the double-layer capacitance). The total impedance of such an equivalent circuit is:

$$Z = R_s + \frac{1}{j\omega C_{dl}} \tag{10}$$

In the case of a simple faradaic reaction (ox + n e^- $\rightarrow$ red), the Randles equivalent circuit is used (Figure A.1).[3]

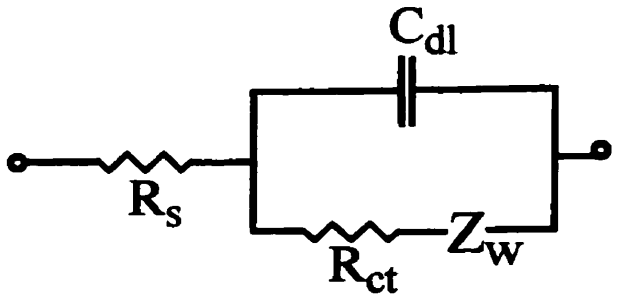

Figure A.1. Equivalent circuit of an electrochemical cell for a simple faradaic process. R_s is the solution resistance, C_{dl} is the double-layer capacitance, R_{ct} is the charge transfer resistance, and Z_w is the Warburg impedance.

The in-phase and out-of-phase components of the Randles equivalent circuit are given by:

$$Z' = R_s + \frac{R_{ct} + \sigma\omega^{-1/2}}{(C_{dl}\sigma\omega^{1/2} + 1)^2 + \omega^2 C_{dl}^2 (R_{ct} + \sigma\omega^{-1/2})^2} \tag{11}$$

$$Z'' = -\frac{\omega C_{dl}(R_{ct} + \sigma\omega^{-1/2})^2 + \sigma\omega^{-1/2}(\omega^{1/2} C_{dl}\sigma + 1)}{(C_{dl}\sigma\omega^{1/2} + 1)^2 + \omega^2 C_{dl}^2 (R_{ct} + \sigma\omega^{-1/2})^2} \tag{12}$$

References

1) Macdonald, J. R. *Impedance Spectroscopy*; Wiley: New York, 1987.

2) Bard, A. J.; Faulkner, L. R. *Electrochemical Methods: Fundamentals and Applications*; John Wiley & Sons: New York, USA, 1980.

3) Randles, J. E. B. *Disc. Faraday Soc.* **1947**, *1*, 11-19.